*Year :* 2019

# THE THALAMIC RETICULAR NUCLEUS: A MULTIFACETED GUARDIAN

Vantomme Gil

UNIL | Université de Lausanne
Faculté de biologie
et de médecine

**Département des Neurosciences Fondamentales**

# THE THALAMIC RETICULAR NUCLEUS: A MULTIFACETED GUARDIAN

**Thèse de doctorat en Neurosciences**

présentée à la

Faculté de Biologie et de Médecine
de l'Université de Lausanne

par

**VANTOMME GIL**

Biologiste diplômé de l'Université de Lausanne, Suisse

**Jury**

Prof. Hornung Jean-Pierre, Président
Prof. Lüthi Anita, Directrice
Prof. Schneggenburger Ralf, Expert
Prof. Fricker Desdemona, Experte

Thèse n° 261

**Lausanne 2019**

***Programme doctoral interuniversitaire en Neurosciences des Universités de Lausanne et Genève***

LEMANIC NEURO SCIENCE DOCTORAL SCHOOL

UNIL | Université de Lausanne

UNIVERSITÉ DE GENÈVE

UNIL | Université de Lausanne
Faculté de biologie
et de médecine

**Département des Neurosciences Fondamentales**

# THE THALAMIC RETICULAR NUCLEUS: A MULTIFACETED GUARDIAN

**Thèse de doctorat en Neurosciences**

présentée à la

Faculté de Biologie et de Médecine
de l'Université de Lausanne

par

**VANTOMME GIL**

Biologiste diplômé de l'Université de Lausanne, Suisse

**Jury**

Prof. Hornung Jean-Pierre, Président
Prof. Lüthi Anita, Directrice
Prof. Schneggenburger Ralf, Expert
Prof. Fricker Desdemona, Experte

Thèse n° 261

**Lausanne 2019**

***Programme doctoral interuniversitaire en Neurosciences des Universités de Lausanne et Genève***

LEMANIC NEURO SCIENCE DOCTORAL SCHOOL

UNIL | Université de Lausanne

UNIVERSITÉ DE GENÈVE

UNIL | Université de Lausanne

UNIVERSITÉ DE GENÈVE

***Programme doctoral interuniversitaire en Neurosciences des Universités de Lausanne et Genève***

# Imprimatur

Vu le rapport présenté par le jury d'examen, composé de

| | | | | |
|---|---|---|---|---|
| **Président·e** | Monsieur | Prof. | Jean-Pierre | **Hornung** |
| **Directeur·trice de thèse** | Madame | Prof. | Anita | **Lüthi** |
| **Expert·e·s** | Monsieur | Prof. | Ralf | **Schneggenburger** |
| | Madame | Prof. | Desdemona | **Fricker** |

le Conseil de Faculté autorise l'impression de la thèse de

**Monsieur Gil Vantomme**

Master en biologie médicale, Université de Lausanne, Suisse

intitulée

**The Thalamic Reticular Nucleus: a Multifaceted Guardian**

Lausanne, le 16 janvier 2020

pour Le Doyen
de la Faculté de Biologie et de Médecine

Prof. Jean-Pierre Hornung

# Table of content

## A. Acknowledgements

I would like to express my very great appreciation to my thesis director, Prof. Anita Lüthi. Since I joined the lab as a master student, her leadership, her professional supervision and her human qualities created an environment where I could and still can grow as a scientist and as a person. She gave me the desire to pursue an academic career and the tools to achieve this goal. I realize how fortunate I am to have learned and worked with her in the last five years and I would like to express again my gratitude.

I would like to offer my special thanks to Dr. Zita Rovó for initiating the major project of my thesis and for her valuable and constructive suggestions during the planning and the development of this research work. She cultivated my interest for *in vivo* methodological approaches that happened to become a keystone of my work.

I am particularly grateful for the assistance given by my colleagues who participated in the realization of the scientific projects. Dr. Laura Fernandez who provided me with very valuable advice on experimental design, scientific writing and data presentation. Dr. Elidie Béard for her support in viral injections and mice handling. Romain Cardis for his help in data analysis. Alejandro Osorio-Forero for his expertise in sleep. The students Georgia Katsioudi, Angelo Guadagno and Virginie Perrenoud for their help in collecting experimental data and the opportunity to share my knowledge with them.

I wish to acknowledge the help provided by Prof. Adrien Peyrache and Dr. Adrian Duszkiewicz from McGill University for teaching me the use of silicone probes.

Beyond the scientific projects, I would like to extend my thanks to all former and present lab members, who created a fantastic working atmosphere. Dr. Simone Astori, Dr. Martina Perin and Chiara Pellegrini who gave me the taste for patch-clamp. Dr. Sandro Lecci who gave me the taste for coffee. Najma Cherrad for her friendship and frank discussions.

I would like to offer my special thanks to Tamara Zehnder for her friendship and the moral and personal support she gave me throughout the thesis. Tamara is the kind of friend and colleague that everyone can wish to have.

My special thanks are extended to Dr. Paul Chu Sin Chung, Dr. Alexandru Deftu, Dr. Ludovic Gillet and Elena Konnova with whom I shared a crowded office where the balance between entertainment and work was excellent, and to all members of the AVS committee for their engagement in the social activities of the department.

Finally, I would like to express my sincerest gratitude to my parents and my brother for their concerns and supports. They have been encouraging and helping me throughout my study and I truly appreciate their efforts.

Lastly, I am thankful to July Ricklin for her continuous support at home, her enthusiastic encouragement in pursuing a career and her implication in many of my activities inside and outside the department.

## B. Abstract

Interactions between the cortex and the thalamus are essential for major brain functions such as sensory information processing and integration, sleep and wake regulation and cognitive processes. The thalamic reticular nucleus (TRN) is strategically positioned within the thalamocortical circuit and has a strong inhibitory control over the thalamus. It can act on a global scale, such as suppressing the flow of sensory information from the thalamus to the cortex during sleep. The TRN also acts locally on the activity of single cells or small cell groups. To reconcile both of these global and local aspects of TRN functions, we studied the cellular, synaptic and functional heterogeneity of the TRN, with a focus on the comparison between the classical sensory TRN and the less well-described limbic TRN.

In study 1, using anatomical tracing and cellular electrophysiology, we identified the dorsal presubiculum (dPreS), the retrosplenial cortex (RSC) and the anterior thalamic nuclei (ATN) as part of a novel thalamo-cortical circuit involving the limbic TRN in mice. The dPreS, RSC and ATN are three key structures for spatial navigation. dPreS/RSC excitatory glutamatergic synapses formed on TRN and ATN are part of a feedforward circuit through which TRN-mediated inhibition generates large burst-mediated inhibitory synaptic currents. The PreS/RSC afferents to the TRN showed driver-like characteristics, which is unprecedented for corticoreticular synapses and expands the scope of the TRN heterogeneity to the nature of its synaptic afferents. We further investigated the role of the limbic TRN in the control of head-direction neurons that were previously described to be located in the anterodorsal thalamus. The width of the tuning curve of head-direction neurons in the thalamus was broadened upon chemogenetic silencing of the TRN, revealing a novel form of internal sensory gating by the TRN. About half of the head-direction neurons showed action potential discharge patterns consistent with feedforward inhibitory responses upon light activation of dPreS/RSC. These data suggest that the limbic TRN sharpens the tuning of thalamic head-direction neurons under dPreS/RSC control. Finally, we investigated the potential function of the limbic TRN in the hidden version of the Morris watermaze. We discovered that chemogenetic silencing of the limbic TRN biased the search patterns towards allocentric strategies and generated perseverance to previously learned escape positions, suggesting an impairment of the egocentric system in which the head-direction system plays a critical role.

In study 2, we combined opto-tagging of TRN sectors with *in vitro* electrophysiological recordings and discovered that the limbic TRN neurons produced less repetitive burst firing than their sensory counterpart. The burst discharge of sensory TRN neurons is known to generate sleep spindles that propagate to the cortex, that are a marker of sleep quality and that correlate with memory consolidation. Consistently, local field potential recordings in the prefrontal cortex that is related to the less bursty limbic TRN revealed smaller amplitude and slower sleep spindles compared to sensory ones, making the heterogeneity of the TRN a critical player in local sleep rhythms.

This thesis summarizes elements supporting the heterogeneity of the TRN, in particular between the sensory and the limbic TRN. It also provides a novel function for the limbic TRN in the spatial navigation system.

## C. Résumé

L'interaction entre le cortex et le thalamus est essentielle aux fonctions majeures du cerveau telles que le traitement et l'intégration des informations sensorielles, la régulation du sommeil, de l'éveil et la cognition. Le noyau réticulé thalamique (TRN) est stratégiquement positionné dans les circuits thalamocorticaux et possède un fort control inhibiteur sur le thalamus. Il peut agir à un niveau global, par exemple en interrompant le flux d'information sensorielle du thalamus vers le cortex pendant le sommeil. Le TRN peut aussi agir de manière localisée sur l'activité d'une seule cellule ou d'un petit groupe. Afin de réconcilier ces aspects globaux et locaux du fonctionnement du TRN, nous avons étudié l'hétérogénéité du TRN au niveau cellulaire, synaptique et fonctionnel, avec une attention particulière à la comparaison entre le TRN sensoriel classique et le TRN limbique qui est moins bien décrit.

Dans l'étude 1, nous avons identifié, à l'aide de méthodes de traçage et d'électrophysiologie cellulaire, le présubiculum dorsal (dPreS), le cortex rétrosplénial (RSC) et les noyaux thalamiques antérieurs (ATN) comme faisant partie d'un circuit thalamocortical impliquant le TRN limbique chez la souris. Le dPreS, le RSC et les ATN sont des structures clés dans le système de navigation spatiale. Les synapses excitatrices glutamatergiques du dPreS/RSC sur le TRN et les ATN font parties d'un circuit dans lequel l'inhibition médiée par le TRN génère de larges courants synaptiques inhibiteurs. Les afférences du PreS/RSC vers le TRN ont montré des caractéristiques de driver, ce qui est sans précédent pour les synapses entre le cortex et le TRN et étend l'hétérogénéité du TRN à la nature de ses afférences synaptiques. Nous avons poussé l'investigation du rôle du TRN limbique sur le control des neurones d'orientation présent dans le thalamus anterodorsal. Le blocage du TRN induit un élargissement de l'arc de cercle pour lequel un neurone d'orientation du thalamus s'active, révélant une nouvelle forme de control de l'information sensorielle interne par le TRN. Environ la moitié des neurones d'orientation montre une activité électrique consistante avec une inhibition disynaptique lors de l'activation du dPreS/RSC. Ces données suggèrent que le TRN limbique affine la précision des neurones d'orientation du thalamus sous le control du dPreS/RSC. Finalement, nous avons investigué le rôle potentiel du TRN limbique dans une tâche d'orientation : le labyrinthe d'eau de Morris. Nous avons découvert que le blocage du TRN limbique biaise les schémas de navigation des souris en faveur de stratégies allocentriques et génère de la persévérance au niveau de la zone d'échappatoire précédemment apprise. Ces résultats suggèrent un déficit du système égocentrique dans lequel les neurones d'orientation jouent un rôle critique.

Dans l'étude 2, nous avons combiné le marquage lumineux des différents secteurs du TRN avec des enregistrements électrophysiologiques *in vitro* et découvert que les neurones du secteur limbique du TRN produisent moins de salves de potentiel d'action que les neurones des secteurs sensoriels. Ces salves des neurones sensoriels du TRN génèrent les fuseaux du sommeil qui se propagent au cortex et sont un marqueur de la qualité du sommeil et de la consolidation de la mémoire. De manière consistante,

les enregistrements des champs de potentiel locaux dans le cortex préfrontal connecté au TRN limbique ont révélé que les fuseaux du sommeil dans ce cortex ont une amplitude et une vitesse réduites en comparaison des fuseaux dans les cortex sensoriels. L'hétérogénéité du TRN semble donc être critique pour la génération locale des rythmes du sommeil.

Cette thèse rassemble les éléments qui supportent l'hétérogénéité du TRN et qui peuvent être à la base des spécificités fonctionnelles du TRN limbique en comparaison du TRN sensoriel. Cette thèse fournit aussi une nouvelle fonction du TRN limbique dans le système de navigation.

## D. Aim

The thalamic reticular nucleus (TRN) has been known for decades to act as the guardian of the gate that controls the information flow between the thalamus and the cortex at two principal levels. On a global scale, the TRN reduces sensory information flow to the cortex during non-rapid-eye-movement sleep (NREMS). Locally, the TRN controls neuronal activity of single cells or small cell groups in the thalamus that form receptive fields for sensory information. The vision of the TRN as a monolithic structure that serves as a global switch for vigilance state is not compatible with these local aspects of the TRN. Recent technological advances have uncovered many TRN subnetworks that differ in cellular identities, efferent and afferent connectivities, and activity patterns during sleep and wakefulness. These could hence play distinct roles in sensory processing and attention, sleep oscillations, but also in novel cognitive processes still to be discovered. Currently, addressing the heterogeneity of the TRN has proven highly successful in advancing the functional understanding of a brain area historically considered as a uniform element.

This thesis aimed to provide novel insights into the heterogeneity of TRN function through asking two main questions:

1) What is the origin and function of synaptic afferents to the anterior portion of the TRN? How do they help refine and revise the classic definition of this nucleus in the gating of information flow?
2) What is the role of cellular and circuit heterogeneities of TRN for sleep?

I pursued these aims through anatomical tracing of afferents to the TRN, electrophysiological recordings *in vitro* and *in vivo* combined with optogenetic and chemogenetic approaches to assess synaptic function and tackled the function of the TRN through behavioral assessment. Both projects presented in this thesis aimed to provide solid cellular and synaptic data that would allow to probe the role of TRN heterogeneity in its function as a gating element and as a pacemaker for sleep rhythms. I have done so first through identifying a synaptic pathway that controls the limbic sector of the TRN and linked it to the spatial navigation system. Second, I have contributed to identify a heterogeneity of TRN burst propensity across sensory and limbic sectors of the TRN. In this thesis, I discuss how these experimental results integrate and expand the current views of the TRN. My thesis emphasizes that the brain also needs to gate internal sensory information such as the head-direction signal and that the TRN has an important say in the local organization of sleep at the cortical level.

## E. Introduction

### Prelude: the brain as an information-processing machine.

There is consensus that one of the major driving forces for the evolution of a central nervous system was to exert a centralized control over the whole body that allows rapid and coordinated responses to the ever-changing environment. Fundamental reflexes do not require the cortex to be involved. For examples, the pupil contracts upon exposure to intense light and the muscles reposition themselves upon percussion of a ligament without the need of cortical processing. However, in order to respond to complex sensory inputs, the brain evolved as a very complex structure in which sensory information can be enhanced, suppressed, refined, compared to expectations and memories and modified according to behavioral needs (hunger, thirst…), internal states (motivation, anxiety, sleepiness…) or environmental contexts.

To bring together all these different requirements for information processing, the brain evolved into multiple anatomically distinct structures (Brodmann, 1909). These segregated structures are dedicated to single functional modalities (Sporns et al., 2000). Briefly, the region dedicated to vision is located in the occipital lobe while audition and touch are in the temporal lobe. The sensory information flows from the external sensory organs in the periphery, to the thalamus and then to the cortex, which form a linear hierarchical system onto which different other brain areas can impose their “contextual” information. The frontal regions of the cortex are dedicated to motor information, as well as executive function, planning and reasoning. The cerebellum is dedicated to complex movement, balance and posture.

Cortico-cortical connections allow the different cortices to communicate and integrate multisensory information. However, some phenomena cannot be explained solely through cortico-cortical interactions. For example, the cortex is capable of generating expectations that alter the perception of the sensory world. Cortical areas processing integrated information feedback onto simpler pathways, down the hierarchy of complexity. An expected stimulus, such as hearing one’s own voice, generates a much lower activity in the auditory cortex than the voice of someone else. Schizophrenic patients are believed to have a dysfunction of this so-called efferent copy mechanism, which is probably one of the causes for the auditory hallucination from which these patients suffer, as they hear their own voice as if it was the voice of someone else.

The thalamus and the thalamic reticular nucleus (TRN) are two subcortical structures that are particularly relevant for fundamental operations of the sensory processing.

The thalamus is the relay center of the brain, which distributes sensory information to the cortex. Most of the sensory inputs perceived by external sensory organs are brought to the thalamus via a few synaptic relays within modality-specific spinal and/or brainstem nuclei. Conversely, cortical outputs also feedback onto the thalamus. The thalamus can thus be considered as the “Gate” to the cortex for sensory information (bottom-up relay) and as a hub for sensory processing (using top-down modulation).

The interconnections between the thalamus and the cortex are called thalamocortical circuits. They form parallel loops mostly dedicated to a single sensory modality. Within these loops, the TRN, strategically positioned between the cortex and the thalamus, receives afferents from both. The TRN contains inhibitory neurons that project only to the thalamus thus controlling the sensory information flow reaching the cortex, resulting in the TRN getting the nickname of “Guardian of the Gate” (Crick, 1984). Indeed, the TRN can promote or inhibit part of the thalamus through a cellular mechanism involving a post-inhibitory rebound (Steriade et al., 1993). Its action can extent on a global scale, suppressing sensory inputs overall during sleep, but also on a local scale such as the sharpening of sensory receptive field of a single thalamic neuron (Crabtree, 2018). Beyond this basic on-off mode, however, the TRN also allows the attentional selection of a modality in a complex environment with conflicting sensory inputs (Wimmer et al., 2015). This shows that the guardian role of the TRN is not limited to that of a neuronal barrier-like element, but it may be relevant to execute higher cognitive demands on organizing and selecting the quantity and quality of information that reaches the cortex.

The mechanisms through which TRN acts are still investigated and even some of the most elementary questions remain unanswered. The different sensory modalities are anatomically segregated in the cortex, thalamus and TRN. Then, how do thalamocortical circuits coordinate the different modalities? Are there circuit specificities for some modalities compared to others, in particular in the TRN? What are the modalities processed by the recently described limbic TRN?

This thesis aims to contribute to these questions, capitalizing on modern neuroscience techniques that allow to characterize and probe heterogeneous cellular and synaptic properties of the TRN. Discovering specificities in molecular marker expression, cellular function and circuit properties of the TRN will unravel how different TRN sectors control the flow of information through the thalamus and maybe reveal insights into the underlying mechanisms.

# Chapter 1. The Thalamic Reticular Nucleus

## Gross anatomical organization and morphology

The Thalamic Reticular Nucleus (TRN) was identified as a structure between the thalamus and the white matter of the interna capsula already in 1889 and received the name «nucleus reticularis» in 1902 (Kölliker, 1889; Münzer and Wiener, 1902).

The TRN is found in most mammals: human, monkey, ferret, cat, rabbit, rat, mouse (Scheibel and Scheibel, 1966; Spreafico et al., 1991; Clemence and Mitrofanis, 1992; Lübke, 1993; Berezhnaya, 2006; Zikopoulos and Barbas, 2006). TRN-like structures have also been described in non-mammalian species such as the caiman *crocodilus* (Pritz, 2018), turtle (Testudo horsfieldi) (Kenigfest et al., 2005) and zebrafish (Mueller, 2012), suggesting that interposed thalamic gating circuits have evolutionarily conserved origin.

The TRN is a shell-shaped nucleus that surrounds the dorsal and lateral portion of the thalamus. It is positioned between the internal capsule laterally, the external medullary lamina medially, the *zona incerta* ventromedially and the ventrolateral geniculate nucleus posteriorly (Fig. 1) (Scheibel and Scheibel, 1966).

The TRN is composed of GABAergic neurons (Houser et al., 1980) and projects exclusively to the thalamus (Jones, 1975). The TRN is the main source of thalamic inhibition in most mammals as the presence of thalamic interneurons is sparse (Arcelli et al., 1997).

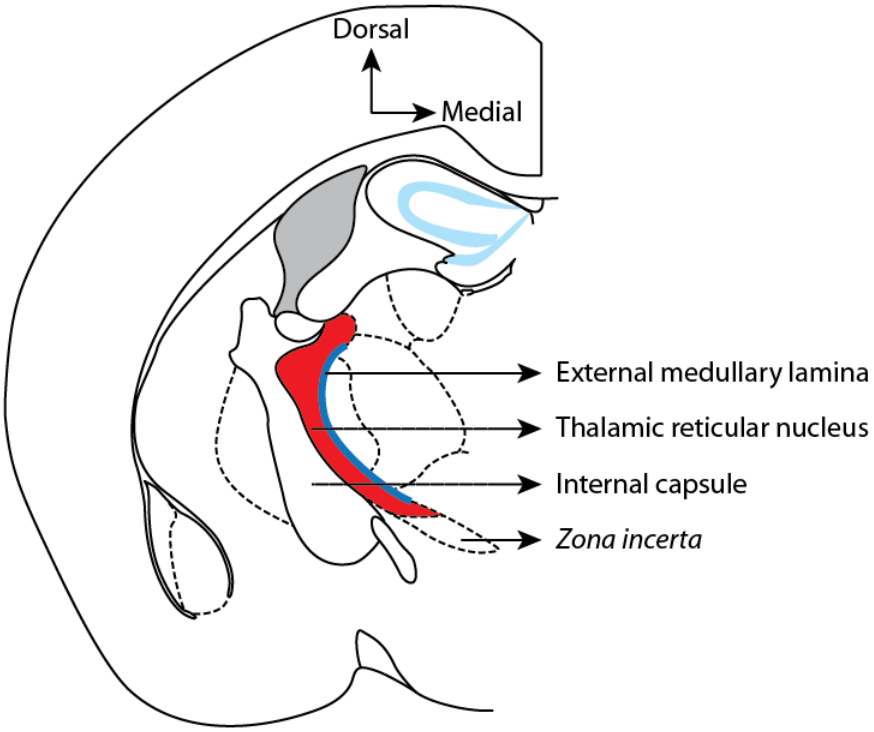


**Figure 1.** Scheme of a coronal mouse brain section at bregma -1.06 mm showing the anatomical position of the TRN. Adapted from The Mouse Brain in Stereotaxic Coordinates 3rd Edition Franklin & Paxinos.

**The TRN in brain circuits: types and organization of afferents and efferents**

Here, I briefly list the origin and characteristics of afferent inputs into the TRN. I pay particular attention to describe the organization of these afferents within the TRN. This anatomical information provides a first idea of the sectorial organization of TRN and of its differential role in treating distinct types of thalamic information. This section also serves to define the major structures, electrophysiological properties of neurons and functional aspects that form the basis to the next, more specialized chapters. For the purpose of avoiding excessive citations, I base my references in this chapter on exhaustive reviews of the topic composed by leading scientists in the field.

Afferents to TRN can be generally subdivided into 1) afferents mediating sensory information flow that ultimately engages the cortex 2) modulatory afferents arising subcortically that bring in contextual information, such as that related to vigilance states 3) novel afferents that have been described mostly anatomically.

1) Afferents related to sensory information flow

Thalamic afferents. It is classically considered that the TRN receives glutamatergic driver inputs from projections neurons of the thalamus called thalamocortical (TC) neurons. The thalamocortical neurons are excitatory neurons that project primarily to the layer 4 of their related cortex (Fig. 2). On their way to the cortex, they send collaterals to the TRN. The thalamus is classically subdivided into three groups of nuclei: the principal or relay nuclei that convey the sensory information, the association or higher-order nuclei that principally receive cortical afferents and are involved in relaying information between cortical areas, and the midline and intralaminar thalamic nuclei defined by their anatomical position and their projection to cortical and subcortical structures. This organization of the thalamic nuclei can be related to the organization of the sectors of the TRN. Indeed, the thalamoreticular circuits are organized in a parallel manner, with a single thalamic nucleus projecting to a restricted sector of the TRN and the TRN projecting back to the same thalamic nucleus (Crabtree, 2018).

Cortical afferents. The TRN receives glutamatergic modulator inputs from the cortical layer 6 neurons called corticothalamic (CT) neurons. These CT neurons project to their related thalamic nucleus and send collaterals to the TRN (Fig. 2). The cortical innervation of the TRN largely overlaps with the thalamic one, at least in sensory sectors, further reinforcing the sectorial organization of the TRN (Desîlets-Roy et al., 2002). These afferents from CT neurons onto the TRN and TC neurons show that top-down input from areas at higher levels of processing feedbacks onto lower ones. Cortical afferents from layer 5 to the TRN are, for the first time, now described for motor cortex, and I participated in the functional characterization of these L5-TRN synapses *in vitro* (Hádinger et al., 2019).

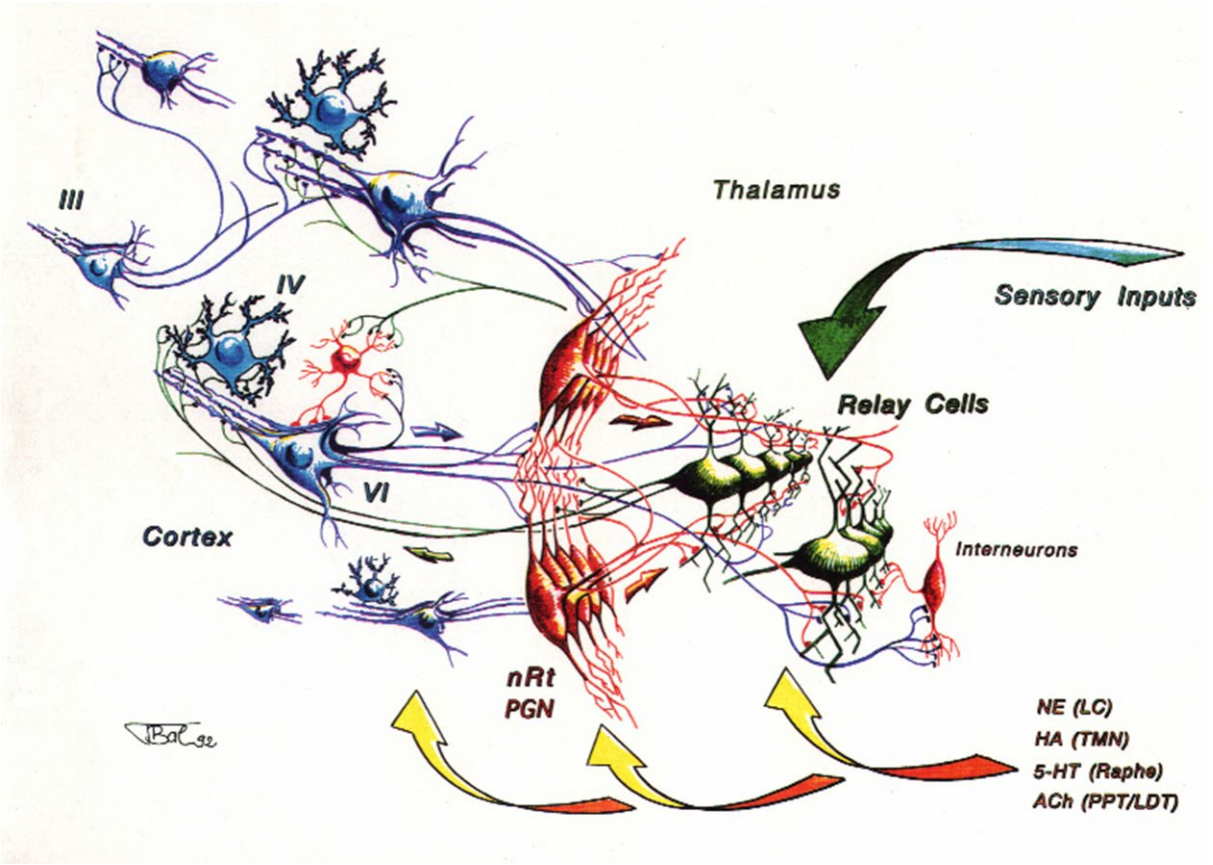


**Figure 2.** Schematic drawing of a thalamocortical network. Thalamic relay cells (green) receive sensory inputs and send projections to the cortical layer 4 and collaterals to the TRN. The cortex (blue) receives thalamic afferents that project to layer 4 neurons and layer 6 neurons project back to the thalamic relay cells and send collaterals to the TRN. TRN neurons (red, nRt) receive afferents from both cortex and thalamus and send inhibitory projections to the thalamus. Neuromodulatory inputs synapse onto the thalamocortical network at all levels, including the TRN. Image by Thierry Bal, 1992.

2) Modulatory afferents

The TRN receives cholinergic, noradrenergic and serotoninergic afferents. So far, the detailed anatomy of their innervation patterns is not known and they seem to reach comparatively large portions of the TRN with similar densities (McCormick, 1992).

Cholinergic afferents. The basal forebrain, pedunculopontine and laterodorsal tegmental nuclei send dense cholinergic projections to the TRN. Cholinergic input indicates that the TRN receives information related to arousal but also to the autonomic nervous system.

Noradrenergic afferents. The TRN is also densely innervated by noradrenergic inputs arising from the locus coeruleus, further showing that arousal-related inputs may dictate TRN activity.

Serotoninergic afferents. A moderate to dense serotoninergic innervation is found throughout the TRN. This innervation is believed to arise from the nucleus raphe pontis and the dorsal raphe nucleus and might be a way that internal states influence TRN activity.

3) Novel, mostly anatomically described afferents

TRN has been shown to receive afferents from the substantia nigra pars reticulata (Paré et al., 1990), the Globus Pallidus (Hazrati and Parent, 1991), the lateral hypothalamus (Herrera et al., 2016) and the basolateral amygdala (Zikopoulos and Barbas, 2012; Clemente-Perez et al., 2017; Aizenberg et al., 2019).

Efferent connections

The TRN projections to the thalamus. The TRN projects to all the anterior, dorsal, intralaminar, posterior and ventral thalamic nuclei, although some differences seem present across species, with the cat TRN not projecting to the anterior thalamic nuclei (Paré et al., 1987). The majority of TRN neurons send their axons in parallel, following a topography with nearest-neighbor relationships that reflect their function as a major and systematic inhibitory regulator of the thalamus. TRN neurons with overlapping dendritic trees have overlapping axonal arbors whereas neighboring TRN neurons with non-overlapping dendritic trees project to adjacent areas (Pinault, 2004). Some TRN neurons can show axon collaterals projecting to a second related thalamic nucleus or a divergent axonal projection to intralaminar and midline nuclei. This indicates that the TRN might be able to combine more than one functional modality and allow the TRN to synchronize several thalamic regions during global brain operation or to favor some thalamic nucleus over the other during attentional processing. TRN projections to the thalamus form feedback inhibitory circuits with the thalamus (TC→TRN→TC) and feedforward inhibitory circuits with both cortex and thalamus (L6 CT→TRN→TC). The feedback inhibitory circuits are mainly forming open loops that result in lateral inhibition to thalamic projecting neurons (Fig. 3). It is generally assumed that the TRN projects only to the ipsilateral thalamic nuclei. However, there are anatomical reports of contralateral projections to thalamic nuclei across species (Paré and Steriade, 1993; Raos and Bentivoglio, 1993) and to the contralateral TRN in rat (Battaglia et al., 1994).

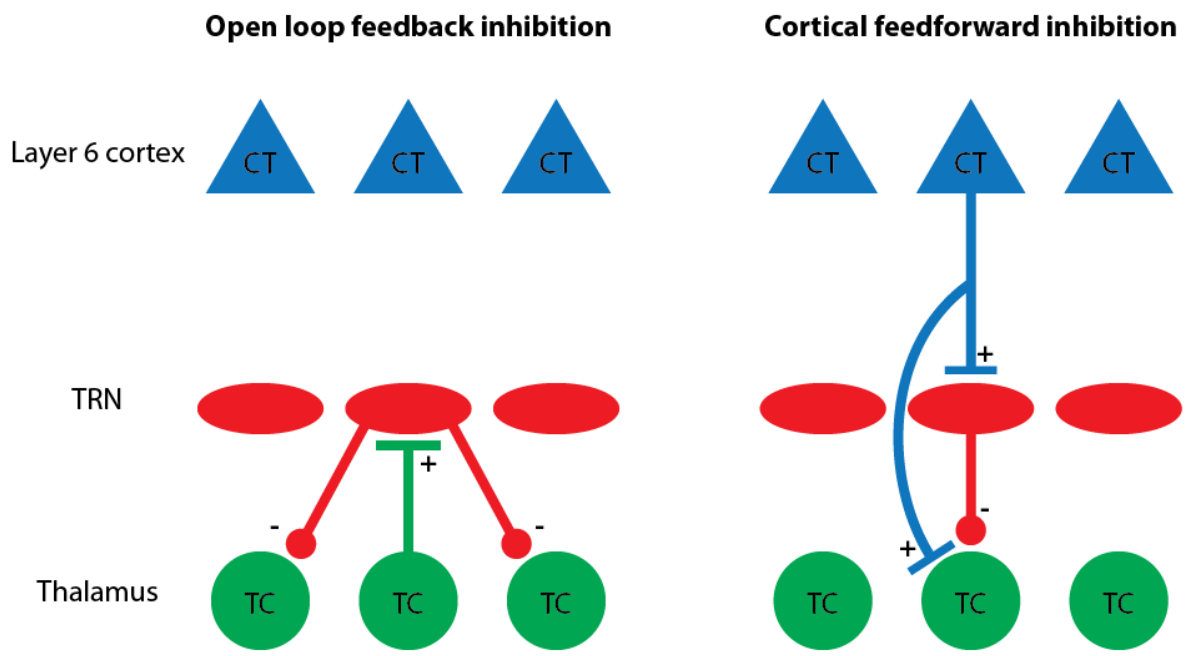


**Figure 3.** Illustration of the feedback (left) and feedforward (right) inhibitory circuits in the thalamocortical network.

Intra TRN connections. The TRN neurons form cell clusters via gap-junctions. This electrical coupling of TRN neurons is present in both rat and mouse and plays an important role in the regulation of firing patterns within the TRN (Landisman et al., 2002). This connection through gap junctions presents a heterogeneous organization as it is mostly found along the dorsoventral axis of the TRN (Deleuze and Huguenard, 2006). The presence of intra-TRN GABAergic synapses has been reported in several studies in mice (Deleuze and Huguenard, 2006; Hou et al., 2016; Makinson et al., 2017), ferrets (Sanchez-Vives et al., 1997; Shu and McCormick, 2002) and rats (de Biasi et al., 1986; Csillik et al., 2005a). These intra TRN connections are critical to control oscillatory activities generated in the thalamoreticular network during normal sleep and they may be relevant for activity-dependent plasticity within TRN (Coulon and Landisman, 2017).

**Dual mode of discharge of TRN neurons**

The TRN neurons have two modes of action potential discharge, the tonic and burst firing modes. The tonic discharge consists in repetitive action potential firing whereas the burst discharge consists in packets of action potentials followed by a period of quiescence. The bursting capacity of TRN neurons is linked to their expression of T-type low-threshold calcium channels, and to their intrinsic cellular properties such as resting membrane potential and membrane resistance (Mulle et al., 1986; Avanzini et al., 1989; Huguenard and McCormick, 2007). At depolarized state, the TRN neurons fire in tonic mode whereas they are generating burst discharge firing from hyperpolarized states. The TRN burst discharges are extremely efficient in generating postsynaptic inhibition and rebound bursting of TC cells (Rovó et al., 2014) and are

hence critical for the generation and maintenance of thalamocortical oscillations. A difference in burst discharge propensity of TRN neurons across sectors or cellular identity would have a huge impact on the thalamocortical activity. Identifying such a cellular heterogeneity is thus critical for the understanding of the TRN functions.

**Major functions**

The strategic position of the TRN between the thalamus and the cortex, its strong inhibitory control over thalamic activity and its rhythmic burst firing capability are features that in combination provide powerful ways to modulate the flow of information through the thalamus and generating changes in thalamic activity during transitions between wakefulness and sleep. This is supported by observations showing a great variety of action potential discharge patterns in relation to different behaviors, such as sleep-wake (Steriade et al., 1986; Gardner et al., 2013), activation by sensory stimuli in a receptive-field like organization (Soto-Sanchez et al., 2017), activation by expected or unexpected stimuli (Yu et al., 2009) and attention-related mechanisms (Halassa et al., 2014). More recent studies have further increased the scope of TRN's function by revealing its role in cognition, emotion (Zikopoulos and Barbas, 2012; Halassa et al., 2014), sensory induced escape (Dong et al., 2019) and pain regulation (Olivéras and Montagne-Clavel, 1994; Liu et al., 2017). Altogether, these functions reveal that the TRN acts both on a global scale (e.g. switch in vigilance state) and on very specific elements of sensory processing (e.g. receptive field sharpening). How does the heterogeneity across the TRN reconcile these two needs for global and local functions? I will further develop this question in the chapters 3 and 4 that are dedicated to the sensory and the limbic TRN functions respectively and discuss how the TRN heterogeneity between sensory and limbic TRN may underlie their different functions in the final section of the thesis.

**Dysfunctions**

Dysfunctions of the TRN have been linked to several mental diseases due to the TRN's functions in attentional modulation, sensory gating and sleep rhythm generation. TRN dysfunction has been strongly associated with absence epilepsy (Huguenard and McCormick, 2007; Makinson et al., 2017). There is also evidence for a TRN involvement in schizophrenia (Steullet et al., 2017; Thankachan et al., 2019) and bipolar disorder (Steullet et al., 2017). The TRN also expresses abundantly some disease-linked genes such as *PTCHD1*, the neurodevelopmental disorder/autism spectrum disorder gene, *Cacna1i* and *Grm3* that are linked to schizophrenia and *CHD2*, a risk gene for autism spectrum disorder (Krol et al., 2018). TRN dysfunctions have also been shown in a mouse model of traumatic brain injury where a delayed TRN astrocytosis was preceding disruption of sleep-wake pattern (Hazra et al., 2014).

## Chapter 2. Heterogeneity of the TRN

The TRN has been viewed as a global inhibitor of the thalamus. However, the TRN is far from being a homogeneous structure. Accumulating evidence shows a rich diversity of neuronal markers, various cell morphologies, relatively precise and focused anatomical organization of TRN sectors and different cellular properties of TRN neurons. These heterogeneities are likely essential in the seemingly diverse functions of TRN, yet still little is known about which ones are relevant and how they link to these functions. In this chapter, I will summarize evidence of the TRN heterogeneity that have been observed in the last decades and that may underlie TRN subnetwork specificities relevant for local sleep regulation that we demonstrated in our recent paper (Study 2: (Fernandez et al., 2018)).

**Sectorial organization: one modality, one sector?**

The TRN can be divided into sectors based on its cortical and subcortical afferents or on its target in the thalamus.

The posterior TRN is heavily connected to thalamic and cortical regions involved in sensory perception and integration. There are clear sectors dedicated to specific sensory modalities. These sectors are so far defined by their synaptic inputs, whereas it is currently unclear how they relate to differences in the cellular properties and whether connectivities between or within the sectors vary. The visual TRN is located in the posterodorsal sector (Crabtree and Killackey, 1989), the somatosensory TRN extends from the intermediate to the posterior sector (Crabtree, 1996) and the auditory TRN is in the posterior sector (Shosaku and Sumitomo, 1983; Crabtree, 1998), all three of them in close proximity to their respective thalamic targets. A gustatory TRN and a visceral TRN were described for the ventroposterior TRN sector (Hayama et al., 1994; Stehberg et al., 2001) (Fig. 4). As previously mentioned, the classical vision of the sensory TRN sectorial organization is that TRN neurons project to the thalamus as a stream of parallel, topographically organized axonal projections (Pinault, 2004). This is particularly the case for visual and somatosensory TRN that show retinotopic (Montero et al., 1977) and somatotopic (Pollin and Rokyta, 1982; Shosaku et al., 1984) organization.

Some TRN neurons in rat and cat sensory sectors show divergent axonal projections (Crabtree, 1996; Pinault and Deschênes, 1998). Only a minority of TRN neurons have bifurcating axons that target a first-order and a related higher-order thalamic nucleus. However, more recent studies shows that the TRN organization goes beyond these parallel sectors dedicated to single modalities. Kimura et al. recorded TRN neurons responding to both visual and auditory stimuli (Kimura, 2014). TRN cells did not produce spikes in response to the alternate modality but only subthreshold responses. However, combination of both stimulations altered TRN response (often reduce TRN output compare to the response to the preferred stimulus). This suggests that the TRN can mediate interactions between sensory stimuli.

A motor TRN, defined by its connection to ventrolateral, ventromedial thalamus and motor cortex, is located in the anterior TRN region in rat (Cicirata et al., 1990). A topographic representation is present in the motor cortex, the thalamus and the motor TRN.

The anterior sector of the TRN is linked to non-sensory/limbic structures. Retrograde tracer studies in rat and monkey show that the anterior TRN receives afferents from limbic cortical regions (cingulate, orbital, infralimbic, RSC, frontal cortex), thalamus (reuniens, paraventricular, anteromedial, anteroventral, anterodorsal, centromedial, mediodorsal), brainstem (substantia nigra pars reticularis, ventral tegmental area, periaqueductal grey, superior vestibular and pontine reticular nuclei) and hippocampal formation (subiculum) (Cornwall et al., 1990; Shibata, 1992; Lozsádi, 1994; Kultas-Ilinsky et al., 1995; Zikopoulos and Barbas, 2007; Çavdar et al., 2008). The cortical projections show a clear topographical organization within rat TRN, with cingulate, orbital and infralimbic cortices projecting to lateral, central and medial sectors of the anterior TRN, respectively. Anterior TRN projections to the mediodorsal thalamus (organized in discontinuous patches or strips, from lateral to medial, (Cornwall and Phillipson, 1988)) and to the anterior thalamic nuclei (ATN) (dorso-ventral axis, (Gonzalo-Ruiz and Lieberman, 1995b, a; Lozsádi, 1995)) also show some degree of topographical organization, but not to the paraventricular thalamus (Cornwall and Phillipson, 1988). It is worth mentioning that species specificities exist as extensive studies in cat anterior TRN failed to show any projections to the ATN (Steriade et al., 1984; Paré et al., 1987; Paré et al., 1991).

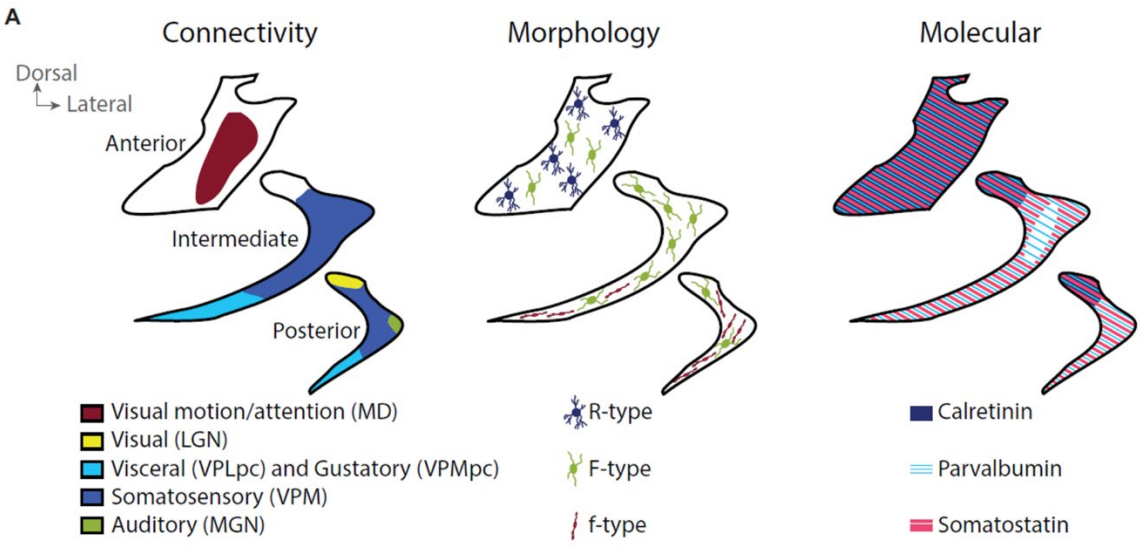


**Figure 4.** Scheme of coronal section through the anterior, intermediate and posterior TRN showing the heterogeneity of the connectivity (left), the neuronal morphology (middle) and the expression pattern of some major molecular markers (right). Adapted from (Vantomme et al., 2019)

## Neurochemical diversity of TRN neurons

The TRN neurons express a variety of neurochemical markers that are not necessarily homogeneously expressed throughout the nucleus and that may also not be conserved across species. Consistent with its inhibitory nature, all TRN neurons described so far are GABAergic. They stain homogeneously and across species for the neurotransmitter γ aminobutyric acid (GABA), for glutamic acid decarboxylase (GAD67) and for vesicular transporter of GABA, such as VGAT2 (see Table 1 for detailed reference). Aside from this seemingly uniform expression of GABA-synthetizing enzymes, there is ample evidence for heterogeneity at the level of a) additional possible neurotransmitter functions, notably neuropeptides and b) cellular expression of calcium-binding proteins, which reflect type and efficiency of the handling of intracellular free calcium levels.

TRN neurons express many neuropeptides that are known for their role in hormonal secretion and metabolism regulation. The expression of these neuropeptides or their related genes were mostly studied in rodents. Therefore, whether their expression is preserved across species remains to be determined. Somatostatin (Sst)-expressing neurons were found in the mouse TRN throughout the nucleus, with the exception of the middle tier of the intermediate portion of the TRN. The Sst affects neurotransmission and cell proliferation. It is also known as the growth hormone-inhibiting hormone. The thyrotropin-releasing hormone (TRH) mRNA and peptide were found in TRN neurons across all sectors in rat. TRH is known for its function in metabolism regulation. The vasoactive intestinal polypeptide (VIP) mRNA and peptide were present throughout the TRN of the rat except in the anterior sector. VIP is known to play a role in the synchronization and modulation of oscillation within the suprachiasmatic nucleus that is involved in circadian rhythm. The prolactin-releasing peptide (PRP) mRNA was found only in the ventro-lateral TRN and was studied for its role in the release of prolactin. The neuropeptide Y (NPY) mRNA was described in the rat TRN without precise intranuclear localization. NPY function has been linked to cell neurogenesis and regulation of the release of hypothalamic hormones. Such a heterogeneity in the distribution of the neuropeptides throughout the TRN may underlie the function of specific subnetworks, however, very little is known about the role of these peptides in thalamocortical activity. For example, the expression of VIP, which seems relevant for synchronization of neuronal activity, is restricted to posterior TRN sectors involved in sensory functions. The heterogeneity of VIP expression could thus underlie the differences in oscillatory pattern between anterior and posterior TRN sectors (Fig. 4).

The calcium-binding protein parvalbumin (PV) is also largely expressed throughout the TRN and across species whereas some others, such as the Calretinin or the Calbindin showed variable expression. The Calretinin is expressed only in the anterodorsal portion of the TRN of the rat. Calbindin-expressing neurons are, however, present in the posterior sector of the rabbit and cat TRN. This heterogeneity of expression of calcium buffer molecules might influence the function of TRN subnetworks (Fig. 4).

| Species / Markers | Mouse | Rat | Rabbit | Ferret | Cat | Non-human primate | Reference |
|---|---|---|---|---|---|---|---|
| GABA | X | X | X | X | X | X | (Ottersen and Storm-Mathisen, 1984) (Houser et al., 1980) (Spreafico et al., 1991) (de Biasi et al., 1986) (Penny et al., 1984) (Clemence and Mitrofanis, 1992) (Hunt et al., 1991) |
| GAD67 | NA | X | X | NA | X | X | (Houser et al., 1980) (Spreafico et al., 1991) (Penny et al., 1984) (Oertel et al., 1983) (Hendrickson et al., 1983) |
| VGAT | X | NA | NA | NA | NA | NA | (Halassa et al., 2011) |
| Parvalbumin | X | X | NA | X | X | X | (Clemente-Perez et al., 2017) (Albéri et al., 2013) (Mitrofanis, 1992b) (Clemence and Mitrofanis, 1992) Jones EG 1989 (Csillik et al., 2005b) |
| Calretinin | NA | X | NA | NA | NA | NA | (Lizier et al., 1997) |
| Calbindin | NA | NA | X | NA | X | NA | (Contreras-Rodriguez et al., 2003) (Mitrofanis, 1992a) |
| Somatostatin | X | NA | NA | NA | X | X | (Clemente-Perez et al., 2017) (Bendotti et al., 1990) (Graybiel and Elde, 1983) (Oertel et al., 1983) (Molinari et al., 1987) (Ahrens et al., 2015) (Wells et al., 2016) |
| TRH | NA | X | NA | NA | NA | NA | (Segerson et al., 1987) (Burgunder et al., 1999) (Mitrofanis, 1992b) (Lechan et al., 1987) |

| | | | | | | | |
|---|---|---|---|---|---|---|---|
| VIP | NA | X | NA | NA | NA | NA | (Burgunder et al., 1999) (Kaneko et al., 1985) |
| PRP | NA | X | NA | NA | NA | NA | (Roland et al., 1999) |
| NPY | NA | X | NA | NA | NA | 0 | (Morris, 1989) |

**Table 1.** Recapitulation of the expression of neuronal markers in TRN neurons across species. X: peptide or mRNA expressed in TRN neurons, 0: absence of peptide and mRNA in TRN neurons, NA: no data available.

**Cell morphology**

Many studies have classified TRN neurons based on the morphology of their somas, dendritic arbors and axons across several species. These aspects are relevant for heterogeneity because they affect the passive properties of neurons and in turn cellular excitability and integrative properties. A small axonal arbor has a greater chance to contact single to few postsynaptic targets and rather participates in closed circuit than a large axonal arbor that can contact multiple postsynaptic targets and may rather serve a synchronization purpose. A large dendritic arbor that spans radially is capable of integrating and sampling a synaptic input from a larger, possibly more diverse set of sources than a small one oriented in space. A small soma size is usually correlating with high membrane resistance and thus possibility high excitability because smaller currents will be required to bring this soma to threshold for action potential generation. Studies of the morphology of TRN neurons found a heterogeneity in their axonal arborization, soma size and orientation of their dendritic trees. I will summarize these findings and illustrate some of the functional impact these morphological differences can have.

Axonal arbors

TRN neurons show variable axonal arborization patterns that were particularly well-described for the sensory sectors of the thalamus (Pinault, 2004). The best described case are rodents, where TRN neurons have compact axon terminals into the first-order somatosensory thalamus and more diffuse axon terminals into the higher-order somatosensory thalamus. In contrast, projections to both first- and higher-order visual thalamus have compact axon terminals (Pinault et al., 1995b, a). These morphological differences of TRN axonal projections correlates with distinct inhibitory responses of thalamic neurons. TRN neurons with diffuse axonal projections have weaker unitary inhibitory currents compared to the ones with more compact axonal arbors (Cox et al., 1997). This suggests that a heterogeneity of the inhibitory control of the thalamic nuclei by the TRN may underlie different functions.

Cell morphology and dendritic arborization

Already in 1966, Scheibel and Scheibel described strong variation in the size of neurons in the different sectors of the TRN. The dendritic arbors are parallel to the border of the TRN, in particular in the thinner sensory sector, whereas the dendrites in the anterior sector seems to leave their soma at all angles (Scheibel and Scheibel,

1966). Similarly, Spreafico described three types of neurons in the TRN. R-type have a round soma and a multipolar dendritic arbor. f-type have a small fusiform soma shape and two main proximal polar dendrites. F-type have a large fusiform soma shape with a flat dendritic domain where the dendrites emerge from the two pole of the soma. R-type neurons were found mostly in the anterior pole of the TRN, whereas f-type were mostly ventral and posterior and F-type where found throughout the TRN (Spreafico et al., 1991). Other studies revealed similar cellular morphological differences across species ((Requena et al., 1991; Clemence and Mitrofanis, 1992; Lübke, 1993) but see (Ohara and Lieberman, 1985; Ohara and Havton, 1996)). This heterogeneity of dendritic arbors orientation is of interest as it can have functional consequences. For example, afferents to the posterior sensory TRN are known to be arranged in slabs (Crabtree and Killackey, 1989). One barrel in the primary somatosensory cortex in rodent is connected to a single barreloids in the thalamus and forms one slab in the TRN. TRN neurons with a flatten dendritic arbor parallel to the main axis of the TRN would be contacted only by a single slab, whereas TRN neurons with multipolar dendrites would reach several slabs and serve as integrators (Fig. 4).

**Functional cellular properties**

The capacity of TRN neurons to switch between tonic and burst firing is essential for many TRN functions such as sleep rhythm generation. There is accumulating evidence that not all TRN neurons have the same propensity for repetitive burst discharge. Differences in burst discharge propensity might underlie distinct sensory processing and attention gating functions in TRN subnetworks. Indeed, tonic firing of TRN neurons recruit mostly synaptic receptors whereas burst firing is capable of recruiting also extrasynaptic receptors and generating major thalamocortical oscillations (Herd et al., 2014; Rovó et al., 2014).

In 1992, Contreras found two functional types of TRN neuron in the anesthetized cat. The type 1 was able to discharge burst of action potential from hyperpolarized state whereas the type 2 did not (Contreras et al., 1992). Similarly, TRN neurons in rat also showed distinct propensity for burst discharge (Brunton and Charpak, 1997). Lee et al. further demonstrated that the proportion of bursting neurons in the dorsal TRN of rat was much lower than in the ventral TRN, suggesting a dorsoventral heterogeneity in burst capacity. Lee et al. defined three functional categories of TRN neurons: non-burst, atypical burst and typical burst TRN neurons (Lee et al., 2007). These functional differences were, however, not linked to different morphological subtypes as previously described (Spreafico et al., 1991) and it was not known at the time whether this variable bursting propensity correlated with the expression of neuronal markers.

Beyond this functional heterogeneity across the dorsoventral axis, Kimura et al. also showed that visual TRN neurons projecting to the dorsolateral geniculate had a higher burst propensity, increased spike per burst with shorter interspike interval than those projecting to the lateroposterior thalamus (Kimura et al., 2012). This suggested a differential inhibitory control over first and higher order thalamic nucleus within the same modality and further increased the complexity of the TRN heterogeneity.

Clemente-Perez et al. compared the bursting capability of TRN neurons based on their expression of PV or Sst. They showed that PV-expressing TRN neurons showed strong repetitive burst discharge whereas the Sst neurons had single to no burst discharge. Activation of PV but not Sst neurons *in vitro* generated oscillations in the TRN-thalamus circuit (Clemente-Perez et al., 2017). This heterogeneity of neuronal markers and burst capacity was further embedded into distinct circuits. The PV+ neurons of the TRN were mainly connected to thalamic principal nuclei whereas Sst+ neurons were connected mostly to intralaminar, parafascicular and anterior thalamic nuclei. Altogether, this suggests a complex organization of TRN subnetworks, which combines neuronal markers, cellular activity and distinct innervation patterns, to support global and local functions of the TRN.

In study 2, we further investigated the impact of the TRN heterogeneity in cellular burst discharge on cortical activity. We showed that the repetitive bursting of TRN neurons is higher in somatosensory TRN and auditory TRN compared to mediodorsal thalamus-connected limbic TRN in mice. This variability in TRN repetitive bursting was correlated with the proportion of cortical sleep spindles and manipulation of TRN bursting capacity affected the cortical oscillation content.

Altogether, these studies show that the view of the TRN as a monolithic structure needs to be abandoned. It is only through dissecting the heterogeneity of the TRN at cellular, functional and anatomical level that we will reveal the mechanisms of action and the local functions of the TRN.

## Chapter 3. What is the sensory TRN and its function?

The sensory TRN is connected to the sensory thalamic nuclei and has been implicated in the control of the flow of sensory information between the thalamus and the cortex for decades. The mechanisms by which the TRN modulates the thalamocortical activity are numerous and often act in concert. This control of the flow of sensory information has two major functions: the gain control and attentional selection of sensory information and the reduction of sensory stimulation during sleep. In this chapter, I will briefly describe some of the mechanisms of sensory processing involving the TRN and focus on the selective sensory attention and the sleep rhythm generation.

### Sensory processing

The sensory processing by the TRN has been linked to the sharpening of thalamic receptive field, sensory gating, sensory gain control and suppression of responses.

The receptive field of a sensory neuron is the portion of the "sensory space" that can elicit neuronal activity once stimulated. For example, the "sensory space" for a somatosensory neuron is the surface of the skin that will trigger the neuronal activity of this neuron. The same applies for the visual field and the sound frequency field. Thalamic neurons in the lateral geniculate nucleus (vision), the medial geniculate nucleus (audition) and the ventrobasal nucleus (somatosensation) have in general a receptive field with a discrete region in the sensory space and a larger suppressive surrounding (Alitto and Usrey, 2003). The properties of the receptive field of sensory thalamic neurons is established by their sensory afferents (Sherman and Guillery, 1998). However, the cortical feedback sharpens the tuning of these sensory thalamic neurons by acting on both the activation of the receptive field and the suppressive surroundings (Alitto and Usrey, 2003). Several studies have demonstrated that lesion (Lee et al., 1994) and pharmacological inhibition (Ergenzinger et al., 1998; Cotillon-Williams et al., 2008) of the different sectors of the sensory TRN mediate enlargement of the connected thalamic neuron receptive field. This enlargement of the thalamic receptive field most probably result from the loss of lateral inhibition by the TRN. TRN neurons also display topographically organized and relatively sharp receptive field to sensory inputs (Shosaku, 1985; Soto-Sanchez et al., 2017). The feedback inhibitory control of the TRN over the thalamus seems to act via lateral inhibition of the thalamic receptive field properties, at least in the visual system (Osaki et al., 2018).

The sensory gain control and sensory suppression is the manipulation of the signal-to-noise ratio for a particular stimulus, particularly important in selective sensory attention. The majority of TRN neurons form open-loop connections with the thalamic neurons (Pinault, 2004), providing the anatomical basis for lateral inhibition. This sensory TRN lateral inhibition of TC cells inhibits the passage of distracting sensory inputs to the cortex while favoring the attended relevant stimuli (Ahrens et al., 2015).

The sensory gating is the process of filtering out repetitive stimuli in the brain. Classically, the auditory gating has been tested by presenting two similar clicks given at short time interval while recording the brain responses. In control subject, the

amplitude of the response to the second stimulus is reduced. Patient suffering from schizophrenia have an impaired auditory gating evident by the lack of reduction of the amplitude of the evoked response to the second stimulus. Sensory gating occurs at many different levels in the brain including thalamus. Krause et al showed the first evidence of auditory gating in the TRN. The TRN responded to the condition stimulus with bursts of action potentials whereas the number of spikes was greatly reduced for the test stimulus. Administration of D-amphetamine into the TRN disrupted the auditory gating (Krause et al., 2003; Yu et al., 2009).

**Selective sensory attention**

The selective attention is the capacity of the brain to select appropriate sensory inputs and to suppress distractors. Among all sensory information perceived, stimuli conveying danger or opportunities must have the priority. These sensory inputs have to be filtered according to behaviorally relevant information to capture limited attentional resources (McAlonan and Brown, 2002).

The TRN strategic position and strong inhibitory control other the thalamus make it a good candidate for selective attention. Indeed, Crick suggested that the TRN might be a key structure that directs internal spotlight of attention to the relevant active thalamocortical circuit, proposing the TRN searchlight hypothesis (Crick, 1984).

Sherman and Guillery described that any brain region that would be dedicated to selective attention has to be topographically organized. Indeed, neurons have to be orderly arranged to allow spatially accurate maps of the environment. This organization in maps allows specific points in the system to be enhanced relative to the others (Sherman and Guillery, 1996). The TRN as well as the thalamocortical and corticothalamic circuits are topographically organized along sensory modalities as I previously described.

To test the implication of TRN in attention, Weese used a covert attention task. Rats were exposed to visual stimulations that indicated the position of a reward. Prior to these visual stimulations, an other visual cue was presented. This cue was either directing the attention to the target or misdirect the attention towards the non-baited area. Valid cues slightly increased the performance of the rats in getting the reward compared to invalid cues. This phenomenon is called the priming effect. Unilateral lesion of the TRN did not impair visual detection nor the ability to perform the task but abolished the priming effect on the contralateral region, suggesting a role of the TRN in monomodal sensory attention (Weese et al., 1999).

In a series of studies, Montero observed the neuronal activation of TRN neurons of rat during exploration of a complex environment (Montero, 1997, 1999, 2000). The rat attended to either visual or somatosensory cues during the exploration. The TRN sector related to the attended stimulus showed neuronal activation (visible as an increase in c-fos staining) whereas TRN sector related to the non-attended stimulus did not express c-fos despite strong labeling in connected thalamus and cortex. This strongly suggest a role of attentional gating of the TRN instead of sensory relay.

McAlonan used the phenomenon of blocking in classical conditioning to test whether the activation of TRN neurons would vary between attended and non-attended stimuli (McAlonan et al., 2000). They showed that c-fos staining was more intense in the TRN sector related to the attended stimulus compare to the non-attended one.

With the development of optogenetic tools, more recent studies are testing the role of the TRN in selective attention. For example, Wimmer et al (Wimmer et al., 2015) manipulated the corticothalamic circuit involving the prefrontal cortex, the visual sector of the TRN and the lateral geniculate nucleus during a cross-modal divided-attention task in mice. The performance of mice to choose correctly between conflicting auditory and visual stimulus was modulated by the activity of the visual TRN. In spontaneously behaving mice, the visual TRN reduced its firing rate when the mouse attended the visual inputs. On the contrary, the visual TRN increased its firing when the mouse attended the auditory inputs, thus inhibiting the “distractor” input. Optogenetically provoked increases of visual TRN firing rate reduced the performance of mice when they had to attend the visual inputs, suggesting a reduction of the visual thalamic gain. Decreasing visual TRN activity diminished the performance when auditory inputs had to be attended to, suggesting an impairment of “distractor removal” (Wimmer et al., 2015). Perturbation of the prefrontal cortex during the anticipation period (prior to the delivering of the cue) also reduced attentional modulation of visual TRN neurons and the performance of mice in this discrimination task. This would suggest a direct input from the prefrontal cortex to the visual TRN. However, direct projection from prefrontal cortex to the visual TRN are scarce (Crabtree, 2018) and recent work suggests that attentional selection is mediated via basal ganglia (Halassa and Kastner, 2017).

An other evidence of the role of the TRN in attention comes from a mouse model for attention deficit and hyperactivity disorder (ADHD). Wells et al revealed that the *PTCHD1* gene is exclusively expressed in the TRN in mice. *PTCHD1* is a gene mutated in some psychiatric disorders in which attention deficits, hyperactivity and sleep abnormalities are frequent co-morbidities. KO mice for *PTCHD1* showed ADHD-like behavior such as attention deficit and the phenotype could be rescued by pharmacological intervention onto the TRN biophysical dysfunction (Wells et al., 2016).

Over the last 20 years, behavioral testing of attention in rodents were combined with lesions of the TRN, measurement of TRN neuronal activity through c-fos staining and unit recording, optogenetic manipulation of TRN activity and genetic manipulation. Altogether, these studies brought a lot of evidence for the importance of the TRN in selective attention, yet the mechanism through which the TRN acts remain elusive.

Guillery et al suggested that the TRN is likely crucial for corticoreticular control of relay cells through promoting a switch from tonic to burst firing, which may change according to changes of the attentional focus across and within cortical areas (Guillery et al., 1998). Classically, burst firing in thalamic relay cells is visible during quiescent state, sleep and anesthesia. Tonic firing in thalamic relay cells is present during alert behavior (Steriade and Llinas, 1988). However, burst responses in visual relays cells have been seen in alert animals, in particular at the beginning of the visual stimulation. This

phenomenon might be a way to increase the intensity of the signal send to the cortex for a novel visual information that might be of importance (Guido and Weyand, 1995; Sherman, 1996; Ramcharan et al., 2000). Similarly, burst firing in somatosensory thalamic nucleus in awake rabbits was shown to be a powerful way to transfer sensory information to the cortex (Swadlow and Gusev, 2001). This burst firing in thalamic relay cells during alert behavior probably depends on TRN inhibition to deinactivate low-threshold t-type calcium channel in the thalamus and allow burst firing.

To summarize, there is ample anatomical, functional and behavioral evidence of the role of the TRN in selective sensory attention. The TRN can act across modalities and within modalities to favor the relevant sensory input and suppress distractors. The heterogeneity of TRN innervation of thalamic nuclei may create subnetworks of TRN neurons dedicated to the removal of distractors and others to increase the gain of the relevant stimulus. The heterogeneity in burst capacity may also influence the mechanism of selective attention, as TRN-burst-dependent burst discharge in thalamic neurons seems to be a powerful way to transfer novel relevant information to the cortex.

**Sleep rhythm generation and arousal**

TRN's activity changes dramatically between sleep and wake periods, adopting burst firing during sleep and tonic action potential activity during wakefulness.

The strong interconnectivity between the thalamus and the cortex allows the thalamus to participate in the generation and modulation of the cortical oscillations detected by electroencephalogram (Fogerson and Huguenard, 2016). The predominant view is that thalamus, by virtue of its interconnectivity with TRN, generates two major types of synchronized network activity that appear predominantly during sleep: delta and spindle. The TC neurons are spontaneously capable of firing bursts of action potential at 1 to 4 Hz during sleep, which is within the frequency range of the EEG delta waves. The synchronous discharge of thalamocortical neurons at this frequency range may underlie the appearance of delta waves in cortex (McCormick and Pape, 1990; Soltesz et al., 1991; Nuñez et al., 1992). The spindle rhythm is generated by the reciprocal connectivity between the thalamus and the TRN and allows the thalamus to generate 10 to 15 Hz oscillations. These sleep spindles are indeed generated in the thalamic networks, as evident by the presence of spontaneous oscillations at the spindle frequencies in thalamic network disconnected from the cortex (Steriade et al., 1993; Huguenard and McCormick, 2007). The TRN is considered as the "sleep spindle pacemaker" (Steriade, 2006). The inhibition generated by the bursting TRN neurons onto the thalamocortical cells is powerful and often coincide with the onset of sleep spindles. The bursting of the TRN is phase-locked to the spindle cycles, intensifies as the spindle evolves (Steriade et al., 1986; Buzsáki, 1991; Gardner et al., 2013) and TRN lesions induce an abolishment of spindles (Fuentealba and Steriade, 2005). A further evidence of the critical role of the TRN in generating sleep spindles comes from one of our recent paper (Study 2: (Fernandez et al., 2018)). We demonstrated that differences in spindle content between cortical areas were tightly linked to differences

in TRN neuron burst discharge across the TRN sectors connected to these cortical areas.

The molecular basis of TRN burst discharge relies on the low-threshold t-type calcium channel ($Ca_V3.3$) (Perez-Reyes, 2003) and the calcium-dependent potassium channel (SK2). Briefly, once a TRN cell has a hyperpolarized membrane potential, typically during sleep when the adrenergic tone is low, the low-threshold calcium channels are deinactivated. An incoming excitation from the cortex of the thalamus becomes then sufficient to activate these low-threshold calcium channels. The entry of calcium generates a depolarizing calcium spike, often carrying action potentials, and activates calcium-dependent potassium channels. These potassium channels induce an after-burst hyperpolarization that, if strong enough, deinactivate the low-threshold calcium channel again, allowing the next cycle of burst to occur (Avanzini et al., 1989; Cueni et al., 2008). The thalamic neurons possess a similar set of low-threshold calcium channels, allowing burst discharge. However, the membrane potential for deinactivation of these calcium channels is more hyperpolarized than in the TRN neurons. Single inhibitory postsynaptic current generated by the TRN in a thalamic neuron may be sufficiently large in amplitude and duration to generate a low-threshold rebound burst in the thalamus (Bal et al., 1995). However, simultaneous discharge of several TRN neurons can activate $GABA_B$ receptor in thalamic neurons. This long lasting $GABA_B$ receptors mediated hyperpolarization facilitate the deinactivation of low-threshold calcium channels and the burst propensity in the thalamus (Sanchez-Vives et al., 1997).

During wakefulness, a set of neurotransmitters such as noradrenalin, serotonin, histamine and glutamate, is released from the brainstem, hypothalamus, basal forebrain and cerebral cortex (McCormick, 1992). These neurotransmitters induce a slow and global depolarization of thalamic and reticular thalamic neurons (Hirsch et al., 1983; Steriade et al., 1986) that results in an abolition of rhythmic rebound burst and the promotion of single-spike firing. This depolarized state of thalamic and reticular neurons thus suppresses the generation of sleep rhythm and promotes sensory-motor processing and cognition that I described before (McCormick and Bal, 1997). Whether the TRN plays an essential role in the arousal systems or whether the TRN is a passive downstream target remains to be determined.

## Chapter 4. What is the limbic TRN and its function?

The limbic TRN sector is located in its anterior portion and is connected to non-sensory thalamic nuclei and cortices, as described in the Chapter 2. Beyond its anatomical connections, very little is known about its function and role in limbic thalamocortical loops. In this chapter, I will focus mostly on the few studies recording or manipulating limbic TRN's neuronal activity and their supportive anatomical evidence.

### Cognition, emotion and memory

Cortical and thalamic limbic structures have been linked to cognition, emotion and memory (Vertes et al., 2015). It is then reasonable to assume that the TRN sectors connected to these structures will assume similar brain functions. However, the morphology of the TRN and in particular the overlap of cortical and thalamic afferents in the anterior sector make it complicated to record and manipulate neuronal activity of the limbic TRN.

By combining implantation of electrodes with 16 independently adjustable microdrives and retrograde opto-tagging of TRN neurons projecting to either anterior thalamic complex or visual thalamus, Halassa et al successfully recorded and manipulated activity of both limbic and sensory TRN neurons of mice (Halassa et al., 2014). Recording of TRN in freely behaving conditions revealed two distinct population of neurons that had opposite modulation by sleep and active waking. Limbic TRN neurons had little activity during sleep and quiescent states, thus disinhibiting limbic thalamus, probably enhancing offline limbic processing such as hippocampal reactivation. The neuronal activity of limbic TRN was increased during waking. However, optogenetic activation and inhibition of these neurons did not show any impact on visual-detection task performance. On the contrary, sensory TRN neurons displayed a pattern of activity consistent with a reduction of sensory processing during sleep and an increase during wake. More precisely, these sensory TRN neurons showed a strong activity time-locked to the cortical spindles during sleep and reduced their activity during attentional sensory detection task.

Further indications of the role of the limbic TRN in cognition, emotion and memory come from extensive anatomical studies of the TRN in non-human primate. Dorsolateral prefrontal cortex, posterior orbitofrontal cortex, mediodorsal thalamus send strong projections to the limbic sector of the TRN that can extend to motor and sensory sectors (Zikopoulos and Barbas, 2012). The amygdala, a key structure for processing signal with emotional importance, was recently shown to send projections to the TRN. About 70% of amygdalar axons projected to the anterior sectors, overlapping with mediodorsal thalamus and posterior orbitofrontal cortex afferents (Zikopoulos and Barbas, 2012). This anatomical observation suggests that amygdala may act in concert with mediodorsal thalamus and posterior orbitofrontal cortex to favor rapid transfer of emotionally relevant information while blocking distractors. John et al explored this hypothesis using a computational model of the amygdala-TRN pathway (John et al., 2016). Their model also supported the hypothesis that the amygdala-TRN

pathway selects emotion-guided signals before sending them to the cortex for further processing and that the amygdala can act as a relevance detection system for the limbic thalamocortical circuit.

**Sensory induced escape**

Dong et al. expanded the scope of functions of the anterior/limbic TRN by describing a corticothalamic circuit involving the cingulate cortex and the intermediodorsal thalamic nucleus. This circuit controls the flight or freeze behavior in mice. The limbic TRN receives glutamatergic inputs from the cingulate cortex and projects to the intermediodorsal thalamic nucleus. Activation of the limbic TRN induced inhibition of the intermediodorsal thalamic nucleus and increased the flight behavior of mice, whereas inhibition of the limbic TRN increased the freezing behavior. Manipulation of the sensory TRN did not affected the flight or freeze behavior (Dong et al., 2019).

**Pain regulation**

A recent study showed that activation of TRN PV neurons in the anterodorsal sector in mice increased pain sensitivity. This increase in pain sensitivity seems to be mediated by changes in inhibitory control over the anterodorsal and/or the paratenial thalamic nucleus, revealing the neuroanatomical basis of TRN's involvement in pain regulation (Liu et al., 2017). This is further supported by evidence of "pain-like" behavior in rat upon blockade of $GABA_A$ receptor in the TRN (Olivéras and Montagne-Clavel, 1994) and the presence of thalamic firing alteration in resting-state functional magnetic resonance imaging of patient suffering from neuropathic pain (Walton and Llinas, 2010).

Altogether these studies expanded the scope of the TRN beyond sensory processing, arousal and sleep rhythm generation. Due to its strong connections with cortical and thalamic structures involved in emotion, memory and attention, the limbic TRN seems to be important for high cognitive processes. Further studies manipulating limbic TRN neuronal activity in behaving animals will certainly unraveled novel functions of the TRN.

# Chapter 5. The head-direction system

In this chapter I will briefly introduce some of the key concepts of the head-direction system as my main project on the limbic sector of the TRN revealed anatomical and functional connections between the TRN and the navigational system. This chapter presents generalities on the head-direction system that do not appear in the introduction of Study 1 and that are meant to complement it.

### Classes of neurons involved in the navigation system

Orienting oneself in the environment is a fundamental cognitive process that relies on brain-wide neuronal circuits. These circuits are constituted of neurons that have distinct functional properties, each of them dedicated to a specific aspect of spatial processing, such as direction, speed and location. For example, the navigation system includes the hippocampal place cells that fire as a function of the animal's position in the environment (O'Keefe and Dostrovsky, 1971), the entorhinal grid cells that fire in multiple place fields that are arranged hexagonally (Hafting et al., 2005) and the border cells that fire when the animal is close to the border of the environment (Hartley et al., 2000) (Fig. 5). The focus of this chapter will be on the head-direction cells. These cells increase their firing when the animal faces a specific direction in space (Taube, 1995).

### The head-direction neuronal circuit

Head-direction cells are found throughout the brain, mostly in the lateral mammillary nucleus, the anterodorsal thalamus, the dorsal presubiculum, the retrosplenial cortex and the medial entorhinal cortex (Dillingham and Vann, 2019). The head-direction signal is generated at the level of the circuit between the dorsal tegmental nucleus and the lateral mammillary nucleus, which receives its main input from the vestibular system when angular velocity of the head changes. The HD signal is additionally updated by landmark, motor and proprioceptive information (Yoder and Taube, 2014). Indeed, the head-direction signal needs to be stable relative to the environment and is thus influenced by sensory inputs. The head-direction signal in the mammillary nucleus is relayed to the anterodorsal thalamus, the dorsal presubiculum (also called postsubiculum) and retrosplenial cortex. The presubiculum and retrosplenial cortex also receive inputs from the visual cortex and feedback on the anterodorsal thalamus, forming a thalamocortical loop in which the head-direction signal and the visual signal are integrated (Fig. 6).

The retrosplenial cortex is connected to the hippocampal and parahippocampal formation, the limbic thalamus and the parietal cortex. It is constituted by a granular and a dysgranular region. The granular region of the retrosplenial cortex has strong reciprocal connections with the anterodorsal thalamus and the dorsal presubiculum, pointing towards its function in the head-direction system and in internally directed navigation. The dysgranular region of the retrosplenial cortex seems to be more connected to visual areas and thus is supposed to be important for visually guided spatial memory and navigation. The retrosplenial cortex has been consistently shown to play a role in navigation and learning in rodents and studies of patients with unilateral or bilateral lesions of the retrosplenial cortex confirmed impairment of the navigation

system as well as memory loss. It is also hypothesized that the retrosplenial cortex plays a role in the transition between the use of egocentric (self-centered) and allocentric (world-centered) reference frames during navigation (Vann et al., 2009).

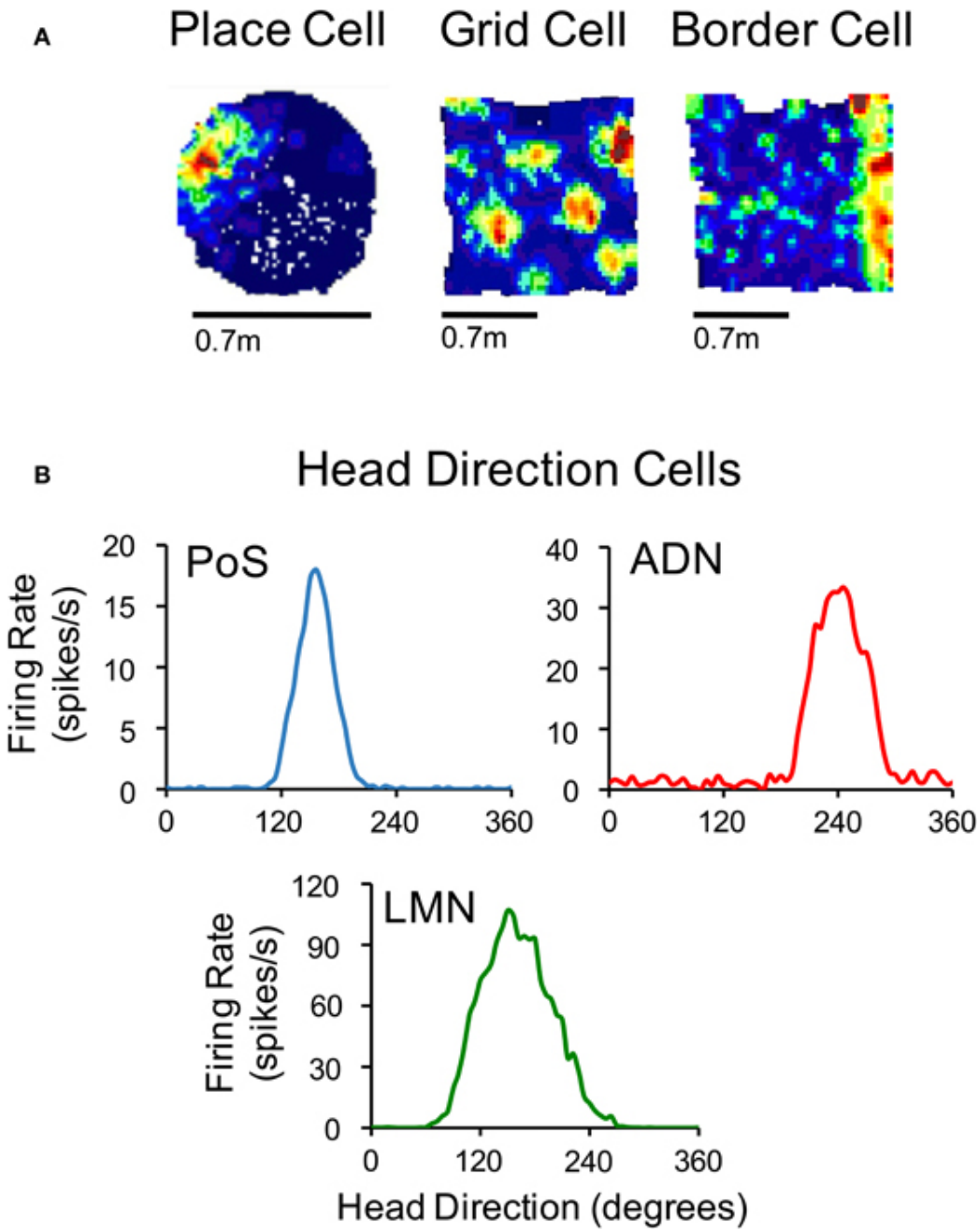


**Figure 5.** Representations of the firing pattern of different classes of neurons involved in the navigation system. (A) Heat maps of the firing rate of a place cell (left), grid cell (middle) and border cell (right). Warmer colors correspond to higher frequency of firing. (B) Plot of the firing rate of head direction units from dorsal presubiculum (PoS, blue), the anterodorsal thalamus (ADN, red) and the lateral mammillary nucleus (LMN, green). Figure from (Clark and Taube, 2012).

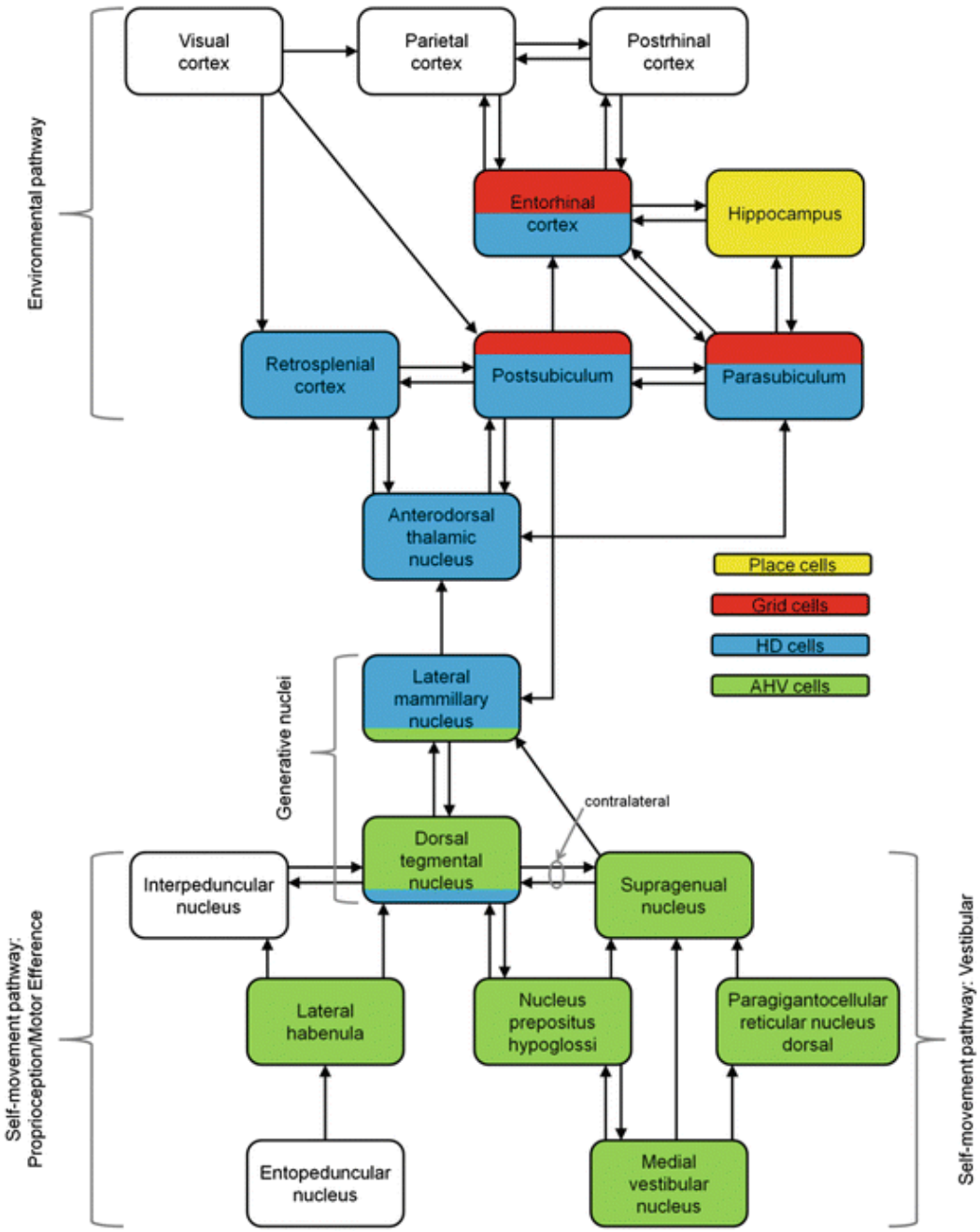


**Figure 6.** Scheme of the overall neuronal circuit for spatial navigation. HD: head-direction. AHV: angular head velocity. Figure from (Winter and Taube, 2014).

The presubiculum is also connected to the hippocampal and parahippocampal formation, the limbic thalamus and entorhinal cortex. The presubiculum is thought to be an entry point for visual information to the head-direction system as well. It receives direct visual inputs from primary and secondary visual cortex and indirect inputs from the retrosplenial cortex. The presubiculum is thus a key relay for the integrated visual/head-direction information to the entorhinal-hippocampal network where grid cells and place cells are located. Lesions of the presubiculum impair spatial learning and memory (Simonnet and Fricker, 2018).

**A role of the limbic TRN in the head-direction system?**

The head-direction signal is processed in the thalamus at least in the anterodorsal nucleus in mice. However, it is not clear what the TRN does to this anterodorsal nucleus in terms of the inhibitory feedback or cortical feedforward inhibition, which I described for classical thalamocortical sensory systems in the chapter 1.

An intriguing observation is that the TRN has never been implicated in these thalamocortical circuits between presubiculum/retrosplenial cortex and the anterodorsal thalamus (Grieves and Jeffery, 2017; Simonnet and Fricker, 2018; Dillingham and Vann, 2019). The anatomical tracing studies described in the chapter 2 suggest that the anterior/limbic portion of the TRN could be connected to thalamic and cortical areas involved in the head-direction signal processing. The hypothesis that the TRN projects to head-direction cells in the thalamus was also very recently proposed by Peyrache et al. (Peyrache et al., 2019) but has never been functionally investigated. Whether the limbic TRN gates the thalamic head-direction signal remains to be explored.

The limbic TRN could be implied in a feedback inhibitory circuit with the anterodorsal thalamus where lateral inhibition would help sharpening the receptive field of thalamic head-direction neurons with an organization similar to the classical sensory thalamoreticular circuit (Osaki et al., 2018). The limbic TRN could also participate in a feedforward inhibitory circuit with the retrosplenial cortex and/or the presubiculum that project back to the anterodorsal thalamus, further sharpening the receptive field of thalamic head-direction cells or anchoring the thalamic head-direction signal to visual landmarks.

My main project (study 1) explored some of these hypotheses through anatomical and functional investigation of the dPreS/RSC projections to the limbic TRN and through recordings of thalamic head-direction neurons with manipulation of the limbic TRN activity.

# F. Results

## Study 1: A thalamic reticular circuit for head direction cell tuning and spatial navigation

Gil Vantomme, Zita Rovó, Romain Cardis, Elidie Béard, Georgia Katsioudi, Angelo Guadagno, Virginie Perrenoud, Laura MJ Fernandez, Anita Lüthi, *in revision Cell Reports*

The ability to detect and localize environmental cues is central for navigation in space. Although cortex is the ultimate site for contextual processing of stimuli and decision making processes, sensory elaboration also takes place at subcortical levels, probably to meet rapid and unexpected behavioral challenges surging on the way. A major site for subcortical gating of sensory stimuli is the TRN thanks to its unique anatomical positioning at the interface between thalamus and cortex. However, the role of the TRN in spatial navigation has never been explored.

The anterodorsal TRN has been shown to project to the anterodorsal thalamic nucleus and to receive afferents from the RSC and the parahippocampal formation across several species (Shibata, 1992; Kultas-Ilinsky et al., 1995; Zikopoulos and Barbas, 2007; Çavdar et al., 2008). These structures are particularly important for the spatial navigation system. Indeed, the head direction signal, generated at the level of the vestibular system, is relayed by the anterodorsal thalamus to the PreS and then to RSC and entorhinal cortices and the hippocampus where place cells and grid cells are generated (Simonnet and Fricker, 2018). The limbic TRN is at the interface between the anterodorsal thalamus that relays the head-direction signal and the parahippocampal formation where the head-direction signal is integrated with multisensory information (Simonnet and Fricker, 2018). Thus the TRN is in a strategic position for regulating the thalamic head-direction firing under the control of the parahippocampal formation. However, a functional connectivity between the limbic TRN and the thalamic nuclei involved in the head-direction/spatial navigation system has never been demonstrated.

In this project, we demonstrated a strong projection from the PreS and RSC to the most anterodorsal sector of the TRN using retrograde and anterograde tracer injections in mice. We further assessed the functional connectivity of these projections using whole-cell patch-clamp recording in acute brain slices in combination with opto and chemogenetic tools. Remarkably, these excitatory projections to the TRN had driver characteristics unlike classical sensory corticoreticular synapses. We further demonstrated both *in vitro* and in freely behaving mice the recruitment of feedforward inhibition by the PreS and RSC cortex to the anterior thalamus via the TRN. Chemogenetic silencing of the anterodorsal TRN reduced the tuning of anterodorsal head-direction neurons and biased the search strategies towards allocentric orientation in the Morris Watermaze. Together these data unraveled a novel function of the TRN in the spatial navigation, expanding our knowledge of the limbic TRN.

This publication represents the core of my work during the doctoral thesis. I designed the *in vivo* and behavioral experiments and carried out most of the experiments and analyses of the anatomical tracing, *in vitro* patch-clamp and *in vivo* single unit recording and Morris Watermaze.

## Study 2: Thalamic reticular control of local sleep in mouse sensory cortex, eLife

Laura MJ Fernandez, Gil Vantomme, Alejandro Osorio-Forero, Romain Cardis, Elidie Béard, Anita Lüthi, eLife 2018;7:e39111, DOI: 10.7554/eLife.39111, 25.12.2018

Sleep is a global vigilance state characterized by a reduction of responsiveness to external stimuli and altered consciousness. However, major electrical sleep rhythms occur at different times in different brain regions. This suggest that on top of a global regulator, some brain structures can generate local oscillatory patterns in the cortex. This local sleep may enable sleep-dependent plasticity in specific neuronal network.

In this paper, we showed that the primary auditory cortex and the primary and secondary somatosensory cortices of mice have larger amplitude and faster sleep spindles than the prefrontal cortex. We investigated whether differences in neuronal activity across TRN sectors may underlie distinct spindle characteristics across the cortex. We demonstrated that TRN neurons in the sensory sector had a strong repetitive bursting capability whereas neurons in the limbic TRN had little to no repetitive burst discharge. This mode of discharge of TRN neurons is dependent on the $Ca_V3.3$ low-threshold T type calcium channel. Blocking TRN repetitive burst discharge via genetic deletion of the $Ca_V3.3$ channels or chemogenetic silencing of TRN neurons induced a switch from spindle to delta enriched sleep and abolished differences in spindle characteristics across the cortex. Altogether, these data identified a novel mechanism underlying local cortical correlates of sleep, showing the critical role of the TRN neuronal activity in shaping the content of cortical oscillations.

In this publication, I carried out and analyzed the results of the anatomical tracing and *in vitro* whole-cell patch clamp recording of TRN neurons.

## G. Discussion

In both studies I aimed to investigate the heterogeneity of the TRN at the cellular, synaptic and functional level, with my principal focus on the so far poorly explored anterior limbic TRN.

In study 1, I characterized a novel thalamocortical circuit that integrates the most anterodorsal part of the limbic TRN. This circuit includes brain structures relevant for the spatial navigation: the presubiculum (PreS), the retrosplenial cortex (RSC) and the anterior thalamic nuclei (ATN). Afferents from PreS and RSC are topographically organized, target a restricted portion of the anterodorsal TRN and recruit feedforward disynaptic inhibition onto the ATN. These properties are quite similar to classical sensory thalamocortical circuits. However, we discovered that Pres/RSC afferents have functional driver characteristics with strong unitary connection and a strong burst coupling onto the TRN, and that limbic TRN neurons have less repetitive bursting than the sensory TRN cells. Functionally, this limbic TRN sharpens the tuning of head-direction thalamic neurons and seems to be relevant in the switch between orientational strategies during spatial navigation.

In study 2, I demonstrated how heterogeneous the TRN is in term of its repetitive bursting capacity. The sensory sectors connected to auditory and somatosensory cortex have strong repetitive burst discharge unlike the limbic, MD-connected TRN neurons. This functional heterogeneity of the TRN correlates with the amplitude and speed of sleep spindles in the related cortices. By ablating the TRN repetitive bursting capacity, we removed this functional heterogeneity at the TRN level but also in sleep spindle characteristics.

In this discussion, I will first develop technical considerations on both studies, then discuss how my results advance the view of the TRN as a heterogeneous nucleus and finally present some of the perspectives arising from my studies.

## Technical considerations

### Tracing

Injections of retrobead into the limbic TRN allowed to target a restricted portion of the anterodorsal TRN that we were interested in. However, the control of the injection volume with a picospritzer was poor and it was almost unavoidable that the retrobead also reached the nearby anteroventral thalamus. By comparing a large number of injected mice, we managed to identify commonalities between large and small injection areas and successfully reproduced prior anatomical studies on the anterior TRN and thalamus. Cortical afferents to the limbic TRN from PreS, RSC, cingulate, prelimbic and infralimbic cortices seemed to arise from the deep layers, according to the position of the beads. Targeting restricted retrobead injections into different region of the limbic TRN or combining retrobead with different fluorescent properties would help to address

the question of whether the limbic TRN is topographically organized around its cortical/thalamic afferents in a similar manner than the sensory TRN or whether it is organized as an integrator in which the afferents from many different regions are colocalized.

We confirmed the projection from the Pres and RSC to the TRN by using Phaseolus Vulgaris leucoagglutinin anterograde tracer (PHAL-L) injections. The PHAL-L was electroporated to permit very restricted injection areas into PreS and RSC. By again comparing a large number of injections, we identified a pattern of projections to the thalamic nuclei and in all cases the projecting fibers crossed the limbic TRN while being closely apposed to somas and dendrites. In spite of a high level of precision we achieved through the PHAL-L injection, we did not manage to tackle the question of the layer specificities of the projection nor to observe a topographic organization in the limbic TRN. For this, many more even smaller injections would be required. Alternatively, driver mouse lines allowing to target specific layers would be a next step to take.

We used viral injections into the PreS/RSC to express the ChR2 in the neurons of these regions. The viral injections were much broader than the PHAL-L injections and it was difficult to distinguished between the site of injection and projections to nearby cortical targets in this heavily interconnected parahippocampal area. The development of mouse Cre lines would help to restrict injection site and to target specific layers or neuronal subtypes. In some initial unpublished observations, we saw that the Neurotensin receptor 1 (NTSR1)-Cre mouse line, widely used to target layer 6 corticothalamic neurons, was absent or much weaker in the PreS, suggesting some level of heterogeneity of the corticothalamic neurons projecting to the sensory or limbic TRN.

### *In vitro* cellular electrophysiology

The whole-cell patch-clamp recording of acute brain slices in combination with optogenetic and chemogenetic tools allowed the identification of functional synapses between the PreS/RSC and the TRN and the elegant demonstration of a feedforward inhibitory circuit with the ATN+ in study 1. In study 2, these *in vitro* recordings allowed the identification of TRN subnetworks, the characterization of their functional heterogeneity in term of bursting and to measure the impact of the activation of inhibitory DREADD receptors on TRN neurons. These *in vitro* recordings also allowed to identify relevant thalamocortical circuits that we could then precisely target *in vivo*.

The combination of *in vitro* recordings with optogenetic stimulation allowed to study specific projections to the TRN to a level that electrical stimulations would not permit. It raises some concerns on the potential effect of viral serotype (used for the expression of the ChR2) and of direct light illumination of synaptic boutons on the synaptic activity. However, cortical afferents to the TRN are intermingled and thus does not allow to use electrical stimulation to control for the side effect of viral transfection. To address this concern, we could deliver the ChR2 with different serotypes of adeno-associated virus

and reproduce the recording. We can also restrict the light stimulation over the interna capsula rather than directly above the TRN for activation of cortical afferents, for example through using a scanning system that would allow us to target with subcellular precision the site of light delivery. Similarly, the use of a faster version of the ChR2, such as ChETA, would be useful to further confirm that the functional driver characteristics of the PreS/RSC-TRN synapses are due to intrinsic properties and not an unexpected limitation of the ChR2 specifically at these synapses.

The minimal stimulation protocol using optogenetic activation of the presynaptic afferents allows to study the unitary properties of specific synapses (Gjoni et al., 2018). However, this procedure showed some limitations compared to classical electrical stimulation. Indeed, the precision of the light intensity control was poor and did not permit to reach the condition of minimal stimulation in most of the cells. Still, in the experiments that fulfilled the criteria for minimal stimulation, differences in unitary currents between afferents to TRN vs ATN came out convincingly.

### *In vivo* electrophysiology

In study 1, the identification of a novel thalamocortical circuit involving the limbic TRN raised the question of its function. PreS, RSC and ATN are known structures in the spatial navigation system, however the role of the limbic TRN on their activity has never been tested. *In vivo* single unit recordings of the thalamic neurons allow to monitor their activity will manipulating their cortical or limbic TRN afferents. I initially used home-made multi-wire electrodes to record from the ATN+. These bundles allowed to sample a large volume of the thalamus but thus lacked spatial precision. These multi-wire electrodes revealed that optogenetic activation of the PreS/RSC induced a reduction of firing of ATN+ units in a time window consistent with disynaptic feedforward inhibition. Furthermore, some of these ATN+ units were tuned to the head-direction, suggesting a role of this cortical feedback to the thalamus in the head-direction signaling. In order to increase the proportion of head-direction neurons recorded, I used linear silicone probes targeted to the anterodorsal thalamus. About 50% of the recorded units in this configuration showed a strong tuning to the head-direction.

In study 2, local recordings of specific cortical regions with local field potential electrodes followed the identification of a heterogeneity of the TRN neuronal activity *in vitro* between the sensory and the limbic sector. Primary auditory (A1), primary and secondary somatosensory (S1, S2) cortices were targeted as they project to the sensory TRN sector and the PFC as it is interconnected to the limbic TRN. The parallel recording of electroencephalogram, electromyogram and four local field potentials allowed the evaluation of the global vigilance state of the mice and the identification of local cortical activity at the same time. This recoding configuration combined with modulation of TRN activity is a powerful tool to tackle both global and local effects of the TRN.

**Morris Watermaze**

In study 1, we investigated the role of the limbic TRN in spatial navigation. Specifically, we used VGAT-Ires-Cre mice expressing the inhibitory DREADD in the anterior portion of the TRN. These mice received intraperitoneal injection of Clozapine N-oxide (CNO) to silence the TRN 40 min prior to the recording session in the hidden version of the Morris watermaze. During the 10 days of learning and 10 days of reversal learning, mice entered the watermaze from randomized quadrant, reinforcing the use of allocentric strategies. Every odd day, the four training sessions were preceded by a probe session where the platform was removed, in order to test the progression in spatial learning.

We showed in study 2 that these injection parameters we used *in vivo* induced changes in brain activity up to 6 h post injection, with a peak effect 30 min post injection. *In vitro*, we confirmed that the inhibitory DREADD activation in sensory TRN neurons induced a strong (~15 mV) hyperpolarization, bringing the cells out of range of firing action potentials. Our results suggest that significant proportion of TRN neurons are silenced by the injection of the CNO and that this inhibition lasts for several hours.

In study 1, the limbic portion of the TRN was silenced during all recording sessions and the post recording resting period. We chose this approach as it permits to tackle the role of the limbic TRN in acute orienting as well as in learning and memory formation. This approach revealed a role of the TRN in biasing search patterns in the Morris watermaze towards egocentric strategy and in reducing perseverance, which points towards acute roles of the limbic TRN in spatial navigation. These results are in accordance with previous studies on the role of prefrontal cortex to limbic thalamus corticothalamic circuit, showing the importance of these structures in the switch between search strategies.

The circuit involving the limbic thalamus, hippocampus and prefrontal cortex is also known to be important for spatial memory formation. We thus hypothesized a decrease in the performance of mice with a silenced limbic TRN in the Morris watermaze. However, there were no significant differences in the performance to find the platform.

Many parameters of the Morris watermaze experiment can be adapted in order to modify the task demands. In the next paragraphs, I would like to speculate on the effect of some of these parameters on our results in study 1.

Chemogenetic silencing of the limbic TRN increased overall the use of allocentric strategies during the learning and reversal learning of the Morris watermaze. Thus, we can hypothesize that the activity of the limbic TRN is required for proper egocentric navigation and that mice with a blockade of the limbic TRN activity switch to more allocentric strategy as a compensatory mechanism. A version of the Morris watermaze promoting egocentric navigation, for example by releasing the mice from a unique entry position all along the experiment, may reveal an impairment of the egocentric navigation system in mice with silencing of the limbic TRN.

The chronic CNO injection protocol we used may result in compensating mechanisms for the impairment of the thalamocortical circuits through other pathways. For example, the head-direction system feeds back information from cortical to subcortical structures through parallel route, one being a PreS to lateral mammillary body, completely bypassing the limbic TRN. An interesting perspective for our study would be to inject CNO only at challenging moments, for example prior to a probe session, where the platform is removed, or at the beginning of the reversal learning. This approach might exacerbate the acute effect of limbic TRN inhibition we observed on the perseverance,

Similarly, we could also reduce the number of probe sessions from one every odd day to only two probe sessions (day 5 and day 11 for learning, day 15 and day 21 for reversal learning) to improve the performance of mice in finding the platform. This may also reinforce the effect we observed on acute orientation and perseverance.

In order to address more specifically the role of the limbic TRN in spatial memory formation and replay, the CNO can be injected right after the recording session in the Morris watermaze. This would allow mice to navigate and orient themselves with a functional thalamocortical circuit. The effect of silencing of the limbic TRN would be restricted to the post recording resting period during which sleep is known to be critical for memory consolidation.

## Heterogeneity of the TRN

My studies revealed novel synaptic and cellular heterogeneities of the TRN. The cortical afferents from PreS and RSC showed functional driver characteristics, which is unprecedented for a corticoreticular synapse. The presence of such a driver cortical input to the limbic TRN that is absent from the cortical afferents to sensory TRN further supports strong functional differences between these circuits. Whether this driver characteristic is recurrent across circuit involving the limbic TRN or a specificity of the corticothalamic circuits between Pres/RSC and ATN+ remains to be determined. At the cellular level, we identified a strong difference in repetitive burst discharge between TRN neurons in the limbic sector compared to the sensory one. This heterogeneity seems to underly the heterogeneity of local cortical oscillations and might be relevant for local sleep regulation. In this section I will develop further how these major findings advance the understanding of the TRN as a heterogeneous structure.

### Cortical modulators vs drivers of the TRN

Glutamatergic synapses have classically been divided into two classes: drivers and modulators. This classification relies on both morphological and functional characteristics. Driver inputs activate only ionotropic glutamatergic receptors, show paired-pulse depression and large evoked postsynaptic potentials. There are very few inputs with poor convergence, thick axons and large terminals on proximal dendrites. On the contrary, modulator inputs activate both ionotropic and metabotropic receptors,

show paired-pulse facilitation and small evoked postsynaptic potentials. Modulator inputs represent the majority of the inputs with a lot of convergence onto the target neurons, with thin axons and small terminals on distal dendrites (Sherman, 2017).

Classical sensory and motor cortices have projections to the TRN with small boutons only (Guillery et al., 1998) and show paired-pulse facilitation (Castro-Alamancos and Calcagnotto, 1999; Astori and Luthi, 2013; Crandall et al., 2015; Fernandez et al., 2018), classifying these layer 6 afferents as modulators. On the contrary, thalamic projections to the sensory TRN have shown driver characteristics (Gentet and Ulrich, 2003).

There is anatomical evidence that the prefrontal cortex projections to the limbic TRN (connected to MD, AV, AM) have both small and large boutons, suggesting a dual origin from layer 5 and 6 (Zikopoulos and Barbas, 2006). These driver-like synapses with large boutons might undergo multivesicular release and could be more efficient in activating the limbic TRN than classical layer 6 modulatory projections. Combined with the presence of gap-junction between TRN neurons (Landisman et al., 2002), few large boutons might be sufficient to trigger widespread activity in subnetworks of the limbic TRN. Until now, only thalamoreticular synapses were described as drivers. Modulator layer 6 afferents were expected to activate TRN neurons only during highly synchronous activity such as during sleep (Crabtree, 2018). Few driver-like connections to the TRN might be able to induce inhibition and disinhibition of subsets of thalamic neurons, allowing discrimination of upcoming information.

The identification of cortical afferents to the limbic TRN showing functional driver characteristics in our study suggests that the limbic TRN conveys direct system-relevant information that is faithfully transmitted to its projection targets. The strong coupling between PreS/RSC presynaptic action potential and bursts in the limbic TRN neurons and the moderate entrainment of firing during repeated stimulation further support this view of a strong feedforward inhibition from the PreS/RSC to their thalamic targets.

**Heterogeneity of TRN: novel insights into neurochemically distinct cell types**

The identification of neurochemically distinct cell types, notably the PV+ and Sst+ subtypes, has been a major impetus for considering TRN as a heterogeneous structure. Although it has been proposed that these cellular subtypes form subnetworks, still little is known about their function. In particular, there has been no study so far that links neurochemical identity to cellular properties to a joint function.

A recent study by Clemente-Perez et al. dissected the role of PV+ and Sst+ neurons of the sensory TRN in thalamocortical oscillations (Clemente-Perez et al., 2017). PV+ neurons in the sensory TRN showed the classical repetitive burst firing upon release from hyperpolarizing current injection. Sst+ neurons in the same sector showed little repetitive burst firing, reminiscent of our observation in the limbic TRN where neurons displayed similar weak repetitive burst capability (Fernandez et al., 2018; Vantomme et al., 2019). However, this weak capability of repetitive burst in the limbic TRN did not

correlate with an increase proportion of Sst+ neurons compared to PV+ neurons (Clemente-Perez et al., 2017). Furthermore, we could not establish a difference in the bursting capacity of limbic TRN neurons between PV+ and PV- neurons recovered after patch-clamp recording (unpublished observation). The mechanism underlying the differences in repetitive burst discharge between the limbic and sensory TRN is still unknown. Our data did not find differences in passive and active membrane properties. Differences in T-type calcium currents and small conductance calcium-activated potassium currents, key players in TRN repetitive burst discharge, might be good candidates for further investigation.

Clemente-Perez et al. also observed that PV+ and Sst+ TRN neurons in the sensory sector project to distinct thalamic targets. PV+ neurons targeted mostly VPM, VPL and PO, three thalamic nuclei involved in sensorimotor signaling. Sst+ neurons projected to the intralaminar thalamic nuclei, the VPL and VM (Clemente-Perez et al., 2017). Looking at projection patterns of PV+ and Sst+ TRN neurons to the ATN and the laterodorsal (LD) thalamus in study 1, we could not observe such specific pattern of projections. Limbic PV+ and Sst+ neurons targeted the anterodorsal (AD), anteroventral (AV) and laterodorsal (LD) thalamic nuclei in a similar manner, suggesting a similar contribution of PV+ and Sst+ neurons to anterior thalamic inhibition. However, we did not investigated whether the PreS and or RSC afferents contacted preferentially PV+ or Sst+ TRN neurons.

Altogether, these data suggest that the TRN inhibition of thalamic nuclei involved in limbic thalamocortical circuits does not serve as an oscillation generator as much as the TRN inhibition of sensory thalamic nuclei. The precise, strong and weakly oscillatory TRN inhibition over limbic thalamus probably reflects distinct needs of limbic thalamocortical networks for their function.

**Possible mechanisms by which TRN can help sharpen the tuning of HD cells – a novel form of gating within the brain.**

The interaction between the inhibitory limbic TRN and anterodorsal head-direction cells has been recently suggested (Peyrache et al., 2019). One of the major elements suggesting that anterodorsal head-direction neurons receive inhibition to suppress spiking activity outside their preferred direction was their narrower angular directional firing range compare to lateral mammillary head-direction neurons that are the main drive for the anterodorsal neurons.

The limbic TRN is a good candidate to explain this difference in angular directional firing range between neurons of the anterodorsal thalamus and the lateral mammillary body. In classical sensory systems that we described in the chapter 3 of the introduction, the TRN is thought to participate in the inhibitory surroundings of thalamic receptive field through lateral inhibition. Thalamo-reticulo-thalamic circuits form open loops allowing lateral inhibition from the TRN neurons to sharpen the sensory receptive field of thalamic cells by inhibiting their activity outside their sensory space. Cortical

afferents also participate to the precision of the sensory receptive field through direct activation and indirect feedforward inhibition (via the TRN) of thalamic neurons.

In the study 1, we found a similar feedforward corticothalamic circuit to AD that recruits inhibition from the limbic TRN. Anatomically, the portion of the limbic TRN that receives PreS/RSC afferents is relatively small in comparison to its thalamic target, suggesting a divergent output from the limbic TRN to AD and that single TRN neurons might project to multiple thalamic ones. Functionally, the responses of ATN+ neurons upon the activation of this feedforward circuit were constituted of compound inhibitory postsynaptic currents of high amplitude, further suggesting that single TRN neurons might contact multiple thalamic targets. Confirming this hypothesis, our data showed an increase in the angular directional firing range of anterodorsal head-direction cells upon chemogenetic inhibition of the limbic TRN. This strongly suggests that the suppression of spiking activity outside the preferred direction of anterodorsal thalamic neurons is mediated, at least partially, by lateral inhibition from the limbic TRN.

**Heterogeneity of TRN's cellular and synaptic properties: Implications for sleep**

In study 2, we correlated the functional heterogeneity of TRN neurons in their repetitive burst discharge to the heterogeneity of sleep spindles in the related cortices. By locally modulating the somatosensory sector of the TRN we could induce changes in the local sleep of somatosensory cortex, establishing causality. Impairment of TRN bursting capacity through deletion of the calcium channel required for such bursting discharge did not impact all TRN sectors and related cortices similarly. Somatosensory and auditory cortex showed a change in their sleep oscillation content, notably a switch from a fast sleep spindles enriched sleep to a delta enriched sleep, whereas there was no differences in the prefrontal cortex. Several factors might underlie this heterogeneity: 1) limbic TRN neurons are not as active as sensory TRN neurons during sleep, 2) the synaptic connectivity of the limbic thalamocortical circuits is different from the sensory circuits, 3) the weaker repetitive bursting capacity of the limbic TRN is indeed relevant for the changes in oscillatory content of the limbic cortex.

Halassa et al. showed that ATN-connected limbic TRN neurons are negatively correlated to the spindle power, are broadly distributed along delta waves, and overall reduce their firing during sleep (Halassa et al., 2014), consistent with the idea that the limbic TRN has a weak spindle-related activity. In this study, the ATN-connected limbic TRN neurons have an increased firing rate during active waking compared to quiescent state and sleep. This suggests that a reduction of activity of the limbic TRN during sleep favors disinhibition of its thalamic targets, perhaps enabling offline processing of the ATN with other limbic structures. On the contrary, sensory connected TRN neurons increase their firing rate overall during sleep and are phase-locked to the sleep spindles, supporting the idea that sensory TRN neurons are more active during sleep than limbic TRN neurons. We found in studies 1 and 2 that limbic TRN neurons involved in thalamocortical loop with the ATN and the mediodorsal thalamus have a

poor repetitive bursting capacity compared to the classical sensory TRN neurons. Blocking burst discharge in the TRN is thus likely to have a stronger impact on brain structures connected to the sensory TRN such as somatosensory cortex than to the limbic TRN such as the PFC.

## Perspectives

### Sleep as a local phenomenon – a result of TRN heterogeneity.

Sleep serves many biological functions, from memory consolidation (Vorster and Born, 2015), to energy balance and metabolic function (Benington and Heller, 1995; Xie et al., 2013), immune protection (Irwin, 2015), macromolecule biosynthesis (Mackiewicz et al., 2007). All the processes required for these functions occur simultaneously and may seem unrelated to each other. Considering sleep only as a global phenomenon thus fails to grab all the local aspects of sleep functions. Considering the local aspects of sleep makes one wonders how sleep is locally regulated. In this section, I will discuss two processes that are known to affect sleep, the homeostatic regulation and learning, and how the TRN might play a role in the local regulation of these processes.

The homeostatic process can be considered as the sleep drive. The longer an individual is awake, the stronger the need to sleep becomes. In terms of brain activity, the delta power (1-4 Hz) was shown to increase with the sleep need. Sleep deprivation protocols revealed a strong increase of the delta power in the subsequent sleep on a global electroencephalogram scale. The delta power can also be upregulated or downregulated locally in the cortex depending on the recent use or absence of use of the related modality (Kattler et al., 1994; Huber et al., 2006). We showed in study 2 that blocking the TRN increases the delta content of sleep. The TRN is thus a potential candidate implicated in the homeostatic mechanisms of delta sleep regulation. Furthermore, the parallel wiring of the TRN in thalamocortical circuits makes it possible to regulate sleep homeostasis locally. A way to investigate the role of the TRN in this local regulation of homeostasis can take advantage of the local increase in sleep delta power induced by excessive sensory stimulation in the preceding wake period. For example, whisker stimulations induce an increase in delta power in the primary somatosensory cortex in rodents (Vyazovskiy et al., 2000). Local depolarization of the somatosensory TRN during the post stimulation sleep can be applied to see whether the use-dependent increase in delta power can be prevented. This approach of local manipulation of the TRN activity and single modality overstimulation circumvents the non-specific effects of sleep deprivation and may unravel the fundamental circuits underlying sleep homeostasis (Vantomme et al., 2019).

The learning process requires specific patterns of synaptic activity that can result in synaptic strengthening or downscaling. The post training sleep is critical for learning and memory as it permits such patterns of synaptic activity to occur and thus synaptic plasticity. In particular, the density of sleep spindles is increased in cortical regions that have been required for learning. Because the TRN is the main generator of sleep

spindles, it suggests that the activity of the TRN might also be relevant to influence the cortical oscillatory content and to promote synaptic plasticity. This hypothesis could be tested through local manipulation of TRN activity in the post training sleep after a learning paradigm. Boosting thalamic bursts firing and cortical spindles through local optogenetic activation of the TRN (Halassa et al., 2011) may enhance learning performance while silencing the TRN locally (Fernandez et al., 2018) may reduce learning performance.

To summarize, the TRN and its heterogeneous connectivity in thalamocortical circuits may underlie local mechanisms of sleep regulation such as the homeostatic and learning processes. Such hypotheses can now be investigated through local manipulation of sleep via interference of the TRN sectors 'activity.

**TRN as part of the head direction system.**

In study 1, we showed that blocking the activity of the limbic TRN increases the tuning width of AD head-direction neurons. We can thus think of the TRN as a constitutive sharpener of the tuning of thalamic head-direction neurons, with AD neurons activating TRN cells that feedback in an open loop circuit and promote lateral inhibition.

We also demonstrated that PreS/RSC has a strong feedforward inhibition onto anterodorsal cells. These cortical inputs, with the contribution of the limbic TRN, might play a role in the re-tuning of anterodorsal thalamic neurons. The PreS and RSC may play an important role in the updating of the head-direction signal with external landmarks. For example, the PreS is an entry point for visual information into the head-direction system. Its strong projections to AD are essential for visual landmark control of the head-direction signal in this nucleus. The limbic TRN is thus in a strategic position to re-tune thalamic head-direction signals under the control of the PreS/RSC. To test whether the TRN plays a role in the visual landmark control of a thalamic cell's preferred direction, we could record thalamic head-direction neurons and combine chemogenetic silencing of the limbic TRN with visual cue rotation. If the limbic TRN plays a role in the visual landmark control of the thalamic head-direction neurons, the precision of the shift in preferred direction induced by the rotation of the visual cues should be lower in mice with chemogenetic silencing of the TRN than in controls.

Head-direction neurons have a persistent high frequency firing when the animal faces the preferred direction. The mechanisms for persistence of directional firing could arise from intrinsic cellular properties of head-direction neurons, network properties that allow strong excitation between neurons with similar tuning, or high recurrent inhibition in combination with direct excitation (Simonnet and Fricker, 2018). The excitatory-excitatory connections between thalamic neurons are rare but very few of them between neurons with similar preferred direction might be sufficient for recurrent excitation. As for the inhibition, the thalamus contains also very few interneurons and we did not find any PV+ cells within the anterodorsal thalamus in our anatomical study. Beyond their role in lateral inhibition, TRN neurons may also help to sustain the firing rate of recurrently connected thalamic neurons similarly to the inhibitory Martinotti cells

with PreS head-direction cells (Simonnet et al., 2017). However, when silencing the limbic TRN, we observed only an increase of the angular directional firing range of thalamic head-direction neurons and no change in maximal firing rate, suggesting a role of the TRN in lateral inhibition but not in recurrent entrainment.

Finally, TRN neurons connected to the ATN correlated very little with sleep spindles and presented overall a reduction of firing during sleep (Halassa et al., 2014). This reduction of activity and lack of synchronization compared to classical sensory TRN may underlie a different function of the limbic TRN in sleep. Thalamic head-direction neurons are active during sleep. The reduction of limbic TRN activity within the head-direction circuit might be necessary for replay and memory formation related to spatial navigation.

**Novel considerations of the limbic TRN**

Abbreviations of the thalamic nuclei:

AD: anterodorsal
AV: anteroventral
AM: anteromedial
LGN: lateral geniculate
MGN: medial geniculate
VPM: ventroposteromedial
VPL: ventroposterolateral
PO: posterior
VL: ventrolateral

VA: ventral anterior
VM: ventromedial
MD: mediodorsal
AD: anterodorsal
AV: anteroventral
AM: anteromedial
SMT: submedial
LD: laterodorsal
LP: lateroposterior
CM: centromedial

PC: paracentral
CL: centrolateral
PF: parafascicular
SPF: subparafascicular
PT: paratenial
PVn: paraventricular
RH: rhomboid
RE: reuniens
IMD: intermediodorsal
IAM: interanteromedial

In this section, I would like to investigate further the potential functions of the limbic TRN. To do so, I will look at the TRN from the perspective of the limbic thalamus. The limbic thalamus was defined as being constituted of the ATN, RE, RH, PV, PT, medial MD, CM, IAM and IMD. This classification is based on functional studies of thalamic nuclei and is different from the original classification that considered three thalamic groups: the principal nuclei (LGN, MGN, VPM, VPL, PO, VL, VA and VM), the associative nuclei (MD, AD, AV, AM, SMT, LD, and LP) and the intralaminar (CM, PC, CL, PF and SPF) and midline (PT, PV, RH, RE and IMD) group.

One can speculate that limbic TRN functions are tightly linked to its thalamic target functions. In the next paragraphs, I will consider some of these limbic thalamic nuclei

that were studied functionally and describe anatomical evidence of TRN projections to these nuclei in an attempt to propose more potential roles of the TRN in limbic functions. The function of these thalamic nuclei were mostly studied using combination of lesion/inactivation of the thalamus with behavioral tasks in rodents.

The ATN is composed of the AD, AV and AM. The ATN is part of the Papez's circuit that forms a loop from the hippocampus to mammillary bodies, ATN, cingulate cortex, parahippocampal formation and back to the hippocampus. The Papez's circuit is critical for mnemonic functions and lesions of the ATN (as well as other structure of the Papez's circuit) disrupt memory (Aggleton and Brown, 1999) and cause severe anterograde amnesia in humans (von Cramon et al., 1985). A particularity of the Papez's circuit is the presence of a theta (5 – 12 Hz) oscillation that propagates in its structures and has been involved in mnemonic function of the hippocampus (Vertes et al., 2001). All subdivisions of the ATN contain neurons that increase their firing rate upon hippocampal theta rhythm. In particular, the AV neurons fired rhythmically in bursts synchronous to this theta. As we already described in study 1, the ATN contains head-direction neurons. The head-direction neurons in the ATN are critical for spatial navigation learning. Indeed, lesion of the ATN disrupted spatial learning and hippocampal place cell activity (Taube et al., 1992; Mizumori et al., 1994; Aggleton and Brown, 1999). ATN lesions were also shown to disrupt conditioned avoidance learning, expanding the role of the ATN beyond spatial navigation (Gabriel et al., 1983; Gabriel et al., 1995). We demonstrated that inhibitory projection from the limbic TRN to the AD and AV are powerful and reliable and that limbic TRN's activity sharpens the tuning of head-direction neurons in the AD. However, we do not know whether ATN-connected TRN neurons play a role in spatial memory formation.

RE and RH will be considered together as their close proximity renders difficult to separate their effect on behavior in lesion studies. RE/RH target mostly the hippocampus and limbic cortices (Vertes et al., 2015). Rats with RE/RH lesion showed a similar performance in acquisition and retention of a watermaze reference memory task than control rats. During probe session following acquisition, rats with RE/RH lesions swam directly to the escape location and, upon realization that the platform was absent, rapidly extended their search to the rest of the watermaze (Dolleman-van der Weel et al., 2009). This observation that a thalamic lesion of RE/RH reduces perseverance in probe session is in accordance with our observation that blockade of the limbic TRN, and thus potentially disinhibiting the RE/RH, promotes perseverance in probe sessions after acquisition. This suggests that shift between strategies can be achieve through changes of thalamic neuronal activity and that the limbic TRN might be a key player in this modulation. Further lesion/inactivation studies of RE/RH revealed the importance of these thalamic nuclei in the medial prefrontal cortex function and in the interaction between the hippocampus and the medial prefrontal cortex, for example in long-term spatial memory formation (Hembrook et al., 2012; Loureiro et al., 2012). Cholvin et al proposed that the RE/RH coordinate the activity of the hippocampus for spatial memory formation and the medial prefrontal cortex for strategy shifting (Cholvin et al., 2013). The dense projections from the medial prefrontal

cortex to the limbic TRN (Zikopoulos and Barbas, 2007) and the evidence of limbic TRN projections to RE (McKenna and Vertes, 2004) further emphasized the potential role of the limbic TRN in modulating the strategy shift in navigation task.

The PVn is known to project mostly to limbic subcortical structures such as the amygdala and nucleus accumbens and thus has been associated with affective functions (Vertes et al., 2015). The PVn has been linked to detection of novel stressors and to adaptation to chronic stress. More precisely, c-fos expression in PVn neurons is increased after exposure to a novel stressor and lesion of the PVn blocked the habituation to repeated restraint stress (Bhatnagar and Dallman, 1998; Bhatnagar et al., 2002). This phenomenon of heightening novel stressor and reduce/suppress already known stressor is reminiscent of the TRN gating function of sensory information. The PVn has also been associated with food consumption and drug seeking behavior, showing increase c-fos staining in PVn neurons is enhanced in anticipation of feeding during food deprivation and after reinstatement of drug seeking behavior. Lesion and/or inactivation of PVn reduce the locomotor activity that precedes feeding and suppress drug-seeking behavior (Nakahara et al., 2004; Angeles-Castellanos et al., 2007; James et al., 2011). As the limbic TRN has been shown to project to the PVn (Cornwall and Phillipson, 1988), we can speculate that TRN inhibitory control over PVn activity may be important in reducing drug seeking behavior and food overconsumption in particular in the context of stress and anxiety.

The medial portion of the MD is strongly connected to the prefrontal cortex and they thus share many functions. In particular, the medial MD is important in behavioral flexibility. Lesion studies have shown that rats with medial MD lesion maintained strategies previously rewarded or showed perseverance despite a change in reward condition (Block et al., 2007). A striking example comes from watermaze experiments where rats stick to thigmotaxis strategy (perseverant swimming in close proximity to the wall), thus delaying their learning of the position of the escape platform. Once the platform location was learned, rats showed perseverant behavior to the former platform position even if the new platform was visible (Dolleman-van der Weel et al., 2009). Beyond this role in behavioral flexibility, the medial MD has been linked to recognition memory. In particular, lesions of medial MD can disrupt associative recognition memory such as place/object association and temporal order of object presentation (Cross et al., 2012). Limbic TRN inhibitory projections to the medial MD (Cornwall and Phillipson, 1988) are then also in a good position to influence flexibility in strategy used in spatial task and maybe even influence memory formation.

Unlike other intralaminar nuclei, the CM projections target mostly limbic structures suggesting that CM's function might be closer to midline thalamic nuclei than intralaminar thalamic nuclei (Van der Werf et al., 2002; Vertes et al., 2012). However, the functions of the CM have not be studied separately from the intralaminar nuclei, probably due to the poor accessibility of the CM for behavioral studies, and this will not be developed further.

## Next steps and conclusion

In the last years, the application of modern neuroscience techniques allowed to link to some extent molecular, cellular, electrical and synaptic heterogeneities of the TRN to its functions. In particular, opto- and chemogenetic manipulation of TRN neuronal activity in combination with electrical recordings of the related circuits or behavioral experimentations allowed to confirm and expand our understanding of the guardian of the gate.

The limbic TRN has barely revealed all its functions as suggested by the strong and numerous afferents from the limbic cortex and thalamus. Before the development of techniques that permit manipulation of specific afferents, it was impossible to disentangle functionally these projections to the limbic TRN. The latest studies revealed the involvement of the limbic TRN into selective attention (Zikopoulos and Barbas, 2006; Halassa et al., 2014), pain regulation (Liu et al., 2017), escape behavior (Dong et al., 2019), navigation (study 1) and how different the limbic TRN participates to sleep spindle generation compared to the sensory TRN (Fernandez et al., 2018; Vantomme et al., 2019). I would expect that the next steps of TRN research would focus on the limbic TRN and how it participates to memory formation and consolidation, emotion and higher cognitive processes.

In particular, I would consider using the thalamocortical circuit of the head-direction system as it offers an interesting framework to further study the function of the limbic TRN in sleep and memory. Unlike cortical structures that process signals from multiple sources, the thalamic head-direction system processes a one-dimensional signal that is the head-angle. This renders the representation of the head-direction system very persistent across brain states. Indeed, parallel recording of the anterodorsal thalamus and dPreS across brain states revealed that the neuronal activity in this thalamocortical network preserved functional organization, inter-area interaction from thalamus to cortex and show similar drifting speed during exploration and REM sleep (Peyrache et al., 2015; Peyrache et al., 2019). This supports the idea that the head-direction system relies mostly on intrinsic wiring and dynamics than on sensory stimuli. Furthermore, the high level of organization of the spatial navigation system and in particular of the head-direction thalamocortical circuit during sleep may play a key role in hippocampal replay and memory consolidation (Peyrache et al., 2019). Whether the limbic TRN plays a role in spatial memory consolidation is still an open question that is being investigated in the context of the head-direction system (Viejo and Peyrache, 2019). The limbic portion of the TRN involved in the head-direction system seems thus to be a good candidate to study the role of the limbic TRN in sleep and memory as the head angle signal offers a simple and reliable readout of the thalamocortical circuit.

In this thesis and in my research projects, I investigated the heterogeneity of the TRN at the cellular, synaptic and functional level, emphasizing the less well-described limbic TRN. I demonstrated how the heterogeneity of the TRN underlies many of its functions

and described how future works will gain from taking into account this heterogeneity. This thesis can serve as a collection of the TRN heterogeneous elements that influence functions of the multifaceted Guardian of the Gate and also provides current hypotheses and ways to address them.

## H. Reference


Aggleton JP, Brown MW (1999) Episodic memory, amnesia, and the hippocampal-anterior thalamic axis. Behav Brain Sci 22:425-444; discussion 444-489.

Ahrens S, Jaramillo S, Yu K, Ghosh S, Hwang GR, Paik R, Lai C, He M, Huang ZJ, Li B (2015) ErbB4 regulation of a thalamic reticular nucleus circuit for sensory selection. Nat Neurosci 18:104-111.

Aizenberg M, Rolon-Martinez S, Pham T, Rao W, Haas JS, Geffen MN (2019) Projection from the Amygdala to the Thalamic Reticular Nucleus Amplifies Cortical Sound Responses. Cell Rep 28:605-615 e604.

Albéri L, Lintas A, Kretz R, Schwaller B, Villa AE (2013) The calcium-binding protein parvalbumin modulates the firing properties of the reticular thalamic nucleus bursting neurons. J Neurophysiol 109:2827-2841.

Alitto HJ, Usrey WM (2003) Corticothalamic feedback and sensory processing. Curr Opin Neurobiol 13:440-445.

Angeles-Castellanos M, Mendoza J, Escobar C (2007) Restricted feeding schedules phase shift daily rhythms of c-Fos and protein Per1 immunoreactivity in corticolimbic regions in rats. Neuroscience 144:344-355.

Arcelli P, Frassoni C, Regondi MC, De Biasi S, Spreafico R (1997) GABAergic neurons in mammalian thalamus: a marker of thalamic complexity? Brain Res Bull 42:27-37.

Astori S, Luthi A (2013) Synaptic plasticity at intrathalamic connections via CaV3.3 T-type Ca2+ channels and GluN2B-containing NMDA receptors. J Neurosci 33:624-630.

Avanzini G, de Curtis M, Panzica F, Spreafico R (1989) Intrinsic properties of nucleus reticularis thalami neurones of the rat studied in vitro. J Physiol 416:111-122.

Bal T, von Krosigk M, McCormick DA (1995) Synaptic and membrane mechanisms underlying synchronized oscillations in the ferret lateral geniculate nucleus in vitro. J Physiol 483 ( Pt 3):641-663.

Battaglia G, Lizier C, Colacitti C, Princivalle A, Spreafico R (1994) A reticuloreticular commissural pathway in the rat thalamus. J Comp Neurol 347:127-138.

Bendotti C, Hohmann C, Forloni G, Reeves R, Coyle JT, Oster-Granite ML (1990) Developmental expression of somatostatin in mouse brain. II. In situ hybridization. Brain Res Dev Brain Res 53:26-39.

Benington JH, Heller HC (1995) Restoration of brain energy metabolism as the function of sleep. Prog Neurobiol 45:347-360.

Berezhnaya LA (2006) Neuronal organization of the reticular nucleus of the thalamus in adult humans. Neurosci Behav Physiol 36:519-525.

Bhatnagar S, Dallman M (1998) Neuroanatomical basis for facilitation of hypothalamic-pituitary-adrenal responses to a novel stressor after chronic stress. Neuroscience 84:1025-1039.

Bhatnagar S, Huber R, Nowak N, Trotter P (2002) Lesions of the posterior paraventricular thalamus block habituation of hypothalamic-pituitary-adrenal responses to repeated restraint. J Neuroendocrinol 14:403-410.

Block AE, Dhanji H, Thompson-Tardif SF, Floresco SB (2007) Thalamic-prefrontal cortical-ventral striatal circuitry mediates dissociable components of strategy set shifting. Cereb Cortex 17:1625-1636.

Brodmann K (1909) Vergleichende Lokalisationslehre der Grosshirnrinde in ihren Prinzipien dargestellt auf Grund des Zellenbaues: Barth.

Brunton J, Charpak S (1997) Heterogeneity of cell firing properties and opioid sensitivity in the thalamic reticular nucleus. Neuroscience 78:303-307.

Burgunder JM, Heyberger B, Lauterburg T (1999) Thalamic reticular nucleus parcellation delineated by VIP and TRH gene expression in the rat. J Chem Neuroanat 17:147-152.

Buzsáki G (1991) The thalamic clock: emergent network properties. Neuroscience 41:351-364.

Castro-Alamancos MA, Calcagnotto ME (1999) Presynaptic long-term potentiation in corticothalamic synapses. J Neurosci 19:9090-9097.

Çavdar S, Onat FY, Çakmak YO, Yananli HR, Gülçebi M, Aker R (2008) The pathways connecting the hippocampal formation, the thalamic reuniens nucleus and the thalamic reticular nucleus in the rat. J Anat 212:249-256.

Cholvin T, Loureiro M, Cassel R, Cosquer B, Geiger K, De Sa Nogueira D, Raingard H, Robelin L, Kelche C, Pereira de Vasconcelos A, Cassel JC (2013) The ventral midline thalamus contributes to strategy shifting in a memory task requiring both prefrontal cortical and hippocampal functions. J Neurosci 33:8772-8783.

Cicirata F, Angaut P, Serapide MF, Panto MR (1990) Functional organization of the direct and indirect projection via the reticularis thalami nuclear complex from the motor cortex to the thalamic nucleus ventralis lateralis. Exp Brain Res 79:325-337.

Clark BJ, Taube JS (2012) Vestibular and attractor network basis of the head direction cell signal in subcortical circuits. Front Neural Circuits 6:7.

Clemence AE, Mitrofanis J (1992) Cytoarchitectonic heterogeneities in the thalamic reticular nucleus of cats and ferrets. J Comp Neurol 322:167-180.

Clemente-Perez A, Makinson SR, Higashikubo B, Brovarney S, Cho FS, Urry A, Holden SS, Wimer M, Dávid C, Fenno LE, Acsády L, Deisseroth K, Paz JT (2017) Distinct thalamic reticular cell types differentially modulate normal and pathological cortical rhythms. Cell Rep 19:2130-2142.

Contreras-Rodriguez J, Gonzalez-Soriano J, Martinez-Sainz P, Marin-Garcia P, Rodriguez-Veiga E (2003) Neurochemical heterogeneity of the thalamic reticular and perireticular nuclei in developing rabbits: patterns of calbindin expression. Brain Res Dev Brain Res 144:211-221.

Contreras D, Curró Dossi R, Steriade M (1992) Bursting and tonic discharges in two classes of reticular thalamic neurons. J Neurophysiol 68:973-977.

Cornwall J, Phillipson OT (1988) Afferent projections to the dorsal thalamus of the rat as shown by retrograde lectin transport. II. The midline nuclei. Brain Res Bull 21:147-161.

Cornwall J, Cooper JD, Phillipson OT (1990) Projections to the rostral reticular thalamic nucleus in the rat. Exp Brain Res 80:157-171.

Cotillon-Williams N, Huetz C, Hennevin E, Edeline JM (2008) Tonotopic control of auditory thalamus frequency tuning by reticular thalamic neurons. J Neurophysiol 99:1137-1151.

Coulon P, Landisman CE (2017) The Potential Role of Gap Junctional Plasticity in the Regulation of State. Neuron 93:1275-1295.

Cox CL, Huguenard JR, Prince DA (1997) Nucleus reticularis neurons mediate diverse inhibitory effects in thalamus. Proc Natl Acad Sci U S A 94:8854-8859.

Crabtree JW (1996) Organization in the somatosensory sector of the cat's thalamic reticular nucleus. J Comp Neurol 366:207-222.

Crabtree JW (1998) Organization in the auditory sector of the cat's thalamic reticular nucleus. J Comp Neurol 390:167-182.

Crabtree JW (2018) Functional Diversity of Thalamic Reticular Subnetworks. Front Syst Neurosci 12:41.

Crabtree JW, Killackey HP (1989) The Topographic Organization and Axis of Projection within the Visual Sector of the Rabbit's Thalamic Reticular Nucleus. Eur J Neurosci 1:94-109.

Crandall SR, Cruikshank SJ, Connors BW (2015) A corticothalamic switch: controlling the thalamus with dynamic synapses. Neuron 86:768-782.

Crick F (1984) Function of the thalamic reticular complex: the searchlight hypothesis. Proc Natl Acad Sci U S A 81:4586-4590.

Cross L, Brown MW, Aggleton JP, Warburton EC (2012) The medial dorsal thalamic nucleus and the medial prefrontal cortex of the rat function together to support associative recognition and recency but not item recognition. Learn Mem 20:41-50.

Csillik B, Mihály A, Krisztin-Péva B, Chadaide Z, Samsam M, Knyihár-Csillik E, Fenyo R (2005a) GABAergic parvalbumin-immunoreactive large calyciform presynaptic complexes in the reticular nucleus of the rat thalamus. J Chem Neuroanat 30:17-26.

Csillik B, Mihaly A, Krisztin-Peva B, Chadaide Z, Samsam M, Knyihar-Csillik E, Fenyo R (2005b) GABAergic parvalbumin-immunoreactive large calyciform presynaptic complexes in the reticular nucleus of the rat thalamus. J Chem Neuroanat 30:17-26.

Cueni L, Canepari M, Lujan R, Emmenegger Y, Watanabe M, Bond CT, Franken P, Adelman JP, Lüthi A (2008) T-type $Ca^{2+}$ channels, SK2 channels and SERCAs gate sleep-related oscillations in thalamic dendrites. Nat Neurosci 11:683-692.

de Biasi S, Frassoni C, Spreafico R (1986) GABA immunoreactivity in the thalamic reticular nucleus of the rat. A light and electron microscopical study. Brain Res 399:143-147.

Deleuze C, Huguenard JR (2006) Distinct electrical and chemical connectivity maps in the thalamic reticular nucleus: potential roles in synchronization and sensation. J Neurosci 26:8633-8645.

Desîlets-Roy B, Varga C, Lavallée P, Deschênes M (2002) Substrate for cross-talk inhibition between thalamic barreloids. J Neurosci 22:RC218.

Dillingham CM, Vann SD (2019) Why Isn't the Head Direction System Necessary for Direction? Lessons From the Lateral Mammillary Nuclei. Front Neural Circuits 13:60.

Dolleman-van der Weel MJ, Morris RG, Witter MP (2009) Neurotoxic lesions of the thalamic reuniens or mediodorsal nucleus in rats affect non-mnemonic aspects of watermaze learning. Brain Struct Funct 213:329-342.

Dong P, Wang H, Shen XF, Jiang P, Zhu XT, Li Y, Gao JH, Lin S, Huang Y, He XB, Xu FQ, Duan S, Lian H, Wang H, Chen J, Li XM (2019) A novel cortico-intrathalamic circuit for flight behavior. Nat Neurosci 22:941-949.

Ergenzinger ER, Glasier MM, Hahm JO, Pons TP (1998) Cortically induced thalamic plasticity in the primate somatosensory system. Nat Neurosci 1:226-229.

Fernandez LM, Vantomme G, Osorio-Forero A, Cardis R, Béard E, Lüthi A (2018) Thalamic reticular control of local sleep in sensory cortex. Elife:in press.

Fogerson PM, Huguenard JR (2016) Tapping the brakes: cellular and synaptic mechanisms that regulate thalamic oscillations. Neuron 92:687-704.

Fuentealba P, Steriade M (2005) The reticular nucleus revisited: intrinsic and network properties of a thalamic pacemaker. Prog Neurobiol 75:125-141.

Gabriel M, Lambert RW, Foster K, Orona E, Sparenborg S, Maiorca RR (1983) Anterior thalamic lesions and neuronal activity in the cingulate and retrosplenial cortices during discriminative avoidance behavior in rabbits. Behav Neurosci 97:675-696.

Gabriel M, Cuppernell C, Shenker JI, Kubota Y, Henzi V, Swanson D (1995) Mamillothalamic tract transection blocks anterior thalamic training-induced neuronal plasticity and impairs discriminative offidance behavior in rabbits. J Neurosci 15:1437-1445.

Gardner RJ, Hughes SW, Jones MW (2013) Differential spike timing and phase dynamics of reticular thalamic and prefrontal cortical neuronal populations during sleep spindles. J Neurosci 33:18469-18480.

Gentet LJ, Ulrich D (2003) Strong, reliable and precise synaptic connections between thalamic relay cells and neurones of the nucleus reticularis in juvenile rats. J Physiol 546:801-811.

Gjoni E, Zenke F, Bouhours B, Schneggenburger R (2018) Specific synaptic input strengths determine the computational properties of excitation-inhibition integration in a sound localization circuit. J Physiol 596:4945-4967.

Gonzalo-Ruiz A, Lieberman AR (1995a) Topographic organization of projections from the thalamic reticular nucleus to the anterior thalamic nuclei in the rat. Brain Res Bull 37:17-35.

Gonzalo-Ruiz A, Lieberman AR (1995b) GABAergic projections from the thalamic reticular nucleus to the anteroventral and anterodorsal thalamic nuclei of the rat. J Chem Neuroanat 9:165-174.

Graybiel AM, Elde RP (1983) Somatostatin-like immunoreactivity characterizes neurons of the nucleus reticularis thalami in the cat and monkey. J Neurosci 3:1308-1321.

Grieves RM, Jeffery KJ (2017) The representation of space in the brain. Behav Processes 135:113-131.

Guido W, Weyand T (1995) Burst responses in thalamic relay cells of the awake behaving cat. J Neurophysiol 74:1782-1786.

Guillery RW, Feig SL, Lozsádi DA (1998) Paying attention to the thalamic reticular nucleus. Trends Neurosci 21:28-32.

Hádinger N, Bősz E, Vantomme G, Tóth B, Lüthi A, Acsády L (2019) Specialized frontal cortical control over the anterior thalamic reticular nucleus. Abstract Society for Neuroscience Meeting 2019.

Hafting T, Fyhn M, Molden S, Moser MB, Moser EI (2005) Microstructure of a spatial map in the entorhinal cortex. Nature 436:801-806.
Halassa MM, Kastner S (2017) Thalamic functions in distributed cognitive control. Nat Neurosci 20:1669-1679.
Halassa MM, Siegle JH, Ritt JT, Ting JT, Feng G, Moore CI (2011) Selective optical drive of thalamic reticular nucleus generates thalamic bursts and cortical spindles. Nat Neurosci 14:1118-1120.
Halassa MM, Chen Z, Wimmer RD, Brunetti PM, Zhao S, Zikopoulos B, Wang F, Brown EN, Wilson MA (2014) State-dependent architecture of thalamic reticular subnetworks. Cell 158:808-821.
Hartley T, Burgess N, Lever C, Cacucci F, O'Keefe J (2000) Modeling place fields in terms of the cortical inputs to the hippocampus. Hippocampus 10:369-379.
Hayama T, Hashimoto K, Ogawa H (1994) Anatomical location of a taste-related region in the thalamic reticular nucleus in rats. Neurosci Res 18:291-299.
Hazra A, Macolino C, Elliott MB, Chin J (2014) Delayed thalamic astrocytosis and disrupted sleep-wake patterns in a preclinical model of traumatic brain injury. J Neurosci Res 92:1434-1445.
Hazrati LN, Parent A (1991) Contralateral pallidothalamic and pallidotegmental projections in primates: an anterograde and retrograde labeling study. Brain Res 567:212-223.
Hembrook JR, Onos KD, Mair RG (2012) Inactivation of ventral midline thalamus produces selective spatial delayed conditional discrimination impairment in the rat. Hippocampus 22:853-860.
Hendrickson AE, Ogren MP, Vaughn JE, Barber RP, Wu JY (1983) Light and electron microscopic immunocytochemical localization of glutamic acid decarboxylase in monkey geniculate complex: evidence for gabaergic neurons and synapses. J Neurosci 3:1245-1262.
Herd MB, Lambert JJ, Belelli D (2014) The general anaesthetic etomidate inhibits the excitability of mouse thalamocortical relay neurons by modulating multiple modes of $GABA_A$ receptor-mediated inhibition. Eur J Neurosci 40:2487-2501.
Herrera CG, Cadavieco MC, Jego S, Ponomarenko A, Korotkova T, Adamantidis A (2016) Hypothalamic feedforward inhibition of thalamocortical network controls arousal and consciousness. Nat Neurosci 19:290-298.
Hirsch JC, Fourment A, Marc ME (1983) Sleep-related variations of membrane potential in the lateral geniculate body relay neurons of the cat. Brain Res 259:308-312.
Hou G, Smith AG, Zhang ZW (2016) Lack of Intrinsic GABAergic Connections in the Thalamic Reticular Nucleus of the Mouse. J Neurosci 36:7246-7252.
Houser CR, Vaughn JE, Barber RP, Roberts E (1980) GABA neurons are the major cell type of the nucleus reticularis thalami. Brain Res 200:341-354.
Huber R, Ghilardi MF, Massimini M, Ferrarelli F, Riedner BA, Peterson MJ, Tononi G (2006) Arm immobilization causes cortical plastic changes and locally decreases sleep slow wave activity. Nat Neurosci 9:1169-1176.
Huguenard JR, McCormick DA (2007) Thalamic synchrony and dynamic regulation of global forebrain oscillations. Trends Neurosci 30:350-356.
Hunt CA, Pang DZ, Jones EG (1991) Distribution and density of GABA cells in intralaminar and adjacent nuclei of monkey thalamus. Neuroscience 43:185-196.
Irwin MR (2015) Why sleep is important for health: a psychoneuroimmunology perspective. Annu Rev Psychol 66:143-172.
James MH, Charnley JL, Flynn JR, Smith DW, Dayas CV (2011) Propensity to 'relapse' following exposure to cocaine cues is associated with the recruitment of specific thalamic and epithalamic nuclei. Neuroscience 199:235-242.
John YJ, Zikopoulos B, Bullock D, Barbas H (2016) The Emotional Gatekeeper: A Computational Model of Attentional Selection and Suppression through the Pathway from the Amygdala to the Inhibitory Thalamic Reticular Nucleus. PLoS Comput Biol 12:e1004722.
Jones EG (1975) Some aspects of the organization of the thalamic reticular complex. J Comp Neurol 162:285-308.
Kaneko T, Tashiro K, Sugimoto T, Konishi A, Mizuno N (1985) Identification of thalamic neurons with vasoactive intestinal polypeptide-like immunoreactivity in the rat. Brain Res 347:390-393.

Kattler H, Dijk DJ, Borbély AA (1994) Effect of unilateral somatosensory stimulation prior to sleep on the sleep EEG in humans. J Sleep Res 3:159-164.
Kenigfest N, Belekhova M, Reperant J, Rio JP, Ward R, Vesselkin N (2005) The turtle thalamic anterior entopeduncular nucleus shares connectional and neurochemical characteristics with the mammalian thalamic reticular nucleus. J Chem Neuroanat 30:129-143.
Kimura A (2014) Diverse subthreshold cross-modal sensory interactions in the thalamic reticular nucleus: implications for new pathways of cross-modal attentional gating function. Eur J Neurosci 39:1405-1418.
Kimura A, Yokoi I, Imbe H, Donishi T, Kaneoke Y (2012) Distinctions in burst spiking between thalamic reticular nucleus cells projecting to the dorsal lateral geniculate and lateral posterior nuclei in the anesthetized rat. Neuroscience 226:208-226.
Kölliker A (1889) Handbuch der Gewebelehre des Menschen, 6th Edition.
Krause M, Hoffmann WE, Hajos M (2003) Auditory sensory gating in hippocampus and reticular thalamic neurons in anesthetized rats. Biol Psychiatry 53:244-253.
Krol A, Wimmer RD, Halassa MM, Feng G (2018) Thalamic reticular dysfunction as a circuit endophenotype in neurodevelopmental disorders. Neuron 98:282-295.
Kultas-Ilinsky K, Yi H, Ilinsky IA (1995) Nucleus reticularis thalami input to the anterior thalamic nuclei in the monkey: a light and electron microscopic study. Neurosci Lett 186:25-28.
Landisman CE, Long MA, Beierlein M, Deans MR, Paul DL, Connors BW (2002) Electrical synapses in the thalamic reticular nucleus. J Neurosci 22:1002-1009.
Lechan RM, Wu P, Jackson IM (1987) Immunocytochemical distribution in rat brain of putative peptides derived from thyrotropin-releasing hormone prohormone. Endocrinology 121:1879-1891.
Lee SH, Govindaiah G, Cox CL (2007) Heterogeneity of firing properties among rat thalamic reticular nucleus neurons. J Physiol 582:195-208.
Lee SM, Friedberg MH, Ebner FF (1994) The role of GABA-mediated inhibition in the rat ventral posterior medial thalamus. I. Assessment of receptive field changes following thalamic reticular nucleus lesions. J Neurophysiol 71:1702-1715.
Liu J, Zhang MQ, Wu X, Lazarus M, Cherasse Y, Yuan MY, Huang ZL, Li RX (2017) Activation of Parvalbumin Neurons in the Rostro-Dorsal Sector of the Thalamic Reticular Nucleus Promotes Sensitivity to Pain in Mice. Neuroscience 366:113-123.
Lizier C, Spreafico R, Battaglia G (1997) Calretinin in the thalamic reticular nucleus of the rat: distribution and relationship with ipsilateral and contralateral efferents. J Comp Neurol 377:217-233.
Loureiro M, Cholvin T, Lopez J, Merienne N, Latreche A, Cosquer B, Geiger K, Kelche C, Cassel JC, Pereira de Vasconcelos A (2012) The ventral midline thalamus (reuniens and rhomboid nuclei) contributes to the persistence of spatial memory in rats. J Neurosci 32:9947-9959.
Lozsádi DA (1994) Organization of cortical afferents to the rostral, limbic sector of the rat thalamic reticular nucleus. J Comp Neurol 341:520-533.
Lozsádi DA (1995) Organization of connections between the thalamic reticular and the anterior thalamic nuclei in the rat. J Comp Neurol 358:233-246.
Lübke J (1993) Morphology of neurons in the thalamic reticular nucleus (TRN) of mammals as revealed by intracellular injections into fixed brain slices. J Comp Neurol 329:458-471.
Mackiewicz M, Shockley KR, Romer MA, Galante RJ, Zimmerman JE, Naidoo N, Baldwin DA, Jensen ST, Churchill GA, Pack AI (2007) Macromolecule biosynthesis: a key function of sleep. Physiol Genomics 31:441-457.
Makinson CD, Tanaka BS, Sorokin JM, Wong JC, Christian CA, Goldin AL, Escayg A, Huguenard JR (2017) Regulation of thalamic and cortical network synchrony by Scn8a. Neuron 93:1165-1179
McAlonan K, Brown VJ (2002) The thalamic reticular nucleus: more than a sensory nucleus? Neuroscientist 8:302-305.
McAlonan K, Brown VJ, Bowman EM (2000) Thalamic reticular nucleus activation reflects attentional gating during classical conditioning. J Neurosci 20:8897-8901.

McCormick DA (1992) Neurotransmitter actions in the thalamus and cerebral cortex and their role in neuromodulation of thalamocortical activity. Prog Neurobiol 39:337-388.
McCormick DA, Pape HC (1990) Properties of a hyperpolarization-activated cation current and its role in rhythmic oscillation in thalamic relay neurones. J Physiol 431:291-318.
McCormick DA, Bal T (1997) Sleep and arousal: thalamocortical mechanisms. Annu Rev Neurosci 20:185-215.
McKenna JT, Vertes RP (2004) Afferent projections to nucleus reuniens of the thalamus. J Comp Neurol 480:115-142.
Mitrofanis J (1992a) Calbindin immunoreactivity in a subset of cat thalamic reticular neurons. J Neurocytol 21:495-505.
Mitrofanis J (1992b) Patterns of antigenic expression in the thalamic reticular nucleus of developing rats. J Comp Neurol 320:161-181.
Mizumori SJ, Miya DY, Ward KE (1994) Reversible inactivation of the lateral dorsal thalamus disrupts hippocampal place representation and impairs spatial learning. Brain Res 644:168-174.
Molinari M, Hendry SH, Jones EG (1987) Distributions of certain neuropeptides in the primate thalamus. Brain Res 426:270-289.
Montero VM (1997) c-fos induction in sensory pathways of rats exploring a novel complex environment: shifts of active thalamic reticular sectors by predominant sensory cues. Neuroscience 76:1069-1081.
Montero VM (1999) Amblyopia decreases activation of the corticogeniculate pathway and visual thalamic reticularis in attentive rats: a 'focal attention' hypothesis. Neuroscience 91:805-817.
Montero VM (2000) Attentional activation of the visual thalamic reticular nucleus depends on 'top-down' inputs from the primary visual cortex via corticogeniculate pathways. Brain Res 864:95-104.
Montero VM, Guillery RW, Woolsey CN (1977) Retinotopic organization within the thalamic reticular nucleus demonstrated by a double label autoradiographic technique. Brain Res 138:407-421.
Morris BJ (1989) Neuronal localisation of neuropeptide Y gene expression in rat brain. J Comp Neurol 290:358-368.
Mueller T (2012) What is the Thalamus in Zebrafish? Front Neurosci 6:64.
Mulle C, Madariaga A, Deschênes M (1986) Morphology and electrophysiological properties of reticularis thalami neurons in cat: in vivo study of a thalamic pacemaker. J Neurosci 6:2134-2145.
Münzer E, Wiener H (1902) Das Zwischen- und Mittelhirn des Kaninchens und die Beziehungen dieser Teile zum übrigen Centralnervensystem, mit besonderer Berücksichtigung der Pyramidenbahn und Schleife. MschrPsychiatNeurol 12:241-259.
Nakahara K, Fukui K, Murakami N (2004) Involvement of thalamic paraventricular nucleus in the anticipatory reaction under food restriction in the rat. J Vet Med Sci 66:1297-1300.
Nuñez A, Curró Dossi R, Contreras D, Steriade M (1992) Intracellular evidence for incompatibility between spindle and delta oscillations in thalamocortical neurons of cat. Neuroscience 48:75-85.
O'Keefe J, Dostrovsky J (1971) The hippocampus as a spatial map. Preliminary evidence from unit activity in the freely-moving rat. Brain Res 34:171-175.
Oertel WH, Graybiel AM, Mugnaini E, Elde RP, Schmechel DE, Kopin IJ (1983) Coexistence of glutamic acid decarboxylase- and somatostatin-like immunoreactivity in neurons of the feline nucleus reticularis thalami. J Neurosci 3:1322-1332.
Ohara PT, Lieberman AR (1985) The thalamic reticular nucleus of the adult rat: experimental anatomical studies. J Neurocytol 14:365-411.
Ohara PT, Havton LA (1996) Dendritic arbors of neurons from different regions of the rat thalamic reticular nucleus share a similar orientation. Brain Res 731:236-240.
Olivéras JL, Montagne-Clavel J (1994) The GABAA receptor antagonist picrotoxin induces a 'pain-like' behavior when administered into the thalamic reticular nucleus of the behaving rat: a possible model for 'central' pain? Neurosci Lett 179:21-24.

Osaki H, Naito T, Soma S, Sato H (2018) Receptive field properties of cat perigeniculate neurons correlate with excitatory and inhibitory connectivity to LGN relay neurons. Neurosci Res 132:26-36.
Ottersen OP, Storm-Mathisen J (1984) GABA-containing neurons in the thalamus and pretectum of the rodent. An immunocytochemical study. Anat Embryol (Berl) 170:197-207.
Paré D, Steriade M (1993) The reticular thalamic nucleus projects to the contralateral dorsal thalamus in macaque monkey. Neurosci Lett 154:96-100.
Paré D, Dossi RC, Steriade M (1991) Three types of inhibitory postsynaptic potentials generated by interneurons in the anterior thalamic complex of cat. J Neurophysiol 66:1190-1204.
Paré D, Steriade M, Deschênes M, Oakson G (1987) Physiological characteristics of anterior thalamic nuclei, a group devoid of inputs from reticular thalamic nucleus. J Neurophysiol 57:1669-1685.
Paré D, Hazrati LN, Parent A, Steriade M (1990) Substantia nigra pars reticulata projects to the reticular thalamic nucleus of the cat: a morphological and electrophysiological study. Brain Res 535:139-146.
Penny GR, Conley M, Schmechel DE, Diamond IT (1984) The distribution of glutamic acid decarboxylase immunoreactivity in the diencephalon of the opossum and rabbit. J Comp Neurol 228:38-56.
Perez-Reyes E (2003) Molecular physiology of low-voltage-activated T-type calcium channels. Physiol Rev 83:117-161.
Peyrache A, Lacroix MM, Petersen PC, Buzsaki G (2015) Internally organized mechanisms of the head direction sense. Nat Neurosci 18:569-575.
Peyrache A, Duszkiewicz AJ, Viejo G, Angeles-Duran S (2019) Thalamocortical processing of the head-direction sense. Prog Neurobiol:101693.
Pinault D (2004) The thalamic reticular nucleus: structure, function and concept. Brain Res Brain Res Rev 46:1-31.
Pinault D, Deschênes M (1998) Projection and innervation patterns of individual thalamic reticular axons in the thalamus of the adult rat: a three-dimensional, graphic, and morphometric analysis. J Comp Neurol 391:180-203.
Pinault D, Bourassa J, Deschênes M (1995a) The axonal arborization of single thalamic reticular neurons in the somatosensory thalamus of the rat. Eur J Neurosci 7:31-40.
Pinault D, Bourassa J, Deschênes M (1995b) Thalamic reticular input to the rat visual thalamus: a single fiber study using biocytin as an anterograde tracer. Brain Res 670:147-152.
Pollin B, Rokyta R (1982) Somatotopic organization of nucleus reticularis thalami in chronic awake cats and monkeys. Brain Res 250:211-221.
Pritz MB (2018) Thalamic Reticular Nucleus in Caiman crocodilus: Immunohistochemical Staining. Brain Behav Evol 92:142-166.
Ramcharan EJ, Gnadt JW, Sherman SM (2000) Burst and tonic firing in thalamic cells of unanesthetized, behaving monkeys. Vis Neurosci 17:55-62.
Raos V, Bentivoglio M (1993) Crosstalk between the two sides of the thalamus through the reticular nucleus: a retrograde and anterograde tracing study in the rat. J Comp Neurol 332:145-154.
Requena V, Diaz F, Villena A, Vidal L, Perez de Vargas I (1991) Histoenzymatic study of the neurons in the visual sector of the thalamic reticular nucleus in the adult rat. J Hirnforsch 32:459-467.
Roland BL, Sutton SW, Wilson SJ, Luo L, Pyati J, Huvar R, Erlander MG, Lovenberg TW (1999) Anatomical distribution of prolactin-releasing peptide and its receptor suggests additional functions in the central nervous system and periphery. Endocrinology 140:5736-5745.
Rovó Z, Mátyás F, Barthó P, Slézia A, Lecci S, Pellegrini C, Astori S, Dávid C, Hangya B, Lüthi A, Acsády L (2014) Phasic, nonsynaptic GABA-A receptor-mediated inhibition entrains thalamocortical oscillations. J Neurosci 34:7137-7147.
Sanchez-Vives MV, Bal T, McCormick DA (1997) Inhibitory interactions between perigeniculate GABAergic neurons. J Neurosci 17:8894-8908.
Scheibel ME, Scheibel AB (1966) The organization of the nucleus reticularis thalami: a Golgi study. Brain Res 1:43-62.

Segerson TP, Hoefler H, Childers H, Wolfe HJ, Wu P, Jackson IM, Lechan RM (1987) Localization of thyrotropin-releasing hormone prohormone messenger ribonucleic acid in rat brain in situ hybridization. Endocrinology 121:98-107.
Sherman SM (1996) Dual response modes in lateral geniculate neurons: mechanisms and functions. Vis Neurosci 13:205-213.
Sherman SM (2017) Functioning of circuits connecting thalamus and cortex. Compr Physiol 7:713-739.
Sherman SM, Guillery RW (1996) Functional organization of thalamocortical relays. J Neurophysiol 76:1367-1395.
Sherman SM, Guillery RW (1998) On the actions that one nerve cell can have on another: distinguishing "drivers" from "modulators". Proc Natl Acad Sci U S A 95:7121-7126.
Shibata H (1992) Topographic organization of subcortical projections to the anterior thalamic nuclei in the rat. J Comp Neurol 323:117-127.
Shosaku A (1985) A comparison of receptive field properties of vibrissa neurons between the rat thalamic reticular and ventro-basal nuclei. Brain Res 347:36-40.
Shosaku A, Sumitomo I (1983) Auditory neurons in the rat thalamic reticular nucleus. Exp Brain Res 49:432-442.
Shosaku A, Kayama Y, Sumitomo I (1984) Somatotopic organization in the rat thalamic reticular nucleus. Brain Res 311:57-63.
Shu Y, McCormick DA (2002) Inhibitory interactions between ferret thalamic reticular neurons. J Neurophysiol 87:2571-2576.
Simonnet J, Fricker D (2018) Cellular components and circuitry of the presubiculum and its functional role in the head direction system. Cell Tissue Res 373:541-556.
Simonnet J, Nassar M, Stella F, Cohen I, Mathon B, Boccara CN, Miles R, Fricker D (2017) Activity dependent feedback inhibition may maintain head direction signals in mouse presubiculum. Nat Commun 8:16032.
Soltesz I, Lightowler S, Leresche N, Jassik-Gerschenfeld D, Pollard CE, Crunelli V (1991) Two inward currents and the transformation of low-frequency oscillations of rat and cat thalamocortical cells. J Physiol 441:175-197.
Soto-Sanchez C, Wang X, Vaingankar V, Sommer FT, Hirsch JA (2017) Spatial scale of receptive fields in the visual sector of the cat thalamic reticular nucleus. Nat Commun 8:800.
Sporns O, Tononi G, Edelman GM (2000) Connectivity and complexity: the relationship between neuroanatomy and brain dynamics. Neural Netw 13:909-922.
Spreafico R, Battaglia G, Frassoni C (1991) The reticular thalamic nucleus (RTN) of the rat: cytoarchitectural, Golgi, immunocytochemical, and horseradish peroxidase study. J Comp Neurol 304:478-490.
Stehberg J, Acuna-Goycolea C, Ceric F, Torrealba F (2001) The visceral sector of the thalamic reticular nucleus in the rat. Neuroscience 106:745-755.
Steriade M (2006) Grouping of brain rhythms in corticothalamic systems. Neuroscience 137:1087-1106.
Steriade M, Llinas RR (1988) The functional states of the thalamus and the associated neuronal interplay. Physiol Rev 68:649-742.
Steriade M, Parent A, Hada J (1984) Thalamic projections of nucleus reticularis thalami of cat: a study using retrograde transport of horseradish peroxidase and fluorescent tracers. J Comp Neurol 229:531-547.
Steriade M, Domich L, Oakson G (1986) Reticularis thalami neurons revisited: activity changes during shifts in states of vigilance. J Neurosci 6:68-81.
Steriade M, McCormick DA, Sejnowski TJ (1993) Thalamocortical oscillations in the sleeping and aroused brain. Science 262:679-685.
Steullet P, Cabungcal JH, Bukhari SA, Ardelt MI, Pantazopoulos H, Hamati F, Salt TE, Cuenod M, Do KQ, Berretta S (2017) The thalamic reticular nucleus in schizophrenia and bipolar disorder: role of parvalbumin-expressing neuron networks and oxidative stress. Mol Psychiatry.

Swadlow HA, Gusev AG (2001) The impact of 'bursting' thalamic impulses at a neocortical synapse. Nat Neurosci 4:402-408.
Taube JS (1995) Head direction cells recorded in the anterior thalamic nuclei of freely moving rats. J Neurosci 15:70-86.
Taube JS, Kesslak JP, Cotman CW (1992) Lesions of the rat postsubiculum impair performance on spatial tasks. Behav Neural Biol 57:131-143.
Thankachan S, Katsuki F, McKenna JT, Yang C, Shukla C, Deisseroth K, Uygun DS, Strecker RE, Brown RE, McNally JM, Basheer R (2019) Thalamic Reticular Nucleus Parvalbumin Neurons Regulate Sleep Spindles and Electrophysiological Aspects of Schizophrenia in Mice. Sci Rep 9:3607.
Van der Werf YD, Witter MP, Groenewegen HJ (2002) The intralaminar and midline nuclei of the thalamus. Anatomical and functional evidence for participation in processes of arousal and awareness. Brain Res Brain Res Rev 39:107-140.
Vann SD, Aggleton JP, Maguire EA (2009) What does the retrosplenial cortex do? Nat Rev Neurosci 10:792-802.
Vantomme G, Osorio-Forero A, Luthi A, Fernandez LMJ (2019) Regulation of Local Sleep by the Thalamic Reticular Nucleus. Front Neurosci 13:576.
Vertes RP, Albo Z, Viana Di Prisco G (2001) Theta-rhythmically firing neurons in the anterior thalamus: implications for mnemonic functions of Papez's circuit. Neuroscience 104:619-625.
Vertes RP, Hoover WB, Rodriguez JJ (2012) Projections of the central medial nucleus of the thalamus in the rat: node in cortical, striatal and limbic forebrain circuitry. Neuroscience 219:120-136.
Vertes RP, Linley SB, Hoover WB (2015) Limbic circuitry of the midline thalamus. Neurosci Biobehav Rev 54:89-107.
Viejo G, Peyrache A (2019) Precise coupling of the thalamic head-direction system to hippocampal ripples. bioRxiv.
von Cramon DY, Hebel N, Schuri U (1985) A contribution to the anatomical basis of thalamic amnesia. Brain 108 ( Pt 4):993-1008.
Vorster AP, Born J (2015) Sleep and memory in mammals, birds and invertebrates. Neurosci Biobehav Rev 50:103-119.
Vyazovskiy V, Borbély AA, Tobler I (2000) Unilateral vibrissae stimulation during waking induces interhemispheric EEG asymmetry during subsequent sleep in the rat. J Sleep Res 9:367-371.
Walton KD, Llinas RR (2010) Central Pain as a Thalamocortical Dysrhythmia: A Thalamic Efference Disconnection? In: Translational Pain Research: From Mouse to Man (Kruger L, Light AR, eds). Boca Raton, FL.
Weese GD, Phillips JM, Brown VJ (1999) Attentional orienting is impaired by unilateral lesions of the thalamic reticular nucleus in the rat. J Neurosci 19:10135-10139.
Wells MF, Wimmer RD, Schmitt LI, Feng G, Halassa MM (2016) Thalamic reticular impairment underlies attention deficit in *Ptchd1*$^{Y/-}$ mice. Nature 532:58-63.
Wimmer RD, Schmitt LI, Davidson TJ, Nakajima M, Deisseroth K, Halassa MM (2015) Thalamic control of sensory selection in divided attention. Nature 526:705-709.
Winter SS, Taube JS (2014) Head Direction Cells: From Generation to Integration. In: Space,Time and Memory in the Hippocampal Formation (Derdikman D, Knierim J, eds), pp 83-106. Vienna: Springer.
Xie L, Kang H, Xu Q, Chen MJ, Liao Y, Thiyagarajan M, O'Donnell J, Christensen DJ, Nicholson C, Iliff JJ, Takano T, Deane R, Nedergaard M (2013) Sleep drives metabolite clearance from the adult brain. Science 342:373-377.
Yoder RM, Taube JS (2014) The vestibular contribution to the head direction signal and navigation. Front Integr Neurosci 8:32.
Yu XJ, Xu XX, He S, He J (2009) Change detection by thalamic reticular neurons. Nat Neurosci 12:1165-1170.
Zikopoulos B, Barbas H (2006) Prefrontal projections to the thalamic reticular nucleus form a unique circuit for attentional mechanisms. J Neurosci 26:7348-7361.

Zikopoulos B, Barbas H (2007) Circuits formultisensory integration and attentional modulation through the prefrontal cortex and the thalamic reticular nucleus in primates. Rev Neurosci 18:417-438.
Zikopoulos B, Barbas H (2012) Pathways for emotions and attention converge on the thalamic reticular nucleus in primates. J Neurosci 32:5338-5350.

# I. Articles

## Study 1:

## A thalamic reticular circuit for head direction cell tuning and spatial navigation

Gil Vantomme, Zita Rovó, Romain Cardis, Elidie Béard, Georgia Katsioudi, Angelo Guadagno, Virginie Perrenoud, Laura MJ Fernandez, Anita Lüthi, *in revision Cell Reports*

## Study 2:

## Thalamic reticular control of local sleep in mouse sensory cortex, eLife

Laura MJ Fernandez, Gil Vantomme, Alejandro Osorio-Forero, Romain Cardis, Elidie Béard, Anita Lüthi, eLife 2018;7:e39111, DOI: 10.7554/eLife.39111, 25.12.2018

# A thalamic reticular circuit for head direction cell tuning and spatial navigation

**Authors:** Gil Vantomme, Zita Rovó, Romain Cardis, Elidie Béard, Georgia Katsioudi, Angelo Guadagno, Virginie Perrenoud, Laura MJ Fernandez, Anita Lüthi*

*Lead contact

**Affiliations:** Department of Fundamental Neurosciences, University of Lausanne, Rue du Bugnon 9, 1005 Lausanne, Vaud, Switzerland

## Summary

To navigate in space, an animal must reference external sensory landmarks to the spatial orientation of its body and head. Circuit and synaptic mechanisms that integrate external cues with internal head-direction (HD) signals to drive navigational behavior remain, however, poorly described. We identify an excitatory synaptic projection from the presubiculum and retrosplenial cortex to the anterodorsalmost sector of the thalamic reticular nucleus (TRN), so far classically implied in gating sensory information flow. Projections to TRN showed driver characteristics and involved AMPA/NMDA-type glutamate receptors that initiated TRN cell burst discharge and feedforward inhibition of anterior thalamic nuclei, where HD-tuned cells relevant for egocentric navigation reside. Chemogenetic anterodorsal TRN inhibition broadened the tuning of thalamic HD cells and compromised egocentric search strategies in the Morris water maze. Besides sensory gating, TRN-dependent thalamic inhibition is an integral part of limbic navigational circuits to recruit HD-cell-dependent search strategies during spatial navigation.

**Keywords**: Anterior thalamus; Retrosplenial cortex; Presubiculum; Allocentric; Egocentric; Synaptic inhibition; Burst discharge; Perseverance; Optogenetics; Chemogenetics

Correspondence: anita.luthi@unil.ch

## Introduction

Spatial navigation requires the ability to notice environmental landmarks, detect their sensory characteristics, and set these in relation to one's self-perceived direction, speed, and location. Cortex is a major site for spatial sensory processing and for creating internal representations of space based on one's own movement, location and body orientation to guide navigation. However, in the interest of survival, environmental cues may need to be detected rapidly to adapt navigational strategies without potentially time-consuming cortical elaboration. A major site for subcortical gating of sensory stimuli is the inhibitory thalamic reticular nucleus (TRN) that shows a unique anatomical positioning at the interface between sensory thalamic nuclei and cortex (Scheibel and Scheibel, 1966; Pinault, 2004; Crabtree, 2018). The significance of TRN in controlling sensory flow is now documented for the gain control of incoming sensory inputs (Le Masson et al., 2002), the sharpening of receptive fields (Lee et al., 1994; Soto-Sánchez et al., 2017), attentional modulation of monomodal (Halassa et al., 2014) or multimodal conflicting sensory inputs (Ahrens et al., 2015; Wimmer et al., 2015), and sensory induced escape (Dong et al., 2019).

In contrast to its role in sensory gating, the TRN has not been implied in the gating of internal signals that underlie one's sense of orientation in space. Lesion studies, however, suggest that TRN contributes to covertly directing a rat's self-orientation to the target stimulus, such that orienting movements can be rapidly executed (Weese et al., 1999). Moreover, anterior thalamic nuclei (ATN) are part of the brain's navigational system (Dumont and Taube, 2015), and there is anatomical evidence in rodent that anterodorsal TRN innervates ATN (Scheibel and Scheibel, 1966; Gonzalo-Ruiz and Lieberman, 1995b, a; Lozsádi, 1995; Pinault and Deschênes, 1998), although this has been questioned in cat (Paré et al., 1987). The anterodorsal (AD) thalamic nucleus, part of the ATN, contains a large proportion of HD cells tuned to the direction of the rodent's head in space (Taube, 1995), which serve as an egocentric, self-centered compass during navigation (van der Meer et al., 2010; Butler et al., 2017). Although the TRN has been proposed to be part of HD circuits (Peyrache et al., 2019), the underlying functional anatomy remains elusive. Possible equivalences and differences to the canonical sensory TRN-thalamocortical circuits thus remain speculative and possible roles for TRN in the gating of HD and spatial navigation signals have not been clarified. Here, we hypothesized that if the TRN is to mediate subcortical sensory gating effectively, it should serve as an entry point for information flow to ATN to control the processing of HD signals.

The anterior thalamic HD representation is controlled by external visual landmarks through input from the dorsal presubiculum (dPreS) (Goodridge and Taube, 1997) and the retrosplenial cortex

(RSC) (Clark et al., 2010). Both areas are reciprocally connected (van Groen and Wyss, 1990) and receive afferents from ATN, primary and secondary visual cortex, integrating information relevant for egocentric and allocentric, external cue-guided, navigation (Dumont and Taube, 2015; Clark et al., 2018; Mitchell et al., 2018; Simonnet and Fricker, 2018). Behaviorally, lesion of dPreS compromises rapid orienting behaviors based on landmarks (Yoder et al., 2019), whereas RSC lesions lead to multiple deficits in spatial navigation and memory formation (Clark et al., 2018; Mitchell et al., 2018). Although there is evidence for a topographically organized cortical feedback from RSC to rat and monkey anterodorsal TRN (Cornwall et al., 1990; Lozsádi, 1994; Zikopoulos and Barbas, 2007), the nature of this cortico-thalamic communication has never been characterized. Indeed, current models of HD circuits involving ATN, dPreS and RSC (Dumont and Taube, 2015; Peyrache et al., 2017; Simonnet and Fricker, 2018; Perry and Mitchell, 2019) and of the brain's 'limbic' navigational system (Bubb et al., 2017) largely disregard a functionally integrated TRN. In spite of this gap of knowledge, the notion of a limbic anterior TRN has been proposed recently (Zikopoulos and Barbas, 2012; Halassa et al., 2014).

In this study, we combined tracing techniques, *in vitro* and *in vivo* electrophysiological recordings together with a spatial navigation task to probe the synaptic integration and the function of TRN in the communication between PreS, RSC and ATN.

# Results

## RSC and PreS send topographically organized projections to ATN and TRN

To determine afferent projection to the anterodorsal portion of the TRN, we injected small volumes (50-100 nl) of red retrobeads into anterodorsal TRN of C57BL6/J mice (4-8-week-old) and identified sites of red punctate fluorescent labeling 5 – 7 days later. Five out of 19 injections were restricted to the anterior TRN in its dorsalmost portion, as verified by parvalbumin (PV)-immunostaining of the TRN (Fig. 1A1). Punctate labeling clearly separated from the injection site was found in the adjacent anterodorsal (AD), laterodorsal (LD) and in the centrolateral (CL) nuclei (Fig. 1A2, Suppl. Fig. 1), consistent with prior tracing studies (Gonzalo-Ruiz and Lieberman, 1995b, a; Lozsádi, 1995; Pinault and Deschênes, 1998). Labeling was also found in deep layers of prelimbic cortex that extended into infralimbic and cingulate, and, in two cases, into motor cortical areas, consistent again with a previous study in rat (Lozsádi, 1994). Our attention was drawn to a distinct stretch of puncta extending from parahippocampal regions into RSC (Fig. 1A2). Labeling included in particular the deep layers of the PreS that is interposed between the subiculum, the parasubiculum and the RSC (Ding, 2013; Simonnet and Fricker, 2018).

93 We next used the anterograde tracer, *Phaseolus vulgaris*-leucoagglutinin (PHAL-L), to confirm
94 projections from RSC and PreS to anterior TRN. Through a panel of injections (n = 20) that
95 targeted restricted portions of RSC, dPreS and ventral PreS (vPreS) (Fig. 1B1), we noted a
96 nucleus-specific labelling pattern in the LD, AD, and anteroventral (AV) thalamus, which is also
97 part of ATN (Fig. 1B2). Injections centered within the RSC labeled large portions of AD and LD,
98 while sparing AV, whereas PreS-centered injections covered more restricted portions of LD, AD
99 and AV. vPreS injections labeled the most lateral portion of LD and AV. All labeled fibers arborized
100 within the most anterodorsal portions of TRN (Fig. 1B3), with fibers surrounding TRN cell bodies,
101 pointing towards putative synaptic connections.

102 **The PreS/RSC establishes functional excitatory synapses onto TRN**

103 We used whole-cell patch-clamp recordings to address the presence of functional connections
104 between PreS/RSC, anterodorsal TRN and ATN in acute coronal slices from brains of mice
105 injected with AAV1-CaMKIIa-ChR2-EYFP into PreS/RSC 3 – 5 weeks earlier (Fig. 2A). Cells
106 patched within anterodorsal TRN showed rebound burst behavior, as recognizable by repetitive
107 high-frequency bursts of action potentials after brief hyperpolarization, similar to posterior sensory
108 TRN cells (Fig. 2B) (Fernandez et al., 2018). Electrical properties were also similar to those of
109 their posterior counterparts (Fig. 2A-C), although cells produced less repetitive bursts (Fernandez
110 et al., 2018; Vantomme et al., 2019). Cells in AD, AV and LD showed properties typical for dorsal
111 thalamocortical neurons, notably the presence of only a single rebound burst discharge
112 (Huguenard, 1996) (Suppl. Fig. 2).

113 Optogenetic stimulation of PreS/RSC fibers was applied while recording from voltage-clamped
114 neurons of the anterodorsal TRN and of AD, AV and LD (Fig. 2D,E). The location of cells within
115 the different thalamic nuclei was evident while guiding the patch pipette to the target region and
116 was confirmed in a subgroup of cells through perfusion with neurobiotin and *post-hoc* recovery
117 (n=33/106) (Fig. 2D1). Rapid synaptic inward currents were elicited in all responsive cells (Fig.
118 2D2). The connectivity, quantified based on the presence of such synaptic currents in the
119 complete set of recorded cells, was > 80 % for all areas (Fig. 2D3). Synaptic currents were time-
120 locked to the stimulus, with a fixed and short latency to response onset and sub-millisecond jitter
121 (Fig. 2D4,D5). Response latency was inversely proportional to light intensity (Suppl. Fig. 2), which
122 is consistent with an action potential-dependent mode of synaptic transmission (Gjoni et al.,
123 2018). There is thus a direct, monosynaptic connection from PreS/RSC to anterodorsal TRN and
124 to AD, AV and LD.

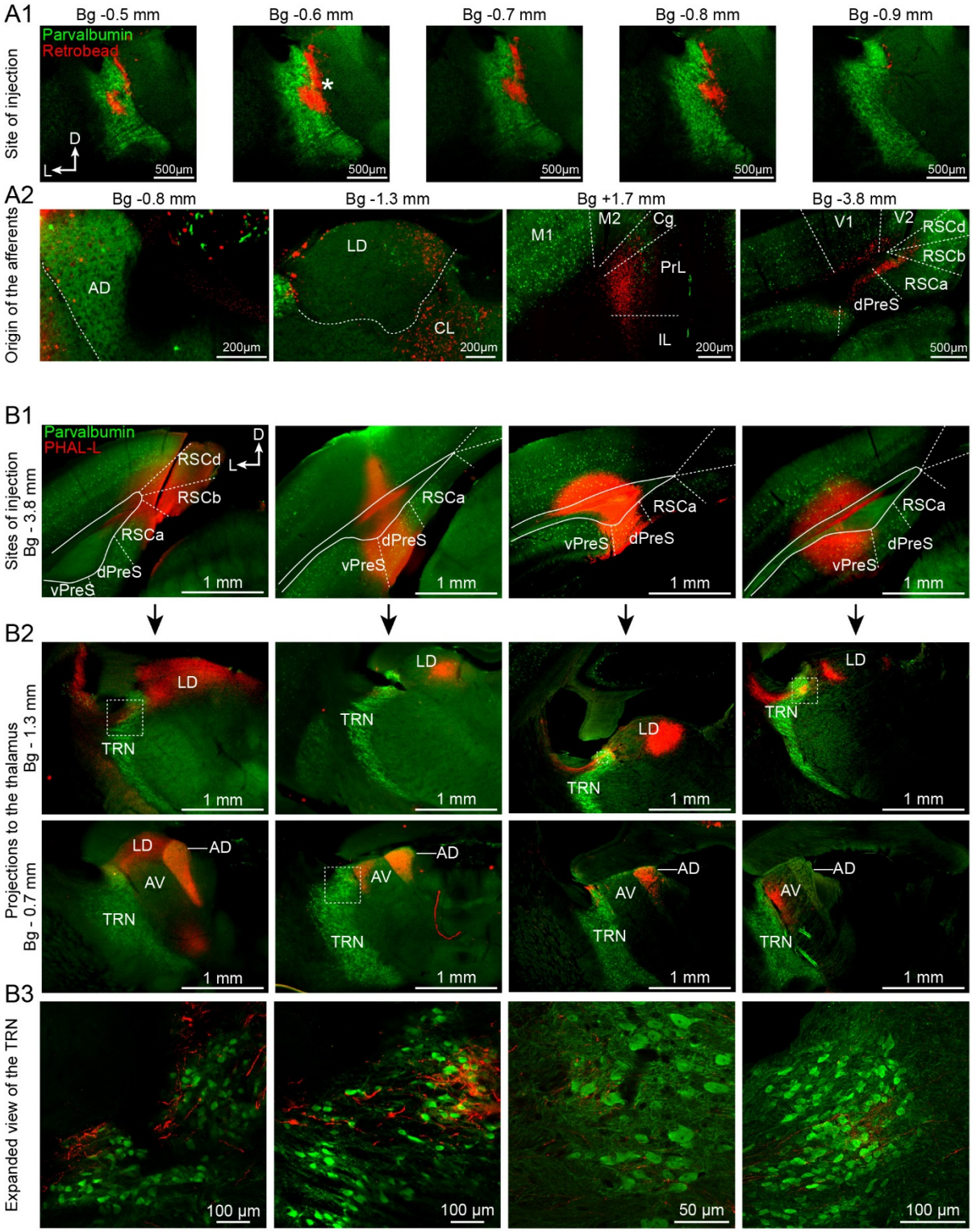
A1
Bg -0.5 mm
Bg -0.6 mm
Bg -0.7 mm
Bg -0.8 mm
Bg -0.9 mm
Parvalbumin
Retrobead
Site of injection
D
L
500μm
A2
Bg -0.8 mm
Bg -1.3 mm
Bg +1.7 mm
Bg -3.8 mm
Origin of the afferents
AD
LD
CL
M1
M2
Cg
PrL
IL
V1
V2
RSCd
RSCb
RSCa
dPreS
200μm
500μm
B1
Parvalbumin
PHAL-L
Sites of injection
Bg - 3.8 mm
RSCd
RSCb
RSCa
dPreS
vPreS
1 mm
B2
Projections to the thalamus
Bg - 1.3 mm
Bg - 0.7 mm
LD
TRN
AD
AV
B3
Expanded view of the TRN
100 μm
50 μm

127 **Figure 1. The RSC and the PreS send topographically organized projections to the anterior**
128 **thalamus and TRN.**

129 **(A1)** Epifluorescent micrographs of mouse coronal brain sections showing a retrobead (red)
130 injection site (*) into the anterior portion of the TRN, which spread ~300 µm along the
131 anteroposterior extent of the TRN (immunostained for PV, green). Bg, Bregma. **(A2)**
132 Epifluorescent micrographs showing retrogradely labeled brain regions. Anterodorsal thalamus
133 (AD) – Laterodorsal thalamus (LD) – Centrolateral thalamus (CL) – Cingulate cortex (Cg) –
134 Prelimbic/Infralimbic cortex (PreL/IL) – dorsal Presubiculum (dPreS) – Retrosplenial cortex (RSC)
135 – Visual cortex (V1/V2) – Motor cortex (M1/M2). **(B1)** Epifluorescent micrographs of 4 different
136 injection sites of PHAL-L (red) into (from left to right) RSC, PreS, dPreS and ventral PreS (vPreS).
137 Green, PV+ neurons. **(B2)** Epifluorescent micrographs of coronal sections in ATN at Bg -1.3 mm
138 (top) and -0.7 mm (middle). Note labeled fibers visible in the anterodorsal TRN (dotted squares).
139 **(B3)** Expanded confocal microscopy views of areas indicated by dotted squares in B2, AV,
140 anteroventral thalamus.

141

142 Light-evoked postsynaptic currents (EPSCs) were mediated by glutamatergic synaptic receptors,
143 as verified in a subset of 5 TRN and 5 neurons of AD, AV or LD (jointly referred to here as ATN+)
144 (Fig. 2E1). Thus, the AMPA receptor antagonist 6,7-Dinitroquinoxaline-2,3(1H,4H)-dione (DNQX,
145 40 µM, bath-application) reduced responses by > 90 % at -60 mV (Fig. 2E1,E2). The block was
146 not complete, suggesting activation of non-AMPA receptors. Indeed, a current component
147 sensitive to the NMDA receptor antagonist DL-2-Amino-5-phosphonovaleric acid (APV) was
148 detectable at +40 mV (Fig. 2E1, E2). NMDA/AMPA ratios were comparable to previous studies in
149 sensory TRN and thalamus (Fernandez et al., 2017). Moreover, the TRN-EPSCs had a twice-
150 shorter half-width than ATN+-EPSCs (Fig. 2E3) and a faster decay time (Fig. 2E4). PreS/RSC
151 inputs thus convey a phasic excitatory input onto anterodorsal TRN cells.

152 **PreS/RSC establishes strong unitary connections with driver characteristics onto**
153 **anterodorsal TRN**

154 TRN and ATN+ neurons were robustly innervated by PreS/RSC afferents, with compound EPSC
155 amplitudes ranging from -25 pA to -1157 pA at high light intensities, although there were nucleus-
156 specific differences (Fig. 3A). Both large and small EPSCs were obtained in slices from the same
157 animals, excluding variable viral transduction as a major reason for this variability. To assess how
158 variability was based on strength and connectivity of PreS/RSC afferents, we used minimal
159 optogenetic stimulation through reducing light intensity to variably evoke failures and successful
160 responses at comparable rates (mean failure rate 47±3 %) (Fig. 3B1). Unitary PreS/RSC EPSCs
161 of TRN cells were 4- to 5-fold larger than the ones established onto AD and AV cells (Fig. 3B2).
162 Dividing the maximally evoked EPSC amplitude by the unitary one, we calculated ranges of 1 –

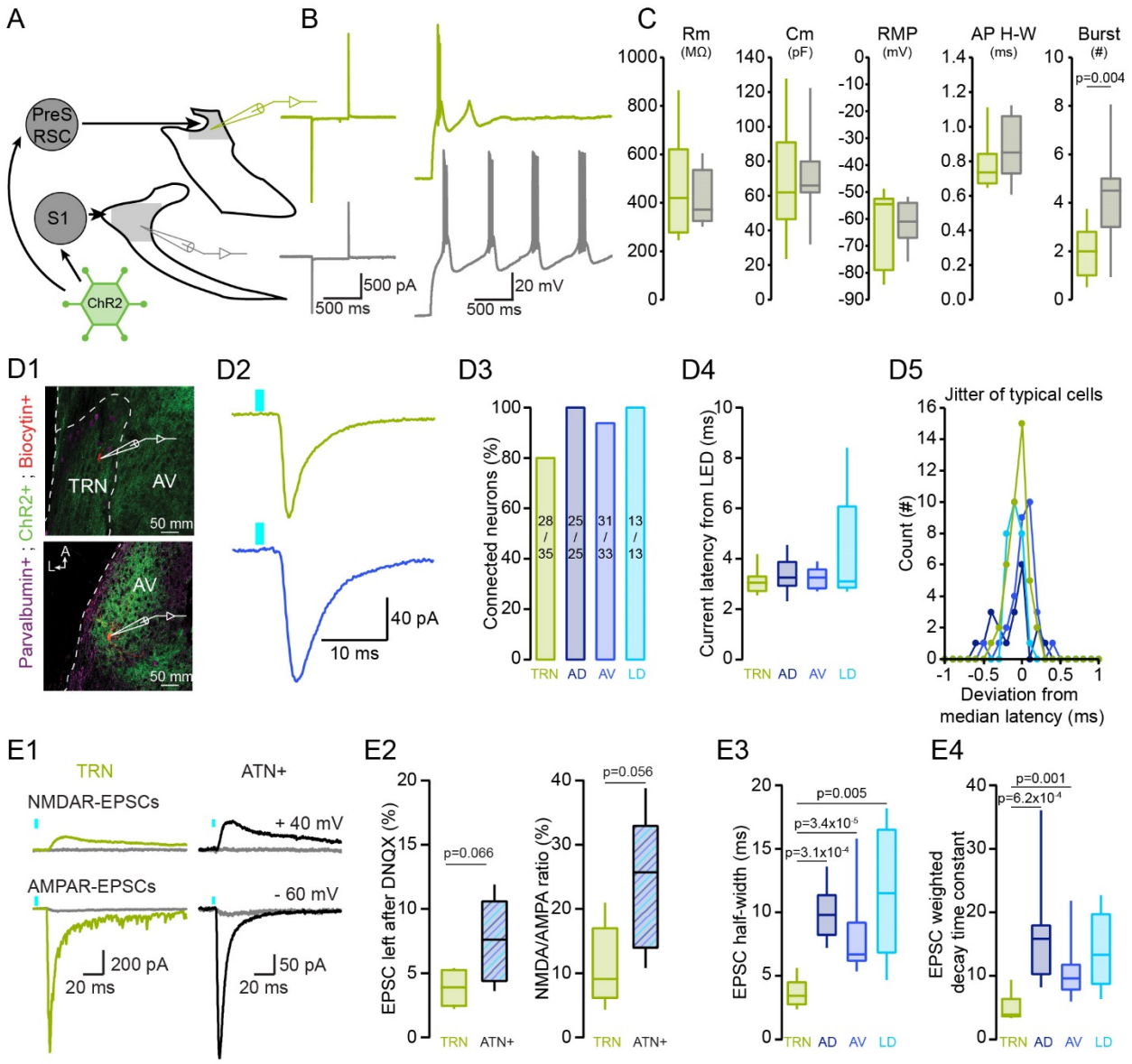


**Figure 2. The PreS/RSC establishes functional excitatory synapses onto TRN**

**(A)** Scheme of viral injections (AAV1-CamKIIa-ChR2-EYFP) into PreS/RSC or primary somatosensory cortex (S1) followed by whole-cell patch-clamp recordings. **(B)** Responses of a PreS/RSC-connected TRN neuron (green) and a S1-connected TRN neuron (grey) to a 10 mV hyperpolarizing step in voltage-clamp (Left) and to negative current injection in current-clamp (Right). **(C)** Box-and-whisker plots of cellular properties of PreS/RSC-connected (n = 16) and S1-connected TRN neurons (n = 11). From left to right: Membrane resistance (Rm), membrane capacitance (Cm), resting membrane potential (RMP), action potential (AP) half-width (H-W), burst number. Mann-Whitney U tests were used for comparing Rm, RMP and AP H-W, Student's *t* tests for Cm and Burst number. Data from S1-connected TRN neurons re-used from a previous study (Fernandez et al., 2018) **(D1)** Confocal micrographs of 300 µm-thick mouse brain sections showing the whole-cell recorded TRN (top) and AV (bottom) neurons filled with neurobiotin (red). Green, ChR2-EYFP-expressing PreS/RSC afferents, magenta, PV+ TRN cells. **(D2)** Current

177 responses of TRN (top) and AV (bottom) neurons to optogenetic activation (blue bars, 1 ms, 3.5
178 mW power, 455 nm) of PreS/RSC afferents, recorded at -60 mV. **(D3)** Connectivity histogram,
179 calculated as the fraction (in %) of neurons responding to optogenetic stimulation. **(D4)** Box-and-
180 whisker plot of response latencies (calculated from LED onset, 'from LED') in the TRN (n = 12),
181 AD (n = 16), AV (n = 16) and LD (n = 6). Mann-Whitney U tests and Bonferroni correction: α =
182 0.0083. **(D5)** Jitter of response latencies (deviation from mean) in one cell from TRN, AD, AV and
183 LD across all stimulation trials. **(E1)** Pharmacological analysis of typical evoked excitatory
184 postsynaptic currents (EPSCs) in TRN and ATN+, showing AMPA- and NMDA-EPSCs and their
185 suppression by DNQX (40 μM) and APV (100 μM), respectively (superimposed grey traces). **(E2)**
186 Box-and-whisker plots of DNQX effects (left, in % of original response amplitude, n = 5 for both
187 TRN and ATN+) and of NMDA/AMPA ratios (right). Values of p from Student's *t* tests. **(E3)** Box-
188 and-whisker plot of EPSC half-widths for TRN (n = 7), AD (n = 8), AV (n = 14) and LD (n = 5).
189 Mann-Whitney U tests and Bonferroni correction: α = 0.0083. Statistically significant p values are
190 indicated. **(E4)** Box-and-whisker plot of the EPSC weighted decay time constant in TRN (n = 7),
191 AD (n = 8), AV (n = 14) and LD (n = 5). Same statistical analysis as E3.

192

193 19 fibers for TRN, 2 – 32 fibers for AD and 8 – 86 fibers for AV. Therefore, although variable, TRN
194 cells are, on average, targeted by a comparatively small number of fibers, but each with greater
195 unitary strength. A large unitary response size has also been described for cortical projections
196 onto sensory TRN (Golshani et al., 2001; Gentet and Ulrich, 2004; Cruikshank et al., 2010). To
197 determine how many of these fibers were necessary to bring TRN cells to threshold for action
198 potential firing, we performed cell-attached patch-clamp recording to preserve cellular integrity
199 during PreS/RSC synaptic stimulation (Fig. 3C1). Action current numbers showed a steep
200 sigmoidal light dependence with half-maximal values reached at 0.63 mW (Fig. 3C2,C3).
201 Subsequent whole-cell mode recording in 5 out of 6 cells confirmed that these were bursts of
202 action potentials riding on a low-threshold calcium spike, which showed similar light dependence
203 (half-maximal number of action potentials at 0.92 mW) (Fig. 3C1,C3). In particular, at a light
204 intensity corresponding to the one used for minimal stimulation (0.19±0.02 mW), single spikes
205 were riding on triangularly shaped calcium spikes. Single or few active synaptic inputs from
206 PreS/RSC appear thus sufficient to bring TRN cells to threshold through reliable EPSP-low
207 threshold burst coupling.

208 Excitatory afferents into thalamus have been divided into 2 major groups, drivers and modulators
209 (Sherman, 2017). To determine the nature of PreS/RSC afferents, we determined paired-pulse
210 ratios (PPRs) of TRN-and ATN+-EPSCs. Under our ionic conditions, PPRs remained close to 1
211 until at least 10 Hz (Fig. 3D1,D2, Suppl. Fig. 3). When plotting results from individual experiments,
212 all data points clustered around 1 for 1-10 Hz, supporting a homogeneity of fibers. This short-term
213 plasticity profile is characteristic for a driver input onto anterodorsal TRN, which is contrary to the

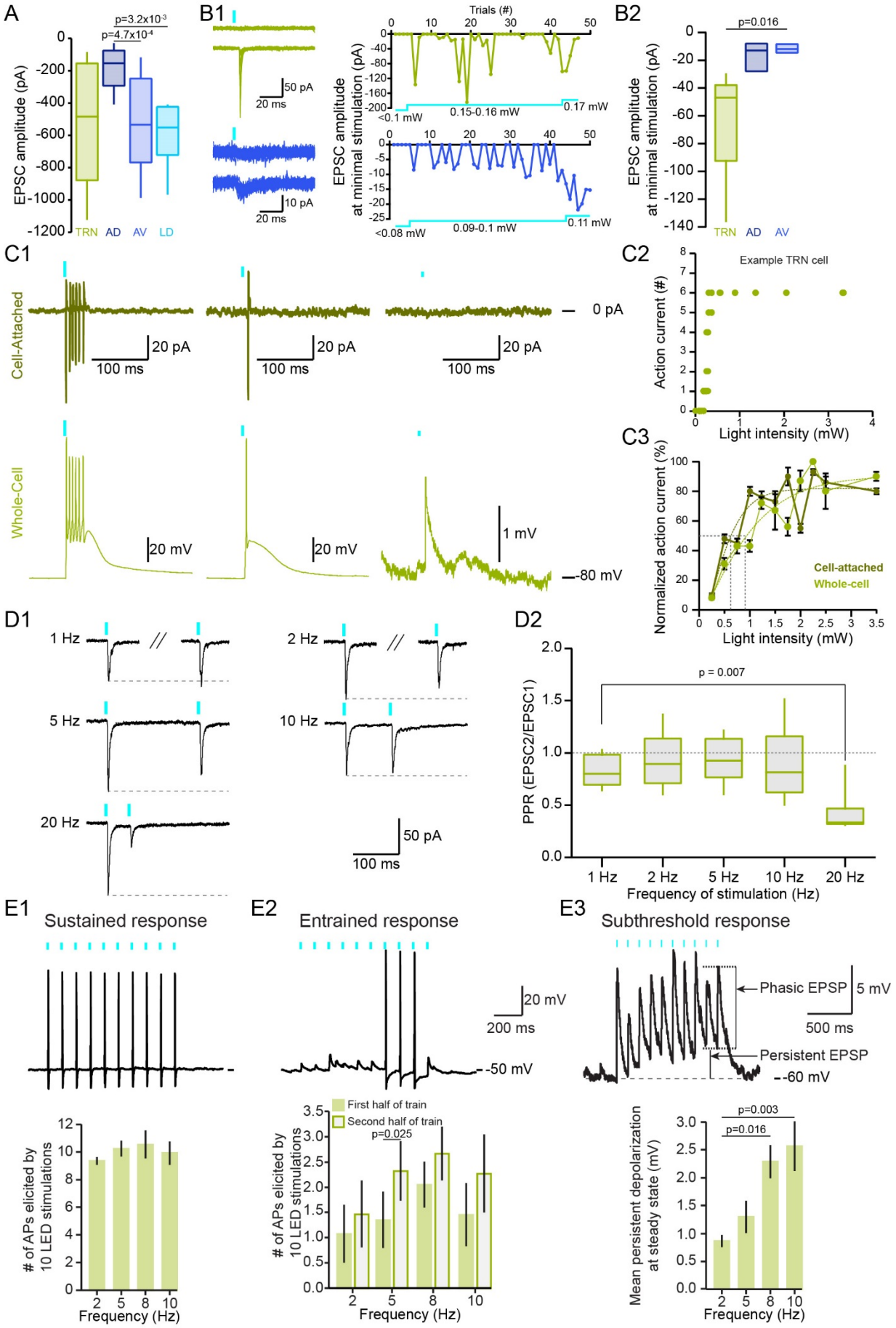
A
p=3.2x10-3
p=4.7x10-4
EPSC amplitude (pA)
TRN AD AV LD
B1
50 pA
20 ms
10 pA
20 ms
Trials (#)
EPSC amplitude at minimal stimulation (pA)
<0.1 mW
0.15-0.16 mW
0.17 mW
<0.08 mW
0.09-0.1 mW
0.11 mW
B2
p=0.016
TRN AD AV
C1
Cell-Attached
Whole-Cell
20 pA
100 ms
0 pA
20 mV
1 mV
-80 mV
C2
Example TRN cell
Action current (#)
Light intensity (mW)
C3
Normalized action current (%)
Cell-attached
Whole-cell
Light intensity (mW)
D1
1 Hz
5 Hz
20 Hz
2 Hz
10 Hz
50 pA
100 ms
D2
p = 0.007
PPR (EPSC2/EPSC1)
1 Hz 2 Hz 5 Hz 10 Hz 20 Hz
Frequency of stimulation (Hz)
E1
Sustained response
# of APs elicited by 10 LED stimulations
Frequency (Hz)
E2
Entrained response
20 mV
200 ms
-50 mV
First half of train
Second half of train
p=0.025
# of APs elicited by 10 LED stimulations
Frequency (Hz)
E3
Subthreshold response
Phasic EPSP
5 mV
500 ms
Persistent EPSP
-60 mV
p=0.003
p=0.016
Mean persistent depolarization at steady state (mV)
Frequency (Hz)

214

**Figure 3. The TRN receives strong unitary connections with driver characteristics from the PreS/RSC.**

**(A)** Box-and-whisker plot of maximally evoked compound EPSC amplitudes in TRN (n = 12), AD (n = 16), AV (n = 16), LD (n = 6). The intensity of the LED was reduced to ~20 % of the maximum in 4/16 AV and 4/6 LD cells to prevent escape currents. 1-factor ANOVA, $p = 1.25x10^{-3}$, post hoc Student's *t* tests with Bonferroni correction: α=0.0083. **(B1)** Minimal stimulation experiment. Left, overlay of successes and failures for a TRN and an AV neuron in one experiment. Right: Time course of the same experiment. Blue trace: intensity of the light stimulation. At minimal stimulation (0.15-0.16 mW for the TRN cell and 0.09-0.1 mW for the AV cell), the failure rate was ~50 % (22/39 failures for the TRN neuron, 20/39 failures for the AV neuron). Increasing the light intensity brought the failure rate to 0 % (right part of the graph). **(B2)** Box-and-whisker plot of the amplitude of successfully evoked unitary EPSCs in TRN (n = 5), AD (n = 3) and AV (n = 4). Repeated Mann-Whitney U tests with Bonferroni correction: α=0.017. **(C1)** Top: representative responses of a cell-attached TRN neuron recording exposed to maximal (left), intermediate (middle) and low (right) light intensities. Bottom: Same experiment in whole-cell current-clamp mode. **(C2)** Graph of action current number for the TRN neuron shown in C1. **(C3)** Same as in C2 for the average of all TRN neurons (cell-attached n = 6, whole-cell n = 5). Data were binned in 0.25 mW light steps. Action current number normalized to the maximum evoked in each neuron. **(D1)** RepresentativeTRN EPSCs at -60 mV upon paired-pulse stimulation at 1, 2, 5, 10 and 20 Hz. Grey dotted lines: amplitude of the first EPSC. **(D2)** Box-and-whisker plot of paired-pulse ratios (TRN: n = 16). Paired Student's t tests or Wilcoxon signed rank-test and Bonferroni correction: α = 0.013. **(E1)** Top: typical membrane voltage response of a TRN neuron to a 10 Hz-light stimulation train. Bottom: Histogram of means (n = 7). Wilcoxon signed rank-tests and Bonferroni correction: α = 0.017. **(E2)** Top: same as in E1 for neurons responding with a subthreshold response at train onset. Bottom: Histogram of means (n = 6). Wilcoxon signed rank-test (at 2 Hz) and Paired Student's *t* tests (at 5, 8, 10 Hz). **(E3)** Top: same as in E1 for subthreshold responses in a TRN neuron held at -60 mV. Bottom: Histogram of the mean persistent depolarization (n = 5). The persistent depolarization measured on the last 3 stimulations. 1-factor RM ANOVA, p = 0.033, post hoc paired Student's *t* tests and Bonferroni correction: α = 0.017.

modulatory profile of cortical input onto sensory TRN, showing paired-pulse facilitation (PPF) (Fernandez et al., 2018).

At depolarized potentials, where tonic discharge is prevalent, PreS/RSC afferents reliably sustained TRN discharge during stimulation trains (Fig. 3E1). Furthermore, initially subthreshold responses could become suprathreshold in the course of a train (Fig. 3E2), most likely due to temporal summation that gave rise to a persistent depolarization on top of the phasic events (Fig. 3E3). Similar results were found at PreS/RSC-ATN+ synapses (Suppl. Fig. 3).

**PreS/RSC afferents mediate feedforward inhibition onto ATN+ through recruiting burst discharge in PV- and somatostatin (Sst)-expressing TRN cells**

How does TRN recruitment by PreS/RSC afferents regulate ATN+ activity? We first tested *in vitro* for Pres/RSC-triggered feedforward inhibition onto ATN+ (Fig. 4A). ATN+ cells were held at

256 voltages to separately monitor EPSC and IPSC components (-60 mV and +15 mV) (see Methods
257 for further details). Out of 22 ATN+ neurons innervated by PreS/RSC, 19 (9 AD, 5 AV, 5 LD)
258 presented with a strong outward current at +15 mV, consistent with an evoked inhibitory
259 postsynaptic current (IPSC) (Fig. 4B). The IPSC latency was higher than the EPSC latency (Fig.
260 4C), consistent with a disynaptic feedforward inhibition. IPSCs were mediated through $GABA_A$
261 receptors (Fig. 4D1,D2). To demonstrate that these IPSCs were indeed mediated by anterodorsal
262 TRN, we combined opto- and chemogenetics in VGAT-Ires-Cre mice expressing the inhibitory
263 Designer Receptor Exclusively Activated by Designer Drugs (DREADD) specifically in the
264 GABAergic cells of anterodorsal TRN and ChR2 in PreS/RSC. Chemogenetic silencing of
265 anterodorsal TRN through bath-application of the DREADD ligand clozapine N-oxide (CNO) while
266 optogenetically activating PreS/RSC afferents indeed reduced the amplitude of the evoked IPSC
267 (Fig. 4E1,E2).

268 The TRN contains subnetworks of PV- or Sst-expressing cells with possibly different functions
269 (Clemente-Perez et al., 2017). We determined the contribution of these subnetworks to ATN+
270 inhibition using PV-Cre and Sst-Cre mice expressing ChR2 in anterodorsal TRN. ChR2-positive
271 fibers were visible throughout the AD, AV and LD in both mouse lines (Fig. 4F), and rapid IPSCs
272 were elicited by activation of both PV- and Sst-expressing TRN cells in all thalamic nuclei (Fig.
273 4G1,G2), suggesting a contribution of both subnetworks to ATN+ inhibition.

274 **Anterodorsal TRN activation regulates action potential firing in ATN+ and sharpens the**
275 **tuning of HD cells**

276 We next addressed the consequences of PreS/RSC activity on unit activity of ATN+ through *in*
277 *vivo* single unit recordings in freely behaving mice while optogenetically activating PreS/RSC
278 bilaterally (Fig. 5A-C). Firing patterns of single units in the ATN+ (n=28/42 responsive units from
279 3 mice), analyzed through raster plots, peri-event histograms and z-score analysis, fell into 4
280 distinct classes. The first group (n=5) diminished firing rate within a time window of 15 – 40 ms
281 that persisted for up to 65 ms (Fig. 5D1). The second group (n=7) showed a late increase in firing,
282 with an onset from the LED stimulation ranging from 25 – 140 ms and persisting for up to 45 ms
283 (Fig. 5D2), reminiscent of a rebound burst discharge. The third group, containing 1 unit only,
284 showed an increase in firing rate only within the first 15 ms after light offset (Fig. 5D3). The last
285 group (n=15) contained units with mixed responses that combined features of the first three
286 groups (Fig. 5D4). In 12 of the mixed cases (Fig. 5D5), inhibition preceded delayed excitation
287 (inhibition onset: 28±2 ms, rebound onset: 70±10 ms, Wilcoxon signed rank-test $p = 3.90 \times 10^{-5}$).
288 Similarly, late increases in firing rate were clearly distinct in latency compared to the rapidly

responding units (early: 9±1 ms, late: 65±7 ms, Mann-Whitney U test p = $4.18 \times 10^{-5}$). Five out of 42 ATN+ units were tuned to the mouse's HD, as quantified by the length of the Rayleigh vector (r) (r = 0.43±0.01, n=5) (Fig. 5E1) (see Methods, (Yoder and Taube, 2009)). PreS/RSC activation induced a rebound firing in 2 of these (Fig. 5E2,E3). These results are consistent with a feedforward inhibitory circuit recruited by PreS/RSC that is present throughout ATN+ and that also targets HD cells.

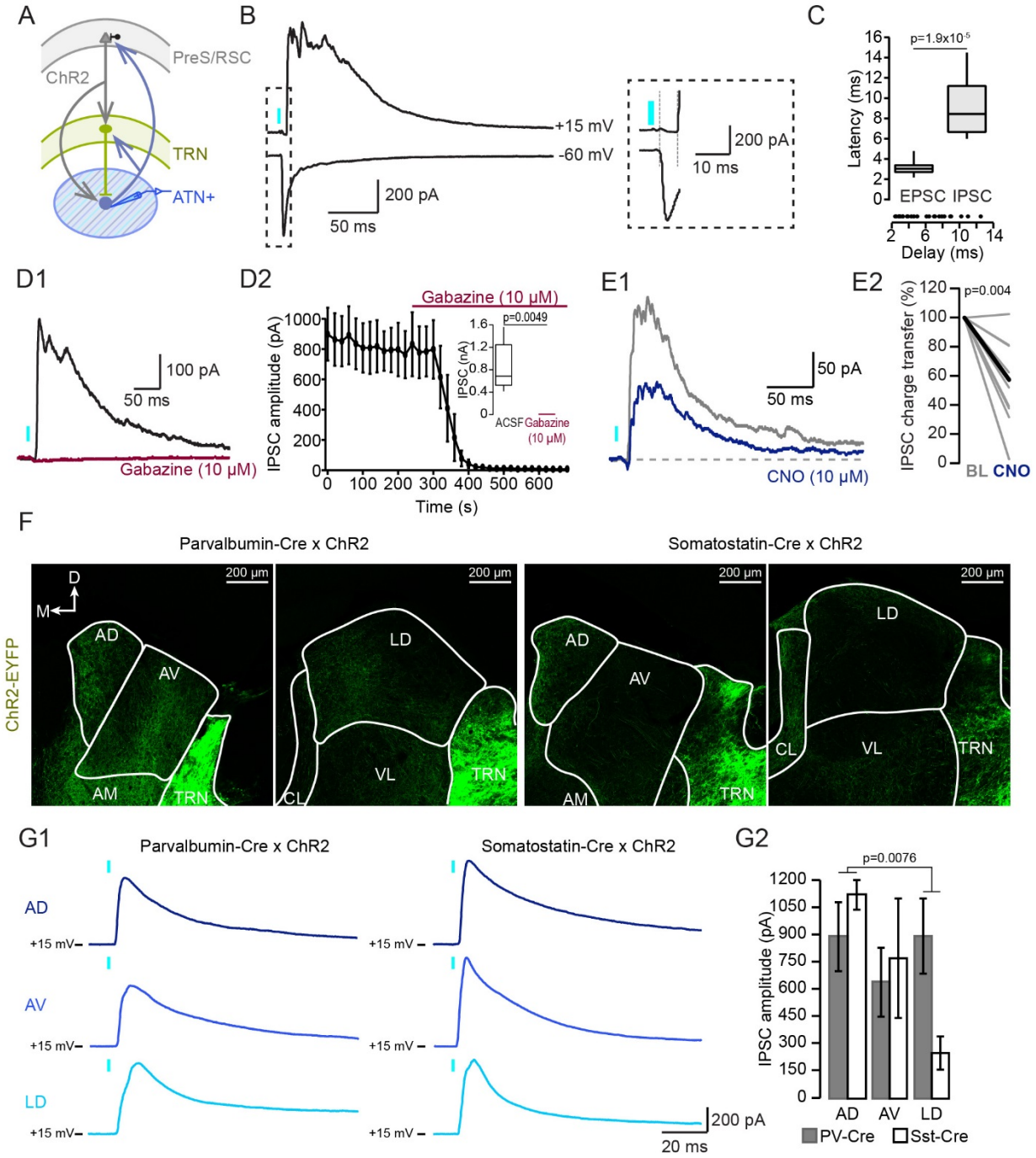

296 **Figure 4. PreS/RSC afferents mediate feedforward inhibition onto anterior thalamus**
297 **through recruiting burst discharge in PV- and Sst-expressing TRN cells.**

298 **(A)** Scheme of the hypothesized circuit studied *in vitro*. **(B)** Typical current responses of an ATN+
299 neuron held successively at -60 and +15 mV to record EPSC and IPSC. Portion indicated by
300 dotted rectangle is expanded on the right. Response latencies were measured from LED onset
301 (grey vertical lines). **(C)** Top: Box-and-Whisker plot of EPSC and IPSC latencies in ATN+ neurons
302 (n = 24). Bottom: Delays between the onset of the IPSC and the EPSC for all experiments.
303 Wilcoxon signed rank-test. **(D1)** A typical ATN+ IPSC before (black) and after (red) bath-
304 application of the $GABA_A$ receptor antagonist gabazine. **(D2)** Time course of gabazine action (n
305 = 6). Inset: Box-and-Whisker plot of steady-state IPSC amplitude in ACSF and gabazine (paired
306 Student's *t* test). **(E1)** IPSC evoked in an ATN+ neuron of a VGAT-Ires-Cre mouse expressing
307 the inhibitory DREADD in anterodorsal TRN. IPSCs measured before (grey) and after (blue) 10
308 µM CNO bath-application. **(E2)** Representation of the charge transfer of IPSCs in ATN+ neurons
309 (n = 10). Wilcoxon signed rank-test. **(F)** Confocal micrographs of ChR2-expressing PV-Cre (left)
310 and Sst-Cre (right) coronal brain sections of ATN+. **(G1)** Representative IPSCs elicited in ATN+
311 neurons held at +15 mV. **(G2)** Histogram of IPSC amplitudes in AD (n = 6 for both PV- and Sst-
312 Cre mice), AV (n = 6 for both) and LD (n = 6 for both). 2-factors ANOVA with factors 'nucleus' and
313 'cell type', $p = 0.036$ for 'nucleus', $p > 0.05$ for 'cell type', post hoc Student's *t* test with Bonferroni
314 correction: $\alpha = 0.017$ for IPSC amplitude between nuclei regardless of cell type.

315

316 Combining chemogenetic inhibition of anterodorsal TRN with silicone probe recordings targeted
317 stereotaxically to the AD, the site of HD cells (Taube, 1995), we probed the role of anterodorsal
318 TRN in further detail (Fig. 5F). Out of 22 sorted units, 11 were HD-tuned (Rayleigh $r \geq 0.4$), 3
319 were head-modulated ($0.2 \leq r < 0.4$) and 8 were untuned, similar to previously observed
320 proportions (Taube, 1995; Yoder and Taube, 2009). We compared the tuning, tuning width,
321 preferred direction and firing rate at the preferred direction of the HD units during a baseline
322 session and 40 min after i.p. injection of CNO (1 – 2 mg/kg) (n=11) (Fig. 5G1,G2) or NaCl (n=10)
323 (Suppl. Fig. 4). There was a trend for decreased tuning and a significant increase in the tuning
324 width after CNO injection compare to baseline. NaCl injection did not induce changes in any of
325 these parameters. There were no significant changes in preferred direction nor in firing rate with
326 CNO nor NaCl. Therefore, the tuning curve of HD cells in AD in freely moving conditions
327 deteriorates upon loss of TRN activity.

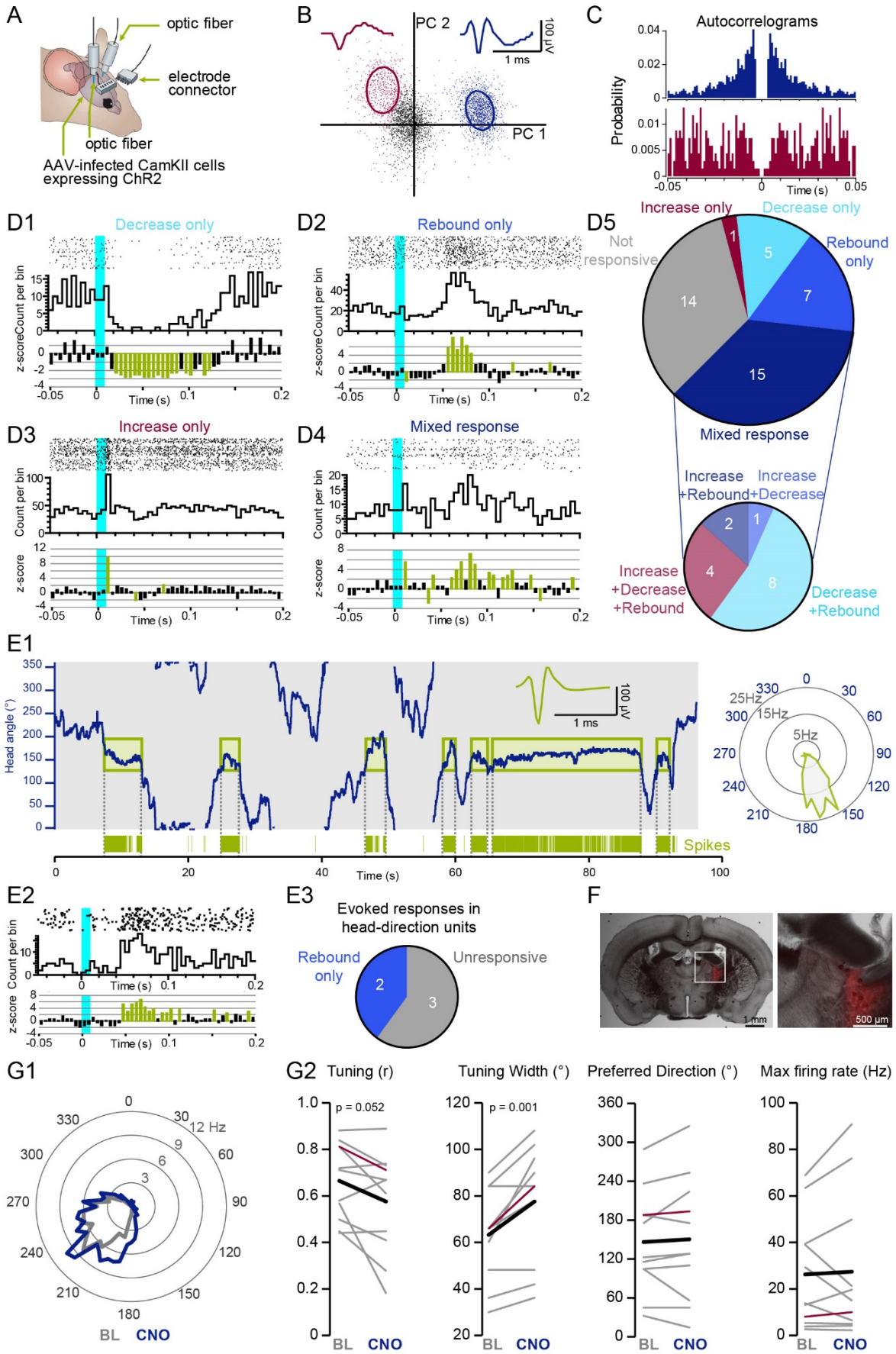
A
optic fiber
electrode connector
optic fiber
AAV-infected CamKII cells expressing ChR2
B
PC 2
PC 1
100 µV
1 ms
C
Autocorrelograms
Probability
Time (s)
D1
Decrease only
D2
Rebound only
D3
Increase only
D4
Mixed response
z-scoreCount per bin
Count per bin
z-score
Time (s)
D5
Increase only
Decrease only
Not responsive
Rebound only
Mixed response
Increase +Rebound
Increase +Decrease
Increase +Decrease +Rebound
Decrease +Rebound
E1
Head angle (°)
Spikes
Time (s)
25Hz
15Hz
5Hz
E2
Count per bin
z-score
Time (s)
E3
Evoked responses in head-direction units
Rebound only
Unresponsive
F
1 mm
500 µm
G1
12 Hz
BL
CNO
G2
Tuning (r)
Tuning Width (°)
Preferred Direction (°)
Max firing rate (Hz)
p = 0.052
p = 0.001
BL
CNO

328

329 **Figure 5. Anterodorsal TRN activation regulates action potential firing in anterior thalamus**
330 **and sharpens the tuning of head direction cells.**

331 **(A)** Scheme of the *in vivo* freely moving recording configuration. **(B, C)** Example of unit sorting
332 based on principal component analysis (B) and autocorrelation (C). Autocorrelograms of the
333 sorted units from panel B showing the typical refractory period around 0. **(D1-D4)** Raster plot,
334 cumulative histogram and z-score analysis for four characteristic unit responses. **(D5)** Pie charts
335 showing the proportion of the four characteristic responses in all putative thalamic units. **(E1)**
336 Graph showing the mouse HD (blue trace) in combination with detected spikes of a putative
337 thalamic HD unit (vertical green lines) tuned around 150°. Insets: mean unit waveform and a polar
338 plot of the tuning curve. **(E2)** Example of a HD unit response to light activation of PreS/RSC
339 afferents. **(E3)** Pie chart of the proportion of head-direction units responsive to light activation of
340 PreS/RSC. **(F)** Sections for the anatomical verification of silicone probe implantation in VGAT-
341 Ires-Cre mice expressing the chemogenetic silencer hM4D-mCherry (red) in anterior TRN. **(G1)**
342 Polar plot of a HD unit's tuning curve during baseline (grey) and after injection of CNO (blue).
343 **(G2)** Quantification of the changes in tuning parameters by CNO (n = 11 HD units). Far left:
344 Rayleigh vector length size. Middle left: width of the tuning curve (measure at half the maximum
345 firing rate). Middle right: preferred direction. Right: the firing rate at the preferred direction. Grey
346 lines: single units. Red line: example unit from G1. Black line: average. Paired Student's *t* tests to
347 compare data during baseline and 40 min after CNO injection.

348

349 **Anterodorsal TRN inhibition biases navigational search strategies in the Morris water maze**

350 We chose the hidden platform version of the Morris water maze (MWM) to probe the role of
351 anterodorsal TRN in spatial navigation. In this maze, both ATN-dependent egocentric and visual
352 cue-dependent allocentric navigational strategies were reported (Stackman et al., 2012; Garthe
353 and Kempermann, 2013). Mice were trained over 10 days to learn the hidden platform in a maze
354 surrounded by visual landmarks, followed by a 10-day reversal learning during which the platform
355 was located in the opposite quadrant (Suppl. Fig. 5A). We hypothesized that chemogenetic
356 suppression of anterodorsal TRN activity, and reduction of PreS/RSC-mediated ATN+ inhibition,
357 would alter navigational behavior once the animal had to rely on HD-dependent, egocentric
358 strategies. We also asked whether there was a bias in search strategies already in the course of
359 spatial learning.

360 We used two groups of mice: "control" VGAT-Ires-Cre and "DREADD" VGAT-Ires-Cre mice that
361 expressed non-DREADD related proteins or the inhibitory DREADD specifically in the
362 anterodorsal TRN, respectively (Fig. 6A). In each of the four daily test sessions, entry points into
363 the maze were randomized across the quadrants to enforce the use of allocentric strategies. Both
364 groups became faster swimmers in the course of the task and showed no significant difference in
365 their mean swimming velocity during the 60-s probe sessions (with platform removed), although
366 there was a light trend for control mice to be faster (Fig. 6B). We thus analyzed the proximity to

367 the platform instead of the latency to platform to account for possible effects of differences in swim
368 speed (Awasthi et al., 2019). Based on this measure, both groups performed similarly, as
369 indicated by a comparable decrease of the mean proximity to the platform during test sessions
370 (Fig. 6C). Moreover, from days 5 – 7 of training, the percentage of time spent in the target
371 quadrant was above chance level for both groups during probe sessions (Fig. 6D) These results
372 show an overall comparable, if not slightly better performance of DREADD mice, but they do not
373 provide information about the navigational strategies used. We hence classified swim trajectories
374 on a trial-by-trial basis for all test sessions according to previously described criteria for allo- and
375 egocentric strategies (Suppl. Fig. 6B-D) (Garthe and Kempermann, 2013; Rogers et al., 2017).
376 Figure 6E shows that mice use a mix of trajectories reflecting the use of both ego- and allocentric
377 strategies (Fig. 6E,I,K). Focusing first on early phases of reversal learning (day 11), DREADD
378 mice showed perseverance around the previous platform location, while control animals reverted
379 to trajectories consistent with egocentric strategies (Fig. 6F). If perseverance was indeed
380 reflecting a decreased ability to change navigational strategy once the correct platform location
381 was learned, signs of perseverance should also be seen in the course of learning. Indeed, when
382 inspecting time-binned occupancy plots during probe sessions, DREADD mice persevered
383 searching at the platform position for the whole 60 s-probe session, whereas control mice shifted
384 to a dispersed search pattern of other regions of the pool during the last 20 s of the session. This
385 was particularly the case during the last 2 probe sessions of the learning (beginning of day 9 and
386 11) (Fig. 6 G,H).

387 Inspired by the finding on the DREADD mice's possibly compromised ability to deploy egocentric
388 strategies during reversal learning, we asked whether evidence for biased strategy selection could
389 also be found during initial platform learning. As is characteristic for the MWM, there was an
390 increase in the proportion of allocentric strategies from day 1-2 to day 9-10 in both control and
391 DREADD mice (Fig. 6 I,J) (Garthe and Kempermann, 2013). However, DREADD mice did so in
392 temporal anticipation, showing significantly more scanning and less random search on day 3, and
393 more direct swimming and less thigmotaxis on day 4 (Fig. 6J). DREADD mice also used an overall
394 greater proportion of allocentric strategies across both learning and reversal learning than control
395 mice (Fig. 6K). Together, suppression of anterodorsal TRN activity 1) alters navigational behavior
396 at reversal learning and 2) biases the search patterns towards allocentric strategies during initial
397 learning.

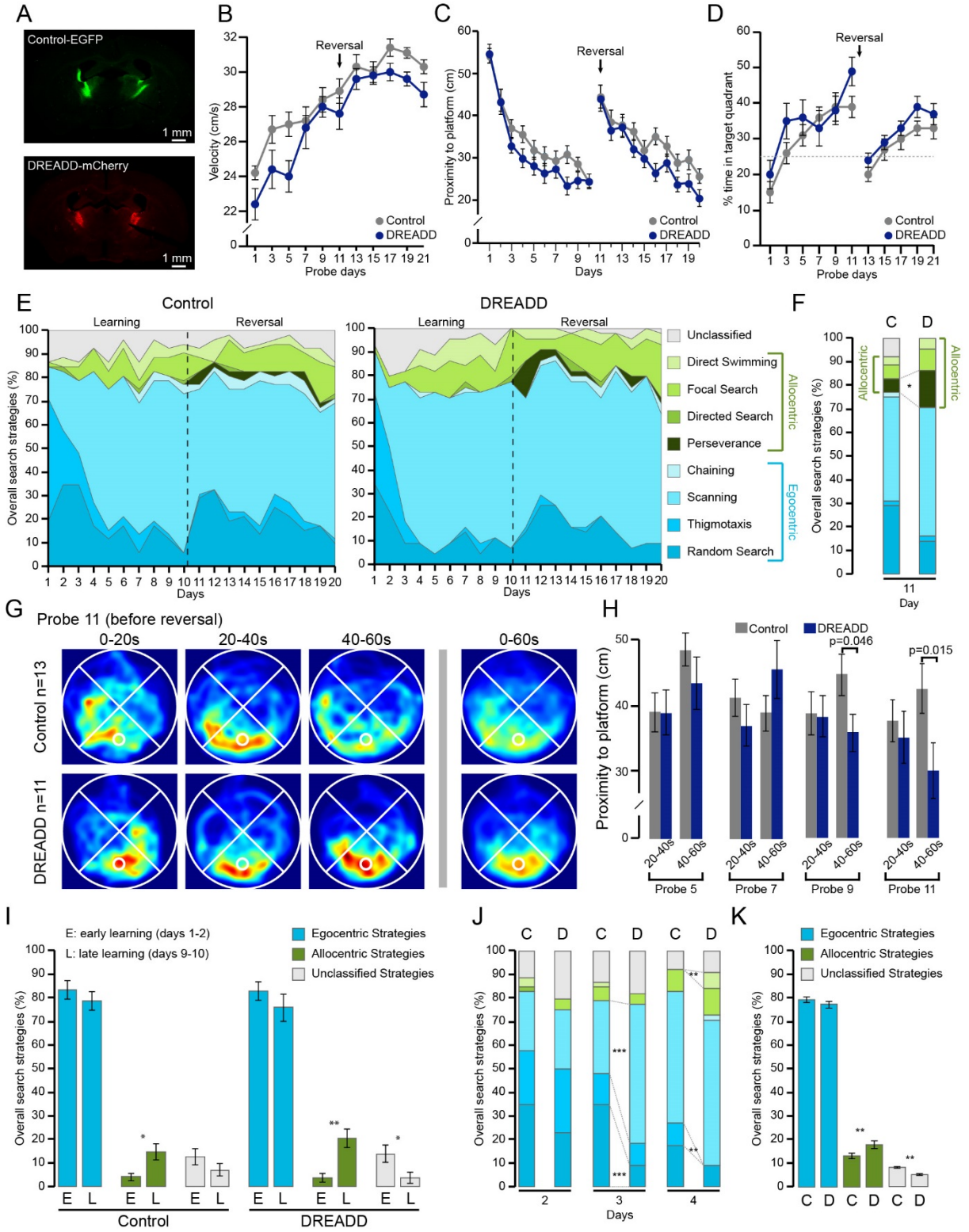
A
Control-EGFP
1 mm
DREADD-mCherry
1 mm
B
Reversal
Velocity (cm/s)
Probe days
Control
DREADD
C
Reversal
Proximity to platform (cm)
Days
Control
DREADD
D
Reversal
% time in target quadrant
Probe days
Control
DREADD
E
Control
DREADD
Learning
Reversal
Overall search strategies (%)
Days
Unclassified
Direct Swimming
Focal Search
Directed Search
Perseverance
Chaining
Scanning
Thigmotaxis
Random Search
Allocentric
Egocentric
F
C
D
Allocentric
Overall search strategies (%)
Day
G
Probe 11 (before reversal)
0-20s
20-40s
40-60s
0-60s
Control n=13
DREADD n=11
H
Control
DREADD
p=0.046
p=0.015
Proximity to platform (cm)
20-40s
40-60s
Probe 5
Probe 7
Probe 9
Probe 11
I
E: early learning (days 1-2)
L: late learning (days 9-10)
Egocentric Strategies
Allocentric Strategies
Unclassified Strategies
Overall search strategies (%)
Control
DREADD
J
C
D
Overall search strategies (%)
Days
K
Egocentric Strategies
Allocentric Strategies
Unclassified Strategies
Overall search strategies (%)

398

399

**Figure 6. Anterodorsal TRN inhibition biases navigational search strategies in the Morris water maze.**

**(A)** Epifluorescent micrographs of VGAT-Ires-Cre mouse coronal brain sections at Bg -0.8 mm for a control mouse (top) and a test mouse (bottom). Color codes indicate expression products. **(B)** Mean swim velocities of control (n = 13) and DREADD (n = 11) mice during probe sessions. 2-factors RM ANOVA with factor 'day' and 'condition', $p < 2x10^{-16}$ for 'day' and p = 0.04 for 'condition'. Post hoc Student's *t* tests with Bonferroni correction: α = 0.005 for 'condition': not significant. **(C)** Graph of the mean proximity to the platform during training sessions. 2-factors RM ANOVA with factor 'day' and 'condition', $p < 2x10^{-16}$ for 'day' and p = 0.04 for 'condition'. Post hoc Student's *t* tests and Mann-Whitney U tests with Bonferroni correction: α = 0.003 for 'condition': not significant. **(D)** Graph of the percentage of time spent in the target quadrant during probe sessions. Chi-square test against 25% chance, significant at days 1, 7, 9, 11 for Control and days 5, 9, 11, 19, 21 for DREADD. **(E)** Stacked area graphs of search strategies used by control (left) and DREADD (right) mice during trial sessions. **(F)** Proportion of overall strategies at day 11 for control (C) and DREADD (D) mice. Chi-square tests for 'allocentric strategy' and for 'Perseverance', p < 0.05 for both. **(G)** Time-binned (20 s bins) and overall average occupancy plots during the last probe session of the learning phase. Hot colors indicate greater occupancy and are equally calibrated in all plots. **(H)** Histogram of the mean proximity to the platform of control and DREADD mice during binned-probe sessions. Student's *t* test for Control vs DREADD at late time bin (40 – 60 s). **(I)** Averaged proportion of egocentric, allocentric and unclassified strategies used during the early (E, days 1 and 2) and late (L, days 9 and 10) learning phase. Wilcoxon signed rank-tests, p = 0.02 for allocentric strategies in control mice, p = 0.008 and p = 0.03 for allocentric and unclassified strategies in DREADD mice, respectively. **(J)** Proportion of overall strategies at day 2, 3 and 4 for control (C) and DREADD (D) mice. Chi-squared tests for 'Scanning' and for 'Random Search' at day 3, p < 0.001 for both. Chi-square tests for 'Direct Swimming' and for 'Thigmotaxis' at day 4, p < 0.01 for both. **(K)** Averaged proportion of egocentric, allocentric and unclassified strategies used during the whole experiment. Student's *t* test comparing Control (C) vs DREADD (D).

# Discussion

Anatomical and physiological identification of synaptic inputs to TRN has repeatedly opened a novel point of view for the TRN's active role in gating sensory information flow to and from the cortex (for review, see (Crabtree, 2018)). We uncover here a previously undescribed excitatory input to TRN from the parahippocampal dPreS and the RSC that shows high connectivity, mediates robust feedforward inhibition to ATN and shapes HD tuning in AD. These findings offer a possible synaptic mechanism contributing to the flexible use of navigational strategies during spatial learning and orientation. We thus identify here a novel thalamocortical loop that integrates TRN and that expands its gating function to the domain of self-orientation and navigation. More generally, we favor a view of the TRN as a multi-modal saliency selector that interfaces between acute cognitive demands, such as attentional switching or spatial re-orientation, and the recruitment of the appropriate sensory and self-orientational HD signals.

441 Retrograde tracing from the anterodorsal portion of the TRN identified several previously
442 described prefrontal cortical afferents (Cornwall et al., 1990; Lozsádi, 1994; Dong et al., 2019).
443 We now additionally demonstrate that there is a continuous band of afferent projections along the
444 presubicular-retrosplenial axis that starts at the border from subiculum to the PreS, thus at the
445 onset of the six-layered presubicular complex. These projections arise in deep layers of PreS and
446 RSC, to where projections to ATN were previously retrogradely traced (Wright et al., 2010). The
447 anterodorsal TRN seems thus to integrate visuospatial and HD input in combination with saliency
448 signals from prefrontal areas. The CL nucleus, a target of the superior colliculus, may convey
449 orienting-movement related signals into TRN (Krout et al., 2001). Moreover, central amygdalar
450 and hypothalamic inputs were recently described (Herrera et al., 2016; Dong et al., 2019).
451 Together, this adds to a complex web of afferents that contrasts with the predominantly
452 monomodal connectional characteristics of posterior sensory sectors of mouse TRN.

453 More work is required to elucidate the detailed organization of the anterodorsal synaptic
454 connectivity from PreS/RSC to anterodorsal TRN and from there to ATN. We note here that both
455 RSC and dPreS target LD and AD preferentially, while projections to AV are minor. AD and LD
456 are thought to functionally cooperate within the HD system (Simonnet and Fricker, 2018; Perry
457 and Mitchell, 2019), possibly acting as first- and higher-order nucleus, respectively (Peyrache et
458 al., 2019). The AV, together with the anteromedial nucleus, has been so far associated with a
459 theta-generating system innervated by vPreS (Perry and Mitchell, 2019). The limited spatial
460 resolution of our tracing methods does not currently allow to verify whether anterodorsal TRN is
461 also subdivided into sectors corresponding to this functional subdivision of ATN+. Interestingly,
462 single-cell labeling identified rat anterodorsal TRN cells with axons bifurcating to innervate both
463 AD and LD (Pinault and Deschênes, 1998). AM-projecting TRN cells were located more ventrally.
464 Anterodorsal TRN may thus contain cells jointly innervating AD and LD, further substantiating a
465 shared function.

466 Our characterization of a cortical excitatory innervation of TRN by PreS/RSC-excitatory input
467 reveals a combination of commonalities but also notable differences to the canonical form of
468 cortical input to sensory TRN that arises from layer 6 corticothalamic neurons of corresponding
469 primary cortex (Usrey and Sherman, 2019). Layer 6 synapses on TRN cells show a high
470 glutamate receptor content (Golshani et al., 2001), high unitary amplitude (Golshani et al., 2001),
471 faster rise and decay times (Gentet and Ulrich, 2004), smaller NMDA/AMPA ratios (Astori and
472 Lüthi, 2013) and marked PPF (Castro-Alamancos and Calcagnotto, 1999; Astori and Lüthi, 2013;
473 Crandall et al., 2015) compared to their thalamocortical counterparts. The presence of PPF

474 classifies layer 6 corticothalamic afferents as modulators rather than drivers (Sherman and
475 Guillery, 1998). While dPreS/RSC-TRN synapses are comparable in terms of unitary amplitude,
476 NMDA/AMPA ratio and EPSC waveform, there is a prominent lack of PPF at dPreS/RSC afferents
477 and a moderate entrainment of firing during repeated stimulation. Rather than being modulators,
478 the PreS/RSC inputs thus shares a short-term plasticity profile reminiscent of the driver inputs
479 that count as the principal information-bearing synapses. Top-down driver input is so far known
480 for corticothalamic layer 5 projections to higher-order thalamic nuclei that show a number of
481 morphological hallmarks (Usrey and Sherman, 2019). A driver profile that we suggest here for the
482 first time for TRN implies that anterodorsal TRN conveys direct system-relevant information that
483 is faithfully transmitted to its projection targets. We cannot exclude, however, that PreS and RSC
484 afferents, if stimulated separately, would show different short-term plasticity including PPF. A
485 further noteworthy point is that both PV+ and Sst+ TRN neurons innervate the AD, AV and LD
486 with comparable strength, pointing to functional differences compared to sensory first-order
487 thalamic nuclei (Clemente-Perez et al., 2017).

488 About 65% of ATN+ units showed a suppression of activity upon PreS/RSC stimulation that was
489 occasionally followed by a rapid increase in discharge. The timing of the inhibition-rebound events
490 is typical for a feedforward inhibitory mechanism (Crandall et al., 2015). Moreover, chemogenetic
491 TRN inhibition degrades HD cell tuning. The rather small effect size may be explained by the only
492 partial reduction of feedforward inhibition by CNO (see Fig. 4E). The anterodorsal TRN is thus
493 part of the top-down circuit so far thought to innervate the ATN+ only monosynaptically (Dumont
494 and Taube, 2015; Peyrache et al., 2017; Simonnet and Fricker, 2018; Perry and Mitchell, 2019).
495 This result advances the mechanistic understanding of the proposed update of thalamic HD cell
496 tuning by visual landmarks (Dumont and Taube, 2015). TRN-dependent inhibition may regulate
497 single AD cells, for example through promoting bursting, which we also observe *in vitro*, although
498 their existence *in vivo* has been questioned (Sheroziya and Timofeev, 2014). Bursting would
499 increase their impact in upstream navigational circuits, in particular in the dPreS circuits
500 (Peyrache et al., 2015), similar to what has been described for sensory thalamocortical circuits
501 (Sherman, 2001). TRN-mediated burst promotion in some AD neurons coupled with inhibition of
502 others could underlie the proposed increase in the precision of HD coding (Peyrache et al., 2015).
503 TRN-driven ATN bursting might also be an important component in oscillatory patterns observed
504 within ATN+, such as the one proposed to occur in AD (Peyrache et al., 2015; Peyrache et al.,
505 2019) or in AV (Tsanov et al., 2011), which are probably relevant for linking spatial information to
506 hippocampal memory processing.

To date, behavioral evidence for a role of the HD system in behavioral navigation is limited (Taube et al., 1992; van der Meer et al., 2010; Valerio and Taube, 2012; Butler et al., 2017) and the role of specific HD circuits, including dPreS and RSC, just starts to be behaviorally explored. Experimental effort typically targets egocentric strategies, for example by moving the MWM relative to landmarks between trials (Stackman et al., 2012), by studying navigation in darkness (Yoder et al., 2019) or by putting rats upside down (Calton and Taube, 2005). In contrast, the idea that spatial navigation requires an on-going switching between a range of possible strategies has not been much pursued, although it is known for human studies (Miniaci and De Leonibus, 2018). For example, a recent study using a hippocampus-specific synaptic knockout animal interpreted perseverant behavior at the platform location as a lack of forgetting (Awasthi et al., 2019), but the question of possible bias in navigational strategies was not addressed. Trajectory analysis in the MWM thus offers itself as an interesting approach to follow on the evolution of navigational behavior under well-controlled landmark conditions while simultaneously allowing egocentric strategies (Dolleman-van der Weel et al., 2009; Garthe and Kempermann, 2013). We found a preferential use of allocentric strategies when anterodorsal TRN was suppressed, suggesting that egocentric navigation was less efficient. This is reminiscent of an ATN lesion study (Stackman et al., 2012), although we cannot currently exclude that TRN-dependent inhibitory effects on nuclei other than ATN, such as on intralaminar nuclei (Dong et al., 2019), contribute. Anterodorsal TRN activity is required for qualitatively high HD signals in AD and/or for a robust activation of these by feedforward inhibition. Anterodorsal TRN activity seems to be critically required at moments when there is a mismatch between allocentric cues and new platform location, such that novel relations between external landmarks and self-perceived orientational strategies, which depend on HD cells, have to be built. Interestingly, the RSC has been proposed as an area involved in allocentric navigation and memory formation, but also in the switching between allo- and egocentric strategies to optimize navigational goals (Mitchell et al., 2018). In particular, its strong connections to limbic thalamus have been implied in the solving of spatial problems (Clark et al., 2018). Similar more complex roles in spatial navigation have recently been proposed for dPreS (Yoder et al., 2019), which has been primarily analyzed as part of the hierarchy of the egocentric coding system (Taube et al., 1990; Dumont and Taube, 2015; Peyrache et al., 2017). Our work does not currently disentangle between the distinct roles of these two brain areas. However, it has managed to pinpoint to the existence of a possibly fine switching mechanism at the interface between major allocentric and egocentric brain areas that, when perturbed, preserved overt navigational performance but compromised it at challenging moments that could pose existential threats.

541 This work integrates TRN function into the brain's balanced control of sensory-guided spatial
542 navigation. The anterodorsal sector of TRN, located at the *limbus*, the 'edge' of the TRN, is a site
543 of complex integration where navigational, attentional, motor and emotional information may be
544 combined for precise activation of egocentric navigation systems. As a perspective arising from
545 this work, we suggest that neuropsychological screening for egocentric navigation deficits may
546 be useful in the diagnosis of disorders linked to TRN dysfunction, such as in neurodevelopmental
547 disorders linked to attentional deficits (Krol et al., 2018) and in schizophrenia (Wilkins et al., 2017).

## 548 Acknowledgements

549 We thank Andreas Lüthi for providing training for the multiwire recordings, Adrien Peyrache for
550 providing training for the silicone probes, Cyril Herry for helping with single unit sorting and
551 analysis, Leonardo Restivo for helping with the design of the Morris water maze experiment and
552 careful reading of the manuscript, Christian Lüscher for providing the VGAT-Ires-Cre mouse line,
553 Desdemona Fricker, John Huguenard, Ralf Schneggenburger for constructive discussions,
554 Simone Astori for critical reading of the manuscript, all lab members for constructive input for the
555 manuscript and discussions in the course of the project.

556 Funding: GV received Travel Grants from the Jean Falk Vairant Foundation, Life Sciences
557 Switzerland and Swiss Society for Neuroscience, ZR was supported by the Marie Heim Vögtlin
558 Foundation, AG received an Erasmus Mobility Grant, AL was supported by Swiss National
559 Science Foundation (Grant No. 31003A-166318 and 310030-184759) and Etat de Vaud.

## 560 Author contributions

561 GV carried out and analyzed all experimental tracing, *in vitro*, *in vivo* and behavioral data, and
562 also contributed to the design of the *in vivo* and behavioral experiments. ZR gained first evidence
563 for the anatomical connectivity between dPreS/RSC and anterodorsal TRN and initiated the *in*
564 *vivo* unit recordings. RC wrote the Matlab code for the analysis of head-direction data and MWM
565 Strategy. EB contributed to viral injections and the MWM experiments, GK to the antero- and
566 retrograde tracing data. AG carried out the *in vitro* recordings in PV- and Sst-Cre mice. VP
567 assisted with anatomical analysis. LMJF contributed to the surgery and analysis for *in vivo*
568 experiments. AL supervised the project and wrote the manuscript with contribution of GV.

## 569 Declaration of interests

570 The authors declare no competing interests.

571 # STAR Methods

572 ## Animal husbandry and ethical approval

573 We used mice of either sex from the C57BL6/J line and from the Slc32a1$^{tm2(cre)Lowl}$ line, commonly
574 referred to as VGAT-Ires-Cre line (Jackson Labs, generated by Dr. B. Lowell, Beth Israel
575 Deaconess Medical Center, Harvard) (Vong et al., 2011), male
576 C57Bl/6J;129P2_Pvalbtm1(cre)Arbr/J mice, referred to here as PV-Cre mice, and male B6N.Cg-
577 Sst<tm2.1(cre)Zjh>/J mice, referred to here as Sst-Cre mice. These three transgenic lines
578 express the Cre-recombinase either in VGAT-, PV- or Sst-positive neurons, respectively. All
579 animals were housed in a temperature and humidity-controlled animal house with a 12/12 h light-
580 dark cycle (lights on at 9 a.m.) and water and food available *ad libitum.* The VGAT-Ires-Cre line
581 was originally generated on a mixed C57BL/6;FVB;129S6 genetic background and backcrossed
582 to C57BL6 ever since. PV-Cre and Sst-Cre lines were maintained on a C57BL6 background.
583 VGAT-Ires-Cre and PV-Cre were used as homozygous, whereas the Sst-Cre mice were
584 heterozygous. For anatomical tracing (retrograde and anterograde), mice (n = 24) were
585 transferred into a housing room with similar conditions on the day prior to injection. They remained
586 there for 7 days after injection before perfusion and tissue processing. For viral injections, mice
587 were transferred into a P2 safety level housing with similar conditions on the day prior to the
588 injection. They remained there 3 – 5 weeks before being used for *in vitro* electrophysiology (n =
589 57), 2 – 3 weeks before surgical implantation for *in vivo* electrophysiology (n = 5), and 2 – 3 weeks
590 before behavioral experiments (n = 24, only males). All experimental procedures complied with
591 the Swiss National Institutional Guidelines on Animal Experimentation and were approved by the
592 Swiss Cantonal Veterinary Office Committee for Animal Experimentation.

593

594 ## Anatomical tracing and verification of recording and injection sites

595 ### Retrograde tracing

596 C57BL6/J mice, 4- 8-week-old, were anesthetized with 5 % isoflurane and fixed onto the
597 stereotaxic frame. During the surgery, the anesthesia level was reduced to 1- 3 % and $N_2O$ was
598 added if the surgery lasted > 1 h. Analgesia was ensured through Carprofen (5 mg/kg i.p.).
599 Craniotomies were performed above the sites of injection at (anteroposterior (AP), mediolateral
600 (ML), depth from cortical surface (DV), in stereotaxic coordinates from Bregma): -0.7, ±1.5, -3.1
601 to target the anterodorsal TRN. Glass pipettes (5-000-1001-X, Drummond Scientific, Broomall,

602 PA) were pulled on a vertical puller (Narishige PP-830, Tokyo, Japan) and backfilled by capillarity
603 with fluorescent latex microspheres (Red Retrobead™, Lumafluor). Using a Picospritzer III,
604 pressurized air pulses (15 psi, 10 ms) were applied every 10 s for 10 min to inject the retrobeads.
605 After 4 – 7 days, mice were perfused and their brains collected for immunostainings.

606 Anterograde tracing

607 The anesthetic and surgical procedures were the same as the ones used for retrograde tracing.
608 The coordinates of injection were (AP, ML, DV): -3.8, ±1.6, -1.0 for RSC, -3.8, ±2.3, -1.6 for PreS.
609 Glass pipettes were backfilled by capillarity with the plant lectin anterograde tracer *Phaseolus*
610 *vulgaris*-leucoagglutinin (PHAL-L, Vector Laboratories, Cat. No. L-1110). PHAL-L was chosen as
611 it permits focal labeling with little spread, which seemed appropriate to target PreS and RSC as
612 specifically as possible. A chlorinated silver wire was inserted into the pipette and a reference
613 electrode attached to the mouse tail. The PHAL-L was electroporated with a 5-µA current, 7 s
614 on/off loop for 20 min, applied with a home-made current isolator and a Master-8 (Master-8 Pulse
615 Stimulator, A.M.P.I., Jerusalem, Israel). After 5 – 7 days, mice were perfused and their brains
616 collected for immunostainings.

617 Perfusion and tissue processing

618 Mice were injected i.p. with a lethal dose of pentobarbital. Intracardial injection of ~45 ml of
619 paraformaldehyde (PFA) 4 % was done at a rate of ~2.5 ml/min. Brains were post-fixed in PFA 4
620 % for at least 24 h at 4°C. Brains were sliced with a Vibratome® (Microtome Leica VT1000 S,
621 section thickness: 100 µm, speed: 0.25-0.5 mm/s and knife sectioning frequency: 65 Hz) in 0.1 M
622 phosphate buffer (PB). Brain sections were either directly mounted on slides or disposed in
623 twelve-well plates filled with 0.1 M PB for immunohistochemistry.

624 Immunofluorescent labeling

625 100 µm-thick brain sections were washed 3 times in 0.1 M PB and transferred to a blocking
626 solution containing 0.1 M PB, 0.3 % Triton, 2 % normal goat serum (NGS) for 30 min. The first
627 antibody solutions also contained 0.1 M PB, 0.3 % Triton, 2 % NGS. For PHAL-L injected mice,
628 we added 1:8000x of rabbit anti-PHAL-L (Vector Laboratories, AS-2300, RRID: AB_2313686) and
629 1:4000x of mouse anti-PV (Swant, PV235, RRID: AB_10000343). For retrobead-injected and
630 virally injected PV-Cre and Sst-Cre mice, we added 1:4000x of mouse anti-PV (Swant, PV235,
631 RRID: AB_10000343). Sections were kept at 4°C for 48 h on a shaking platform. After 3 washings
632 in 0.1 M PB, we added a secondary antibody solution containing 0.1 M PB, 0.3 % Triton, 2 %

633 NGS and, when appropriate, 1:500x of goat anti-rabbit Cyanine Cy3™ (Jackson Immunoresearch,
634 111-165-003, RRID: AB_2338000), 1:500x of goat anti-mouse Cy5™ Jackson Immunoresearch,
635 115-175-146, RRID: AB_2338713) and/or 1:500x of goat anti-mouse Alexa Fluor® 488 (Jackson
636 Immunoresearch, 115-545-003, RRID: AB_2338840). Sections were mounted on slides and
637 covered with a mounting medium (Vectashield).

638 300 µm-thick brain sections obtained from patch-clamp recording sessions were post-fixed in 4
639 % PFA for at least 24 h. Brain sections were washed 3x in 0.1 M PB and then pretreated with a
640 solution containing 0.1 M PB and 1 % Triton for 30 min. The blocking solution was 0.1 M PB, 1 %
641 Triton, 2 % NGS and was applied for 30 min. The first antibody solution contained 0.1 M PB, 1 %
642 Triton, 2 % NGS, 1:4000x mouse anti-PV (Swant, PV235, RRID: AB_10000343) and was applied
643 for 5 days at 4°C. The secondary antibody solution contained 0.1 M PB, 0.3 % Triton, 2 % NGS,
644 1:500x goat anti-mouse CY5, (Jackson ImmunoResearch, 115-175-146, RRID: AB_2338713),
645 1:8000x Streptavidin ALEXA594 (Jackson ImmunoResearch, 016-580-084, RRID: AB_2337250)
646 and was applied for 24 h at 4°C. Sections were mounted on slides and covered with a mounting
647 medium (Vectashield).

648 Microscopy

649 Electromicrographs of brain slices were taken with a fluorescent stereomicroscope (Nikon SMZ
650 25) or a confocal microscope (Zeiss LSM 780 Quasar Confocal Microscope). NIS-Elements 4.5
651 (Nikon), Adobe Photoshop CS5 and Zen lite 2012 were used to merge images from different
652 channels.
653

654 **Viral injections**

655 Mice 3- 5-week-old were anesthetized using Ketamine-Xylazine (83 and 3.5 mg/kg, respectively)
656 and placed on a heating blanket to maintain the body temperature at 37°C. An initial dose of
657 analgesic was administrated i.p. at the beginning of the surgery (Carprofen 5 mg/kg). The animal
658 was head-fixed on a stereotactic apparatus equipped with an ear and mouth adaptor for young
659 animals (Stoelting 51925, Wood Dale, IL). The bone was exposed at the desired injection site
660 through a small skin incision. Viruses were injected with a thin glass pipette (5-000-1001-X,
661 Drummond Scientific, Broomall, PA) pulled on a vertical puller (Narishige PP-830, Tokyo, Japan).
662 C57BL6/J mice were injected bilaterally with a virus encoding ChR2 (500 nl of AAV1-hSyn-
663 ChR2(H134R)_eYFP-WPRE-hGH, $10^{12}$ GC, ~100–200 nl/min) into the PreS (AP, ML, DV): -3.8,
664 +/-2.5, -1.7. VGAT-Ires-Cre mice were injected bilaterally with 500 nl of AAV1-hSyn-

665 ChR2(H134R)_eYFP-WPRE-hGH (1x$10^{12}$ GC, ~100–200 nl/min) into the PreS and/or unilaterally
666 or bilaterally with a virus encoding DREADD-mCherry (500 nl of AAV8-hSyn-DIO-
667 hM4D(Gi)_mCherry, 6.4x$10^{12}$ GC), or DREADD-IRES-mCitrine (500 nl of ssAAV8/2-hSyn1-dlox-
668 A_hM4D(Gi)_IRES_mCitrine-dlox-WPRE-hGHp(A), 3.1x$10^{12}$ GC) or a control AAV8 encoding a
669 DREADD-unrelated construct (500 nl of AAV8-hSyn-FLEX-Jaws_KGC_GFP_ER2, 3.2x$10^{12}$ GC)
670 in the anterior sector of the TRN (AP, ML, DV: -0.8, ±1.35, -3.1). PV-Cre and Sst-Cre mice were
671 injected into the anterior TRN (AP, ML, DV: -0.8, ±1.35, -3.1) with AAV1-EF1a-DIO-
672 ChR2(H134R)_eYFP-WPRE-hGH (1x$10^{12}$ GC, 500 nl, ~100–200 nl/min).

673

674 ***In vitro* electrophysiological recordings**

675 Slice preparation, solutions and recordings.

676 Brain slice preparation, storage and recordings were performed essentially as described
677 (Fernandez et al., 2018). Adult 8- 10-week-old C57BL6/J and VGAT-Ires-Cre mice (3 – 4 weeks
678 post viral injection) were briefly anesthetized with isoflurane and their brains quickly extracted.
679 Acute 300-µm-thick coronal brain slices were prepared in ice-cold oxygenated sucrose solution
680 (which contained in mM: 66 NaCl, 2.5 KCl, 1.25 $NaH_2PO_4$, 26 $NaHCO_3$, 105 D(+)-saccharose, 27
681 D(+)-glucose, 1.7 L(+)-ascorbic acid, 0.5 $CaCl_2$ and 7 $MgCl_2$), using a sliding vibratome (Histocom,
682 Zug, Switzerland). Slices were kept for 30 min in a recovery solution at 35°C (in mM: 131 NaCl,
683 2.5 KCl, 1.25 $NaH_2PO_4$, 26 $NaHCO_3$, 20 D(+)-glucose, 1.7 L(+)-ascorbic acid, 2 $CaCl_2$, 1.2 $MgCl_2$,
684 3 myo-inositol, 2 pyruvate) before being transferred to room temperature for at least 30 min before
685 starting the recording. Slices were placed in the recording chamber of an upright microscope
686 (Olympus BX50WI, Volketswil, Switzerland) and continuously perfused at room temperature with
687 oxygenated ACSF containing (in mM): 131 NaCl, 2.5 KCl, 1.25 $NaH_2PO_4$, 26 $NaHCO_3$, 20 D(+)-
688 glucose, 1.7 L(+)-ascorbic acid, 2 $CaCl_2$ and 1.2 $MgCl_2$. This solution was supplemented in all
689 experiments with 0.1 picrotoxin, 0.01 glycine, with picrotoxin removed for the recordings testing
690 for feedforward inhibition (see Fig. 4). Borders of anterior TRN and ATN+ were visually identified
691 in transillumination using a 10x water-immersion objective. Within a selected nucleus, cells were
692 visualized through differential interference contrast optics a 40x water-immersion objective.
693 Infrared images were acquired with an iXon Camera X2481 (Andor, Belfast, Northern Ireland).
694 Cells were patched using borosilicate glass pipettes (TW150F-4) (World Precision Instruments,
695 Sarasota, FL) pulled with a DMZ horizontal puller (Zeitz Instruments, Martinsried, Germany) to a
696 final resistance of 2.5-5 MΩ. A $K^+$-based intracellular solution that contained (in mM) 140

697 KGluconate, 10 Hepes, 10 KCl, 0.1 EGTA, 10 phosphocreatine, 4 Mg-ATP, 0.4 Na-GTP, pH 7.3,
698 290–305 mOsm, supplemented with ~2 mg/ml of neurobiotin (Vector Labs, Servion, Switzerland)
699 was used for comparative measurements of the passive cellular properties (Fig. 2B,2C), for the
700 cell-attached recordings (Fig. 3C) and for all current-clamp recordings (Fig. 3E). A $Cs^+$-based
701 intracellular solution containing (in mM) 127 CsGluconate, 10 Hepes, 2 CsBAPTA, 6 $MgCl_2$, 10
702 phosphocreatine, 2 Mg-ATP, 0.4 Na-GTP, 2 QX314-Cl, supplemented with ~2 mg/ml of
703 neurobiotin, pH 7.3, 290–305 mOsm) was used with all the other voltage-clamp protocols. For
704 these solutions, a liquid junction potential of -10 mV was taken into account for the current-clamp
705 data. Signals were amplified using a Multiclamp 700B amplifier, digitized via a Digidata1322A and
706 sampled at 10 kHz with Clampex10.2 (Molecular Devices, San José, CA).

707 Recording protocols, optogenetic stimulation and analysis.

708 Immediately after gaining whole-cell access, cell resistance ($R_m$) and cell capacitance ($C_m$) were
709 measured in voltage-clamp at -60 mV through applying 500 ms-long, 10-20 mV hyperpolarizing
710 steps (5 steps/cell). Then the recording was switched to current-clamp to measure the resting
711 membrane potential (RMP). Squared somatic current injections (-50 to -300 pA for 500 ms, 4
712 injections/cell) hyperpolarized neurons below -100 mV from membrane potentials between -50 to
713 -60 mV and induced repetitive burst discharge in TRN neurons and single burst discharge in
714 thalamic neurons (Fig. 2B, 2C). Squared current injections of increasing amplitude (step size, 50
715 pA, 500 ms) were used to depolarize the neurons and generate tonic firing. Action potential
716 properties were measured at the rheobase.

717 Whole-field blue LED (Cairn Res, Faversham, UK) stimulation (455 nm, duration: 0.1 to 1 ms,
718 maximal light intensity 3.5 mW, 0.16 $mW/mm^2$) in voltage-clamp (-60 mV) was used to assess the
719 connectivity of TRN and ATN+ neurons through fibers arising from the PreS/RSC. EPSCs were
720 elicited through single light pulses every 20 s, with a 5 mV hyperpolarizing step to control for the
721 access resistance. After a stable baseline of > 2 min, drugs were applied in the bath (40 µM
722 DNQX, 100 µM D,L-APV). To measure NMDA-components, the holding membrane potential was
723 slowly brought to +40 mV where NMDAR-mediated currents were recorded for 2 min before bath-
724 application of D,L-APV. Single light pulses were used in protocols to measure EPSC kinetics and
725 pharmacological properties (Fig. 2D, 2E). The latency from LED onset, EPSC half-width and
726 EPSC weighted decay time constant were measured with Clampfit 10.2. The effect of bath-
727 application of 40 µM DNQX was measured once the reduction of EPSC amplitude reached a
728 steady state. The NMDA/AMPA ratio was measured by dividing the amplitude of the EPSC at +40

729 mV in DNQX by the amplitude of the EPSC at -60 mV during the baseline and was expressed in
730 percentage.

731 Minimal stimulation was achieved by progressively reducing the intensity of a single light pulse
732 from its maximum (3.5 mW) to a level where only ~50 % of the stimuli induced a successful EPSC.
733 The light intensity potentiometer allowing a limited graduation of light intensities, we could include
734 only a few cells (n=12/50) in which this condition was achieved at 0.28±0.05 mW. In the case of
735 LD neurons, which showed very high amplitude EPSCs with frequent escape currents, none of
736 them reached the criterion to be included. Minimal stimulation was observed for light intensities
737 averaging 0.28±0.05 mW, less than 10 % of the maximum. In a subset of cells (n=8), we slightly
738 increased light intensity to 0.40±0.08 mW to verify whether failure rate decreased but the
739 amplitude of successful responses was maintained. This was achieved in 5 cells in which failure
740 rate decreased to 0 % but the amplitude of successes was 109±4 % of that found during minimal
741 stimulation, whereas it increased to > 140 % in the remaining 3 cases. All successful EPSCs at
742 minimal light stimulation were visually identified and measured in Clampfit10.2.

743 Cell-attached recordings of TRN cells (Fig. 3C) were achieved with recording pipettes of ~5 MΩ
744 resistance, voltage-clamped at 0 mV and ~0 pA of holding current, while applying single light
745 stimuli at varying light intensity (~100 stimuli/cell, one every 10 s). Whole-cell access was then
746 established and cells held in current-clamp at their resting membrane potential. Single light
747 stimulations with similar light intensities were given ~30 times for each cell every 10 s. The number
748 of action currents/action potentials and the interspike interval (ISI) were manually measured on
749 Clampfit10.2. The number of spikes was normalized to the maximum number evoked by the light
750 stimulation. Data were grouped in bins of 0.25 mW of light (Fig. 3C3) and a sigmoidal fit was
751 applied using Igor Pro 7 (WaveMetrics Inc., Lake Oswego, OR). The sigmoidal fit for cell-attached
752 evoked spikes was $= \frac{-78+160}{1+e^{\frac{-(x-0.18)}{0.32}}}$ . The sigmoid fit for whole-cell evoked spikes was $= \frac{-142+232}{1+e^{\frac{-(x-0.2)}{0.73}}}$ .

753 Paired light stimulations at 1, 2, 5, 10 and 20 Hz were used to assess the short-term plasticity of
754 PreS/RSC-TRN and PreS/RSC-ATN+ synapses. The paired pulse ration (PPR) was expressed
755 as the ratio between the second and the first EPSC amplitude (Fig. 3D). Four responses were
756 elicited for each frequency, with an interval of 20 s between each protocol. The amplitude of
757 EPSCs was measured on the average trace in Clampfit10.2, and traces were not included if
758 spontaneous currents appeared in between the paired stimuli.

759 For train stimulation, PreS-RSC afferents to TRN and ATN+ neurons were stimulated with 10 light
760 pulses delivered 1/30 s at 2, 5, 8 and 10 Hz while cells were held at -50 to -60 mV in current-

761 clamp (Fig. 3E). Per stimulation frequency and cell, 5 responses were recorded and averaged.
762 Responses were subdivided into sustained (Fig. 3E1) or entrained (Fig. 3E2) responses based
763 on whether or not the first light pulse elicited an action potential. The number of action potentials
764 generated by the train of stimulation was counted on Clampfit10.2. To quantify sustained and
765 entrained responses, the number of action potentials during the 5 first stimulations was compared
766 to the number of action potentials during the 5 last stimulations. In subthreshold responses, the
767 amplitudes of the phasic responses were calculated from the point of positive inflection after a
768 light stimulation to the next positive peak for each of the 10 subthreshold responses. The
769 persistent depolarization was measured as the difference between the baseline value before the
770 train of stimulation and the point of positive inflexion after each light stimulation. The mean
771 persistent depolarization for the last 3 stimulations was used to quantify the steady state
772 response.

773 To record feedforward inhibitory currents, using the Cs-based intracellular solution defined above,
774 we studied single light-evoked EPSCs recorded in ATN+ cells at -60 mV (uncorrected for a 10
775 mV junction potential). Then the membrane potential of the cell was slowly brought to +15 mV
776 (uncorrected for a 10 mV junction potential). In 6 ATN+ cells, IPSCs were recorded for 4 min (12
777 protocols, once every 20 s) for a baseline, then 10 µM gabazine were bath-applied. The amplitude
778 of the IPSCs in gabazine was measured at the steady state. A similar protocol was applied for 10
779 ATN+ cells recorded in VGAT-Ires-Cre mice expressing the inhibitory DREADD in TRN cells.
780 Instead of gabazine, 10 µM CNO were bath-applied after the baseline recording of IPSCs.
781 Measures of charge transfer were used to take into account the variable waveform of the IPSCs
782 that were composed of multiple superimposed burst-like synaptic events.

783 To determine the connectivity of PV- and Sst-expressing TRN cells, brain slices were prepared
784 from PV-Cre and Sst-Cre lines previously injected with ChR2-expressing virus (see above). Using
785 identical recording and light stimulation conditions, evoked IPSCs were quantified in neurons
786 recorded in the different thalamic nuclei AD, AV and LD.

## 787 ***In vivo* single-unit recordings and head-direction monitoring**

### 788 Electrode and fiber preparation.

789 Two types of recording configurations were used. Multi-wire electrodes were implanted for
790 studying response properties of ATN+ to PreS/RSC stimulation. Silicon probes were used for
791 identification and recording of HD-tuned units in combination with chemogenetic silencing of the
792 anterodorsal TRN.

793 The multi-wire electrodes consisted of 16 individually insulated nichrome wires (13-µm inner
794 diameter, impedance 1 – 3 MΩ; California Fine Wire) contained in a 26-gauge stainless steel
795 guide canula. The wires were attached to a 16-pin connector (CON/16m-V-t, Omnetics) (Courtin
796 et al., 2014), cut at a length of ~2 mm from the edge of the metal guiding tube and gold-plated
797 using a nanoZ™ device (White Matter LLC, provided by Plexon Inc., Dallas, TX) to a final
798 impedance of 50 – 100 kΩ. A silver wire (Warner Instr.) was soldered to the ground pin of the
799 connector. Two animals were implanted with a single shank linear silicone probe (Neuronexus
800 A1x16-5mm-50-703-Z16).

801 The optic fibers were built from a standard hard cladding multimode fiber (225 µm outer diameter,
802 Thorlabs, BFL37-2000/FT200EMT), inserted and glued (Heat-curable epoxy, Precision Fiber
803 Products, ET-353ND-16OZ) to a multimode ceramic zirconia ferrule (Precision Fiber Products,
804 MM-FER2007C-2300). The penetrating end was cut at the desired length (~2 mm) with a Carbide-
805 tip fiber optic scribe (Precision Fiber Products, M1-46124). The other end was polished with fiber-
806 polishing films (Thorlabs). The optic fibers were connected to a PlexBright Optogenetic
807 Stimulation System (Plexon) via home-made patch chord. The connection to the PlexBright Table-
808 top LED Module (Wavelength 465 nm) was achieved through a Mini MM FC 900µm Connector
809 (Precision Fiber Products, MM-CON2004-2300-14-BLK). The other end of the patch chord was
810 inserted into a ceramic zirconia ferrule, fixed with glue and heat-shrinking tube (Allied Electronics,
811 689-0267) and polished. Before the recording, the patch chord was attached to the implanted
812 optic fiber via a ceramic split sleeve (Precision Fiber Products, SM-CS125S).

813 Surgery.

814 Virally injected C57BL6/J and VGAT-Ires-Cre mice were anesthetized with 5 % isoflurane, fixed
815 on a stereotaxic frame and kept on a feedback-controlled heating pad (Phymep). The level of
816 isoflurane was reduced along the surgery until 1 % and mixed with $N_2O$. Craniotomies were
817 opened above the PreS (AP, ML, DV: -3.8, +/-2.5, -1.7), the left ATN (AP, ML, DV: -0.8, +0.75, -
818 2.8) and the lateral cerebellum with a microdrill (1/005 drill-size). The conjunctive tissue on the
819 skull was removed with a scalpel and the skull was cleaned with iodine-based disinfectant. The
820 skull was then scratched with the tip of the scalpel in a grid-like meshwork of grooves to improve
821 the attachment of the glue (Loctite 401, Koening). Multi-wire electrodes and linear silicone probes
822 were lowered vertically, at approximately 10 µm/s initially and then 1 µm/s when reaching the ATN
823 and glued to the skull. Optic fibers were lowered vertically above the PreS at similar rates. For
824 the multi-wire electrodes, the ground silver wire was implanted at the surface of the lateral
825 cerebellum. For silicone probes, the reference and ground wires were twisted together and

826 implanted at the surface of the lateral cerebellum. Carprofen (5 mg/kg, i.p.) and paracetamol (2
827 mg/mL, drinking water) were provided during the peri-operative period. The mice were left in their
828 home cage for a week to recover from the surgery and their weight, behavior and all aspects were
829 monitored in score sheets established with the veterinary protocols. During this period, mice were
830 also habituated to the handling and the recording cables.

831 Unit recordings and HD monitoring.

832 Mice were placed into a large cylindrical Plexiglas cage (diameter: 50 cm, height: 40 cm) where
833 they could freely behave all along the recording sessions. The cage was positioned below a vision
834 color camera inside a Faraday cage. Implanted animals were connected to the pre-amplifier PZ5-
835 32 (Tucker-Davis Technologies (TDT)) via a ZIF-Clip Headstage adaptor (TDT, ZCA-OMN16) for
836 the multi-wire electrodes and a ZIF-Clip Headstage (TDT) for the silicone probes. The camera
837 was connected to a RV2 collection device (TDT) capable of tracking red and green LEDs mounted
838 on the ZIF-Clip Headstage. The preamplifier was connected to a main amplifier RZ5D (TDT). The
839 main computer (WS8, TDT) used the Real-time Processor Visual Design Studio (RPvdsEx) tool
840 to design the recording sessions, activate light stimulation from the PlexBright Optogenetic
841 Stimulation System (Plexon), and acquire the electrophysiological data from the headstage and
842 tracking data from the camera.

843 For C57Bl6/J mice implanted with a multi-wire electrode, a recording session consisted in a 10 –
844 20 min baseline recording followed by a 10 – 20 min recording with optogenetic activation of the
845 PreS/RSC. The stimulation consisted in 300 – 600 light stimulations of 10 ms duration, one
846 stimulation every 2 s. The intensity of the light ranged from 2 – 6 mW depending on the quality of
847 the homemade optic fibers. For VGAT-Ires-Cre mice implanted with a silicone probe, a recording
848 session consisted in a 10 – 20 min baseline recording, i.p. injection of CNO (1 – 2 mg/kg) or NaCl,
849 40 min resting in homecage and 10 – 20 min test recording. The timing of the CNO injection is
850 based on previous *in vivo* work using the same mouse line and CNO products, showing that the
851 CNO effect peaked ~30 min post i.p. injection (Fernandez et al., 2018).

852 Spike sorting.

853 The Offline Sorter software (Plexon), Neuroexplorer (Nex Technologies) and MATLAB
854 (MathWorks) were used to sort and analyze single-unit spikes. The waveforms were manually
855 delineated in the two-dimensional space of principal components using their voltage features.
856 Single units were defined as discrete clusters of waveforms in the principal component space,
857 and did not contain spikes with a refractory period less than 1 ms. The quantification of the clusters

separation was further measured with multivariate ANOVA and J3 statistics. Cross-correlation analyses were used to control that a single unit was not recorded on multiple channels. Target units that had a peak of spike discharge when the reference unit fired were considered as duplicates and only one of the copy was used for analysis (Adapted from (Rozeske et al., 2018)). To compare the recordings during baseline and after injection of CNO, units were sorted with two different methods. At first, both recording sessions were manually sorted as described above while the experimenter was blind to the baseline/CNO condition. In a second step, the baseline sorting template was used for the CNO recording. Both methods gave similar results and only the manual sorted data are shown.

## Unit analysis.

The discharge pattern of well-defined single units in the ATN+ was aligned to the optogenetic stimulation using peri-event raster plots and cumulative histogram (5 ms bins, starting 50 ms before LED onset and lasting 200 ms after LED onset, Neuroexplorer). The firing rate 50 ms before the LED onset was used as a baseline to calculate the Z-score of each bin as follow: $= \frac{measured\ valued - baseline\ average}{baseline\ standard\ error}$. Z-scores were considered significant when > 1.96 and < -1.96. Significant changes in the firing rate fell into 4 distinct classes depending on the direction of the change (increase or decrease firing) and the timing of the change.

Using a custom-made Matlab routine, the discharge patterns of ATN+ units were binned to the HD of the mice. The angles of direction were binned in 6°. The firing rate was averaged for each of the 60 portions of the circle. The length of the Rayleigh vector (r) was calculated and units were considered as HD if $r \geq 0.4$, as head-modulated if $0.2 \leq r < 0.4$ and as not tuned if $r < 0.2$ (Yoder and Taube, 2009). The maximal firing rate, the width and the preferred direction were calculated for HD units. The width of the tuning curve was measured as the span of the angle between the two directions for which the firing rate was equal to 50 % of the maximal firing rate at the preferred direction (Blair and Sharp, 1995).

884 **Behavioral experiment**

885 Recording.

886 One week before the beginning of the behavioral task, VGAT-Ires-Cre mice expressing either an
887 inhibitory DREADD (DREADD mice) or a non DREADD-related (control mice) construct into the
888 anterodorsal TRN were habituated to the handling and i.p. injection. Naïve VGAT-Ires-Cre male
889 mice were trained to find a 12 cm wide circular platform submerged 0.5 – 0.8 cm below the surface
890 in a 150 cm diameter circular pool filled with white opaque water at 23±1°C. Mice were trained in
891 daily sessions composed of 4 consecutive trials, with a 60 s probe session without the platform
892 preceding the first trial session every odd days. A trial ended when the mice spent 5 s onto the
893 platform. Mice were left 10 s more before being placed below a heating lamp before the next trial,
894 10 – 15 s later. Four shapes around the pool (cross, horizontal stripes, vertical stripes, coffee
895 grain) served as visual cues and were placed in the SW, NW, NE, SE corner of the room
896 respectively. If the mouse failed to find the platform after 60 s, the experimenter guided it to the
897 platform where it was left for 15 s. Mice were placed in the pool facing the wall. The position of
898 pool entry was randomly shuffled every day between NE, SE, NW and NE. During a 60 s probe
899 session, the platform was removed and mice were released from the wall of the quadrant opposite
900 to the target one. The experimenter was blind to the condition of the mice (control or DREADD).
901 The session duration (between the first and the last animal) was ~2 hours, the first trial starting at
902 Zeitgeber time 0 + 1.5 h. Daily i.p. injection of CNO (1 – 2 mg/kg) were performed 40 min before
903 the beginning of the session. The timing of the CNO injection is based on previous *in vivo* work
904 using the same mouse line and CNO products, showing that the CNO effect peaked ~30 min post
905 i.p. injection (Fernandez et al., 2018).

906 Analysis and automatic strategy detection.

907 The video tracking data were analyzed using EthoVisionXT14 (Noldus) to quantify the average
908 swimming speed, escape latency, proximity (mean distance of all the tracked points of the path
909 to the platform center), percentage time spent in target quadrant and platform crossings.
910 Heatmaps were generated by superimposing all the path points of every mouse in a group.
911 Heatmaps were linearly scaled using the global minimum and maximum for both groups to allow
912 comparison between the two. To attribute a specific strategy to each MWM trial, we used a
913 homemade matlab algorithm based on (Garthe et al., 2009). For each trial, the animal path in the
914 MWM was extracted as timed-tagged x and y coordinates from which specific variables were
915 computed in order to take a decision. The 8 strategies are described in Suppl. Fig. 5 and the

916 decision was made in the following sequential order with the 4 allocentric strategies first followed
917 by the 4 egocentric strategies: 1-Direct swimming; if 95 % of the time-points are spent in the goal
918 cone (isosceles triangle with its height going from starting point to goal platform with an origin
919 angle of 40°). 2-Focal search; if the mean distance of the path to its centroid (MDTC) was inferior
920 to 35 % standard unit (STDU) corresponding to the radius of the MWM, and the mean distance
921 to the edge of the goal platform was inferior to 30% STDU. 3-directed search; if total time spent
922 in the goal cone was superior to 80 %. 4-perseverance; if the MDTC was inferior to 45 % STDU
923 and the mean distance to the previous platform edge was inferior to 40 % STDU. In our case, the
924 perseverance strategy was only possible after day 10, during the reversal learning period. 5-
925 chaining; if the time spent in the annulus zone (spanning from 33 to 70 % STDU) was superior to
926 80 %. 6-scanning; if the total coverage of the MWM (the pool was divided in 15 cm squares and
927 the coverage was obtained as the ratio of crossed squares over the total number of squares) was
928 superior to 10% and inferior to 60 %, and the mean distance of the path to the center of the MWM
929 was inferior to 70% STDU. 7-thigmotaxis; if the time spent in the closer wall zone (spanning from
930 87 % STDU to the edge of the MWM) was superior to 35 % and the time spend in the wider wall
931 zone (spanning from 70 % STDU to the edge of the MWM) was superior to 65 %. 8-random
932 search; if the total coverage of the MWM was superior to 60 %. If none the conditions could be
933 met in this order, no strategy were attributed.

934 **Statistics**

935 All tests were done using R programming software (2.15.0, R Core Team, The R Foundation for
936 Statistical Computing (www.rproject.org/foundation), 2007]. The normality of the data sets was
937 assessed using Shapiro-Wilk normality test. Comparison of two data sets were done using
938 Student's *t* test and paired Student's *t* test, for non-repeated and repeated measures respectively,
939 or their non-parametric equivalent, Mann-Whitney U test and Wilcoxon signed rank-test. Chi-
940 square tests were used to assess whether the swimming region of mice during probe sessions of
941 the MWM were different from the expected frequencies and the proportion of strategies used
942 between mouse groups. 1-way/2-way (non-)repeated measure ANOVAs followed by post hoc *t*
943 tests were used when necessary on normally distributed data sets whereas non-normally
944 distributed data were analyzed directly with the post hoc tests. A Bonferroni correction was
945 applied when more than two comparisons were done on the same data set and the new alpha
946 threshold is indicated. All statistical tests are specifically indicated in the figure legends if they are
947 not given in the main text.

948

949 # References


950 Ahrens S, Jaramillo S, Yu K, Ghosh S, Hwang GR, Paik R, Lai C, He M, Huang ZJ, Li B (2015) ErbB4 regulation
951 of a thalamic reticular nucleus circuit for sensory selection. Nat Neurosci 18:104-111.
952 Astori S, Lüthi A (2013) Synaptic plasticity at intrathalamic connections via $Ca_V3.3$ T-type $Ca^{2+}$ channels and
953 GluN2B-containing NMDA receptors. J Neurosci 33:624-630.
954 Awasthi A, Ramachandran B, Ahmed S, Benito E, Shinoda Y, Nitzan N, Heukamp A, Rannio S, Martens H,
955 Barth J, Burk K, Wang YT, Fischer A, Dean C (2019) Synaptotagmin-3 drives AMPA receptor
956 endocytosis, depression of synapse strength, and forgetting. Science 363.
957 Blair HT, Sharp PE (1995) Anticipatory head direction signals in anterior thalamus: evidence for a
958 thalamocortical circuit that integrates angular head motion to compute head direction. J Neurosci
959 15:6260-6270.
960 Bubb EJ, Kinnavane L, Aggleton JP (2017) Hippocampal - diencephalic - cingulate networks for memory
961 and emotion: An anatomical guide. Brain Neurosci Adv 1.
962 Butler WN, Smith KS, van der Meer MAA, Taube JS (2017) The head-direction signal plays a functional role
963 as a neural compass during navigation. Curr Biol 27:2406.
964 Calton JL, Taube JS (2005) Degradation of head direction cell activity during inverted locomotion. J
965 Neurosci 25:2420-2428.
966 Castro-Alamancos MA, Calcagnotto ME (1999) Presynaptic long-term potentiation in corticothalamic
967 synapses. J Neurosci 19:9090-9097.
968 Clark BJ, Bassett JP, Wang SS, Taube JS (2010) Impaired head direction cell representation in the
969 anterodorsal thalamus after lesions of the retrosplenial cortex. J Neurosci 30:5289-5302.
970 Clark BJ, Simmons CM, Berkowitz LE, Wilber AA (2018) The retrosplenial-parietal network and reference
971 frame coordination for spatial navigation. Behav Neurosci 132:416-429.
972 Clemente-Perez A, Makinson SR, Higashikubo B, Brovarney S, Cho FS, Urry A, Holden SS, Wimer M, David
973 C, Fenno LE, Acsády L, Deisseroth K, Paz JT (2017) Distinct thalamic reticular cell types differentially
974 modulate normal and pathological cortical rhythms. Cell Rep 19:2130-2142.
975 Cornwall J, Cooper JD, Phillipson OT (1990) Projections to the rostral reticular thalamic nucleus in the rat.
976 Exp Brain Res 80:157-171.
977 Courtin J, Chaudun F, Rozeske RR, Karalis N, Gonzalez-Campo C, Wurtz H, Abdi A, Baufreton J, Bienvenu
978 TC, Herry C (2014) Prefrontal parvalbumin interneurons shape neuronal activity to drive fear
979 expression. Nature 505:92-96.
980 Crabtree JW (2018) Functional diversity of thalamic reticular subnetworks. Front Syst Neurosci 12:41.
981 Crandall SR, Cruikshank SJ, Connors BW (2015) A corticothalamic switch: controlling the thalamus with
982 dynamic synapses. Neuron 86:768-782.
983 Cruikshank SJ, Urabe H, Nurmikko AV, Connors BW (2010) Pathway-specific feedforward circuits between
984 thalamus and neocortex revealed by selective optical stimulation of axons. Neuron 65:230-245.
985 Ding SL (2013) Comparative anatomy of the prosubiculum, subiculum, presubiculum, postsubiculum, and
986 parasubiculum in human, monkey, and rodent. J Comp Neurol 521:4145-4162.
987 Dolleman-van der Weel MJ, Morris RG, Witter MP (2009) Neurotoxic lesions of the thalamic reuniens or
988 mediodorsal nucleus in rats affect non-mnemonic aspects of watermaze learning. Brain Struct
989 Funct 213:329-342.
990 Dong P, Wang H, Shen XF, Jiang P, Zhu XT, Li Y, Gao JH, Lin S, Huang Y, He XB, Xu FQ, Duan S, Lian H, Wang
991 H, Chen J, Li XM (2019) A novel cortico-intrathalamic circuit for flight behavior. Nat Neurosci
992 22:941-949.
993 Dumont JR, Taube JS (2015) The neural correlates of navigation beyond the hippocampus. Prog Brain Res
994 219:83-102.

Fernandez LM, Vantomme G, Osorio-Forero A, Cardis R, Béard E, Lüthi A (2018) Thalamic reticular control of local sleep in mouse sensory cortex. Elife 7.

Fernandez LMJ, Pellegrini C, Vantomme G, Béard E, Lüthi A, Astori S (2017) Cortical afferents onto the nucleus Reticularis thalami promote plasticity of low-threshold excitability through GluN2C-NMDARs. Sci Rep 7:12271.

Garthe A, Kempermann G (2013) An old test for new neurons: refining the Morris water maze to study the functional relevance of adult hippocampal neurogenesis. Front Neurosci 7:63.

Gentet LJ, Ulrich D (2004) Electrophysiological characterization of synaptic connections between layer VI cortical cells and neurons of the nucleus reticularis thalami in juvenile rats. Eur J Neurosci 19:625-633.

Gjoni E, Zenke F, Bouhours B, Schneggenburger R (2018) Specific synaptic input strengths determine the computational properties of excitation-inhibition integration in a sound localization circuit. J Physiol 596:4945-4967.

Golshani P, Liu XB, Jones EG (2001) Differences in quantal amplitude reflect GluR4- subunit number at corticothalamic synapses on two populations of thalamic neurons. Proc Natl Acad Sci U S A 98:4172-4177.

Gonzalo-Ruiz A, Lieberman AR (1995a) Topographic organization of projections from the thalamic reticular nucleus to the anterior thalamic nuclei in the rat. Brain Res Bull 37:17-35.

Gonzalo-Ruiz A, Lieberman AR (1995b) GABAergic projections from the thalamic reticular nucleus to the anteroventral and anterodorsal thalamic nuclei of the rat. J Chem Neuroanat 9:165-174.

Goodridge JP, Taube JS (1997) Interaction between the postsubiculum and anterior thalamus in the generation of head direction cell activity. J Neurosci 17:9315-9330.

Halassa MM, Chen Z, Wimmer RD, Brunetti PM, Zhao S, Zikopoulos B, Wang F, Brown EN, Wilson MA (2014) State-dependent architecture of thalamic reticular subnetworks. Cell 158:808-821.

Herrera CG, Cadavieco MC, Jego S, Ponomarenko A, Korotkova T, Adamantidis A (2016) Hypothalamic feed-forward inhibition of thalamocortical network controls arousal and consciousness. Nat Neurosci 19:290-298.

Huguenard JR (1996) Low-threshold calcium currents in central nervous system neurons. Annu Rev Physiol 58:329-348.

Krol A, Wimmer RD, Halassa MM, Feng G (2018) Thalamic reticular dysfunction as a circuit endophenotype in neurodevelopmental disorders. Neuron 98:282-295.

Krout KE, Loewy AD, Westby GW, Redgrave P (2001) Superior colliculus projections to midline and intralaminar thalamic nuclei of the rat. J Comp Neurol 431:198-216.

Le Masson G, Renaud-Le Masson S, Debay D, Bal T (2002) Feedback inhibition controls spike transfer in hybrid thalamic circuits. Nature 417:854-858.

Lee SM, Friedberg MH, Ebner FF (1994) The role of GABA-mediated inhibition in the rat ventral posterior medial thalamus. II. Differential effects of GABAA and GABAB receptor antagonists on responses of VPM neurons. J Neurophysiol 71:1716-1726.

Lozsádi DA (1994) Organization of cortical afferents to the rostral, limbic sector of the rat thalamic reticular nucleus. J Comp Neurol 341:520-533.

Lozsádi DA (1995) Organization of connections between the thalamic reticular and the anterior thalamic nuclei in the rat. J Comp Neurol 358:233-246.

Miniaci MC, De Leonibus E (2018) Missing the egocentric spatial reference: a blank on the map. F1000Res 7:168.

Mitchell AS, Czajkowski R, Zhang N, Jeffery K, Nelson AJD (2018) Retrosplenial cortex and its role in spatial cognition. Brain Neurosci Adv 2:2398212818757098.

Paré D, Steriade M, Deschênes M, Oakson G (1987) Physiological characteristics of anterior thalamic nuclei, a group devoid of inputs from reticular thalamic nucleus. J Neurophysiol 57:1669-1685.

1043 Perry BAL, Mitchell AS (2019) Considering the evidence for anterior and laterodorsal thalamic nuclei as
1044 higher order relays to cortex. Front Mol Neurosci 12:167.
1045 Peyrache A, Schieferstein N, Buzsáki G (2017) Transformation of the head-direction signal into a spatial
1046 code. Nat Commun 8:1752.
1047 Peyrache A, Lacroix MM, Petersen PC, Buzsáki G (2015) Internally organized mechanisms of the head
1048 direction sense. Nat Neurosci 18:569-575.
1049 Peyrache A, Duszkiewicz AJ, Viejo G, Angeles-Duran S (2019) Thalamocortical processing of the head-
1050 direction sense. Prog Neurobiol:101693.
1051 Pinault D (2004) The thalamic reticular nucleus: structure, function and concept. Brain Res Brain Res Rev
1052 46:1-31.
1053 Pinault D, Deschênes M (1998) Projection and innervation patterns of individual thalamic reticular axons
1054 in the thalamus of the adult rat: a three-dimensional, graphic, and morphometric analysis. J Comp
1055 Neurol 391:180-203.
1056 Rogers J, Churilov L, Hannan AJ, Renoir T (2017) Search strategy selection in the Morris water maze
1057 indicates allocentric map formation during learning that underpins spatial memory formation.
1058 Neurobiol Learn Mem 139:37-49.
1059 Rozeske RR, Jercog D, Karalis N, Chaudun F, Khoder S, Girard D, Winke N, Herry C (2018) Prefrontal-
1060 periaqueductal gray-projecting neurons mediate context fear discrimination. Neuron 97:898-910
1061 e896.
1062 Scheibel ME, Scheibel AB (1966) The organization of the nucleus reticularis thalami: a Golgi study. Brain
1063 Res 1:43-62.
1064 Sherman SM (2001) Thalamic relay functions. Prog Brain Res 134:51-69.
1065 Sherman SM (2017) Functioning of circuits connecting thalamus and cortex. Compr Physiol 7:713-739.
1066 Sherman SM, Guillery RW (1998) On the actions that one nerve cell can have on another: distinguishing
1067 "drivers" from "modulators". Proc Natl Acad Sci U S A 95:7121-7126.
1068 Sheroziya M, Timofeev I (2014) Global intracellular slow-wave dynamics of the thalamocortical system. J
1069 Neurosci 34:8875-8893.
1070 Simonnet J, Fricker D (2018) Cellular components and circuitry of the presubiculum and its functional role
1071 in the head direction system. Cell Tissue Res 373:541-556.
1072 Soto-Sánchez C, Wang X, Vaingankar V, Sommer FT, Hirsch JA (2017) Spatial scale of receptive fields in the
1073 visual sector of the cat thalamic reticular nucleus. Nat Commun 8:800.
1074 Stackman RW, Jr., Lora JC, Williams SB (2012) Directional responding of C57BL/6J mice in the Morris water
1075 maze is influenced by visual and vestibular cues and is dependent on the anterior thalamic nuclei.
1076 J Neurosci 32:10211-10225.
1077 Taube JS (1995) Head direction cells recorded in the anterior thalamic nuclei of freely moving rats. J
1078 Neurosci 15:70-86.
1079 Taube JS, Muller RU, Ranck JB, Jr. (1990) Head-direction cells recorded from the postsubiculum in freely
1080 moving rats. I. Description and quantitative analysis. J Neurosci 10:420-435.
1081 Taube JS, Kesslak JP, Cotman CW (1992) Lesions of the rat postsubiculum impair performance on spatial
1082 tasks. Behav Neural Biol 57:131-143.
1083 Tsanov M, Chah E, Vann SD, Reilly RB, Erichsen JT, Aggleton JP, O'Mara SM (2011) Theta-modulated head
1084 direction cells in the rat anterior thalamus. J Neurosci 31:9489-9502.
1085 Usrey WM, Sherman SM (2019) Corticofugal circuits: Communication lines from the cortex to the rest of
1086 the brain. J Comp Neurol 527:640-650.
1087 Valerio S, Taube JS (2012) Path integration: how the head direction signal maintains and corrects spatial
1088 orientation. Nat Neurosci 15:1445-1453.
1089 van der Meer MAA, Richmond Z, Braga RM, Wood ER, Dudchenko PA (2010) Evidence for the use of an
1090 internal sense of direction in homing. Behav Neurosci 124:164-169.

1091 van Groen T, Wyss JM (1990) The postsubicular cortex in the rat: characterization of the fourth region of
1092 the subicular cortex and its connections. Brain Res 529:165-177.
1093 Vantomme G, Osorio-Forero A, Lüthi A, Fernandez LMJ (2019) Regulation of local sleep by the thalamic
1094 reticular nucleus. Front Neurosci 13:576.
1095 Vong L, Ye C, Yang Z, Choi B, Chua S, Jr., Lowell BB (2011) Leptin action on GABAergic neurons prevents
1096 obesity and reduces inhibitory tone to POMC neurons. Neuron 71:142-154.
1097 Weese GD, Phillips JM, Brown VJ (1999) Attentional orienting is impaired by unilateral lesions of the
1098 thalamic reticular nucleus in the rat. J Neurosci 19:10135-10139.
1099 Wilkins LK, Girard TA, Herdman KA, Christensen BK, King J, Kiang M, Bohbot VD (2017) Hippocampal
1100 activation and memory performance in schizophrenia depend on strategy use in a virtual maze.
1101 Psychiatry Res Neuroimaging 268:1-8.
1102 Wimmer RD, Schmitt LI, Davidson TJ, Nakajima M, Deisseroth K, Halassa MM (2015) Thalamic control of
1103 sensory selection in divided attention. Nature 526:705-709.
1104 Wright NF, Erichsen JT, Vann SD, O'Mara SM, Aggleton JP (2010) Parallel but separate inputs from limbic
1105 cortices to the mammillary bodies and anterior thalamic nuclei in the rat. J Comp Neurol
1106 518:2334-2354.
1107 Yoder RM, Taube JS (2009) Head direction cell activity in mice: robust directional signal depends on intact
1108 otolith organs. J Neurosci 29:1061-1076.
1109 Yoder RM, Valerio S, Crego ACG, Clark BJ, Taube JS (2019) Bilateral postsubiculum lesions impair visual
1110 and nonvisual homing performance in rats. Behav Neurosci 133:496-507.
1111 Zikopoulos B, Barbas H (2007) Circuits formultisensory integration and attentional modulation through
1112 the prefrontal cortex and the thalamic reticular nucleus in primates. Rev Neurosci 18:417-438.
1113 Zikopoulos B, Barbas H (2012) Pathways for emotions and attention converge on the thalamic reticular
1114 nucleus in primates. J Neurosci 32:5338-5350.

1115

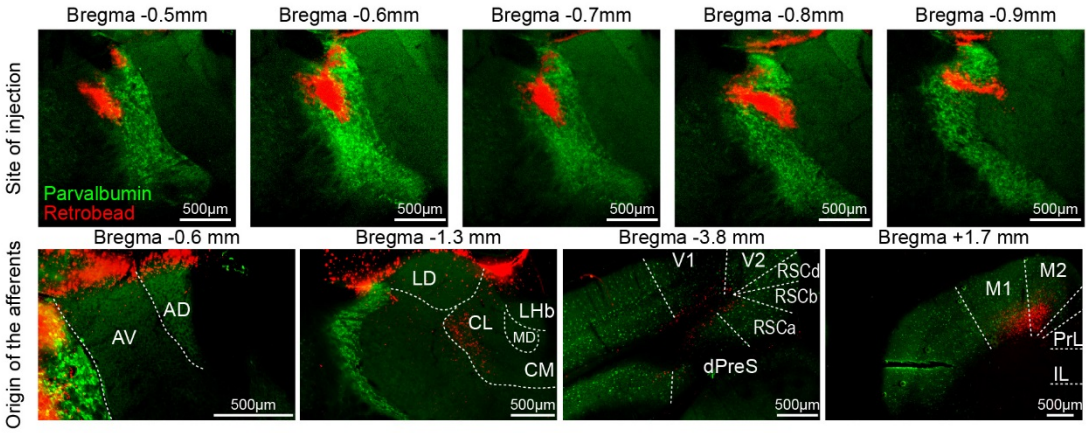
Bregma -0.5mm
Bregma -0.6mm
Bregma -0.7mm
Bregma -0.8mm
Bregma -0.9mm
Site of injection
Parvalbumin
Retrobead
500μm
Bregma -0.6 mm
Bregma -1.3 mm
Bregma -3.8 mm
Bregma +1.7 mm
Origin of the afferents
AV
AD
LD
CL
LHb
MD
CM
V1
V2
RSCd
RSCb
RSCa
dPreS
M1
M2
PrL
IL

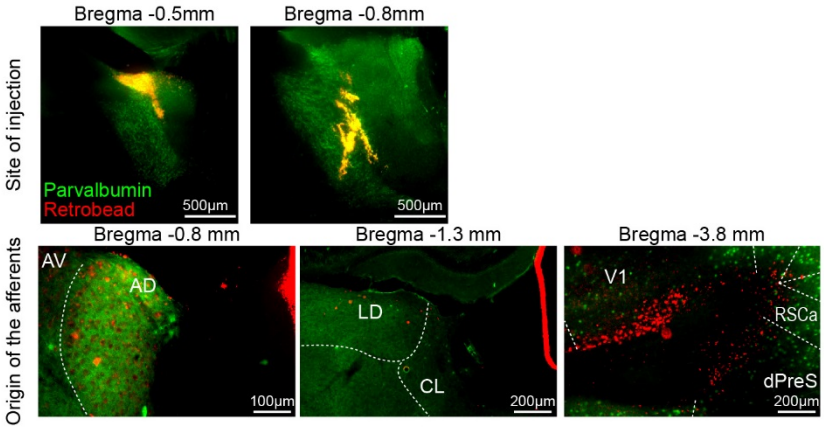
Bregma -0.5mm
Bregma -0.8mm
Site of injection
Parvalbumin
Retrobead
500μm
Bregma -0.8 mm
Bregma -1.3 mm
Bregma -3.8 mm
Origin of the afferents
AV
AD
100μm
LD
CL
200μm
V1
RSCa
dPreS

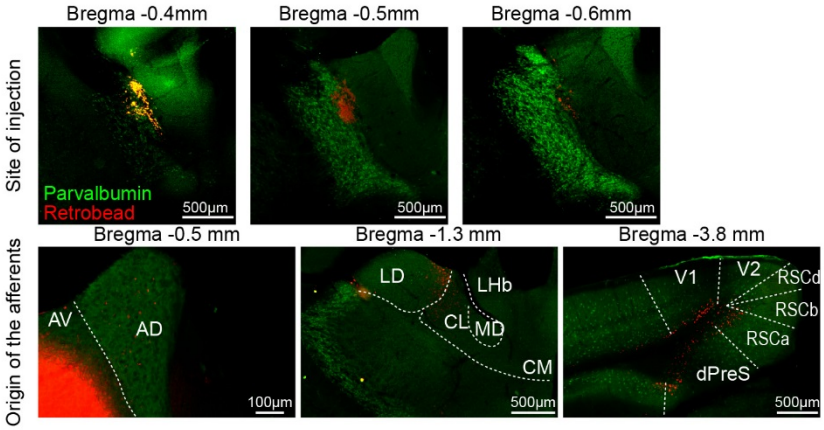
Bregma -0.4mm
Bregma -0.5mm
Bregma -0.6mm
Site of injection
Parvalbumin
Retrobead
500μm
Bregma -0.5 mm
Bregma -1.3 mm
Bregma -3.8 mm
Origin of the afferents
AV
AD
100μm
LD
LHb
CL
MD
CM
V1
V2
RSCd
RSCb
RSCa
dPreS

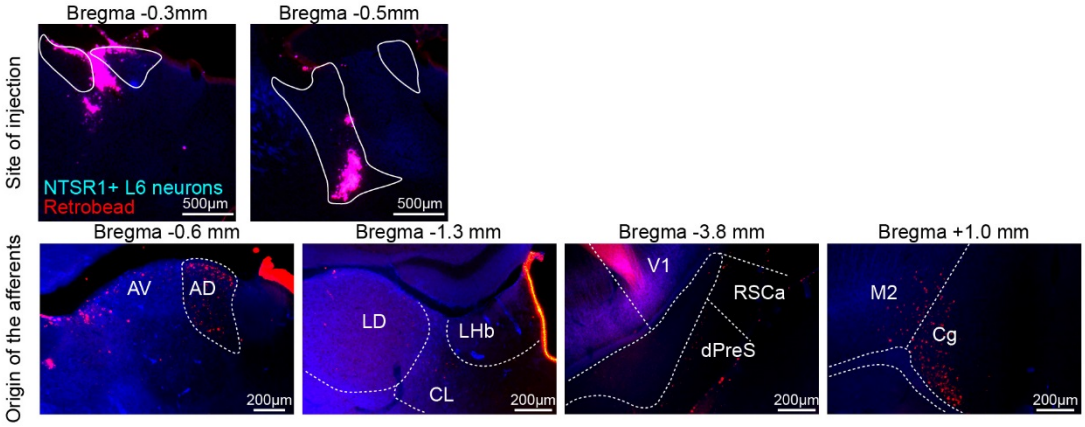
Bregma -0.3mm
Bregma -0.5mm
Site of injection
NTSR1+ L6 neurons
Retrobead
500μm
Bregma -0.6 mm
Bregma -1.3 mm
Bregma -3.8 mm
Bregma +1.0 mm
Origin of the afferents
AV
AD
200μm
LD
LHb
CL
V1
RSCa
dPreS
M2
Cg

**Supplementary Figure 1. The anterior TRN receives afferents from ATN+, RSC, PreS, cingulate, visual and motor cortices.**

**(A-D)** Five Epifluorescent micrographs of mouse coronal brain sections showing the full extent of a retrobead (red) injection into the anterior portion of the TRN (top) and brain regions where retrobeads were retrogradely transported, thus indicating afferent origin (bottom). **(A-C)** immunostaining for PV (green). **(D)** Immunostaining for NTSR1+ L6 cortical neurons and their projection to the thalamus (blue). Anterodorsal thalamus (AD) – Anteroventral thalamus (AV) – Laterodorsal thalamus (LD) – Mediodorsal thalamus (MD) – Lateral habenula (LHb) – Centrolateral thalamus (CL) – Centromedial thalamus (CM) – Cingulate cortex (Cg) – prelimbic/infralimbic cortex (PreL/IL) – Dorsal presubiculum (dPreS) – Retrosplenial cortex (RSC) – Visual cortex (V1/V2) – Motor cortex (M1/M2) – Prelimbic cortex (PrL) – Infralimbic cortex (IL).

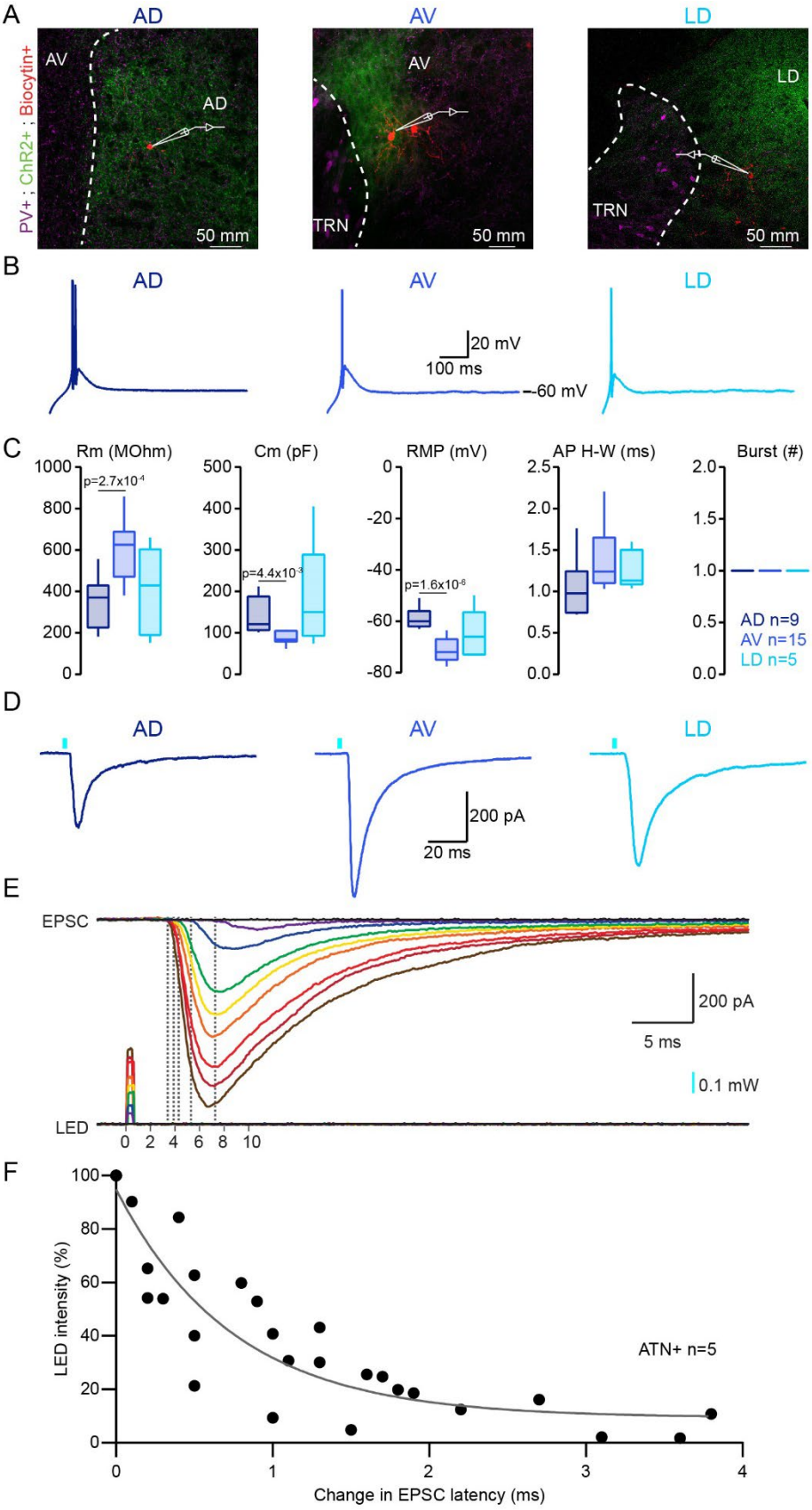
A
AD
AV
LD
PV+ ; ChR2+ ; Biocytin+
AV
AD
50 mm
AV
TRN
50 mm
LD
TRN
50 mm
B
AD
AV
LD
20 mV
100 ms
-60 mV
C
Rm (MOhm)
p=2.7x10-4
Cm (pF)
p=4.4x10-3
RMP (mV)
p=1.6x10-6
AP H-W (ms)
Burst (#)
AD n=9
AV n=15
LD n=5
D
AD
AV
LD
200 pA
20 ms
E
EPSC
200 pA
5 ms
0.1 mW
LED
0 2 4 6 8 10
F
LED intensity (%)
ATN+ n=5
Change in EPSC latency (ms)

**Supplementary Figure 2. The PreS/RSC establish functional excitatory synapses onto AD, AV and LD.**

**(A)** Confocal micrographs of 300 µm-thick mouse brain sections showing the whole-cell recorded AD (left), AV (middle) and LD (right) neurons filled with neurobiotin (red). Green, ChR2-EYFP-expressing PreS/RSC afferents, magenta, PV+ TRN cells. **(B)** Voltage responses of neurons shown in A to a negative current injection. (C) Box-and-whisker plots of passive and active cellular properties of PreS/RSC-connected AD (green, n=9), AV (orange, n=15) and LD (blue, n=5) neurons. From left to right: Membrane resistance (Rm), membrane capacitance (Cm), resting membrane potential (RMP), action potential (AP) half-width (H-W), burst number. Student's *t* tests were used to compare Vm, Rm and Cm. A Mann-Whitney U test was used for comparing HW. **(D)** Current responses of AD (left), AV (middle) and LD (right) neurons to optogenetic activation (blue bars, 1 ms, 3.5 mW power, 455 nm) of PreS/RSC afferents, recorded at -60 mV. **(E)** Current responses of a thalamic neuron to optogenetic stimulation of PreS/RSC afferents at different intensities. **(F)** Graph showing the increasing latency of the EPSC latency when reducing light stimulation intensity in 5 ATN+ neurons.

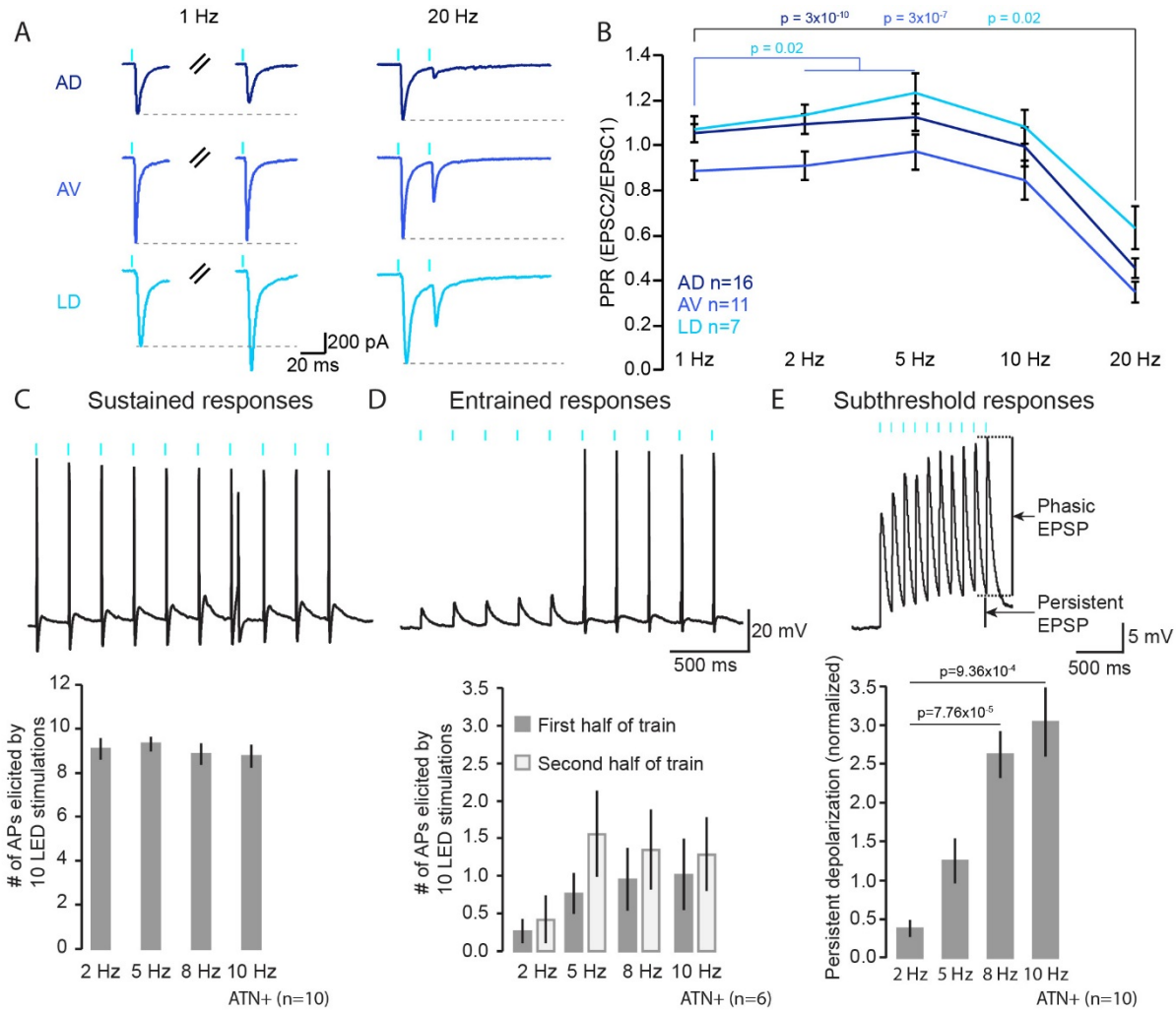


**Supplementary Figure 3. The ATN+ receives strong unitary connections with 'driver' characteristics from the PreS/RSC.**

**(A)** Representative current responses of AD, AV and LD neurons held at -60 mV upon paired-pulse stimulation at 1 and 20 Hz. Grey dotted lines correspond to the amplitude of the first EPSC. **(B)** Graph of the paired-pulse ratios. Paired Student's *t* tests with Bonferroni correction for multiple comparisons for PPR at 1 Hz vs PPR at other frequencies (α = 0.013). **(C)** Top: typical membrane voltage response of an ATN+ neuron to a train of 10 light stimulations at 10 Hz. Action potentials are elicited from the first light stimulation, classifying it as a sustained response. Bottom: Histogram of action potential numbers during such train stimulations in ATN+ neurons (n = 10) showing sustained response patterns. Wilcoxon signed rank-tests were used to compare between the 2 Hz and the other frequencies of stimulation, with Bonferroni correction for multiple comparison (α = 0.017). **(D)** Top: same as in C when neurons responded with a subthreshold response at train onset, classifying them as an entrained response. Bottom: Histogram of action potential numbers during the first half (5 first light stimulation) and the second half of the train of 10 light stimulations in ATN+ neurons (n = 6). A Wilcoxon signed rank-test (at 2 Hz) and Paired Student's *t* tests (at 5, 8, 10 Hz) were used to compare the number of action potentials elicited during the first half vs the second half of the train of stimulation. **(E)** Top: same as in C for subthreshold responses in an ATN+ neuron held at -60 mV. Bottom: Histogram of the persistent depolarization induced by trains in TRN neurons (n = 5). The persistent depolarization was measured on the last 3 stimulations of the train, see methods for the details. Paired Student's *t* tests with Bonferroni correction for multiple comparison (α = 0.017) were used to compare the persistent depolarization at 2 Hz with the persistent depolarization at other frequencies.

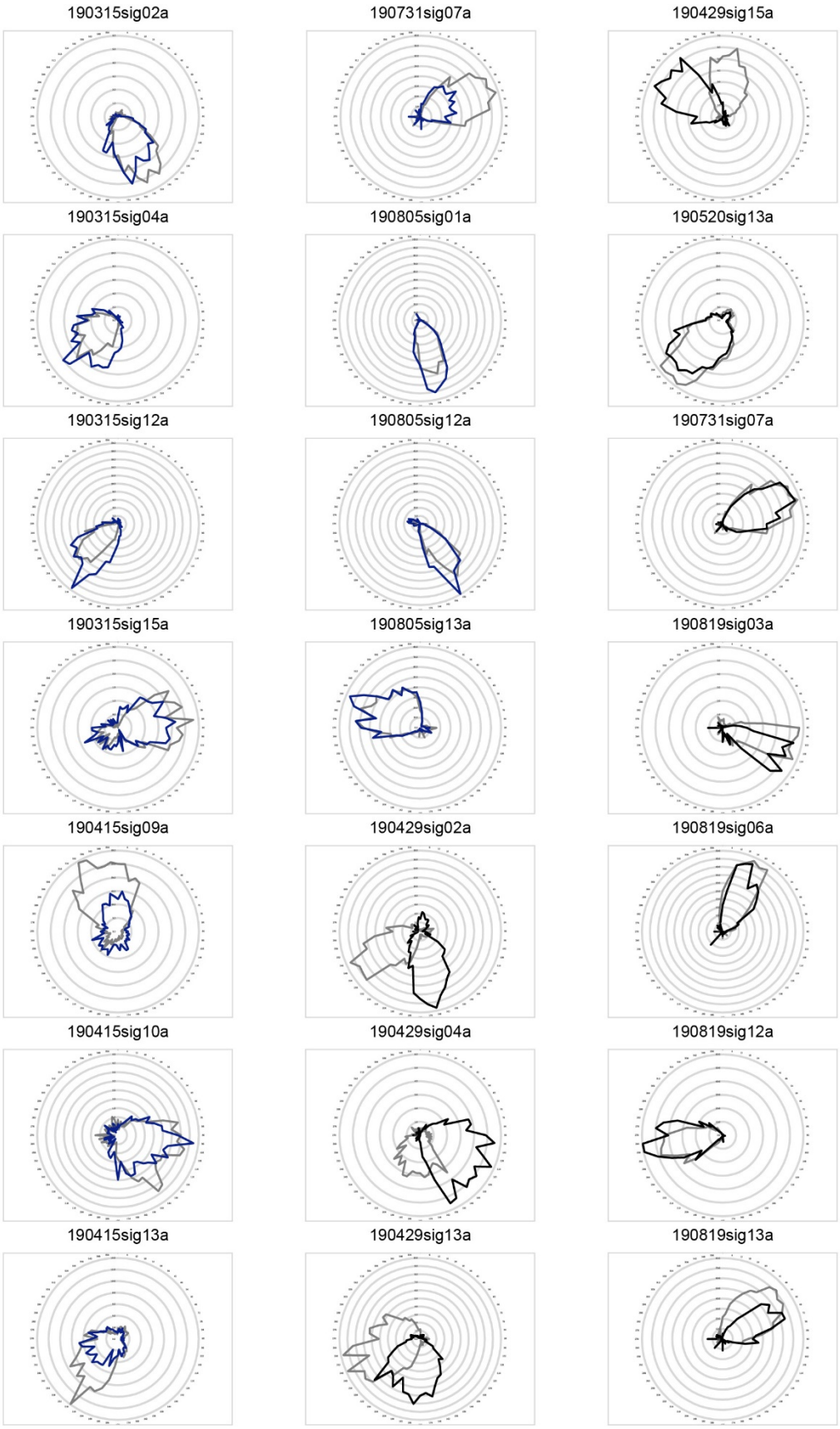


**Supplementary Figure 4. Effect of chemogenetic silencing of anterodorsal TRN neurons onto the tuning of thalamic head-direction neurons.**

Polar plots of all HD units recorded before (grey) and after CNO (blue) or NaCl (black) injection.

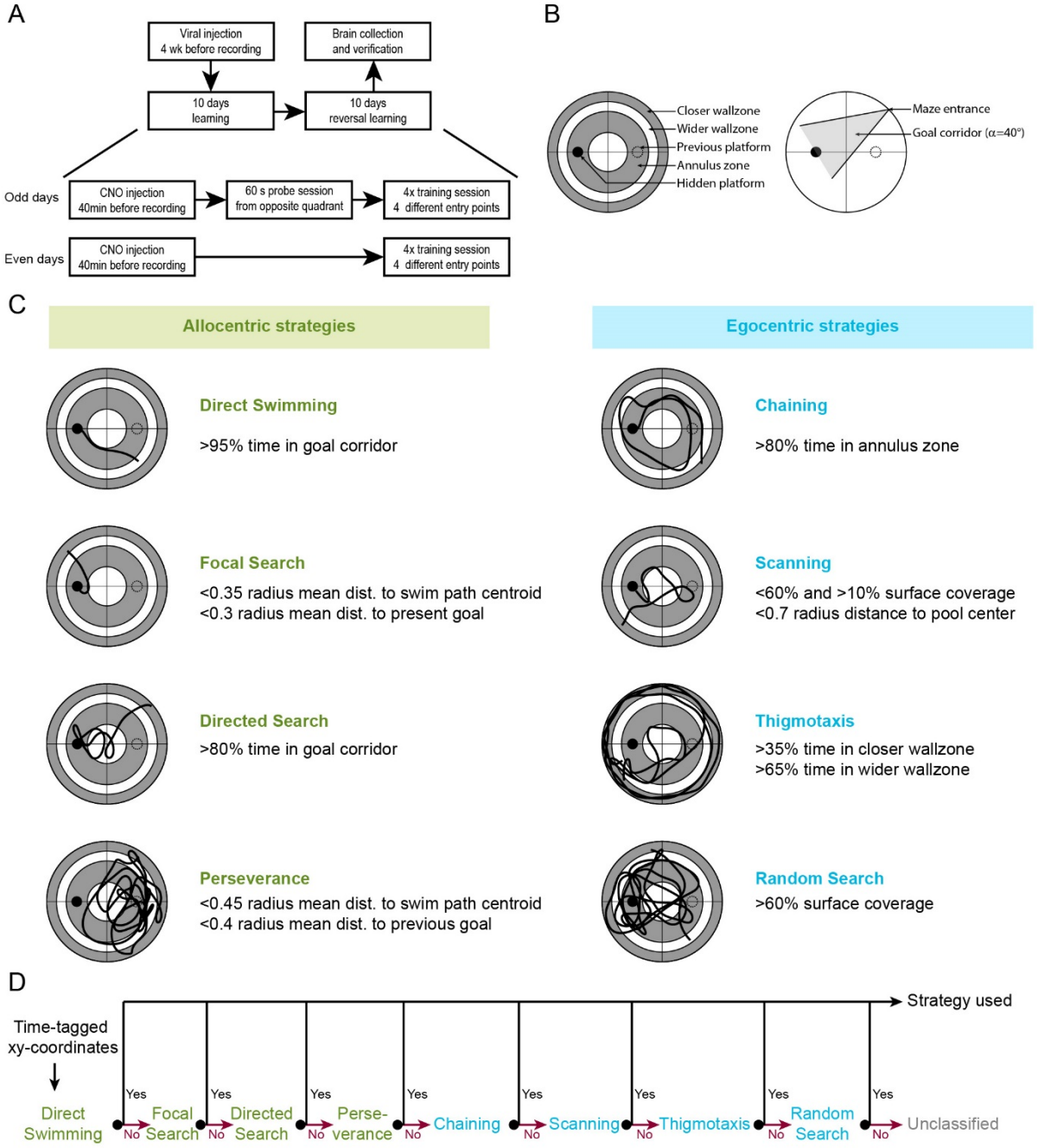


**Supplementary Figure 5. Design of Morris Water tasks and algorithm-based classification of search strategies.**

**(A)** Scheme of the experimental design. For further details, see methods. **(B)** Representation of the variables used for the classification process. The pool was divided into several areas to calculate the respective amount of time spent into these specifics areas (left). The average distance of all the data points constituting the search path to its centroid, the present platform and the former platform was used for the classification. Search patterns based on a directional preference for the actual platform were identified using a triangular shaped corridor expanding from the entry point of the mice with its bisecting line towards the platform (right). **(C)** Strategies were identified by one or two parameters representing their major properties. **(D)** The algorithm excluded strategies from the more to the less specific search patterns. Search patterns not recognized were grouped as unclassified strategies.

eLIFE
elifesciences.org

RESEARCH ARTICLE

# Thalamic reticular control of local sleep in mouse sensory cortex

**Laura MJ Fernandez, Gil Vantomme, Alejandro Osorio-Forero, Romain Cardis, Elidie Béard, Anita Lüthi***

Department of Fundamental Neurosciences, University of Lausanne, Lausanne, Switzerland

**Abstract** Sleep affects brain activity globally, but many cortical sleep waves are spatially confined. Local rhythms serve cortical area-specific sleep needs and functions; however, mechanisms controlling locality are unclear. We identify the thalamic reticular nucleus (TRN) as a source for local, sensory-cortex-specific non-rapid-eye-movement sleep (NREMS) in mouse. Neurons in optogenetically identified sensory TRN sectors showed stronger repetitive burst discharge compared to non-sensory TRN cells due to higher activity of the low-threshold $Ca^{2+}$ channel $Ca_V3.3$. Major NREMS rhythms in sensory but not non-sensory cortical areas were regulated in a $Ca_V3.3$-dependent manner. In particular, NREMS in somatosensory cortex was enriched in fast spindles, but switched to delta wave-dominated sleep when $Ca_V3.3$ channels were genetically eliminated or somatosensory TRN cells chemogenetically hyperpolarized. Our data indicate a previously unrecognized heterogeneity in a powerful forebrain oscillator that contributes to sensory-cortex-specific and dually regulated NREMS, enabling local sleep regulation according to use- and experience-dependence.
DOI: https://doi.org/10.7554/eLife.39111.001

***For correspondence:** anita.luthi@unil.ch

**Competing interests:** The authors declare that no competing interests exist.

**Funding:** See page 20

**Received:** 15 June 2018
**Accepted:** 19 December 2018
**Published:** 25 December 2018

**Reviewing editor:** John Huguenard, Stanford University School of Medicine, United States



## Introduction

Sleep is a global vigilance state with well-known behavioral, electroencephalographic and neuromodulatory attributes. However, cerebral correlates of non-rapid-eye-movement sleep (NREMS) and REMS, notably several major EEG sleep rhythms, occur variably at different times in different brain regions (***Massimini et al., 2004***; ***Nir et al., 2011***; ***Siclari and Tononi, 2017***). This suggests that, on top of a global regulation, forebrain pacemakers with regionally specific oscillatory properties shape sleep across the cortex (***Krueger et al., 2013***). Such local aspects probably underlie the sleeping brain's decreased capacity to integrate external information and enable plasticity in specific neural circuits (***Siclari and Tononi, 2017***; ***Crunelli et al., 2018***). For example, sleep-dependent memory consolidation is linked to spatially confined regulation of NREMS rhythms in the brain areas involved in recent learning (***Rasch and Born, 2013***). Furthermore, sleep disorders may arise from a pathologically altered spatial heterogeneity that negatively impacts sleep as a global state (***Krueger et al., 2013***; ***Siclari and Tononi, 2017***).

Prototype cellular pacemakers for NREMS rhythms, notably for the slow-oscillation (SO) (<1 Hz), delta waves (1–4 Hz) and sleep spindles (10–15 Hz) have been known for decades (for review, see (***Steriade et al., 1993***; ***Astori et al., 2013***; ***Sanchez-Vives et al., 2017***)). However, the spatiotemporal variability of cortical rhythms challenges the idea that these are homogeneous sources across the cortical surface (***Piantoni et al., 2016***; ***Siclari and Tononi, 2017***). For example, 'fast' and 'slow' human sleep spindles distribute variably and correlate differentially with memory consolidation, which has prompted a search for at least two, if not several, separately active spindle generators (***Schabus et al., 2007***; ***Frauscher et al., 2015***). Interestingly, anatomical and functional boundaries of cortical areas go in parallel with variations of sleep rhythms (***Fernandez et al., 2017***;

**eLife digest** Falling asleep affects our behavior immediately and profoundly. During sleep, large electrical waves appear across the brain in areas responsible for consciousness, sensation and movement. In the cortex – the outer layer of the brain – sleep waves arise from networks that connect to the thalamus, a deeper structure within the brain. However, not all areas of the brain sleep equally. We know this intuitively because sensory stimuli, such as an alarm clock or a baby's cry, can still wake us up. By contrast, we typically do not move much or take major decisions while we sleep. Therefore, the brain areas involved in sensation should not be expected to sleep in the same way as areas involved in movement or reasoning.

Neighboring brain areas generally show very different sleep waves. The brain regions that we use during the day can also affect how sleep varies from one area to the next. It is not well understood what determines these 'local' sleep properties.

By studying the brains of mice, Fernandez et al. now show that the networks between the cortex and thalamus are much more varied than previously thought, in particular regarding a thalamic nucleus that is relevant for sleep wave generation. These previously unrecognized differences deep within the brain are part of the origin of local sleep in the outer layer of the brain. Sleep wave activity differed depending on whether the networks were involved in sensory or non-sensory roles. The networks allow sensory areas to switch efficiently between different forms of local sleep. This might underlie how the brain's sensory activity during the day can influence local sleep at night.

There is growing evidence that major sleep disorders are due to disturbances to local sleep. Techniques to modify or restore specific sleep waves locally in the brain could help to develop new sleep therapies. For example, having a detailed map of electrical waves within the sleep-disordered brain could help researchers to apply transcranial stimulation techniques in ways that might help to treat these debilitating disorders.

DOI: https://doi.org/10.7554/eLife.39111.002

***Piantoni et al., 2017***). Moreover, sleep rhythms can show local singularities within a single cortical area according to developmental stage, or as a result of experience and learning during the day (***Huber et al., 2004***; ***Kurth et al., 2010***; ***Johnson et al., 2012***; ***Laventure et al., 2016***). There is also evidence for the localized appearance of sleep-related patterns in individual cortical columns (***Pigarev et al., 1997***; ***Rector et al., 2005***). Therefore, modality-specific thalamocortical loops could account for diversity in local NREMS. Moreover, there should be powerful local tuning mechanisms to locally switch between different NREMS rhythms. The current view is dominated by cortical focal influences as essential to shape local rhythms (***Contreras et al., 1996***; ***Piantoni et al., 2017***; ***Siclari and Tononi, 2017***). In contrast, thalamic oscillators are seen as broad and relatively homogeneous sources of oscillatory power that can spread focally or globally to cortex (***Bonjean et al., 2012***), but that have little bearing on their ultimate cortical correlates.

This view is becoming revised as novel observations on heterogeneous thalamic pacemaker mechanisms are reported. Of interest is the thalamic reticular nucleus (TRN), typically referred to as an inhibitory shell of highly oscillatory, burst-prone cells surrounding the dorsal thalamus (***Pinault, 2004***; ***Fogerson and Huguenard, 2016***). Burst discharge generates large inhibitory synaptic potentials (***Herd et al., 2013***; ***Rovó et al., 2014***) that entrain thalamocortical neurons into rhythmicity. Bursting is based on the $Ca_V3.3$ channel that is crucial for sleep spindle generation (***Astori et al., 2011***; ***Pellegrini et al., 2016***), but many studies indicate that not all TRN cells burst equally (***Contreras et al., 1992***; ***Brunton and Charpak, 1997***; ***Lee et al., 2007***; ***Kimura et al., 2012***; ***Clemente-Perez et al., 2017***; ***Higashikubo and Moore, 2018***). Then, the TRN is parcellated into at least five modality-specific sectors, sensory, motor or limbic ones, according to their innervation by a particular dorsal thalamic nucleus and the reciprocally connected cortical area (***Crabtree, 1999***; ***Pinault, 2004***). Moreover, optogenetic activation of TRN promotes cortical spindles or delta waves (***Halassa et al., 2011***; ***Lewis et al., 2015***), suggesting that the exact patterns of TRN cell activity may determine the contribution of these two rhythms at the cortical surface. Most recently, various discharge propensity in TRN cells was linked to the differential expression of parvalbumin (PV) or somatostatin (***Clemente-Perez et al., 2017***). The number of PV-expressing cells is

smaller in TRN of schizophrenic patients and mouse models (**Steullet et al., 2018**) in which reduced sleep spindle density is a common observation (**Manoach et al., 2016**). Together, there is accruing evidence for marked molecular and functional TRN cell heterogeneity. However, whether TRN heterogeneity is relevant for brain correlates of NREMS has so far not been tested.

This study shows that the heterogeneous cellular properties of optogenetically identified TRN sectors are a major source of local NREMS rhythms in sensory cortices. We identify the ionic mechanisms underlying this heterogeneity and study its impact on major NREMS correlates in sensory and non-sensory cortices using genetic and chemogenetic approaches. We thereby unravel novel organizing principles of NREMS topography in mouse and show that heterogeneity in TRN sectors accounts for a previously unrecognized enrichment of fast and large sleep spindles in somatosensory cortices that are coupled to the SO. We also find that TRN heterogeneity enables rapid switching between different forms of NREMS rhythms, suggesting that this could underlie the regulation of local NREMS by use and experience.

## Results

### TRN cell burst discharge propensity in acute slices varies across sensory and non-sensory sectors

To identify TRN cells belonging to a sensory sector, we used stereotaxic injections of AAV-ChR2_EYFP into somatosensory (S1, barrel field) or auditory cortex (AC) of 3- to 4-week-old mice. Non-sensory TRN sectors related to associative areas, such as the medial prefrontal cortex (PFC), were instead targeted through injections into the mediodorsal (MD) thalamic nucleus that is the input structure forming reciprocal loops with several areas of the PFC (**Mátyás et al., 2014**; **Delevich et al., 2015**; **Collins et al., 2018**) and that forms reciprocal circuits with the TRN (**Mitchell, 2015**). Enhanced yellow fluorescent protein (EYFP) fluorescence was present at injection sites and in restricted portions of TRN 3–4 weeks after injection, as verified on coronal sections stained

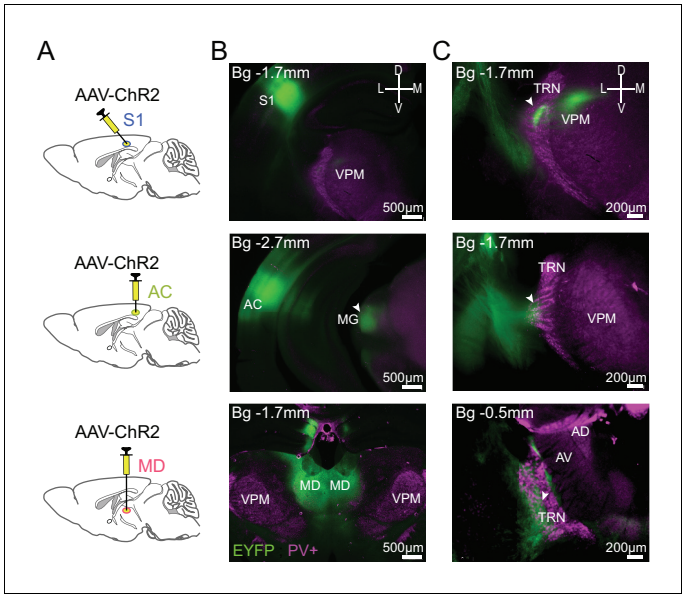


**Figure 1.** Identification of TRN sectors through anterograde tracing. (**A**) Scheme illustrating injection of AAV-ChR2_EYFP into S1 (top), AC (middle) and MD (bottom). (**B**) Epifluorescent micrographs of coronal sections at 2.5x magnification, anteroposterior position indicated with respect to bregma (Bg). ChR2-EYFP (green) expression in infected S1 neurons and their projection to TRN and VPM (top), in AC neurons and their projection to medial geniculate nucleus (MG) (middle) and in MD neurons (bottom), with immunostaining for PV-positive (PV+, magenta) TRN neurons. The VPM appears in light magenta due to its innervation by TRN. (**C**) Expanded view of the target TRN sector at 5x magnification. White arrowheads indicate sites of projection into TRN.
DOI: https://doi.org/10.7554/eLife.39111.003

immunohistochemically for PV to delineate the dorso-ventral extent of the TRN (**Figure 1**). The observed sectorial portions coincided with the ones established previously (**Pinault and Deschênes, 1998**; **Pinault, 2004**). Thus, injections into S1 revealed fibers navigating through the postero-dorsal portion of the TRN that terminated in elongated fluorescent spots in the thalamic ventral posterior medial nucleus corresponding to thalamic barreloids (**Bourassa et al., 1995**). AC injections resulted in fluorescent labeling of postero-central regions of the TRN that are anterior to the medial geniculate nucleus. Finally, MD injections labeled antero-ventral portions of the TRN, overlapping with TRN areas innervating motor and intralaminar nuclei (**Pinault and Deschênes, 1998**; **Pinault, 2004**).

In acute coronal slices prepared from injected animals, TRN cells recorded in the green fluorescent areas through whole-cell patch clamp recordings reliably (> 85 % of the cells across sectors) responded to optogenetic stimulation (470 nm light, pulse duration $\leq$1 ms, 0.16 mW/mm$^2$) with rapid excitatory postsynaptic currents ranging between -42 to -938 pA (**Figure 2A**). Paired stimuli (interstimulus interval: 100 ms) yielded paired-pulse facilitation for cortical afferents (S1-innervated TRN cells: 203 ± 12%, n = 12, Wilcoxon signed rank-test, p=4.9x10$^{-4}$ for 2$^{nd}$ vs 1$^{st}$ stimulus; for AC-innervated TRN cells: 175 ± 21%, n = 6, p=0.03), as described previously (**Astori and Lüthi, 2013**), whereas paired responses to MD stimulation showed comparable size (105 ± 4 %, n = 13, p=0.27). Cells showed values for resting membrane potential and capacitance consistent with previous data (**Figure 2B**; **Astori et al., 2011**). Rebound action potential discharge was elicited in response to square somatic current injections (negative current injections of -50 to -300 pA for 500 ms to hyperpolarize the somatic membrane potential < -100 mV, yielding cell input resistance values of 344 ± 18 MΩ for all three sectors). Rebound oscillatory bursting hallmarks the capacity of TRN cells to engage in rhythm generation (**Astori et al., 2011**; **Wimmer et al., 2012**; **Clemente-Perez et al., 2017**). S1- and AC-innervated TRN cells showed the rhythmic, repetitive burst discharge described previously (**Figure 2C**; **Cueni et al., 2008**; **Astori et al., 2011**), evident as several groups of high-frequency action potentials each riding on a triangular-shaped membrane depolarization and followed by a pronounced afterhyperpolarization. Repetitive burst discharge strongly depended on the membrane voltage, showing an inverted U-shaped voltage dependence that peaked at -65 to -60 mV for S1-innervated cells (**Figure 2D1,E**). Only 1/12 S1-innervated TRN cells was a non-repetitive bursting cell (**Figure 2F**). Similar burst propensity was found for TRN cells innervated from AC (**Figure 2E**), but 4/13 cells were non-repetitive bursters (**Figure 2F**). In TRN cells responding to MD inputs, repetitive bursting was weak (**Figure 2C,D1**) and 9/14 cells discharged maximally one burst (**Figure 2F**). These results show that repetitive burst propensity is stronger in sensory compared to non-sensory TRN sectors. Within sensory sectors, the somatosensory sector displayed the highest density of strongly bursting cells, whereas the auditory sector had a smaller proportion of cells with rhythmic bursting.

To test whether the heterogeneity of burst discharge across TRN sectors depended on $Ca_V3.3$ channels, the optogenetic strategy described above was applied to animals with a genetic deletion of the *Cacna1i* ($Ca_V3.3$, $\alpha$1I) gene (**Astori et al., 2011**). This channel is primarily responsible for burst discharge in TRN cells, while co-expressed $Ca_V3.2$ channels play a minor role (**Pellegrini et al., 2016**). Accordingly, TRN cells of these animals are unable to burst repetitively, whereas tonic action potential discharge is preserved. Cells patched in acute slices from *Cacna1i*$^{-/-}$ ($Ca_V3.3$ KO) animals showed passive properties comparable to those in C57BL/6J (WT) cells of the corresponding sectors (**Figure 2B**), although S1-innervated cells had a smaller capacitance indicative of reduced cell size, perhaps resulting from morphological alterations in these constitutive knock-outs. Light-evoked synaptic responses showed a similar range of amplitudes (−10 to −1076 pA) and a short-term plasticity that was comparable to the one found for WT cells (S1-innervated TRN cells: 188 ± 32%, n = 7, p=0.016; for AC-innervated TRN cells: 203 ± 13%, n = 8, p=0.008; for MD-innervated TRN cells: 87 ± 8, n = 10, p=0.31; two-way ANOVA with factors 'genotype' and 'sector', p=0.28 for interaction). However, the vigorous bursting in somatosensory and auditory TRN cells was suppressed, thus abolishing the dependence of repetitive burst discharge propensity on TRN sector type (Kruskal-Wallis with factor 'sector', p=3×10$^{-4}$ for WT, p=0.14 for $Ca_V3.3$ KO) (**Figure 2D2, E**). Together, these data indicate that the $Ca_V3.3$ channel endows superior bursting capacity to sensory over non-sensory TRN cells.

It has been shown that TRN bursting capacities are sensitive to cortical lesions (**Paz et al., 2010**). To exclude the possibility that the viral injections compromised TRN discharge, we also recorded from TRN cells in slices prepared from uninjected animals and identified putative sensory and non-

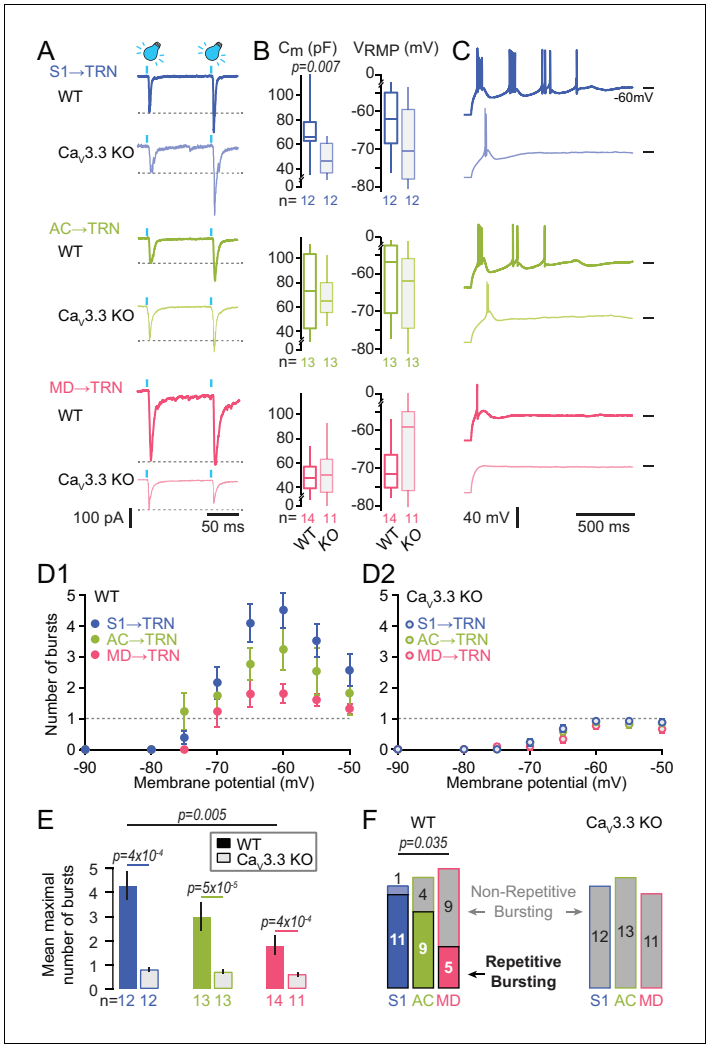


**Figure 2.** Oscillatory burst firing varies across TRN sectors and depends on $Ca_V3.3$ $Ca^{2+}$ channels. (**A**) Representative traces of paired EPSCs in whole-cell voltage-clamped TRN neurons at −60 mV of WT and $Ca_V3.3$ KO mice upon light activation of S1 (top), AC (middle) and MD (bottom) afferents. Afferent-specific forms of short-term plasticity are preserved across genotypes (see Results for averaged data). (**B**) Box-and-whisker-plots of the mean capacitance ($C_m$) and the resting membrane potential ($V_{RMP}$) of the recorded TRN neurons (WT: n = 12 for S1, n = 13 for AC, n = 14 for MD; $Ca_V3.3$ KO: n = 12 for S1, n = 13 for AC, n = 11 for MD). It can be noted that the $C_m$ of S1-innervated TRN neurons in $Ca_V3.3$ KO showed a reduction compared to WT, suggesting smaller cell size (Mann-Whitney test, p=0.007). (**C**) Representative current-clamp recordings of oscillatory bursting responses of TRN neurons across sectors, induced through hyperpolarizing current injections (−50 to −300 pA for 500 ms). Horizontal lines denote −60 mV. Note the strong repetitive burst firing in sensory sectors that is impaired in the $Ca_V3.3$ KO cells, whereas MD-innervated cells mostly discharge a single burst. (**D**) Graph of the number of repetitive bursts as a function of the membrane potential prior to the hyperpolarizing pulse (***Cueni et al., 2008***). This yields a U-shaped curve reaching a peak at −65 and −60 mV in all sectors of WT mice (**D1**) that was abolished in $Ca_V3.3$ KO mice (**D2**). Dashed horizontal lines at ordinate value one indicate the border between repetitive and not-repetitive bursting conditions. (**E**) Mean number of repetitive bursts of TRN neurons (between −60 and −65 mV) across sectors and genotype. Mann-Whitney tests were used for comparison between genotypes, and p-values are given above the bars. (**F**) Histogram of the proportion of repetitive (colored rectangles) and non-repetitive bursting (grey rectangles with color surroundings) TRN neurons in the different sectors. Chi-square test followed by pairwise proportion test with Holm's p-value adjustment was used for statistical evaluation, with significant value given above the bars.

DOI: https://doi.org/10.7554/eLife.39111.004

The following source data and figure supplement are available for figure 2:

**Source data 1.** Numerical data values and statistics underlying ***Figure 2***.

*Figure 2 continued on next page*

*Figure 2 continued*

DOI: https://doi.org/10.7554/eLife.39111.006

**Figure supplement 1.** Oscillatory burst firing varies across the anteroposterior extent of TRN and depends on $Ca_V3.3$ $Ca^{2+}$ channels.

DOI: https://doi.org/10.7554/eLife.39111.005

sensory sectors in horizontal slices along the anteroposterior axis. These experiments confirmed the different burst propensity in sensory vs non-sensory sectors (***Figure 2—figure supplement 1***).

## Mouse NREMS shows spectral features that are specific to functional cortical areas

We next monitored local NREMS in cortical areas connected to the TRN sectors studied *in vitro*. Under stereotaxic guidance, animals were implanted for *in vivo* multi-site recordings of local field potentials (LFPs) in the same cortical areas that were previously targeted for the anterograde viral tracing of TRN sectors, along with electroencephalography/electromyography (EEG/EMG) (***Figure 3A,B***). For S1 and AC, electrodes were positioned in deep layers (layers 5 and 6), whereas infra-/prelimbic cortical areas (collectively referred to as PFC) were implanted in middle layers (layers 3 and 5, see Materials and methods for exact stereotaxic coordinates), according to the majority of thalamocortical input received in the respective areas. Additionally, the secondary somatosensory cortex (S2) was implanted (layers 2/3 and 4) to monitor NREMS in an associative sensory cortical area with strong reciprocal connections to S1 (***Zingg et al., 2014***). We chose high-impedance electrodes (~10–12 MΩ) for LFP recordings to maximize detection of local signals. Simultaneous EEG/EMG recordings on the contralateral hemisphere were used for vigilance state scoring (***Figure 3A, B***).

Animals were recorded in head-restrained mode, which yields a sleep profile comparable to that in freely moving conditions, as previously shown (***Fernandez et al., 2017***; ***Lecci et al., 2017***). Each mouse was recorded for 2–3 hr/day and spontaneously switched between periods of wakefulness, NREMS and REMS with power spectra typical for each vigilance state (***Figure 3—figure supplement 1A***).

NREMS was accompanied by distinct LFP waveforms across cortical areas of WT animals (***Figure 3C***). In S1 and S2, prominent activity in the SO (0.5–1.5 Hz, frequency band chosen based on visual inspection of the power spectrum) and the sleep spindle (sigma, 10–15 Hz) frequency ranges was visible (***Figure 3—figure supplement 1B***). Activity in the delta (1.5–4 Hz) frequency range was evident as large positive deflections (***Figure 3—figure supplement 1B***). Similar, yet weaker rhythmic activity was observed in AC and PFC. The PFC showed signals dominated by slow events, as reported (***Fernandez et al., 2017***), which included a component around 4 Hz resembling a respiratory-related rhythm in frontal brain areas (***Figure 3C,D***; ***Zhong et al., 2017***). Power spectral analyses over total NREMS times of 2200–6100 s per animal (average 4487 ± 603 s, concatenated from NREMS bouts across recording days) showed that NREMS in all recorded areas had broadly elevated power in the low-frequency range covering both the SO and the delta range (0.5–4 Hz), whereas a 'shoulder' in the sigma band was present only in somatosensory areas (n = 9 for S1 and n = 8 for S2) but not in AC (n = 6) and PFC (n = 6) (***Figure 3D***).

NREMS in animals lacking $Ca_V3.3$ channels showed several marked changes that were apparent in both the raw traces and in characteristic alterations of the power spectra (NREMS recording times of 1800–7000 s per animal, average 3459 ± 421 s). First, there was a striking lack of visually recognizable sleep spindle activity in S1 and S2, and a sigma power shoulder was not present in the power spectrum (***Figure 3C,D***, bottom panel showing enlarged portions of the power spectrum and ***Figure 3—figure supplement 1B***). Second, activity in the delta range was augmented, whereas the SO was less prominent in LFP traces from S1, S2 and AC. These visual observations manifested as a rightward shift of the low-frequency activity in the power spectrum, with a clear power peak present in the delta band that dominated over power values < 1.5 Hz. The power spectra for WT and $Ca_V3.3$ KO animals intersected in the slow frequencies around 1.6–1.8 Hz for S1, S2 and AC, suggesting a consistent spectral border between the SO and the delta bands. Separate quantification of total power in the SO, the delta and the sigma frequency band confirmed these observations (***Figure 3E***). After Bonferroni correction, the sigma power reduction in S1 appeared as a trend. However, this is

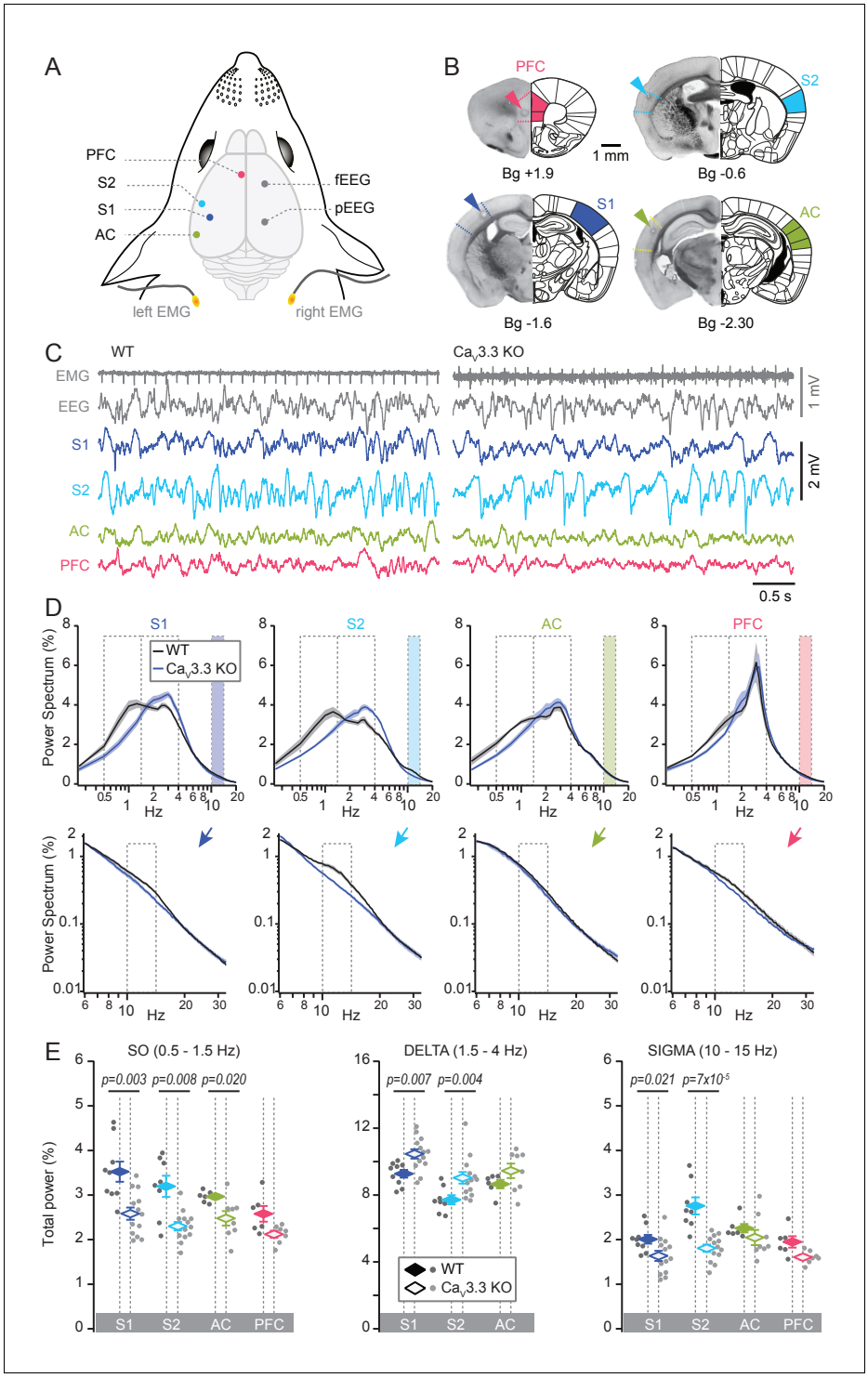


**Figure 3.** Cortical-area specific NREMS features depend on $Ca_V3.3$ $Ca^{2+}$ channels. (**A**) Schematic illustrating implantation sites for LFP, EEG (fEEG and pEEG; frontal and parietal EEG) and EMG electrodes. S1, S2; primary and secondary somatosensory areas; AC, auditory cortex; PFC, medial prefrontal cortex. (**B**) Histological sections of representative cases confirming the location of the recording sites. Arrowheads mark site of lesion caused by electrocoagulation. Anteroposterior stereotaxic coordinates are given relative to Bregma (Bg). (**C**) Representative raw traces of NREMS for WT (left) and $Ca_V3.3$ KO (right) animals, showing (from top to bottom) the EMG, EEG and LFP signals for S1, S2, AC and PFC (infra-/prelimbic area). The heart beat is visible on the EMG trace. (**D**) Power spectra corresponding to the LFP recordings, plotted in a linear-log plot to emphasize the three frequency bands of interest: the SO (0.5–1.5 Hz), the delta (1.5–4 Hz) and the sigma band (10–15 Hz). The sigma band is colored and

*Figure 3 continued on next page*

*Figure 3 continued*

shown in expanded log-log plots at the bottom. Normalized mean ±S.E.M. values of power spectral density are shown for S1, S2, AC and PFC for both genotypes (WT: n = 9 for S1, n = 8 for S2, n = 6 for AC, n = 6 for PFC; $Ca_V3.3$ KO: n = 13 for S1, n = 13 for S2, n = 8 for AC, n = 7 for PFC). (**E**) Mean total power for the three frequency bands across S1, S2, AC and PFC, with values for individual animals shown in points (dark gray for WT, light gray for $Ca_V3.3$ KO animals), and mean values ± S.E.M. in color diamonds. Statistical significance was tested for each area separately, comparing WT and $Ca_V3.3$ KO. Mann-Whitney non-parametric test for WT *vs* $Ca_V3.3$ KO, for S1, p=0.003 for the SO, p=0.007 for delta, p=0.021 for sigma; for S2, p=0.008 for the SO, p=0.005 for delta, $p=6.9\times10^{-5}$ for sigma; for AC, p=0.02 for the SO, p>0.05 for delta and sigma; for PFC, all p-values>0.05. Bonferroni-corrected α-threshold for the three frequency bands was 0.017.

DOI: https://doi.org/10.7554/eLife.39111.007

The following source data and figure supplement are available for figure 3:

**Source data 1.** Numerical data values and statistics underlying ***Figure 3***.

DOI: https://doi.org/10.7554/eLife.39111.009

**Figure supplement 1.** Head-fixed animals present spectra typical for each vigilance state accompanied by distinct LFP waveforms across cortical areas in WT and $Ca_V3.3$ KO animals.

DOI: https://doi.org/10.7554/eLife.39111.008

an underestimation because the difference between the two curves extends up to ~18 Hz. In PFC, in contrast, no alterations in the power spectrum were observed, with in particular no significant change in the sigma power and in the SO peak. The delta band was not analyzed in this area due to the superposition of the respiratory rhythm on top of the delta waves.

Together, the lack of $Ca_V3.3$ channels altered the spectral mix of NREMS in sensory circuits, whereby power in the delta frequency band became overrepresented compared to the SO. This shift was greatest in S1 and S2, where in addition sigma power activity was suppressed. In contrast, the PFC did not show these alterations in two of the three major frequency bands, suggesting a minor dependence on $Ca_V3.3$ channels.

## Chemogenetic inhibition of TRN cells reproduces the switch from spindle- to delta-enriched sleep

The results from $Ca_V3.3$ KO animals suggest that strong $Ca_V3.3$-dependent burst discharge is required for spindle-enriched NREMS. Therefore, acute reduction of TRN excitability to suppress bursting should also deplete spindles and lead to a NREMS enriched in delta waves. To test this, we hyperpolarized TRN cells with a chemogenetic approach, whereby we expressed the inhibitory DREADD receptor hM4Di in VGAT-Ires-Cre animals (***Vong et al., 2011***) through bilateral injection of AAV-hM4D(Gi)_mCherry or AAV-hM4D(Gi)_IRES_mCitrine in the region of the somatosensory TRN sector (***Figure 4—figure supplement 1A***). In acute slices prepared 3 weeks after injection, bath application of the DREADD-ligand Clozapine N-oxide (CNO, 10 μM) induced a marked membrane hyperpolarization ($\Delta V = -13.9 \pm 1.5$ mV, n = 10, paired *t*-test, $p=6\times10^{-6}$) of fluorescent cells held in whole-cell current-clamp at resting membrane potentials ranging from −50 to −70 mV (***Figure 4A, B***). Cellular input resistance was reduced and rebound burst discharge suppressed in the continuous presence of CNO. Bursting could be recovered upon direct current (d.c.) injection to restore the original membrane potential (d.c. injection tested in n = 3 cells, ***Figure 4A***). Non-fluorescent cells in the vicinity of the injected area did not respond to CNO (***Figure 4B***). This result is consistent with CNO-induced activation of $K^+$ conductances and shows that TRN neurons become silenced without impairing rebound bursting and action potential firing. Treatment with CNO thus overall reduces TRN excitability, and in particular specifically reproduces the decreased burst propensity of TRN cells found in the $Ca_V3.3$-KO animals that is relevant for the altered NREMS spectral properties.

Similarly injected animals were also implanted *in vivo* for S1 LFP and EEG/EMG freely moving recordings and treated with CNO (i.p. 1 mg/kg) or NaCl at 2 hr into the light phase (ZT2). The latencies to fall asleep were comparable after drug or NaCl injections (31.4 ± 3.7 min for CNO, 24.8 ± 2.1 min for NaCl; n = 5, paired *t*-test, p=0.16). NREMS analysis was done for the time period of 20–65 min after drug injection, which is the period where drug effects peak (***Figure 4—figure supplement 1B***). Total time spent in NREMS was not different between CNO and NaCl injections in the analysis period (24.1 ± 1.7 min for CNO, 27.7 ± 1.9 min for NaCl injections, Wilcoxon signed rank-test,

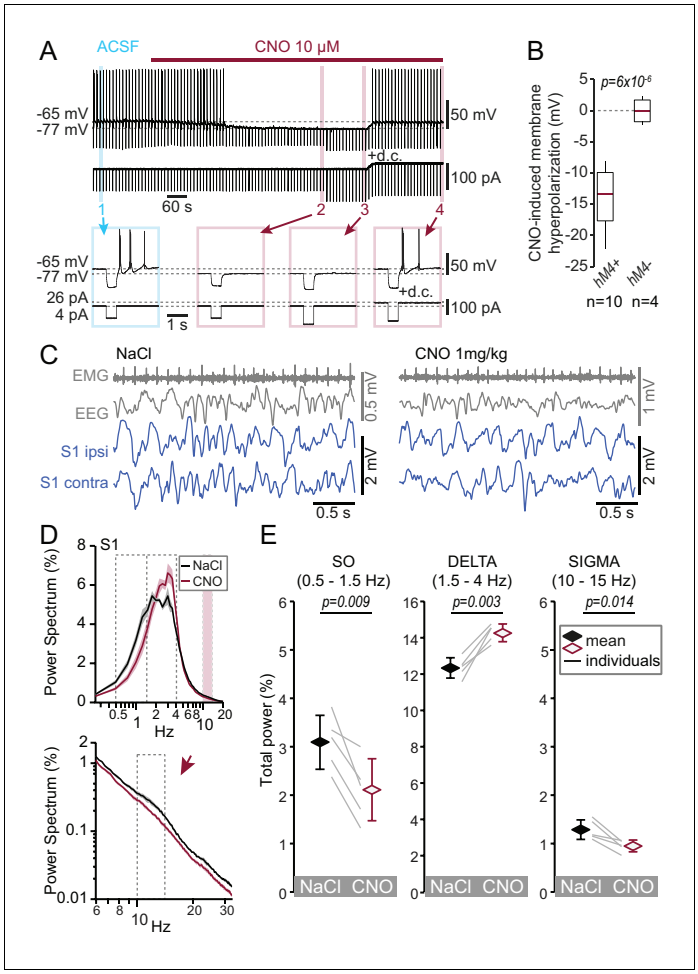


**Figure 4.** Chemogenetic hyperpolarization of TRN cells mimics the NREMS phenotype of the $Ca_V3.3$ KO mice. (**A**) Representative membrane voltage recording of a whole-cell patch-clamped TRN cell *in vitro* exposed to CNO (10 μM, bath application indicated by horizontal bar) recorded in a slice from a mouse injected with AAV8-hM4D(Gi)_IRES_mCitrine. The cell was injected every 10 s with brief negative current pulses to elicit rebound discharge. The application of CNO hyperpolarized the membrane potential, suppressed rebound bursting and decreased membrane input resistance, as evident by the smaller voltage deflection in response to the negative current step (−80 pA). Current step size was increased to −120 pA to compensate for the decreased membrane resistance. Subsequent injection of direct current (d.c.) to counteract membrane hyperpolarization then reinstated burst discharge. Numbers indicate portions of the trace shown expanded below. Horizontal dotted lines indicate mean membrane potential before and during CNO application. (**B**) Box-and-whisker plot of membrane hyperpolarization *in vitro* (ΔV, calculated as the difference before and during CNO) for fluorescent (hM4+, n = 10, ΔV = −13.9 ± 1.5 mV, paired *t*-test, $p=6\times10^{-6}$) and non-fluorescent cells (hM4-, n = 4, ΔV = 0.0 ± 0.9 mV, paired *t*-test, p=0.97). The CNO-effects between the two-cell groups differed significantly (unpaired *t*-test, $p=1.1\times10^{-4}$). (**C**) Representative traces *in vivo* during NREMS 30 min after the injection of NaCl (left) or CNO (right) in the same animal, showing (from top to bottom) the EMG, EEG and S1-LFP (ipsilateral and contralateral to EEG) signals. (**D**) Mean ±S.E.M. power spectra of the S1-LFPs for NaCl and CNO injections *in vivo* during the NREMS periods 20 to 65 min after injection. Expanded portion is shown below in log-log scale to emphasize the sigma band (10–15 Hz). (**E**) Mean total power for the three frequency bands of interest. Diamonds and error bars show the Mean ±S.E.M. across subjects. Gray lines represent individual animals. Repeated-measures ANOVA for factors 'frequency' and 'treatment', $p=7.7\times10^{-5}$ was followed by paired *t*-tests for individual frequency bands, with values given above the bars. Bonferroni-corrected, α threshold was 0.017.

DOI: https://doi.org/10.7554/eLife.39111.010

The following source data and figure supplement are available for figure 4:

**Source data 1.** Numerical data values and statistics underlying ***Figure 4***.

DOI: https://doi.org/10.7554/eLife.39111.012

*Figure 4 continued on next page*

*Figure 4 continued*

**Figure supplement 1.** Chemogenetic inhibition of TRN cells acutely increases delta activity in a DREADD-dependent expression.

DOI: https://doi.org/10.7554/eLife.39111.011

p=0.22) and mean NREMS bout durations were comparable (93.3 ± 12.3 s for CNO, 91.2 ± 32.5 s for NaCl, Wilcoxon signed rank-test, p=0.31). Following CNO injections, S1 LFP signals during NREMS showed reduced spindle activity and instead became enriched in activity in the delta frequency range (***Figure 4C,D***, repeated-measures ANOVA with factors 'frequency' and 'treatment', $p=7.7\times10^{-5}$). Compared to NaCl injections, total power in the delta frequency range was increased, whereas the SO and spindle activity were suppressed (***Figure 4D,E***). Control animals injected with AAV8 carrying a DREADD-unrelated optogenetic construct (see Materials and methods) did not respond to CNO (***Figure 4—figure supplement 1C–F***). The CNO-induced acute membrane hyperpolarization thus reproduced the major power spectral changes observed in NREMS of the $Ca_V3.3$ KO mouse: the suppression of the SO and sleep spindle power, and the enhancement of delta power. As CNO-induced hyperpolarization suppressed burst discharge (see also ***Figure 2D1***), the joint results from the genetic and the chemogenetic manipulations identify decreased TRN bursting as the primary factor relevant for the enrichment of delta power at the expense of sigma and SO power in NREMS.

## $Ca_V3.3$ channels amplify and accelerate spindles in the somatosensory areas

Given the importance of $Ca_V3.3$-dependent TRN burst discharge for NREMS in sensory cortices, the question remains open of how this discharge pattern controls the properties of local, discrete spindle events. The exact sources of regional spindle properties have recently received considerable attention (***Schabus et al., 2007***; ***Frauscher et al., 2015***; ***Piantoni et al., 2017***). Therefore, we developed an algorithm to isolate discrete spindle events in NREMS of WT and $Ca_V3.3$ KO mice. We followed a previously established thresholding approach in rat that successfully characterized spindles in both rodent and human (***Mölle et al., 2009***) complemented with additional criteria, as detailed in the Materials and methods (***Figure 5—figure supplement 1***). For the band-pass filtering, we were guided by the observation that in both S1 and S2 of the $Ca_V3.3$ KO animals, power was attenuated beyond the widely used sigma band of 10–15 Hz. Therefore, we chose 9–16 Hz to allow for the possible inclusion of comparatively slow and fast spindles.

We isolated 727–2289 events per WT mouse and area that showed the typical spindle-shaped, waxing-waning waveform (***Figure 5A***). Spindles in S1 and S2 showed large amplitudes that were comparable to that of the SO, whereas those in AC and PFC were less prominent (***Figure 5A***). In the $Ca_V3.3$ KO animals, the large spindle events were reduced in S1 and S2, but remained comparable in AC. There was also a reduction of event amplitude in PFC (***Figure 5B1***). Cumulative probability density curves showed a marked leftward shift of the amplitude distribution in S1 and S2, but not in AC and PFC (***Figure 5B2***). We also analyzed the intra-spindle frequencies, one of the major markers of spindle heterogeneity (***Figure 5C***). The frequency of detected events was distributed according to a Gaussian between 9 and 16 Hz, with a maximum around 10–12 Hz, yielding means of 11.6 ± 0.09 Hz for S1; 11.7 ± 0.05 Hz for S2; 11.2 ± 0.05 Hz for AC; 11.5 ± 0.03 Hz for PFC (***Figure 5C1***). All distributions showed a tail indicating a small proportion of events with a frequency >14 Hz (***Figure 5C2***). In the $Ca_V3.3$ KO animals, frequencies were specifically attenuated in S1 and S2, but remained comparable in AC and PFC. The greater activity of $Ca_V3.3$ channels in the sensory sectors of TRN thus correlated strongly with higher amplitudes and frequencies of individual spindles in S1 and S2.

## $Ca_V3.3$ channels ensure the temporal coordination of sleep spindles with the active state of the SO

Sleep spindles are temporally grouped by the active state of the SO, which reflects the strong role of corticothalamic volleys in recruiting thalamic circuits (***Contreras et al., 1996***). This grouping is key for the promotion of sleep-dependent memory consolidation (***Mölle et al., 2009***) and it may be

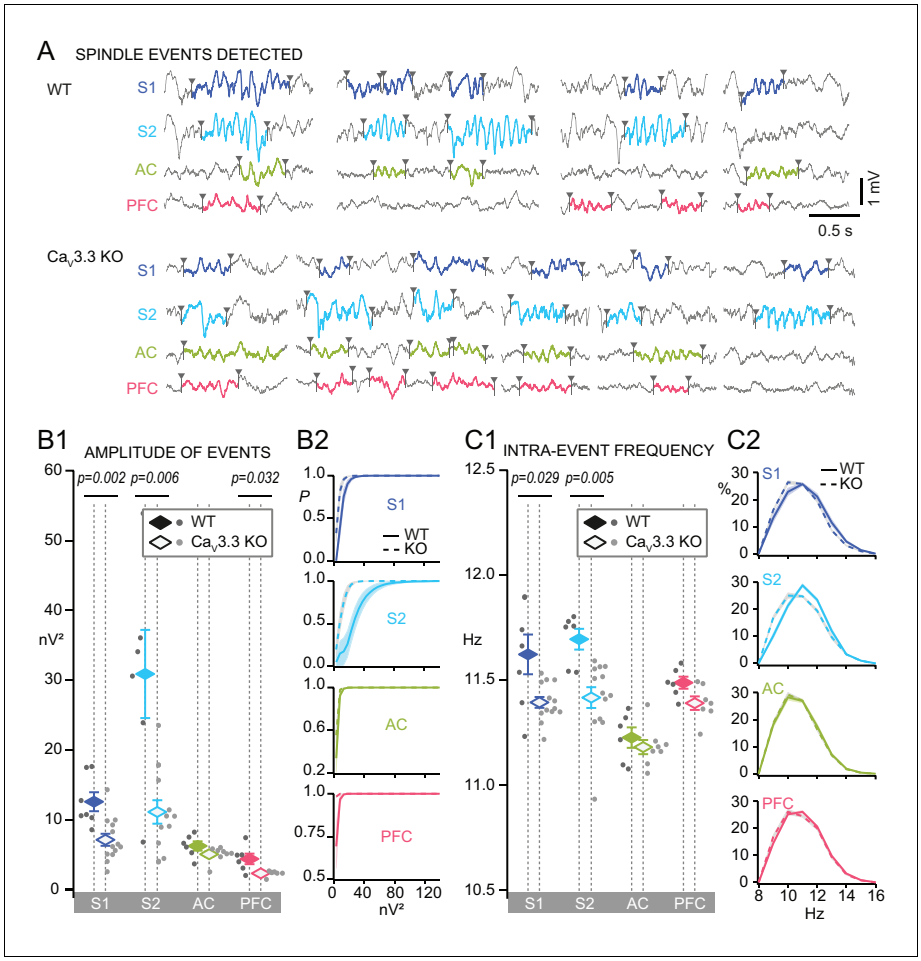


**Figure 5.** Discrete spindle events are amplified and accelerated in somatosensory areas by $Ca_V3.3$ channels. (**A**) Representative traces during NREMS for WT and $Ca_V3.3$ KO for S1, S2, AC and PFC, showing examples of algorithm-detected discrete spindle events (9–16 Hz, colored and bordered by arrowheads). (**B**) Mean amplitude of detected spindles quantified as mean power of the band-pass filtered signal (9–16 Hz). (**B1**) Mean spindle power levels across animals, values for individual animals shown by dots (dark gray for WT, light gray for $Ca_V3.3$ KO animals) and mean values ± S.E.M. by colored diamonds. Statistical significance was tested for each area separately using Mann-Whitney test, comparing WT (S1, n = 7; S2, n = 6; AC, n = 6; PFC, n = 6) and $Ca_V3.3$ KO (S1, n = 13; S2, n = 13; AC, n = 8; PFC, n = 7). p-values obtained were: for S1, p=0.002; for S2, p=0.006; for AC, p>0.05; for PFC, p=0.032. (**B2**) Cumulative probability distributions. (**C**) Same for intra-spindle frequencies. (**C1**) p-values obtained were: for S1, p=0.029; for S2, p=0.005; for AC and PFC, p>0.05. (**C2**) Probability distribution of spindle events according to their intra-spindle frequency.

DOI: https://doi.org/10.7554/eLife.39111.013

The following source data and figure supplement are available for figure 5:

**Source data 1.** Numerical data values and statistics underlying ***Figure 5***.

DOI: https://doi.org/10.7554/eLife.39111.015

**Figure supplement 1.** Illustration of procedure for automated spindle detection Representative traces for the four areas, S1, S2, AC and PFC in a WT animal, showing for each (from top to bottom): raw trace, band-pass filtered 9–16 Hz, power of the filtered trace.

DOI: https://doi.org/10.7554/eLife.39111.014

disrupted in some cases of schizophrenia (***Manoach et al., 2016***). We determined the onset times of detected spindles with respect to the phase of the SO (***Figure 6A***) and confirmed such time-locking throughout all areas, with ~60% and 40% of detected spindles initiating during the cortical active and silent states (also named UP and DOWN states), respectively (***Figure 6B,C***). Remarkably, the same analysis in the $Ca_V3.3$ KO animals showed that the time-locking of sleep spindles to the SO

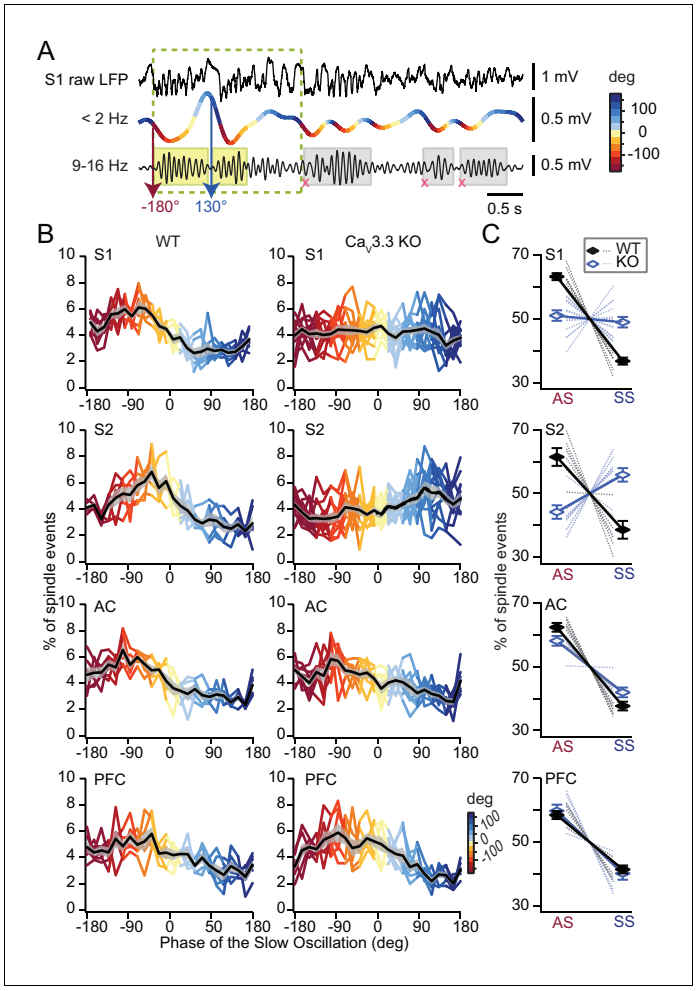


**Figure 6.** Phase-locking of spindles to the active state of the SO depends on $Ca_V3.3$ channels in somatosensory cortices. (**A**) Illustration of the method to determine the phase value of the SO at which a detected spindle event starts (yellow shaded rectangles). SO periods were determined based on (***Mölle et al., 2009***) and indicated as dashed rectangle. Spindles that did not coincide with detected SO were not included in this analysis (gray shaded rectangles). (**B**) Graphs presenting sleep spindle occurrence as a function of SO phase. Colored lines represent individual animals, black lines the mean ±S.E.M. (gray-shaded curve). Same animal numbers as in ***Figure 5***. (**C**) Mean occurrence of spindle onsets for the active (AS, −180°, 0°) and the silent (SS, 0°, 180°) state of the SO. Statistical significance was tested for each area separately with respect to spindle occurrence as a function of AS and SS. All tests were paired *t*-test, except for S2 for which we used Wilcoxon signed rank-test. For WT, p-values obtained were: for S1, $p=2\times10^{-5}$; for S2, p=0.031; for AC, $p=3\times10^{-4}$; for PFC, p=0.001. For $Ca_V3.3$ KO, p-values obtained were: for S1, p=0.543; for S2, p=0.033; for AC, p=0.001; for PFC, p=0.003. Comparison between genotypes was done for the active state (AS) using unpaired *t*-test, except for S2 for which we used Mann-Whitney test. p-values obtained were: for S1, $p=8.3\times10^{-6}$; for S2, $p=5\times10^{-4}$; for AC, p=0.06; for PFC, p=0.59.

DOI: https://doi.org/10.7554/eLife.39111.016

The following source data is available for figure 6:

**Source data 1.** Numerical data values and statistics underlying ***Figure 6***.

DOI: https://doi.org/10.7554/eLife.39111.017

was altered for S1 and S2 (***Figure 6B,C***), but not for AC and PFC. In both S1 and S2, the presence of spindles on the active state was diminished in favor of spindles in the silent state. In S1 from $Ca_V3.3$ KO animals, the occurrence of spindles was comparable between active and silent states, whereas events occurred preferentially in the silent state in S2. This difference in the coupling was not due to a less faithful detection of the smaller spindles in the $Ca_V3.3$ KO animals, because the analysis produced similar results when it was limited to WT spindles with amplitudes corresponding to those of

the $Ca_V3.3$ KO animals. Therefore, the presence of $Ca_V3.3$ ensures the timely occurrence of sleep spindles with respect to the cortical active state.

## Discussion

We identify a novel mechanism underlying local cortical correlates of NREMS. It arises through heterogeneity in thalamic circuits and correlates with variable oscillatory bursting propensity across TRN sectors. Strong $Ca_V3.3$-dependent bursting in the somatosensory TRN sector led to local NREMS with fast and large spindles coupled to the SO, whereas this was not the case for cortical areas corresponding to TRN sectors with weakly bursting cells. Intriguingly, high burst propensity was also coupled to a dual regulation of local NREMS, such that the SO and spindles could be suppressed in favor of delta waves. Sectorial attributes of TRN circuits thus emerge as a powerful source for local NREMS correlates. They additionally facilitate a tuning of NREMS between major spectral correlates, offering a candidate mechanism for local sleep modulation, possibly in response to use, experience and learning. A sectorial heterogeneity of TRN will also advance insight into a proposed common vulnerability of TRN circuitry for both sleep as well as wakefulness-driven selective attention in neuropsychiatric disorders (***Krol et al., 2018***).

The TRN has been traditionally regarded as a homogeneous sleep rhythm pacemaker (***Fuentealba and Steriade, 2005***; ***Fogerson and Huguenard, 2016***) that underlies global thalamic inhibition (***Halassa and Acsády, 2016***). Although its molecular and functional heterogeneity is increasingly recognized, consequences for NREMS are so far poorly explored and the role of sector-specific TRN cell characteristics is unknown. Thus, it is not clear whether heterogeneous cellular discharge properties (***Contreras et al., 1992***; ***Brunton and Charpak, 1997***; ***Lee et al., 2007***; ***Kimura et al., 2012***; ***Higashikubo and Moore, 2018***) or variable expression of PV and somatostatin are important for local sleep (***Clemente-Perez et al., 2017***). Furthermore, sensory but not limbic TRN cells preferentially engage in sleep-related activity (***Halassa et al., 2014***), but it is not known whether they are cellularly distinct. Therefore, this study is the first to bring together TRN heterogeneities at both the *in vitro* and the *in vivo* levels using optogenetically assisted mapping of TRN sectors. We show that cellular heterogeneities align with identified TRN sectors, and TRN sectors with area-specific NREMS, thus establishing the TRN sector-specific cellular properties as a source for local and tunable NREMS. Based on a previous study demonstrating that PV-positive cells are stronger bursters than cells enriched in somatostatin (***Clemente-Perez et al., 2017***), we propose that PV-positive TRN cells are primary determinants of the unique sleep spindle properties in somatosensory cortex.

The focus on NREMS in specific cortical areas using LFP recordings, combined with genetic and chemogenetic manipulation and cellular analysis, reveals novel and surprising topographical aspects of mouse NREMS (***Terrier and Gottesmann, 1978***; ***Kim et al., 2015***; ***Fernandez et al., 2017***). One remarkable observation is that somatosensory cortices showed a clear sigma power 'shoulder' and strong, fast, $Ca_V3.3$-dependent spindle events. The widespread idea from EEG recordings that sleep spindle generation in mouse NREMS is weak (***Astori et al., 2011***) should thus be revised as we now show that full-fledged spindle activity is generated in local regions of the mouse brain. The highly focal synaptic organization of the barrel system, where TRN-thalamic, thalamocortical and cortico-thalamic projections between barreloid and barrel topographically match on a cell-to-cell basis (***Desílets-Roy et al., 2002***; ***Wimmer et al., 2010***), together with a high density of PV-positive, bursty cells in the TRN somatosensory sector (***Clemente-Perez et al., 2017***), are likely important anatomical substrates enabling strong local spindles. The tight alignment of thalamic unit and S1 LFP activity recorded simultaneously during spindles in urethane anaesthesia (***Rovó et al., 2014***) supports this interpretation. We also observed prominent sigma power and high-amplitude spindles in S2 that exceeded levels in S1. High reciprocal cortical connectivity between S1 and S2 (***Feldmeyer et al., 2013***), and a differential recruitment of first- and higher order thalamic nuclei in these two areas, could be some of the reasons behind this difference. In contrast to S1 and S2, no discernable sigma power shoulder was present in AC, and detected spindles showed no dependence on the $Ca_V3.3$ channel. We found a tendency for a decreased density of highly burst-prone cells in mouse, which possibly reduces the strength of spindle generation in auditory sectors. It also remains to be seen whether there exist functional and anatomical differences in the overall connectivity of each sensory TRN sector (***Crabtree, 1999***). Similarly, the spectral composition of NREMS in pre- and infralimbic

portions of the PFC showed no prominent sigma power and no overall dependence on $Ca_V3.3$ channels, consistent with a minor expression of $Ca_V3.3$ channels in the MD-innervated sector and with the presence of a majority of somatostatin-positive, weakly bursting cells in these areas of the TRN (**Clemente-Perez et al., 2017**). However, discrete spindles could be detected in mouse and they are well-described for rat PFC (**Siapas and Wilson, 1998**; **Peyrache et al., 2011**; **Maingret et al., 2016**). Discrete spindle events were accompanied by a phase entrainment of TRN discharge in sleeping rats, although mean firing rates seemed low (**Gardner et al., 2013**). There could thus be a spindle-generating circuitry independent of the powerful $Ca_V3.3$-dependent mechanisms in sensory TC loops, in which anterior and midline thalamic nuclei and hippocampus are involved. Such ideas remain to be tested also regarding the notion of distinct frontal spindles in both human (**Schabus et al., 2007**) and mouse (**Kim et al., 2015**).

Power in the SO band was consistently co-modulated with sleep spindle activity in both the $Ca_V3.3$ KO mouse and during chemogenetic TRN inhibition. This could be evidence in favor of a role of TRN in the generation of the SO (**Crunelli et al., 2015**). Our chemogenetic results generally support the idea that the TRN sustains low-frequency activity in cortico-thalamocortical loops, an effect which could possibly also result secondarily from its phasic recruitment by cortex to generate sleep spindles. Also, the increase of delta power could have de-emphasized the relative presence of SOs. Additionally, possible roles of $Ca_V3.3$ channels in cortically generated rhythms could arise from a subgroup of cortical interneurons (**Liu et al., 2011**).

The genetic removal of the $Ca_V3.3$ channel enhanced delta power in S1 and S2 at the expense of sleep spindles. Chemogenetic hyperpolarization reproduced this observation closely. Although the chemogenetic approach suppresses excitability in a manner that is not limited to bursting, the close correspondence with the observations in the $Ca_V3.3$-KO animals, in which only bursting but not tonic firing is impaired (**Astori et al., 2011**), strongly suggests that suppressed bursting, which is the common denominator of both experimental approaches, is the principal mechanism involved in the effects at the level of NREMS. While the reduction in sleep spindle activity under these conditions is expected (**Astori et al., 2011**), an enhancement and/or unmasking of delta wave-generating activity in thalamocortical circuits has now become apparent thanks to the locality of our recordings. It is reminiscent of previous observations of an opposite regulation of slow wave/delta and spindle power during NREMS (**Dijk et al., 1993**; **Steriade et al., 1993**; **Franken et al., 1998**), which has been explained based on the different membrane potential polarizations of TC cells involved in spindle or delta rhythm generation (**Nuñez et al., 1992**). Here, we identify TRN cell membrane potential polarization as a determinant for such regulation in somatosensory thalamocortical circuits during NREMS. Remarkably, the capability of TRN in generating either spindles or delta waves was also evident based on whether brief or prolonged optogenetic stimulation was applied (**Halassa et al., 2011**; **Lewis et al., 2015**). This underscores the power of TRN-dependent inhibition in controlling thalamocortical synchrony according to discharge patterns. We add to this the capability of a local, switchable tuning of NREMS spectral properties in somatosensory cortex. In agreement with pioneering work on delta waves, we propose that TRN hyperpolarization liberates TC cells from phasic hyperpolarization to engage in a clock-like rhythm at delta frequencies (**Steriade et al., 1993**). Results consistent with this interpretation were also obtained in animals doubly deficient in $Ca_V3$ channels (**Pellegrini et al., 2016**). Recently, it was also shown that optogenetic inhibition of anterior TRN cells may suppress rather than strengthen low-frequency EEG activity (**Herrera et al., 2016**), yet this effect occurred with a 10-s-long delay after acute inhibition of TRN cell discharge.

The powerful control of delta power by TRN-dependent mechanism could be relevant for the role of delta waves in the homeostatic regulation of NREMS. The increase in low-frequency power of NREMS over the 0.75–4 Hz power band, referred to as slow-wave activity, is the most widely used marker to quantify homeostatic sleep pressure (**Borbély and Tobler, 2011**). We find here that slow-wave activity contains a thalamically controlled component that can be rapidly and bidirectionally modulated through TRN membrane polarization. Such mechanisms could contribute to sleep-deprivation induced boosting of the high- but not the low-frequency component of slow-wave activity (**Achermann and Borbély, 1997**; **Huber et al., 2000**). Bidirectional regulation of slow-wave activity in local brain areas according to use dependence has also been described (**Kattler et al., 1994**; **Pigarev et al., 1997**; **Vyazovskiy et al., 2000**; **Miyamoto and Hensch, 2003**; **Huber et al., 2006**). More complex localized alterations in NREMS are observed following exposure to learning tasks that involve enhanced power in both the low-frequency range (SO and delta waves in the slow wave

activity frequency range of 0.5–4 Hz) and in the fast sleep spindle range (**Huber et al., 2004**). Learning tasks involving motor cortex increase the density of individual spindle events in a manner specifically restricted to motor cortex (**Johnson et al., 2012**) or augmented both slow wave and sleep spindle power in supplementary motor cortex (**Tamaki et al., 2013**). Therefore, cortical modules are capable of generating qualitatively different forms of local NREMS spontaneously and according to recent use and experience. Membrane potential polarization within TRN sectors could represent a powerful addition to previously proposed mechanisms that primarily imply changes in cortical synaptic strength (**Tononi and Cirelli, 2014**). Both ascending brainstem and basal forebrain (**McCormick and Bal, 1997**; **Beierlein, 2014**) as well as descending cortical inputs (**McCormick and von Krosigk, 1992**; **Zhang et al., 2012**) regulate TRN membrane potential and burst propensity. Whether differential neuromodulation of TRN sectors contributes to use- and experience-dependent sleep regulation remains an intriguing topic for further study.

Compromised sleep spindle generation is a promising read-out for neuropsychiatric disorders involving aberrant sensory percepts and attentional deficits, such as schizophrenia (**Manoach et al., 2016**). In large-scale genome-wide association studies, the gene encoding $Ca_V3.3$ channels ranks in the top list of candidate risk genes in schizophrenia, together with several genes that are highly enriched in TRN and implied in repetitive burst discharge (**Krol et al., 2018**). Based on our data, we propose that wake-related deficits in some of these patients may show a specificity for certain sensory modalities that co-vary with local deficits in sleep spindles and their coupling to the SO. This could help to further refine the classification and diagnosis of these complex disorders.

# Materials and methods

### Key resources table

| Reagent type (species) or resource | Designation | Source or reference | Identifiers | Additional information |
|---|---|---|---|---|
| Genetic reagent (*M. musculus*) | $Ca_V3.3$ KO | PMID: 21808016 | MGI:5637591 | generated by Dr. H. Prosser, then at GSK |
| Genetic reagent (*M. musculus*) | VGAT-Ires-Cre | PMID: 21745644 | MGI:5141270 | generated by Dr. B. Lowell, Harvard |
| Recombinant DNA reagent | AAV1-hSyn-ChR2(H134R)_eYFP-WPRE-hGH | Penn Vector Core | 26973P | |
| Recombinant DNA reagent | AAV8-hSyn-DIO-hM4D(Gi)_mCherry | UNC Vector Core | N/A | |
| Recombinant DNA reagent | ssAAV8/2-hSyn1-dlox-HA_hM4D(Gi)_IRES_mCitrine-dlox-WPRE-hGHp(A) | Zurich viral vector repository | v93-8 | |
| Antibody | mouse anti-PV RRID:AB_10000343 | Swant | PV 235 | Dilution 1/4000 |
| Antibody | goat anti-mouse CY5 RRID:AB_2338713 | Jackson ImmunoResearch | 115-175-146 | Dilution 1/500 |
| Peptide, recombinant protein | streptavidin coupled with Alexa Fluor 594 RRID:AB_2337250 | Jackson ImmunoResearch | 016-580-084 | Dilution 1/8000 |
| Chemical compound, drug | CNO | Tocris | 6329 | |
| Software, algorithm | Neuroexplorer | Plexon | | |

*Continued on next page*

*Continued*

| Reagent type (species) or resource | Designation | Source or reference | Identifiers | Additional information |
|---|---|---|---|---|
| Software, algorithm | Intan RHD2000 recording system with Matlab toolbox 1.2.2 | IntanTeck | | |
| Software, algorithm | PClamp10.2 | Molecular Devices | | |
| Software, algorithm | Igor Pro 7 | WaveMetrics | | |
| Software, algorithm | Matlab 2018 a | MathWorks | | |
| Software, algorithm | R 3.5.1 | R Core Team | | |

## Animal handling

Mice from the C57BL/6J line (also referred to as wild-type, WT), the $Ca_V3.3$ KO line and the VGAT-Ires-Cre line (Jackson Labs, generated by Dr. B. Lowell, Beth Israel Deaconess Medical Center, Harvard) (***Vong et al., 2011***) were bred on a C57BL/6J background and housed in a temperature- and humidity-controlled animal house with a 12 hr/12 hr light-dark cycle (lights on at 9 am). Food and water were available *ad libitum*. For viral injections, 3- to 4-week-old mice of either sex were transferred to a P2 safety level housing room with identical conditions 1 day prior to injection. Then, for *in vitro* experimentation, animals were transferred 3 to 4 weeks later to a housing room with identical conditions, 3–5 days prior to sacrifice. For *in vivo* experimentation, animals were brought to the recording room at least one week prior to experimentation. All experimental procedures complied with the Swiss National Institutional Guidelines on Animal Experimentation and were approved by the Swiss Cantonal Veterinary Office Committee for Animal Experimentation.

## Viral injections

Mice 3- to 4-week-old were anaesthetized using Ketamine-Xylazine (83 and 3.5 mg/kg, respectively). Mice were placed on a heating blanket to maintain the body temperature at 37°C. An initial dose of analgesic was administrated at the beginning of the surgery (Carprofen i.p. 5 mg/kg). The animal was head-fixed on a stereotactic apparatus equipped with a head adaptor for young animals (Stoelting 51925, Wood Dale, IL). A small incision was made on the skin and the bone exposed at the desired injection site. Viruses were injected with a thin glass pipette (5-000-1001-X, Drummond Scientific, Broomall, PA) pulled on a vertical puller (Narishige, Tokyo, Japan). WT and $Ca_V3.3$ KO mice were injected bilaterally with a virus encoding ChR2-EYFP (500 nl of AAV1-hSyn-ChR2(H134R)_eYFP-WPRE-hGH, $10^{12}$ GC, ~100–200 nl/min) for one of the following sites (in stereotaxic coordinates, relative to bregma: anteroposterior, lateral, depth from surface): S1 (-1.7, ±3.1, -0.8), AC (-2.5, ±4, -1.1), MD (-1.7, ±0.4, -3.2). VGAT-Ires-Cre mice were injected bilaterally with a virus encoding DREADD-mCherry (500 nl of AAV8-hSyn-DIO-hM4D(Gi)_mCherry, $6.4x10^{12}$ GC), or DREADD-IRES-mCitrine (500 nl of ssAAV8/2-hSyn1-dlox-HA_hM4D(Gi)_IRES_mCitrine-dlox-WPRE-hGHp(A), $3.1x10^{12}$ GC) or a control AAV8 encoding a DREADD-unrelated construct (500 nl of AAV8-hSyn-FLEX-Jaws_KGC_GFP_ER2, $3.2x10^{12}$ GC) in the sensory sector of the TRN (-1.7, ±2.25, -2.9).

## *In vitro* electrophysiological recordings

Adult WT, $Ca_V3.3$ KO and VGAT-Ires-Cre mice (3–4 weeks post viral injection), 7- to 9-week-old, were briefly anaesthetized with isoflurane and their brains quickly extracted. Acute 300-µm-thick coronal brain slices were prepared in ice-cold oxygenated sucrose solution (which contained in mM: NaCl 66, KCl 2.5, $NaH_2PO_4$ 1.25, $NaHCO_3$ 26, *D*-saccharose 105, *D*-glucose 27, *L(+)*-ascorbic acid 1.7, $CaCl_2$ 0.5 and $MgCl_2$ 7), using a sliding vibratome (Histocom, Zug, Switzerland). Slices were kept for 30 min in a recovery solution at 35°C (in mM: NaCl 131, KCl 2.5, $NaH_2PO_4$ 1.25, $NaHCO_3$ 26, *D*-glucose 20, *L(+)*-ascorbic acid 1.7, $CaCl_2$ 2, $MgCl_2$ 1.2, *myo*-inositol 3, pyruvate 2) before being transferred to room temperature for at least 30 more min before starting the recording.

Recording glass pipettes were pulled from borosilicate glass (TW150F-4) (World Precision Instruments, Sarasota, FL) with a DMZ horizontal puller (Zeitz Instruments, Martinsried, Germany) to a final resistance of 2–4 MΩ. Pipettes were filled with a $K^+$-based intracellular solution that contained in mM: KGluconate 140, Hepes 10, KCl 10, EGTA 0.1, phosphocreatine 10, Mg-ATP 4, Na-GTP 0.4, pH 7.3, 290–305 mOsm, supplemented with ~2 mg/ml of neurobiotin (Vector Labs, Servion, Switzerland). Slices were placed in the recording chamber of an upright microscope (Olympus BX50WI, Volketswil, Switzerland) and continuously superfused at room temperature with oxygenated ACSF containing in mM: NaCl 131, KCl 2.5, $NaH_2PO_4$ 1.25, $NaHCO_3$ 26, *D*-glucose 20, *L(+)*-ascorbic acid 1.7, $CaCl_2$ 2 and $MgCl_2$ 1.2, picrotoxin 0.1, glycine 0.01. Cells were visualized with differential interference contrast optics and 10X and 40X immersion objectives. Infrared images were acquired with an iXon Camera X2481 (Andor, Belfast, Northern Ireland). Signals were amplified using a Multiclamp 700B amplifier, digitized via a Digidata1322A and sampled at 10 kHz with Clampex10.2 (Molecular Devices, San José, CA). Immediately after gaining whole-cell access, cell capacitance $C_m$ was measured in voltage-clamp at −60 mV through applying 500 ms-long, 20 mV hyperpolarizing steps (5 steps/cell). Whole-field blue LED (Cairn Res, Faversham, UK) stimulation (455 nm, duration: 0.1 to 1 ms, maximal light intensity 0.16 $mW/mm^2$) in voltage-clamp (−60 mV) was used to assess the connectivity of TRN neurons through fibers arising from the previously injected area (S1, AC or MD). Once identified, squared somatic current injections (−50 to −300 pA for 500 ms, 4 injections/cell and membrane potential) hyperpolarized neurons below −100 mV from membrane potentials between −90 and −50 mV (corrected for a liquid junction potential of 10 mV) and induced repetitive burst discharge in TRN neurons. For comparison between neurons from different TRN sectors, the response to this current injection was also used to assess cellular input resistance $R_i$. For CNO application, a stable baseline of at least 2 min was recorded before bath application of water-soluble CNO (10 µM, Tocris, Bristol, UK) for at least 2 min until its hyperpolarizing effect reached a plateau. Washout of CNO did not reverse the hyperpolarizing effect for up to 10 min of washout. Two VPM and two TRN neurons outside the visually identified fluorescent site of injection were used as control for CNO's effect on membrane potential.

Cell parameters were calculated on Clampfit v.10.2. and IgorPro Wavemetrics (Lake Oswego, OR). Input and access resistances were evaluated all along the recordings. Neurons presenting a variation of the access resistance >20% or a holding current at −60 mV < −150 pA were excluded from analysis. Light-evoked excitatory postsynaptic current (EPSC) amplitudes were measured in traces presenting monophasic synaptic events that occurred at fixed latency after LED onset and that were not contaminated by asynchronous release. In the subset of neurons that underwent paired-pulse stimulation, traces containing spontaneous activity between the two LED stimulations were discarded. Paired-pulse ratios are expressed as percentage of the second over the first EPSC amplitude (6 paired-stimuli/cell). The bursting of TRN neurons was assessed by counting the number of $Ca^{2+}$ spikes following a 500 ms hyperpolarization below −100 mV. $Ca^{2+}$ spikes were counted as bursts if they generated triangular-shaped membrane depolarizations followed by a clear afterhyperpolarization, regardless of the presence of high-frequency action potentials on top of the $Ca^{2+}$ spikes.

## *In vivo* multi-site electrophysiological recordings

Surgery was performed as recently described (***Lecci et al., 2017***). Briefly, animals were subjected to gas anaesthesia (isoflurane supplemented with a mixture $O_2$ and $N_2O$) and small craniotomies (0.3–0.5 mm) were performed at the location for implantation of high-impedance fine tungsten LFP microelectrodes (10–12 MΩ, 75 µm shaft diameter, FHC, Bowdoin, ME) at the following sites (in stereotaxic coordinates, relative to bregma: anteroposterior, lateral, depth from surface): sensory regions S1 (−1.7, 3.0, -1.0), S2 (−0.7, 4.2, -1.1), and AC (−2.5, 4.0, -1.1), limbic areas of PFC (+1.8, 0.3, -1.85). Implantations were guided through calculating the corresponding interaural coordinates. As a neutral reference for LFP electrodes, a silver wire (Harvard Apparatus, Holliston, MA) was inserted in the bone over lateral portions of the cerebellum. On the contralateral skull site, two conventional gold-coated low-impedance electrodes were implanted over the *dura mater* through frontal and parietal bones for differential surface EEG recordings. Two gold pellets inserted into the muscles of the neck served as EMG electrodes. Multi-site recordings were carried out in head-restrained conditions, for which a light-weight metal head-post (Bourgeois Mécanique SAS, Lyon, France) was glued and cemented onto the midline skull in order to perform painless head-fixed recording sessions (***Fernandez et al., 2017***; ***Lecci et al., 2017***). Carprofen (5 mg/kg, i.p.) and

paracetamol (2 mg/mL, drinking water) were provided during the pre- and post-operative periods. Mice were gently and gradually habituated to a custom-made head-fixation system (Bourgeois Mécanique SAS, Lyon, France) by increasing the amount of time spent in head fixation daily from 10 to 30 min to 2–3 hr/day. Mice sat within a cardboard roll such that only the head protruded. Occasionally, a heating pad was placed underneath the cardboard. After each head-restrained period, mice were rewarded with *ad libitum* drops of sweetened water. Mice typically started sleeping spontaneously after 7–14 d of habituation, generating periods of both NREMS and REMS. LFP and EEG/EMG signals were amplified 1000x through a 16-channel Multiple Acquisition Processor System (Plexon Inc., Dallas, TX), high- and low-pass filtered at 0.8 and 300 Hz, respectively, and digitized at 1 kHz. For multi-site recordings, 5 WT and 6 $Ca_V3.3$ KO animals had all four recording sites histologically confirmed, 1 WT (S1, S2, PFC) and 3 $Ca_V3.3$ KO (2x S1, S2, AC; 1x S1, S2, PFC) animals had three confirmed recording sites, 3 WT (1x S1, AC; 2x S1, S2) and 4 $Ca_V3.3$ KO (S1, S2) animals had two confirmed sites. Four animals were excluded because recording sites could not be identified or because brain appearance was not satisfying (ventricle dilatation or damaged brain slice).

## *In vivo* chemogenetics

After 1 week of recovery from viral injection, bilateral S1 LFP electrodes, and EEG/EMG electrodes were implanted as described above, followed by a week of recovery. After 4 days of habituation to the tethering cable, baseline activity was recorded in freely moving conditions during 3 to 4 days. 3 weeks after viral injections, intra-peritoneal injection of CNO (water-soluble diluted in NaCl 0.9%, dosis 1 mg/kg, Ref. 6329, Tocris, Bristol, UK) or NaCl 0.9% was performed at Zeitgeber time ZT2 in a random cross-over design, with the experimenter blind to the injection. Recordings under each condition took place on 4–5 successive days, with 2–3 CNO and 1–2 NaCl injections per animal. Signals were acquired at 1 kHz with an Intan digital RHD2132 amplifier board and a RHD2000 USB Interface board, with a high-pass filter set at 0.8 Hz (Intan Technologies, Los Angeles, CA). Data were acquired in Matlab using the RHD2000 Matlab toolbox and customized display software in Matlab. To assess the time course of CNO action, 3 DREADD-mCherry and 3 AAV8-control animals were recorded starting at ZT0. Based on these dynamics, we chose a window of 45 min (starting 20 min after the injection) for comparison of CNO and NaCl effects (***Figure 4—figure supplement 1B, D***). The average power spectrum per animal was calculated as mean between recording sites and repetition-days for the two conditions (CNO or NaCl). Spectral analysis of the signals was performed as described in the data analysis section. For chemogenetic recordings, a total of 3 DREADD-mCherry and 2 control AAV8 mice had bilateral S1 recording sites histologically confirmed, 2 DREADD-mCherry and 1 control AAV8 had one confirmed S1 recording sites.

## Histology and immunofluorescent labeling

After completion of patch-clamp recordings *in vitro*, slices were post-fixed in paraformaldehyde (4%) for >24 hr. An immunostaining on free-floating sections was used to outline PV-positive (PV+) neurons in the TRN and to recover neurobiotin-filled neurons. To ensure proper staining of PV+ neurons, a 5-day incubation at 4°C of the primary antibody (mouse anti-PV, 1/4000, Swant Inc., Marly, Switzerland) in 1% Triton was required. The secondary antibody (goat anti-mouse CY5, 1/500, Jackson ImmunoResearch, Ely, Nevada) and Streptavidin (coupled with Alexa Fluor 594, 1/8000, Jackson ImmunoResearch) were incubated at 4°C for 24 hr. Sections were observed with an Axiovision Imager Z1 (Carl Zeiss) microscope equipped with an AxioCam MRc5 camera. Objectives were EC-Plan Neofluar 2.5x/0.075 ∞/0.17, 5x/0.16 ∞/0.17. The AxioVision Rel. 4.7 and Adobe Photoshop CS5 software were used to merge micrographs from the different channels. The nomenclature of the location of TRN sectors in ***Figure 1*** follows the descriptions established by ***Pinault and Deschênes (1998)***.

After completion of *in vivo* recordings (multi-site or chemogenetics recordings), recording sites were marked through electro-coagulation (50 µA, 8–10 s) during deep pentobarbital anaesthesia (80 mg/kg) before transcardiac perfusion (4% paraformaldehyde in 0.1 M phosphate buffer). After >24 hr post-fixation, 100 µm coronal brain sections were cut and imaged to confirm electrocoagulation sites of LFP implantation or fluorescent expression of viral injection site.

## *In vivo* data analysis

Data were analyzed using IgorPro (Wavemetrics, v7, Lake Oswego, OR), MatLab (MathWorks) and Excel (Microsoft).

### Scoring of vigilance states

Sleep and wake episodes were detected manually according to standard scoring procedures (***Fernandez et al., 2017***). Briefly, wakefulness was accompanied by large or tonic EMG signal (active and quiet wakefulness), EEG of low-voltage and exhibiting fast oscillatory components, such as theta and gamma oscillations. Drowsiness period between wakefulness and NREMS were discarded, as well as intermediate sleep periods between NREMS and REMS. Only consolidated clear episodes of NREMS were selected for the analysis: high amplitude voltage and slow EEG components, such as periods of slow oscillation (<1.5 Hz), delta waves (1.5–4 Hz) and spindles (10–15 Hz). REMS was clearly distinguishable with reduced EMG activity (atonia) and predominant theta (~6–10 Hz) on the low-amplitude EEG. For the chemogenetic data analysis, NREMS was scored in 4 s epochs with the same criteria and only consolidated NREMS (>20 s) were included in further analysis. All scorings were done with custom-made software prepared in Igor and Matlab.

### Spectral analysis of the signals

Power spectra were computed on raw signals using a squared Fast Fourier Transform (FFT) on 4 s windows after offset correction (mean substracted for each window). Each mean power spectrum per mouse and per channel was normalized by its sum between 0 and 35 Hz and expressed in percentage to compare between animals. The total power per frequency band of interest, SO 0.5–1.5 Hz, delta 1.5–4 Hz and sigma 10–15 Hz, was measured using the integral of the normalized power spectrum in-between frequency band borders.

### Dynamics of delta time course (Chemogenetics)

The dynamics of delta activity were extracted from the area under the power spectrum in the delta band (1.5–4 Hz) for each 4 s epoch of consolidated NREMS (>20 s continuous bouts). The time-series were calculated in quantiles of identical amounts of NREMS (12 for baseline and 36 for post-injections) and normalized by the mean of the first two baseline bins.

### Spindle event detection

The square-power of the filtered enlarged sigma band (9–16 Hz, Finite Impulse Response) calculated separately for the recordings from each brain area was used to detect onset and offset of spindles. We applied a threshold of [1.5 x the S.D. + 1 x the mean] of the sigma power, and detected all events above this threshold that lasted at least 3 cycles (***Figure 5—figure supplement 1A***). The onset and offset times of a spindle event were extended to the closest cycle at 0 crossing before and after the threshold. Events that were overlapping or that were separated by <10 ms were fused. Events that were at the beginning time point or last time point of a NREMS bout were discarded. Amplitudes of spindles were computed from the average amplitude of the sigma power between onset and offset time and averaged per mouse. Frequency of spindles were determined by extracting the peak frequency from the magnitude FFT on each spindle event (86.3% of events had a distinguishable frequency peak and were included), followed by calculating the mean intra-frequency per mouse. Two WT mice with S1 and S2 recording sites were omitted due to an unusually reduced signal amplitude that prevented comparison to other mice (note that no normalization was applied for spindle detection).

### Slow oscillation detection

Periods of clear and visible SOs were detected based on (***Mölle et al., 2009***). Briefly, each signal was 2 Hz low-pass filtered, minimum (y1) and maximum (y2) were detected, as well as the corresponding time point (x1 and x2). The mean minima (Y1) and the mean maxima (Y2) as well as their difference (Y2-Y1) were calculated. Constraints for selecting periods of SOs were: (1) times between x1 and x2 were comprised between 0.5 s and 2 s, (2) if y1 was lower than 2/3 of the mean Y1, (3) y2-y1 was at least 2/3 of Y2-Y1. These constraints allowed to select the largest SOs periods. Only events

that had a time overlap ≥95% to a SO were selected for the phase-locking analysis. Angle phase values of the SO at each spindle event onset time detected were extracted using a Hilbert transform.

### Statistics

*In vitro*. Statistical analysis was done using R programming language (2.15.0, R Core Team) [The R Development Core Team, The R Foundation for Statistical Computing (www.r-project.org/foundation), 2007]. The normality of the data sets was assessed using Shapiro-Wilk normality test. Comparisons between paired conditions (amplitude of $1^{st}$ versus $2^{nd}$ EPSCs during paired-stimulation and effect of CNO on membrane potential) were done using Wilcoxon signed rank-test and paired Student's *t*-test, respectively. Comparisons between unpaired conditions in non-normally distributed datasets (passive cellular properties, sector effect on repetitive bursting in WT, sector effect on repetitive bursting in $Ca_V3.3$ KO, genotype effect on repetitive bursting) were done using Mann-Whitney or Kruskal-Wallis H tests. Comparisons between unpaired conditions in normally distributed datasets (sector and genotype effect onto PPR and CNO effect onto WT vs $Ca_V3.3$ KO) were done using unpaired Student's *t*-tests or two-way ANOVAs. Bonferroni correction was applied whenever more than two comparisons were done for the same data set. The proportion of repetitive bursting neurons in the different TRN sectors was compared using Chi-square test for independence followed by a pairwise proportion test with Holm's adjustment method. Exact significant p-values are indicated.

*In vivo*. Statistical analysis was done using IgorPro, R programming language and Matlab. The normality of the data sets was assessed using Shapiro-Wilk normality test. Comparisons between genotypes per site of recording were done using Student's *t*-test (parametric data set) or Mann-Whitney (non-parametric unpaired data set). Comparisons between paired conditions (CNO versus NaCl, or SO Active state versus Silent state) were done using paired Student's *t*-test (parametric data set) or Wilcoxon signed-rank test (non-parametric paired data). Bonferroni correction was applied when more than two comparisons were done for the same data set.

## Acknowledgements

We are grateful to all lab members for critical input at all stages of this manuscript. In particular, Sandro Lecci was heavily involved in supporting experimentation and in data analysis discussions. The excellent animal care and support by the Team of our Animalerie, headed by Alain Gnecchi and Michelle Blom, and the expert veterinary advice and support of Drs. Gisèle Ferrand and Laure Sériot are highly appreciated. We thank Christiane Devenoges for excellent technical support on histology and genotyping. We are indebted to Antoine Adamantidis, Simone Astori, Paul Franken, Manuel Mameli and Mehdi Tafti for many constructive discussions and experimental input. Simone Astori, Sylvain Crochet, Sandro Lecci and Francesca Siclari provided critical comments on prefinal versions of the manuscript. Many thanks to Christian Lüscher and Manuel Mameli for making the VGAT-Ires-Cre animals available to us. This study was supported by the Swiss National Science Foundation, the Fondation Pro-Femmes, and Etat de Vaud.

## Additional information

### Funding


| Funder | Grant reference number | Author |
|---|---|---|
| Swiss National Science Foundation | 31003A_166318 | Laura MJ Fernandez<br>Gil Vantomme<br>Alejandro Osorio-Forero<br>Romain Cardis<br>Elidie Béard<br>Anita Lüthi |
| État de Vaud | | Laura MJ Fernandez<br>Gil Vantomme<br>Alejandro Osorio-Forero<br>Romain Cardis<br>Elidie Béard<br>Anita Lüthi |

| | |
|---|---|
| FBM Poste de soutien à un congé parental | Laura MJ Fernandez |

The funders had no role in study design, data collection and interpretation, or the decision to submit the work for publication.

### Author contributions

Laura MJ Fernandez, Conceptualization, Data curation, Formal analysis, Supervision, Validation, Investigation, Visualization, Methodology, Writing—original draft, Project administration, Writing—review and editing; Gil Vantomme, Alejandro Osorio-Forero, Data curation, Formal analysis, Validation, Investigation, Visualization, Methodology, Writing—original draft, Writing—review and editing; Romain Cardis, Resources, Software, Formal analysis, Visualization, Methodology, Writing—review and editing; Elidie Béard, Data curation, Formal analysis, Validation, Investigation, Methodology, Writing—review and editing; Anita Lüthi, Conceptualization, Data curation, Supervision, Funding acquisition, Validation, Visualization, Writing—original draft, Project administration, Writing—review and editing

### Author ORCIDs

Laura MJ Fernandez http://orcid.org/0000-0002-7942-3369
Gil Vantomme http://orcid.org/0000-0002-7441-0737
Alejandro Osorio-Forero http://orcid.org/0000-0003-4341-4206
Anita Lüthi https://orcid.org/0000-0002-4954-4143

### Ethics

Animal experimentation: All experimental procedures complied with the Swiss National Institutional Guidelines on Animal Experimentation (Swiss Federal Act on Animal Protection, LPA 2005) and were approved by the Swiss Cantonal Veterinary Office Committee for Animal Experimentation. All experiments were carried out in accordance with approved protocols by the Swiss Cantonal Veterinary Office Committee for in vitro experimentation on mice (reference VD2062) and for in vivo experimentation on mice (references VD2387 and VD2401).

### Decision letter and Author response

Decision letter https://doi.org/10.7554/eLife.39111.022
Author response https://doi.org/10.7554/eLife.39111.023

## Additional files

### Supplementary files

- Transparent reporting form

DOI: https://doi.org/10.7554/eLife.39111.018

### Data availability

All data generated or analysed during this study are included in the manuscript and supporting files.

## References

**Achermann P**, Borbély AA. 1997. Low-frequency (< 1 Hz) oscillations in the human sleep electroencephalogram. *Neuroscience* **81**:213–222. DOI: https://doi.org/10.1016/S0306-4522(97)00186-3, PMID: 9300413

**Astori S**, Wimmer RD, Prosser HM, Corti C, Corsi M, Liaudet N, Volterra A, Franken P, Adelman JP, Lüthi A. 2011. The $Ca_V3.3$ calcium channel is the major sleep spindle pacemaker in thalamus. *PNAS* **108**:13823–13828. DOI: https://doi.org/10.1073/pnas.1105115108, PMID: 21808016

**Astori S**, Lüthi A. 2013. Synaptic plasticity at intrathalamic connections via $Ca_V3.3$ T-type $Ca^{2+}$channels and GluN2B-containing NMDA receptors. *Journal of Neuroscience* **33**:624–630. DOI: https://doi.org/10.1523/JNEUROSCI.3185-12.2013

**Astori S**, Wimmer RD, Lüthi A. 2013. Manipulating sleep spindles–expanding views on sleep, memory, and disease. *Trends in Neurosciences* **36**:738–748. DOI: https://doi.org/10.1016/j.tins.2013.10.001, PMID: 24210901

**Beierlein M**. 2014. Synaptic mechanisms underlying cholinergic control of thalamic reticular nucleus neurons. *The Journal of Physiology* **592**:4137–4145. DOI: https://doi.org/10.1113/jphysiol.2014.277376, PMID: 24973413

**Bonjean M**, Baker T, Bazhenov M, Cash S, Halgren E, Sejnowski T. 2012. Interactions between core and matrix thalamocortical projections in human sleep spindle synchronization. *Journal of Neuroscience* **32**:5250–5263. DOI: https://doi.org/10.1523/JNEUROSCI.6141-11.2012, PMID: 22496571

**Borbély AA**, Tobler I. 2011. Manifestations and functional implications of sleep homeostasis. *Handbook of Clinical Neurology* **98**:205–213. DOI: https://doi.org/10.1016/B978-0-444-52006-7.00013-7, PMID: 21056188

**Bourassa J**, Pinault D, Deschênes M. 1995. Corticothalamic projections from the cortical barrel field to the somatosensory thalamus in rats: a single-fibre study using biocytin as an anterograde tracer. *European Journal of Neuroscience* **7**:19–30. DOI: https://doi.org/10.1111/j.1460-9568.1995.tb01016.x, PMID: 7711933

**Brunton J**, Charpak S. 1997. Heterogeneity of cell firing properties and opioid sensitivity in the thalamic reticular nucleus. *Neuroscience* **78**:303–307. DOI: https://doi.org/10.1113/jphysiol.2007.134254, PMID: 9145788

**Clemente-Perez A**, Makinson SR, Higashikubo B, Brovarney S, Cho FS, Urry A, Holden SS, Wimer M, Dávid C, Fenno LE, Acsády L, Deisseroth K, Paz JT. 2017. Distinct thalamic reticular cell types differentially modulate normal and pathological cortical rhythms. *Cell Reports* **19**:2130–2142. DOI: https://doi.org/10.1016/j.celrep.2017.05.044, PMID: 28591583

**Collins DP**, Anastasiades PG, Marlin JJ, Carter AG. 2018. Reciprocal circuits linking the prefrontal cortex with dorsal and ventral thalamic nuclei. *Neuron* **98**:366–379. DOI: https://doi.org/10.1016/j.neuron.2018.03.024

**Contreras D**, Curró Dossi R, Steriade M. 1992. Bursting and tonic discharges in two classes of reticular thalamic neurons. *Journal of Neurophysiology* **68**:973–977. DOI: https://doi.org/10.1152/jn.1992.68.3.973, PMID: 1432063

**Contreras D**, Destexhe A, Sejnowski TJ, Steriade M. 1996. Control of spatiotemporal coherence of a thalamic oscillation by corticothalamic feedback. *Science* **274**:771–774. DOI: https://doi.org/10.1126/science.274.5288.771, PMID: 8864114

**Crabtree JW**. 1999. Intrathalamic sensory connections mediated by the thalamic reticular nucleus. *Cellular and Molecular Life Sciences* **56**:683–700. DOI: https://doi.org/10.1007/s000180050462, PMID: 11212315

**Crunelli V**, David F, Lőrincz ML, Hughes SW. 2015. The thalamocortical network as a single slow wave-generating unit. *Current Opinion in Neurobiology* **31**:72–80. DOI: https://doi.org/10.1016/j.conb.2014.09.001, PMID: 25233254

**Crunelli V**, Lőrincz ML, Connelly WM, David F, Hughes SW, Lambert RC, Leresche N, Errington AC. 2018. Dual function of thalamic low-vigilance state oscillations: rhythm-regulation and plasticity. *Nature Reviews Neuroscience* **19**:107–118. DOI: https://doi.org/10.1038/nrn.2017.151, PMID: 29321683

**Cueni L**, Canepari M, Luján R, Emmenegger Y, Watanabe M, Bond CT, Franken P, Adelman JP, Lüthi A. 2008. T-type $Ca^{2+}$ channels, SK2 channels and SERCAs gate sleep-related oscillations in thalamic dendrites. *Nature Neuroscience* **11**:683–692. DOI: https://doi.org/10.1038/nn.2124, PMID: 18488023

**Delevich K**, Tucciarone J, Huang ZJ, Li B. 2015. The mediodorsal thalamus drives feedforward inhibition in the anterior cingulate cortex via parvalbumin interneurons. *Journal of Neuroscience* **35**:5743–5753. DOI: https://doi.org/10.1523/JNEUROSCI.4565-14.2015, PMID: 25855185

**Desîlets-Roy B**, Varga C, Lavallée P, Deschênes M. 2002. Substrate for cross-talk inhibition between thalamic barreloids. *The Journal of Neuroscience* **22**:RC218. DOI: https://doi.org/10.1523/JNEUROSCI.22-09-j0002.2002, PMID: 11978859

**Dijk DJ**, Hayes B, Czeisler CA. 1993. Dynamics of electroencephalographic sleep spindles and slow wave activity in men: effect of sleep deprivation. *Brain Research* **626**:190–199. DOI: https://doi.org/10.1016/0006-8993(93)90579-C, PMID: 8281430

**Feldmeyer D**, Brecht M, Helmchen F, Petersen CC, Poulet JF, Staiger JF, Luhmann HJ, Schwarz C. 2013. Barrel cortex function. *Progress in Neurobiology* **103**:3–27. DOI: https://doi.org/10.1016/j.pneurobio.2012.11.002, PMID: 23195880

**Fernandez LMJ**, Comte JC, Le Merre P, Lin JS, Salin PA, Crochet S. 2017. Highly dynamic spatiotemporal organization of low-frequency activities during behavioral states in the mouse cerebral cortex. *Cerebral Cortex* **27**:5444–5462. DOI: https://doi.org/10.1093/cercor/bhw311, PMID: 27742711

**Fogerson PM**, Huguenard JR. 2016. Tapping the brakes: cellular and synaptic mechanisms that regulate thalamic oscillations. *Neuron* **92**:687–704. DOI: https://doi.org/10.1016/j.neuron.2016.10.024, PMID: 27883901

**Franken P**, Malafosse A, Tafti M. 1998. Genetic variation in EEG activity during sleep in inbred mice. *American Journal of Physiology-Regulatory, Integrative and Comparative Physiology* **275**:R1127–R1137. DOI: https://doi.org/10.1152/ajpregu.1998.275.4.R1127

**Frauscher B**, von Ellenrieder N, Dubeau F, Gotman J. 2015. Scalp spindles are associated with widespread intracranial activity with unexpectedly low synchrony. *NeuroImage* **105**:1–12. DOI: https://doi.org/10.1016/j.neuroimage.2014.10.048, PMID: 25450108

**Fuentealba P**, Steriade M. 2005. The reticular nucleus revisited: intrinsic and network properties of a thalamic pacemaker. *Progress in Neurobiology* **75**:125–141. DOI: https://doi.org/10.1016/j.pneurobio.2005.01.002, PMID: 15784303

**Gardner RJ**, Hughes SW, Jones MW. 2013. Differential spike timing and phase dynamics of reticular thalamic and prefrontal cortical neuronal populations during sleep spindles. *Journal of Neuroscience* **33**:18469–18480. DOI: https://doi.org/10.1523/JNEUROSCI.2197-13.2013, PMID: 24259570

**Halassa MM**, Siegle JH, Ritt JT, Ting JT, Feng G, Moore CI. 2011. Selective optical drive of thalamic reticular nucleus generates thalamic bursts and cortical spindles. *Nature Neuroscience* **14**:1118–1120. DOI: https://doi.org/10.1038/nn.2880, PMID: 21785436

**Halassa MM**, Chen Z, Wimmer RD, Brunetti PM, Zhao S, Zikopoulos B, Wang F, Brown EN, Wilson MA. 2014. State-dependent architecture of thalamic reticular subnetworks. *Cell* **158**:808–821. DOI: https://doi.org/10.1016/j.cell.2014.06.025, PMID: 25126786

**Halassa MM**, Acsády L. 2016. Thalamic inhibition: diverse sources, diverse scales. *Trends in Neurosciences* **39**:680–693. DOI: https://doi.org/10.1016/j.tins.2016.08.001, PMID: 27589879

**Herd MB**, Brown AR, Lambert JJ, Belelli D. 2013. Extrasynaptic $GABA_A$ receptors couple presynaptic activity to postsynaptic inhibition in the somatosensory thalamus. *Journal of Neuroscience* **33**:14850–14868. DOI: https://doi.org/10.1523/JNEUROSCI.1174-13.2013, PMID: 24027285

**Herrera CG**, Cadavieco MC, Jego S, Ponomarenko A, Korotkova T, Adamantidis A. 2016. Hypothalamic feedforward inhibition of thalamocortical network controls arousal and consciousness. *Nature Neuroscience* **19**:290–298. DOI: https://doi.org/10.1038/nn.4209

**Higashikubo B**, Moore CI. 2018. Systematic examination of the impact of depolarization duration on thalamic reticular nucleus firing *in vivo*. *Neuroscience* **368**:187–198. DOI: https://doi.org/10.1016/j.neuroscience.2017.09.038, PMID: 28965837

**Huber R**, Deboer T, Tobler I. 2000. Topography of EEG dynamics after sleep deprivation in mice. *Journal of Neurophysiology* **84**:1888–1893. DOI: https://doi.org/10.1152/jn.2000.84.4.1888, PMID: 11024081

**Huber R**, Ghilardi MF, Massimini M, Tononi G. 2004. Local sleep and learning. *Nature* **430**:78–81. DOI: https://doi.org/10.1038/nature02663, PMID: 15184907

**Huber R**, Ghilardi MF, Massimini M, Ferrarelli F, Riedner BA, Peterson MJ, Tononi G. 2006. Arm immobilization causes cortical plastic changes and locally decreases sleep slow wave activity. *Nature Neuroscience* **9**:1169–1176. DOI: https://doi.org/10.1038/nn1758, PMID: 16936722

**Johnson LA**, Blakely T, Hermes D, Hakimian S, Ramsey NF, Ojemann JG. 2012. Sleep spindles are locally modulated by training on a brain-computer interface. *PNAS* **109**:18583–18588. DOI: https://doi.org/10.1073/pnas.1207532109, PMID: 23091013

**Kattler H**, Dijk DJ, Borbély AA. 1994. Effect of unilateral somatosensory stimulation prior to sleep on the sleep EEG in humans. *Journal of Sleep Research* **3**:159–164. DOI: https://doi.org/10.1111/j.1365-2869.1994.tb00123.x, PMID: 10607121

**Kim D**, Hwang E, Lee M, Sung H, Choi JH. 2015. Characterization of topographically specific sleep spindles in mice. *Sleep* **38**:85–96. DOI: https://doi.org/10.5665/sleep.4330, PMID: 25325451

**Kimura A**, Yokoi I, Imbe H, Donishi T, Kaneoke Y. 2012. Distinctions in burst spiking between thalamic reticular nucleus cells projecting to the dorsal lateral geniculate and lateral posterior nuclei in the anesthetized rat. *Neuroscience* **226**:208–226. DOI: https://doi.org/10.1016/j.neuroscience.2012.09.016, PMID: 22989916

**Krol A**, Wimmer RD, Halassa MM, Feng G. 2018. Thalamic reticular dysfunction as a circuit endophenotype in neurodevelopmental disorders. *Neuron* **98**:282–295. DOI: https://doi.org/10.1016/j.neuron.2018.03.021, PMID: 29673480

**Krueger JM**, Huang YH, Rector DM, Buysse DJ. 2013. Sleep: a synchrony of cell activity-driven small network states. *European Journal of Neuroscience* **38**:2199–2209. DOI: https://doi.org/10.1111/ejn.12238, PMID: 23651209

**Kurth S**, Ringli M, Geiger A, LeBourgeois M, Jenni OG, Huber R. 2010. Mapping of cortical activity in the first two decades of life: a high-density sleep electroencephalogram study. *Journal of Neuroscience* **30**:13211–13219. DOI: https://doi.org/10.1523/JNEUROSCI.2532-10.2010, PMID: 20926647

**Laventure S**, Fogel S, Lungu O, Albouy G, Sévigny-Dupont P, Vien C, Sayour C, Carrier J, Benali H, Doyon J. 2016. NREM2 and sleep spindles are instrumental to the consolidation of motor sequence memories. *PLOS Biology* **14**:e1002429. DOI: https://doi.org/10.1371/journal.pbio.1002429, PMID: 27032084

**Lecci S**, Fernandez LM, Weber FD, Cardis R, Chatton JY, Born J, Lüthi A. 2017. Coordinated infraslow neural and cardiac oscillations mark fragility and offline periods in mammalian sleep. *Science Advances* **3**:e1602026. DOI: https://doi.org/10.1126/sciadv.1602026, PMID: 28246641

**Lee SH**, Govindaiah G, Cox CL. 2007. Heterogeneity of firing properties among rat thalamic reticular nucleus neurons. *The Journal of Physiology* **582**:195–208. DOI: https://doi.org/10.1113/jphysiol.2007.134254, PMID: 17463035

**Lewis LD**, Voigts J, Flores FJ, Schmitt LI, Wilson MA, Halassa MM, Brown EN. 2015. Thalamic reticular nucleus induces fast and local modulation of arousal state. *eLife* **4**:e08760. DOI: https://doi.org/10.7554/eLife.08760, PMID: 26460547

**Liu XB**, Murray KD, Jones EG. 2011. Low-threshold calcium channel subunit $Ca_V3.3$ is specifically localized in GABAergic neurons of rodent thalamus and cerebral cortex. *The Journal of Comparative Neurology* **519**:1181–1195. DOI: https://doi.org/10.1002/cne.22567, PMID: 21344408

**Maingret N**, Girardeau G, Todorova R, Goutierre M, Zugaro M. 2016. Hippocampo-cortical coupling mediates memory consolidation during sleep. *Nature Neuroscience* **19**:959–964. DOI: https://doi.org/10.1038/nn.4304, PMID: 27182818

**Manoach DS**, Pan JQ, Purcell SM, Stickgold R. 2016. Reduced sleep spindles in schizophrenia: a treatable endophenotype that links risk genes to impaired cognition? *Biological Psychiatry* **80**:599–608. DOI: https://doi.org/10.1016/j.biopsych.2015.10.003, PMID: 26602589

**Massimini M**, Huber R, Ferrarelli F, Hill S, Tononi G. 2004. The sleep slow oscillation as a traveling wave. *Journal of Neuroscience* **24**:6862–6870. DOI: https://doi.org/10.1523/JNEUROSCI.1318-04.2004, PMID: 15295020

**Mátyás F**, Lee J, Shin HS, Acsády L. 2014. The fear circuit of the mouse forebrain: connections between the mediodorsal thalamus, frontal cortices and basolateral amygdala. *European Journal of Neuroscience* **39**:1810–1823. DOI: https://doi.org/10.1111/ejn.12610, PMID: 24819022

**McCormick DA**, Bal T. 1997. Sleep and arousal: thalamocortical mechanisms. *Annual Review of Neuroscience* **20**:185–215. DOI: https://doi.org/10.1146/annurev.neuro.20.1.185, PMID: 9056712

**McCormick DA**, von Krosigk M. 1992. Corticothalamic activation modulates thalamic firing through glutamate "metabotropic" receptors. *PNAS* **89**:2774–2778. DOI: https://doi.org/10.1073/pnas.89.7.2774, PMID: 1313567

**Mitchell AS**. 2015. The mediodorsal thalamus as a higher order thalamic relay nucleus important for learning and decision-making. *Neuroscience & Biobehavioral Reviews* **54**:76–88. DOI: https://doi.org/10.1016/j.neubiorev.2015.03.001, PMID: 25757689

**Miyamoto H**, Hensch TK. 2003. Reciprocal interaction of sleep and synaptic plasticity. *Molecular Interventions* **3**:404–417. DOI: https://doi.org/10.1124/mi.3.7.404, PMID: 14993461

**Mölle M**, Eschenko O, Gais S, Sara SJ, Born J. 2009. The influence of learning on sleep slow oscillations and associated spindles and ripples in humans and rats. *European Journal of Neuroscience* **29**:1071–1081. DOI: https://doi.org/10.1111/j.1460-9568.2009.06654.x, PMID: 19245368

**Nir Y**, Staba RJ, Andrillon T, Vyazovskiy VV, Cirelli C, Fried I, Tononi G. 2011. Regional slow waves and spindles in human sleep. *Neuron* **70**:153–169. DOI: https://doi.org/10.1016/j.neuron.2011.02.043, PMID: 21482364

**Nuñez A**, Curró Dossi R, Contreras D, Steriade M. 1992. Intracellular evidence for incompatibility between spindle and delta oscillations in thalamocortical neurons of cat. *Neuroscience* **48**:75–85. DOI: https://doi.org/10.1016/0306-4522(92)90339-4, PMID: 1584427

**Paz JT**, Christian CA, Parada I, Prince DA, Huguenard JR. 2010. Focal cortical infarcts alter intrinsic excitability and synaptic excitation in the reticular thalamic nucleus. *Journal of Neuroscience* **30**:5465–5479. DOI: https://doi.org/10.1523/JNEUROSCI.5083-09.2010, PMID: 20392967

**Pellegrini C**, Lecci S, Lüthi A, Astori S. 2016. Suppression of sleep spindle rhythmogenesis in mice with deletion of $Ca_V3.2$ and $Ca_V3.3$ T-type $Ca^{2+}$ channels. *Sleep* **39**:875–885. DOI: https://doi.org/10.5665/sleep.5646, PMID: 26612388

**Peyrache A**, Battaglia FP, Destexhe A. 2011. Inhibition recruitment in prefrontal cortex during sleep spindles and gating of hippocampal inputs. *PNAS* **108**:17207–17212. DOI: https://doi.org/10.1073/pnas.1103612108, PMID: 21949372

**Piantoni G**, Halgren E, Cash SS. 2016. The contribution of thalamocortical core and matrix pathways to sleep spindles. *Neural Plasticity* **2016**:1–10. DOI: https://doi.org/10.1155/2016/3024342, PMID: 27144033

**Piantoni G**, Halgren E, Cash SS. 2017. Spatiotemporal characteristics of sleep spindles depend on cortical location. *NeuroImage* **146**:236–245. DOI: https://doi.org/10.1016/j.neuroimage.2016.11.010, PMID: 27840241

**Pigarev IN**, Nothdurft HC, Kastner S. 1997. Evidence for asynchronous development of sleep in cortical areas. *NeuroReport* **8**:2557–2560. DOI: https://doi.org/10.1097/00001756-199707280-00027, PMID: 9261826

**Pinault D**, Deschênes M. 1998. Projection and innervation patterns of individual thalamic reticular axons in the thalamus of the adult rat: a three-dimensional, graphic, and morphometric analysis. *The Journal of Comparative Neurology* **391**:180–203. DOI: https://doi.org/10.1002/(SICI)1096-9861(19980209)391:2<180::AID-CNE3>3.0.CO;2-Z, PMID: 9518268

**Pinault D**. 2004. The thalamic reticular nucleus: structure, function and concept. *Brain Research Reviews* **46**:1–31. DOI: https://doi.org/10.1016/j.brainresrev.2004.04.008, PMID: 15297152

**Rasch B**, Born J. 2013. About sleep's role in memory. *Physiological Reviews* **93**:681–766. DOI: https://doi.org/10.1152/physrev.00032.2012, PMID: 23589831

**Rector DM**, Topchiy IA, Carter KM, Rojas MJ. 2005. Local functional state differences between rat cortical columns. *Brain Research* **1047**:45–55. DOI: https://doi.org/10.1016/j.brainres.2005.04.002, PMID: 15882842

**Rovó Z**, Mátyás F, Barthó P, Slézia A, Lecci S, Pellegrini C, Astori S, Dávid C, Hangya B, Lüthi A, Acsády L. 2014. Phasic, nonsynaptic GABA-A receptor-mediated inhibition entrains thalamocortical oscillations. *Journal of Neuroscience* **34**:7137–7147. DOI: https://doi.org/10.1523/JNEUROSCI.4386-13.2014, PMID: 24849349

**Sanchez-Vives MV**, Massimini M, Mattia M. 2017. Shaping the default activity pattern of the cortical network. *Neuron* **94**:993–1001. DOI: https://doi.org/10.1016/j.neuron.2017.05.015, PMID: 28595056

**Schabus M**, Dang-Vu TT, Albouy G, Balteau E, Boly M, Carrier J, Darsaud A, Degueldre C, Desseilles M, Gais S, Phillips C, Rauchs G, Schnakers C, Sterpenich V, Vandewalle G, Luxen A, Maquet P. 2007. Hemodynamic cerebral correlates of sleep spindles during human non-rapid eye movement sleep. *PNAS* **104**:13164–13169. DOI: https://doi.org/10.1073/pnas.0703084104

**Siapas AG**, Wilson MA. 1998. Coordinated interactions between hippocampal ripples and cortical spindles during slow-wave sleep. *Neuron* **21**:1123–1128. DOI: https://doi.org/10.1016/S0896-6273(00)80629-7, PMID: 9856467

**Siclari F**, Tononi G. 2017. Local aspects of sleep and wakefulness. *Current Opinion in Neurobiology* **44**:222–227. DOI: https://doi.org/10.1016/j.conb.2017.05.008, PMID: 28575720

**Steriade M**, McCormick DA, Sejnowski TJ. 1993. Thalamocortical oscillations in the sleeping and aroused brain. *Science* **262**:679–685. DOI: https://doi.org/10.1126/science.8235588, PMID: 8235588

**Steullet P**, Cabungcal JH, Bukhari SA, Ardelt MI, Pantazopoulos H, Hamati F, Salt TE, Cuénod M, Do KQ, Berretta S. 2018. The thalamic reticular nucleus in schizophrenia and bipolar disorder: role of parvalbumin-expressing neuron networks and oxidative stress. *Molecular Psychiatry* **23**:2057–2065. DOI: https://doi.org/10.1038/mp.2017.230, PMID: 29180672

**Tamaki M**, Huang TR, Yotsumoto Y, Hämäläinen M, Lin FH, Náñez JE, Watanabe T, Sasaki Y. 2013. Enhanced spontaneous oscillations in the supplementary motor area are associated with sleep-dependent offline learning

of finger-tapping motor-sequence task. *Journal of Neuroscience* **33**:13894–13902. DOI: https://doi.org/10.1523/JNEUROSCI.1198-13.2013, PMID: 23966709

**Terrier G**, Gottesmann CL. 1978. Study of cortical spindles during sleep in the rat. *Brain Research Bulletin* **3**:701–706. DOI: https://doi.org/10.1016/0361-9230(78)90021-7, PMID: 162576

**Tononi G**, Cirelli C. 2014. Sleep and the price of plasticity: from synaptic and cellular homeostasis to memory consolidation and integration. *Neuron* **81**:12–34. DOI: https://doi.org/10.1016/j.neuron.2013.12.025, PMID: 24411729

**Vong L**, Ye C, Yang Z, Choi B, Chua S, Lowell BB. 2011. Leptin action on GABAergic neurons prevents obesity and reduces inhibitory tone to POMC neurons. *Neuron* **71**:142–154. DOI: https://doi.org/10.1016/j.neuron.2011.05.028, PMID: 21745644

**Vyazovskiy V**, Borbély AA, Tobler I. 2000. Unilateral vibrissae stimulation during waking induces interhemispheric EEG asymmetry during subsequent sleep in the rat. *Journal of Sleep Research* **9**:367–371. DOI: https://doi.org/10.1046/j.1365-2869.2000.00230.x, PMID: 11123523

**Wimmer VC**, Bruno RM, de Kock CP, Kuner T, Sakmann B. 2010. Dimensions of a projection column and architecture of VPM and POm axons in rat vibrissal cortex. *Cerebral Cortex* **20**:2265–2276. DOI: https://doi.org/10.1093/cercor/bhq068, PMID: 20453248

**Wimmer RD**, Astori S, Bond CT, Rovó Z, Chatton JY, Adelman JP, Franken P, Lüthi A. 2012. Sustaining sleep spindles through enhanced SK2-channel activity consolidates sleep and elevates arousal threshold. *Journal of Neuroscience* **32**:13917–13928. DOI: https://doi.org/10.1523/JNEUROSCI.2313-12.2012, PMID: 23035101

**Zhang Y**, Buonanno A, Vertes RP, Hoover WB, Lisman JE. 2012. NR2C in the thalamic reticular nucleus; effects of the NR2C knockout. *PLOS ONE* **7**:e41908. DOI: https://doi.org/10.1371/journal.pone.0041908, PMID: 22848654

**Zhong W**, Ciatipis M, Wolfenstetter T, Jessberger J, Müller C, Ponsel S, Yanovsky Y, Brankačk J, Tort ABL, Draguhn A. 2017. Selective entrainment of gamma subbands by different slow network oscillations. *PNAS* **114**:4519–4524. DOI: https://doi.org/10.1073/pnas.1617249114, PMID: 28396398

**Zingg B**, Hintiryan H, Gou L, Song MY, Bay M, Bienkowski MS, Foster NN, Yamashita S, Bowman I, Toga AW, Dong HW. 2014. Neural networks of the mouse neocortex. *Cell* **156**:1096–1111. DOI: https://doi.org/10.1016/j.cell.2014.02.023, PMID: 24581503